

SUPPORTING INFORMATION

Governing efficiency and thermoresponsivity of luminescence in dirhenium(V) molecules  
by a highly tunable emission mechanism

Michał Liberka,<sup>a,b</sup> Mikołaj Zychowicz,<sup>a,b</sup> Laurine Vasseur,<sup>a,c</sup> James Hooper,<sup>a</sup> and Szymon Chorazy<sup>\*,a</sup>

<sup>a</sup>Faculty of Chemistry, Jagiellonian University, Gronostajowa 2, 30-387 Kraków, Poland

<sup>b</sup>Doctoral School of Exact and Natural Sciences, Jagiellonian University, Łojasiewicza 11, 30-348 Kraków, Poland

<sup>c</sup>Université Paris Cité and CNRS, ITODYS, F-75006 Paris, France

\*Corresponding author: simon.chorazy@uj.edu.pl

Thermogravimetric (TG) curves for the whole series of <b>Re<sub>2</sub>-L</b> materials. (Fig. S1)	- S2
Infrared (IR) absorption spectra for the whole series of <b>Re<sub>2</sub>-L</b> materials. (Fig. S2)	- S3
Crystal data and structure refinement parameters for <b>Re<sub>2</sub>-L</b> materials under variable temperature conditions. (Tables S1-S8)	- S4-S27
Detailed structural views, crystal structure parameters, and temperature variation of unit cell parameters and bond lengths within bimetallic {Re <sup>V</sup> <sub>2</sub> } <sup>4-</sup> assemblies in the structure of all obtained materials of <b>Re<sub>2</sub>-L</b> . (Fig. S3-S18, Tables S9-S16)	- S28-S51
Orientation of dinuclear {Re <sup>V</sup> <sub>2</sub> } <sup>4-</sup> molecular anions in the unit cell of the crystal structure of <b>Re<sub>2</sub>-L</b> materials. (Fig. S19)	- S52
Results of Continuous Shape Measure analysis for rhenium(V) complexes in the crystal structure of <b>Re<sub>2</sub>-L</b> materials. (Tables S17-S24)	- S53-S57
Temperature variation of the OC-6 Continuous Shape Measure parameters for rhenium(V) complexes in the crystal structure of <b>Re<sub>2</sub>-L</b> materials, and the related comment. (Fig. S20)	- S58-S59
Comparison of experimental and calculated powder X-ray diffraction patterns for the whole series of <b>Re<sub>2</sub>-L</b> materials. (Fig. S21)	- S60
Solid-state room-temperature UV-vis absorption spectra of all <b>Re<sub>2</sub>-L</b> materials. (Fig. S22)	- S61
Crystal data, structure refinement, and detailed crystal structure parameters of the reference compound <b>Re-en</b> , as well as the related representative structural views. (Fig. S23, Table S25)	- S62
Comparison of the emission spectra at 77 and 300 K, and the related spectroscopic parameters of the reference compounds of <b>Re-L</b> and selected reported <b>Re<sub>2</sub>-L</b> materials. (Fig. S24, Table S26)	- S63
Representative graphs illustrating solid-state photoluminescent properties of <b>Re<sub>2</sub>-L</b> materials and tables containing their selected spectroscopic parameters. (Fig. S25-S32, Tables S27-S42)	- S64-S87
Description of the molecular DFT/TD-DFT theoretical calculations, and their results obtained using the Gaussian software, including the metric parameters of optimized geometries, contour plots of chosen MO corresponding to the TD-DFT theoretical calculations, the excitation and emission energies predicted for the lowest energy excited states, and the related comparison with the experiment, all sets for the whole series of <b>Re<sub>2</sub>-L</b> materials, as well as the analogous sets for results obtained using ORCA software for selected compounds. (Fig. S33-S46, Tables S43-S62)	- S88-S116
Description of the periodic DFT calculations for selected <b>Re<sub>2</sub>-L</b> materials and the related results including computed bond distances in optimized geometries, computed interaction energies, computed density of states, and computed energy spacings corresponding to the observed emission events. (Fig. S47, Tables S63-S65)	- S117-S119
Temperature dependencies of selected spectroscopic parameters of <b>Re<sub>2</sub>-L</b> materials, shown together with the related relative thermal sensitivity curves and thermal repeatability cycles. (Fig. S48-S63)	- S120-S135
Best-fit parameters for the linear and Mott-Seitz fittings of the temperature dependencies of selected spectroscopic parameters for <b>Re<sub>2</sub>-L</b> materials. (Tables S66-S70)	- S136-S140
Temperature-variable emission decay profiles for <b>Re<sub>2</sub>-L</b> materials, shown with the best-fit curves to the double exponential function and the related best-fit parameters. (Fig. S64-S70, Tables S71-S77)	- S141-S166
Temperature dependencies of the emission lifetimes for <b>Re<sub>2</sub>-L</b> materials, shown together with the related relative thermal sensitivity and thermal repeatability curves. (Fig. S71 and S72)	- S167-S168
Best-fit parameters for the exponential fitting of the temperature dependencies of average emission lifetime for <b>Re<sub>2</sub>-L</b> materials. (Table S78)	- S169
The detailed insight into the dependence of emission maximum energy on the Re1-N1 and Re1-N6 bond distances under variable temperatures in all obtained materials of <b>Re<sub>2</sub>-L</b> . (Fig. S73)	- S170
The correlation of non-radiative decay rate constant with the emission energies in <b>Re<sub>2</sub>-L</b> . (Fig. S74)	- S171
References to the Supporting Information.	- S172-173

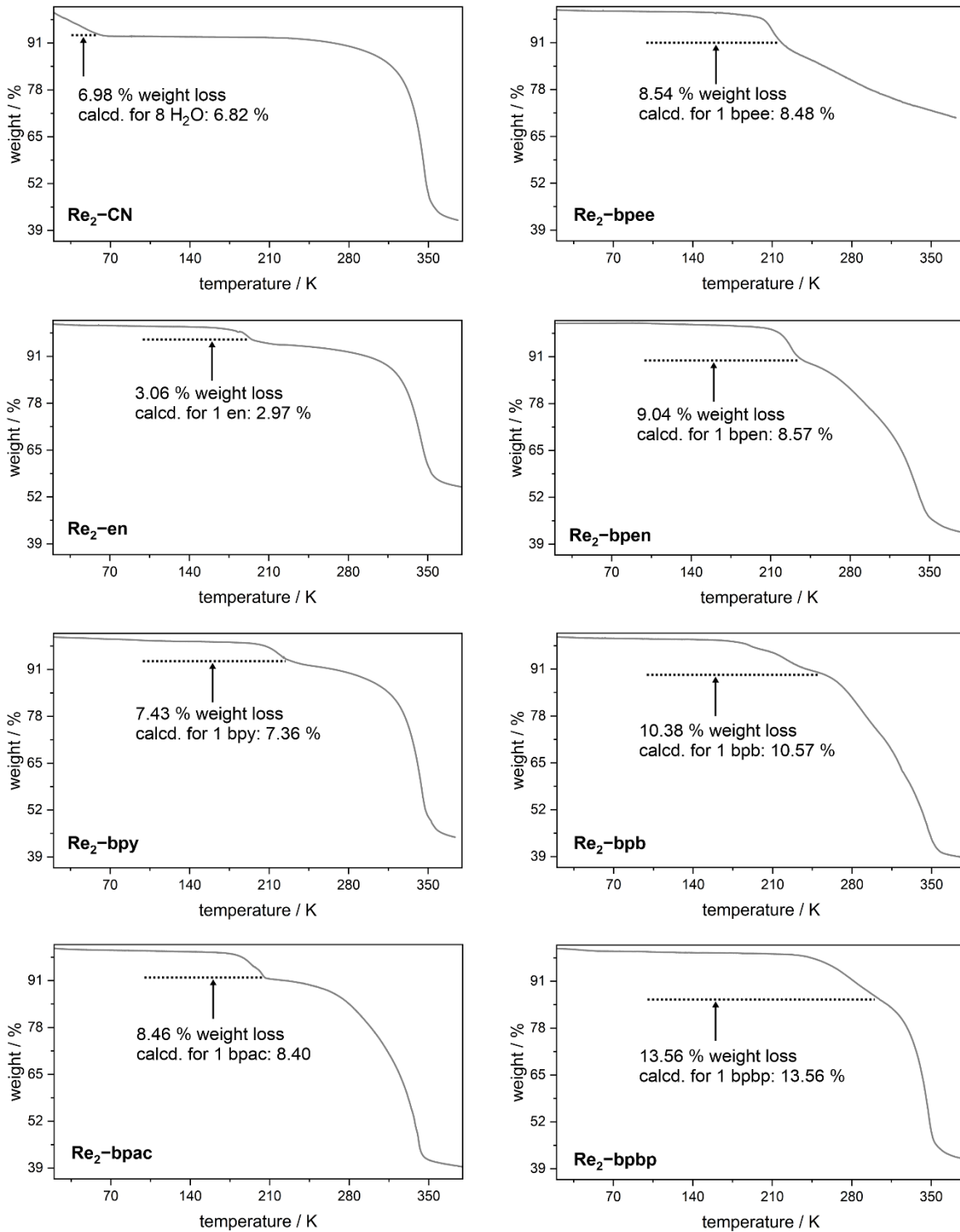


**Fig. S1** Thermogravimetric (TG) curves collected in the temperature range of 20–390 °C for crystalline samples of **Re<sub>2</sub>-CN**, **Re<sub>2</sub>-en**, **Re<sub>2</sub>-bpy**, **Re<sub>2</sub>-bpac**, **Re<sub>2</sub>-bpee**, **Re<sub>2</sub>-bpn**, **Re<sub>2</sub>-bpb**, and **Re<sub>2</sub>-bpbp**. The steps related to the loss of water molecules, diamine, or diimine ligands (depending on the material) are depicted.

**Comment to Fig. S1:** All presented compounds are stable with heating up to ca. 200 °C when the two-step weight loss of the sample mass is detected. The first can be ascribed to the loss of an organic linker connecting the Re(V) centers (except for **Re<sub>2</sub>-CN**, where water molecules are present and removed under heating). The related weight loss is consistent with the theoretical value in each case (as depicted in the Fig. S1). The mass decrease at higher temperatures is related to the loss of cyanido ligands leading to the sample decomposition. No mass changes below 100 °C prove that the methanol molecules, initially present in the materials after syntheses, were removed when the crystals were air-dried. The only exception to this is the **Re<sub>2</sub>-CN** compound, where the weight loss below 100 °C results from the removal of water molecules of crystallization.

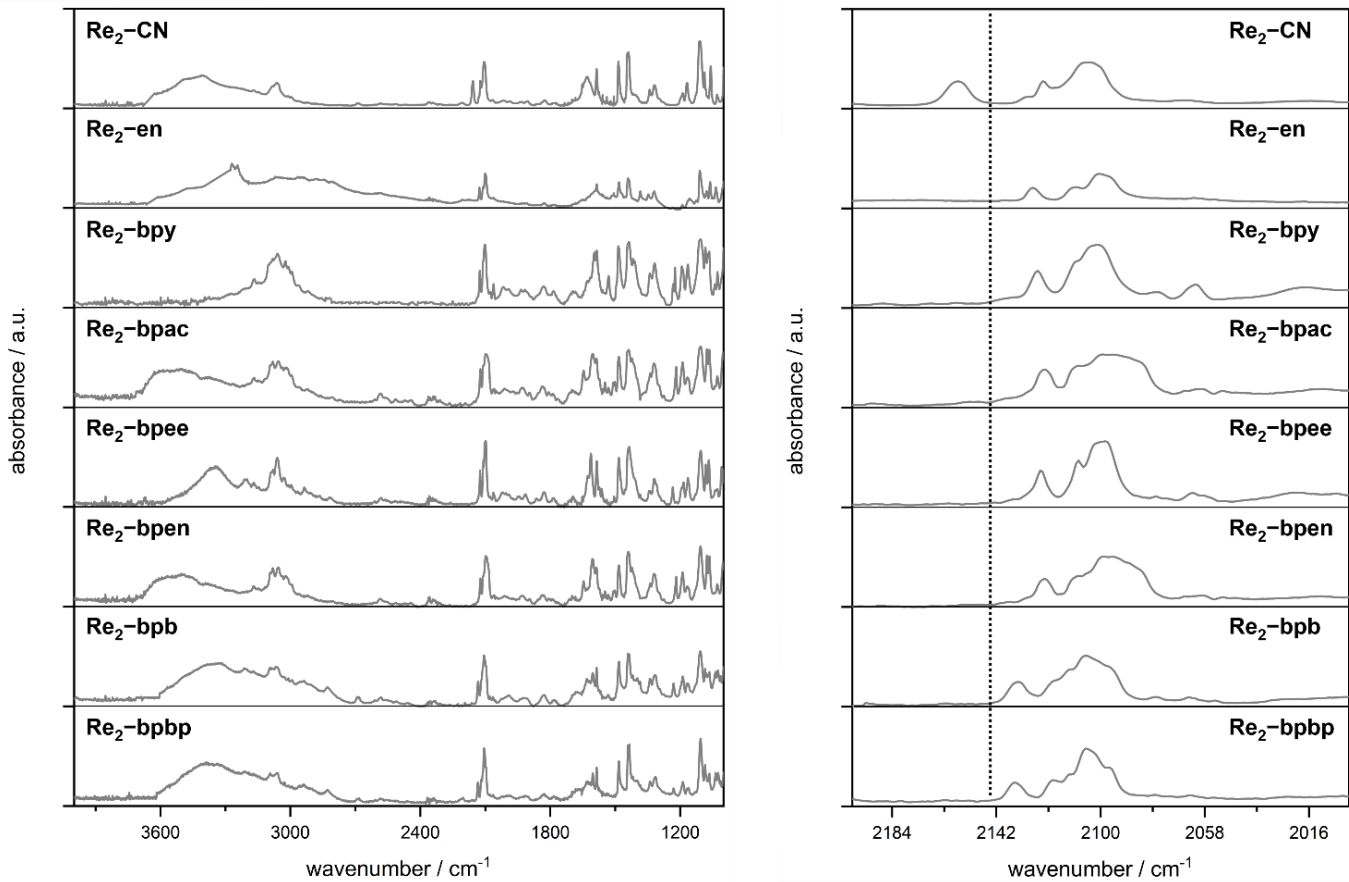


**Fig. S2** Infrared (IR) absorption spectra of crystalline samples of **Re<sub>2</sub>-CN**, **Re<sub>2</sub>-en**, **Re<sub>2</sub>-bpy**, **Re<sub>2</sub>-bpac**, **Re<sub>2</sub>-bpee**, **Re<sub>2</sub>-bpen**, **Re<sub>2</sub>-bpb**, and **Re<sub>2</sub>-bpbp** presented in the broad 4000–1000 cm<sup>-1</sup> region (left), and in the limited 2200–2000 cm<sup>-1</sup> related to cyanido stretching vibrations (right).

**Comment to Fig. S2:** The IR spectra of the crystalline samples of **Re<sub>2</sub>-CN**, **Re<sub>2</sub>-en**, **Re<sub>2</sub>-bpy**, **Re<sub>2</sub>-bpac**, **Re<sub>2</sub>-bpee**, **Re<sub>2</sub>-bpen**, **Re<sub>2</sub>-bpb**, and **Re<sub>2</sub>-bpbp** are very similar. In all samples, the wide absorption above 2850 cm<sup>-1</sup>, as well as the extensive area of absorption bands in the 1500–700 cm<sup>-1</sup> range, are related to the stretching and skeletal vibrations of organic ligands and PPh<sub>4</sub><sup>+</sup> cations. In the range of 2145–2070 cm<sup>-1</sup>, characteristic peaks related to stretching vibrations of terminal cyanido ligands can be observed. In the infrared absorption spectra of **Re<sub>2</sub>-CN**, also higher energy bands above 2145 cm<sup>-1</sup> are observed, which can be attributed to stretching cyanido vibrations within the Re<sup>V</sup>–N≡C–Re<sup>V</sup> linkages (i.e., bridging cyanido ligands). Those results are in line with the single-crystal structural analysis for reported materials and previous works on similar compounds.<sup>[S1,S2]</sup>

**Table S1** Crystal data and structure refinement parameters for **Re<sub>2</sub>-CN**.

compound	Re <sub>2</sub> -CN			
formula	C <sub>104</sub> H <sub>96</sub> N <sub>10</sub> O <sub>8</sub> P <sub>4</sub> Re <sub>2</sub>			
formula weight / g·mol <sup>-1</sup>	2110.21			
λ / Å	0.71073 Å (Mo Kα)			
T / K	100(2)	120(2)	140(2)	160(2)
crystal system	triclinic			
space group	P -1			
a / Å	13.9923(5)	14.0034(6)	14.0159(6)	14.0299(7)
b / Å	14.1642(6)	14.1745(6)	14.1869(6)	14.2017(7)
c / Å	25.3154(9)	25.3337(10)	25.3565(10)	25.3809(12)
α / deg	103.6180(10)	103.5990(10)	103.6050(10)	103.583(2)
β / deg	103.4640(10)	103.4880(10)	103.5190(10)	103.539(2)
γ / deg	92.1280(10)	92.1190(10)	92.0740(10)	92.051(2)
V / Å <sup>3</sup>	4719.7(3)	4730.3(3)	4742.5(3)	4757.0(4)
Z	2	2	2	2
calcd. density / g·cm <sup>-3</sup>	1.485	1.482	1.478	1.473
abs. coeff. / cm <sup>-1</sup>	2.693	2.687	2.680	2.672
F(000)	2128	2128	2128	2128
Θ range / deg	2.531–25.027	2.529–25.027	2.527–25.027	2.524–25.027
collected refl.	75574	75975	76043	76444
R <sub>int</sub>	0.0747	0.0773	0.0777	0.0775
completeness / %	99.9	99.9	99.9	99.9
data/restraints/parameters	16654/41/1216	16691/41/1216	16729/41/1216	16778/21/1216
GOF on F <sup>2</sup>	1.015	1.013	1.013	1.016
final R <sub>1</sub> [ <i>I</i> > 2σ( <i>I</i> )]	0.0367	0.0378	0.0377	0.0375
final wR <sub>2</sub> [all data]	0.0705	0.0723	0.0715	0.0723
diff. peak and hole / e·Å <sup>-3</sup>	1.447 and -0.671	1.116 and -0.729	0.926 and -0.720	0.894 and -0.778

**Table S1** (continuation) Crystal data and structure refinement parameters for **Re<sub>2</sub>-CN**.

compound	Re <sub>2</sub> -CN			
formula	C <sub>104</sub> H <sub>96</sub> N <sub>10</sub> O <sub>8</sub> P <sub>4</sub> Re <sub>2</sub>			
formula weight / g·mol <sup>-1</sup>	2110.21			
λ / Å	0.71073 Å (Mo Kα)			
T / K	180(2)	200(2)	220(2)	240(2)
crystal system	triclinic			
space group	P -1			
a / Å	14.0373(8)	14.0563(7)	14.0726(5)	14.0953(4)
b / Å	14.2090(8)	14.2270(7)	14.2406(5)	14.2538(4)
c / Å	25.3857(13)	25.4144(12)	25.4424(8)	25.4628(6)
α / deg	103.545(2)	103.521(2)	103.5210(10)	103.5400(10)
β / deg	103.557(2)	103.580(2)	103.6160(10)	103.6440(10)
γ / deg	92.064(2)	92.073(2)	92.0980(10)	92.1340(10)
V / Å <sup>3</sup>	4763.1(5)	4781.0(4)	4795.4(3)	4810.0(2)
Z	2	2	2	2
calcd. density / g·cm <sup>-3</sup>	1.471	1.466	1.461	1.457
abs. coeff. / cm <sup>-1</sup>	2.668	2.659	2.651	2.642
F(000)	2128	2128	2128	2128
Θ range / deg	2.176–25.026	2.519–25.028	2.517–25.027	2.516–25.027
collected refl.	76641	77079	77330	77612
R <sub>int</sub>	0.0787	0.0799	0.0809	0.0826
completeness / %	99.9	99.9	99.9	99.9
data/restraints/parameters	16799/41/1216	16857/41/1216	16913/41/1216	16965/41/1216
GOF on F <sup>2</sup>	1.018	1.001	1.005	1.017
final R <sub>1</sub> [ <i>I</i> > 2σ( <i>I</i> )]	0.0381	0.0393	0.0398	0.0411
final wR <sub>2</sub> [all data]	0.0757	0.0823	0.0798	0.0818
diff. peak and hole / e·Å <sup>-3</sup>	1.192 and -0.65	1.373 and -0.712	1.262 and -0.649	1.485 and -0.707

**Table S1** (continuation) Crystal data and structure refinement parameters for **Re<sub>2</sub>-CN**.

compound	Re <sub>2</sub> -CN		
formula	C <sub>104</sub> H <sub>96</sub> N <sub>10</sub> O <sub>8</sub> P <sub>4</sub> Re <sub>2</sub>		-
formula weight / g·mol <sup>-1</sup>	2110.21		-
λ / Å	0.71073 Å (Mo Kα)		-
T / K	260(2)	280(2)	300(2)
crystal system	triclinic		-
space group	P -1		-
a / Å	14.1206(3)	14.1590(4)	14.198(6)
b / Å	14.2661(4)	14.2832(4)	14.301(6)
c / Å	25.4760(6)	25.4884(6)	25.516(11)
α / deg	103.5730(10)	103.6220(10)	103.684(13)
β / deg	103.6710(10)	103.6870(10)	103.703(13)
γ / deg	92.1900(10)	92.2990(10)	92.366(13)
V / Å <sup>3</sup>	4823.5(2)	4842.3(2)	4890(4)
Z	2	2	2
calcd. density / g·cm <sup>-3</sup>	1.453	1.447	1.433
abs. coeff. / cm <sup>-1</sup>	2.635	2.625	2.599
F(000)	2128	2128	2128
Θ range / deg	2.516 25.027	2.516 25.027	2.519 25.027
collected refl.	77895	78090	78643
R <sub>int</sub>	0.0860	0.0898	0.1011
completeness / %	99.9	99.9	99.9
data/restraints/parameters	17011/41/1216	17078/41/1216	17247/25/1163
GOF on F <sup>2</sup>	1.006	1.029	1.013
final R <sub>1</sub> [ <i>I</i> > 2σ( <i>I</i> )]	0.0435	0.0459	0.0529
final wR <sub>2</sub> [all data]	0.0912	0.0981	0.1263
diff. peak and hole / e·Å <sup>-3</sup>	1.564 and -0.616	1.690 and -0.973	2.028 and -0.967

**Table S2** Crystal data and structure refinement parameters for **Re<sub>2</sub>-en**.

compound	Re <sub>2</sub> -en			
formula	C <sub>110</sub> H <sub>88</sub> N <sub>12</sub> O <sub>4</sub> P <sub>4</sub> Re <sub>2</sub>			
formula weight / g·mol <sup>-1</sup>	2137.22			
λ / Å	0.71073 Å (Mo Kα)			
T / K	100(2)	120(2)	140(2)	160(2)
crystal system	triclinic			
space group	P -1			
a / Å	13.1236(4)	13.1444(4)	13.1660(4)	13.1933(4)
b / Å	14.9709(5)	14.9928(4)	15.0152(4)	15.0423(4)
c / Å	28.1670(8)	28.1685(8)	28.1764(8)	28.1950(8)
α / deg	98.7810(10)	98.7650(10)	98.7440(10)	98.7200(10)
β / deg	98.4310(10)	98.4560(10)	98.4740(10)	98.5000(10)
γ / deg	111.2940(10)	111.3640(10)	111.4340(10)	111.5050(10)
V / Å <sup>3</sup>	4971.6(3)	4984.1(2)	4998.5(2)	5018.4(3)
Z	2	2	2	2
calcd. density / g·cm <sup>-3</sup>	1.428	1.424	1.420	1.414
abs. coeff. / cm <sup>-1</sup>	2.556	2.549	2.542	2.532
F(000)	2146	2146	2146	2146
Θ range / deg	2.508–25.027	2.506–25.027	2.505–25.025	2.501–25.027
collected refl.	79903	80340	80612	81166
R <sub>int</sub>	0.0302	0.0305	0.0308	0.0311
completeness / %	99.8	99.9	99.9	99.8
data/restraints/parameters	17541/48/1213	17586/48/1213	17633/48/1213	17690/48/1213
GOF on F <sup>2</sup>	1.077	1.035	1.034	1.069
final R <sub>1</sub> [ <i>I</i> > 2σ( <i>I</i> )]	0.0266	0.0264	0.0262	0.0261
final wR <sub>2</sub> [all data]	0.0655	0.0699	0.0703	0.0664
diff. peak and hole / e·Å <sup>-3</sup>	1.684 and -0.960	1.570 and -1.002	1.416 and -0.970	1.362 and -0.879

**Table S2** (continuation) Crystal data and structure refinement parameters for **Re<sub>2</sub>-en**.

compound	Re <sub>2</sub> -en			
formula	C <sub>110</sub> H <sub>88</sub> N <sub>12</sub> O <sub>4</sub> P <sub>4</sub> Re <sub>2</sub>			
formula weight / g·mol <sup>-1</sup>	2137.22			
λ / Å	0.71073 Å (Mo Kα)			
T / K	180(2)	200(2)	220(2)	240(2)
crystal system	triclinic			
space group	P -1			
a / Å	13.2171(4)	13.2418(4)	13.2624(5)	13.2865(4)
b / Å	15.0643(5)	15.0883(5)	15.1080(5)	15.1313(4)
c / Å	28.2084(8)	28.2265(9)	28.2447(9)	28.2656(8)
α / deg	98.6940(10)	98.6710(10)	98.6400(10)	98.6090(10)
β / deg	98.5230(10)	98.5490(10)	98.5790(10)	98.5800(10)
γ / deg	111.5790(10)	111.6520(10)	111.7180(10)	111.8150(10)
V / Å <sup>3</sup>	5034.3(3)	5052.0(3)	5067.1(3)	5084.7(3)
Z	2	2	2	2
calcd. density / g·cm <sup>-3</sup>	1.410	1.405	1.401	1.396
abs. coeff. / cm <sup>-1</sup>	2.524	2.515	2.507	2.499
F(000)	2146	2146	2146	2146
Θ range / deg	2.499–25.027	2.496–25.027	2.400–25.027	2.398–26.365
collected refl.	81420	82265	82482	91405
R <sub>int</sub>	0.0317	0.0619	0.0327	0.0352
completeness / %	99.8	99.9	99.9	99.8
data/restraints/parameters	17734/48/1213	17804/48/1213	17843/48/1213	20729/48/1213
GOF on F <sup>2</sup>	1.017	1.037	1.051	1.046
final R <sub>1</sub> [ <i>I</i> > 2σ( <i>I</i> )]	0.0262	0.0398	0.0270	0.0296
final wR <sub>2</sub> [all data]	0.0716	0.1116	0.0690	0.0763
diff. peak and hole / e·Å <sup>-3</sup>	1.384 and -0.824	1.484 and -2.076	1.282 and -0.778	1.309 and -0.689

**Table S2** (cont.) Crystal data and structure refinement parameters for **Re<sub>2</sub>-en**.

compound	Re <sub>2</sub> -en		
formula	C <sub>110</sub> H <sub>88</sub> N <sub>12</sub> O <sub>4</sub> P <sub>4</sub> Re <sub>2</sub>		-
formula weight / g·mol <sup>-1</sup>	2137.22		-
λ / Å	0.71073 Å (Mo Kα)		-
T / K	260(2)	280(2)	300(2)
crystal system	triclinic		
space group	P -1		
a / Å	13.3110(4)	13.3463(6)	13.3522(15)
b / Å	15.1554(4)	15.1859(7)	15.2047(16)
c / Å	28.2862(8)	28.3267(12)	28.325(3)
α / deg	98.5690(10)	98.5010(10)	98.515(3)
β / deg	98.5850(10)	98.615(2)	98.557(4)
γ / deg	111.9170(10)	112.031(2)	112.143(4)
V / Å <sup>3</sup>	5102.5(3)	5129.9(4)	5134.6(10)
Z	2	2	2
calcd. density / g·cm <sup>-3</sup>	1.391	1.384	1.382
abs. coeff. / cm <sup>-1</sup>	2.490	2.477	2.474
F(000)	2146	2146	2146
Θ range / deg	2.397–25.027	2.394–25.026	2.393–25.028
collected refl.	82657	83595	83479
R <sub>int</sub>	0.0340	0.0347	0.0356
completeness / %	99.8	99.9	99.9
data/restraints/parameters	17734/48/1213	18080/48/1213	18100/48/1213
GOF on F <sup>2</sup>	1.003	1.047	1.006
final R <sub>1</sub> [ <i>I</i> > 2σ( <i>I</i> )]	0.0282	0.0294	0.0302
final wR <sub>2</sub> [all data]	0.0754	0.0746	0.0822
diff. peak and hole / e·Å <sup>-3</sup>	1.148 and -0.583	1.118 and -0.634	1.048 and -0.639

**Table S3** Crystal data and structure refinement parameters for **Re<sub>2</sub>-bpy**.

compound	Re <sub>2</sub> -bpy			
formula	C <sub>114</sub> H <sub>88</sub> N <sub>12</sub> P <sub>4</sub> Re <sub>2</sub>			
formula weight / g·mol <sup>-1</sup>	2122.26			
λ / Å	0.71073 Å (Mo Kα)			
T / K	100(2)	120(2)	140(2)	160(2)
crystal system	monoclinic			
space group	P 2 <sub>1</sub> /c			
a / Å	20.5759(17)	20.5801(12)	20.5890(9)	20.5985(8)
b / Å	13.1338(11)	13.1593(8)	13.1770(6)	13.1960(6)
c / Å	19.7224(17)	19.7375(11)	19.7443(9)	19.7530(8)
α / deg	90	90	90	90
β / deg	116.435(2)	116.390(2)	116.3770(10)	116.3530(10)
γ / deg	90	90	90	90
V / Å <sup>3</sup>	4772.5(7)	4788.3(5)	4799.0(4)	4811.2(3)
Z	2	2	2	2
calcd. density / g·cm <sup>-3</sup>	1.477	1.472	1.469	1.465
abs. coeff. / cm <sup>-1</sup>	2.659	2.650	2.644	2.637
F(000)	2132	2132	2132	2132
Θ range / deg	2.52–25.682	2.581–25.682	2.462–25.681	2.46–25.681
collected refl.	54731	55667	55512	57943
R <sub>int</sub>	0.0350	0.0976	0.0970	0.0959
completeness / %	99.9	99.9	99.9	99.9
data/restraints/parameters	9038/0/595	9069/0/595	9038/0/595	9038/0/595
GOF on F <sup>2</sup>	1.062	1.061	1.054	1.066
final R <sub>1</sub> [ <i>I</i> > 2σ( <i>I</i> )]	0.0233	0.0311	0.0306	0.0316
final wR <sub>2</sub> [all data]	0.0533	0.0834	0.0830	0.0844
diff. peak and hole / e·Å <sup>-3</sup>	1.194 and -0.610	1.805 and -1.442	1.637 and -1.399	1.791 and -1.383

**Table S3** (continuation) Crystal data and structure refinement parameters for **Re<sub>2</sub>-bpy**.

compound	Re <sub>2</sub> -bpy			
formula	C <sub>114</sub> H <sub>88</sub> N <sub>12</sub> P <sub>4</sub> Re <sub>2</sub>			
formula weight / g·mol <sup>-1</sup>	2122.26			
λ / Å	0.71073 Å (Mo Kα)			
T / K	180(2)	200(2)	220(2)	240(2)
crystal system	monoclinic			
space group	P 2 <sub>1</sub> /c			
a / Å	20.6151(13)	20.6315(10)	20.6466(9)	20.6596(6)
b / Å	13.2176(8)	13.2387(6)	13.2616(6)	13.2791(4)
c / Å	19.7617(12)	19.7707(9)	19.7818(9)	19.7936(6)
α / deg	90	90	90	90
β / deg	116.336(2)	116.3120(10)	116.2890(10)	116.2660(10)
γ / deg	90	90	90	90
V / Å <sup>3</sup>	4825.8(5)	4840.6(4)	4856.2(4)	4869.5(3)
Z	2	2	2	2
calcd. density / g·cm <sup>-3</sup>	1.461	1.456	1.451	1.447
abs. coeff. / cm <sup>-1</sup>	2.629	2.621	2.613	2.606
F(000)	2132	2132	2132	2132
Θ range / deg	2.690–25.027	2.454–25.681	2.451–26.371	2.448–25.681
collected refl.	56343	60006	63729	60613
R <sub>int</sub>	0.0299	0.0967	0.0981	0.0963
completeness / %	99.9	99.9	99.9	99.9
data/restraints/parameters	8525/0/595	9172/0/595	9923/0/595	9224/0/595
GOF on F <sup>2</sup>	1.057	1.035	1.048	1.049
final R <sub>1</sub> [ <i>I</i> > 2σ( <i>I</i> )]	0.0224	0.0314	0.0330	0.0326
final wR <sub>2</sub> [all data]	0.0530	0.0861	0.0867	0.0852
diff. peak and hole / e·Å <sup>-3</sup>	0.892 and -0.449	1.644 and -1.130	1.832 and -1.160	1.665 and -1.067

**Table S3** (continuation) Crystal data and structure refinement parameters for **Re<sub>2</sub>-bpy**.

compound	Re <sub>2</sub> -bpy			
formula	C <sub>114</sub> H <sub>88</sub> N <sub>12</sub> P <sub>4</sub> Re <sub>2</sub>			-
formula weight / g·mol <sup>-1</sup>	2122.26			-
λ / Å	0.71073 Å (Mo Kα)			-
T / K	260(2)	280(2)	300(2)	-
crystal system	monoclinic			-
space group	P 2 <sub>1</sub> /c			-
a / Å	20.6739(5)	20.6860(6)	20.6982(6)	-
b / Å	13.2990(3)	13.3138(4)	13.3255(4)	-
c / Å	19.8066(5)	19.8227(5)	19.8415(6)	-
α / deg	90	90	90	-
β / deg	116.2490(10)	116.2360(10)	116.2270(10)	-
γ / deg	90	90	90	-
V / Å <sup>3</sup>	4884.1(2)	4896.9(2)	4909.2(3)	-
Z	2	2	2	-
calcd. density / g·cm <sup>-3</sup>	1.443	1.439	1.436	-
abs. coeff. / cm <sup>-1</sup>	2.598	2.591	2.585	-
F(000)	2132	2132	2132	-
Θ range / deg	2.445–26.372	2.443–26.372	2.561–25.681	-
collected refl.	63864	64611	61515	-
R <sub>int</sub>	0.1004	0.1005	0.0335	-
completeness / %	99.9	99.9	99.9	-
data/restraints/parameters	9992/0/595	10020/0/595	9312/0/595	-
GOF on F <sup>2</sup>	1.052	1.037	1.024	-
final R <sub>1</sub> [ <i>I</i> > 2σ( <i>I</i> )]	0.0350	0.0347	0.0262	-
final wR <sub>2</sub> [all data]	0.0900	0.0899	0.0602	-
diff. peak and hole / e·Å <sup>-3</sup>	1.773 and -1.096	1.561 and -1.074	0.664 and -0.535	-

**Table S4** Crystal data and structure refinement parameters for **Re<sub>2</sub>-bpac**.

compound	Re <sub>2</sub> -bpac			
formula	C <sub>122</sub> H <sub>112</sub> N <sub>12</sub> O <sub>6</sub> P <sub>4</sub> Re <sub>2</sub>			
formula weight / g·mol <sup>-1</sup>	2338.54			
λ / Å	0.71073 Å (Mo Kα)			
T / K	100(2)	120(2)	140(2)	160(2)
crystal system	triclinic			
space group	P -1			
a / Å	9.8159(6)	9.8183(5)	9.8295(4)	9.8364(4)
b / Å	12.1799(7)	12.1928(6)	12.2159(5)	12.2378(5)
c / Å	23.1732(14)	23.1971(12)	23.2418(10)	23.2792(9)
α / deg	75.457(2)	75.417(2)	75.3890(10)	75.3630(10)
β / deg	81.048(2)	80.981(2)	80.9260(10)	80.9060(10)
γ / deg	82.351(2)	82.349(2)	82.3470(10)	82.3530(10)
V / Å <sup>3</sup>	2636.2(3)	2641.5(2)	2653.97(19)	2664.48(19)
Z	1	1	1	1
calcd. density / g·cm <sup>-3</sup>	1.473	1.470	1.463	1.457
abs. coeff. / cm <sup>-1</sup>	2.413	2.413	2.402	2.392
F(000)	1186	1186	1186	1186
Θ range / deg	25.680–25.242	2.610–25.682	2.594–25.680	2.602–25.682
collected refl.	43820	44216	44692	45092
R <sub>int</sub>	0.0340	0.0345	0.0350	0.0675
completeness / %	99.9	99.9	99.9	99.9
data/restraints/parameters	9983/0/664	10006/0/664	10046/12/664	9983/0/664
GOF on F <sup>2</sup>	1.018	1.059	1.044	1.041
final R <sub>1</sub> [ <i>I</i> > 2σ( <i>I</i> )]	0.0246	0.0250	0.0253	0.0284
final wR <sub>2</sub> [all data]	0.0592	0.0619	0.0616	0.0700
diff. peak and hole / e·Å <sup>-3</sup>	1.301 and -0.848	1.146 and -0.796	1.286 and -0.735	1.197 and -0.948

**Table S4** (continuation) Crystal data and structure refinement parameters for **Re<sub>2</sub>-bpac**.

compound	Re <sub>2</sub> -bpac			
formula	C <sub>122</sub> H <sub>112</sub> N <sub>12</sub> O <sub>6</sub> P <sub>4</sub> Re <sub>2</sub>			
formula weight / g·mol <sup>-1</sup>	2338.54			
λ / Å	0.71073 Å (Mo Kα)			
T / K	180(2)	200(2)	220(2)	240(2)
crystal system	triclinic			
space group	P -1			
a / Å	9.8448(3)	9.8521(4)	9.8583(3)	9.8673(3)
b / Å	12.2621(4)	12.2847(4)	12.3042(4)	12.3291(3)
c / Å	23.3174(7)	23.3540(8)	23.3775(8)	23.4052(6)
α / deg	75.3310(10)	75.3130(10)	75.3170(10)	75.3490(10)
β / deg	80.8720(10)	80.8710(10)	80.9070(10)	81.0080(10)
γ / deg	82.3340(10)	82.3200(10)	82.3180(10)	82.3340(10)
V / Å <sup>3</sup>	2675.76(14)	2686.61(17)	2695.54(15)	2707.76(13)
Z	1	1	1	1
calcd. density / g·cm <sup>-3</sup>	1.451	1.445	1.441	1.434
abs. coeff. / cm <sup>-1</sup>	2.382	2.373	2.365	2.354
F(000)	1186	1186	1186	1186
Θ range / deg	2.589–25.681	2.728–25.679	2.582–25.681	2.578–25.680
collected refl.	45473	45599	45695	45995
R <sub>int</sub>	0.0660	0.0342	0.0669	0.0351
completeness / %	99.9	99.9	99.9	99.9
data/restraints/parameters	10121/0/664	10149/0/664	10188/0/664	10121/0/664
GOF on F <sup>2</sup>	1.042	1.029	1.042	1.024
final R <sub>1</sub> [ <i>I</i> > 2σ( <i>I</i> )]	0.0280	0.0248	0.0295	0.0264
final wR <sub>2</sub> [all data]	0.0675	0.0560	0.0720	0.0605
diff. peak and hole / e·Å <sup>-3</sup>	1.183 and -0.860	1.064 and -0.629	0.951 and -0.960	0.853 and -0.538

**Table S4** (continuation) Crystal data and structure refinement parameters for **Re<sub>2</sub>-bpac**.

compound	Re <sub>2</sub> -bpac			
formula	C <sub>122</sub> H <sub>112</sub> N <sub>12</sub> O <sub>6</sub> P <sub>4</sub> Re <sub>2</sub>	–	–	–
formula weight / g·mol <sup>−1</sup>	2338.54	–	–	–
λ / Å	0.71073 Å (Mo Kα)	–	–	–
T / K	260(2)	280(2)	–	–
crystal system	triclinic	–	–	–
space group	P −1	–	–	–
a / Å	9.8745(3)	9.8936(15)	–	–
b / Å	12.3491(3)	12.3547(19)	–	–
c / Å	23.4288(6)	23.496(4)	–	–
α / deg	75.4090(10)	75.531(5)	–	–
β / deg	81.1210(10)	81.119(5)	–	–
γ / deg	82.3270(10)	82.363(5)	–	–
V / Å <sup>3</sup>	2718.25(13)	2734.1(7)	–	–
Z	1	1	–	–
calcd. density / g·cm <sup>−3</sup>	1.429	1.42	–	–
abs. coeff. / cm <sup>−1</sup>	2.345	2.331	–	–
F(000)	1186	1186	–	–
Θ range / deg	2.574–25.681	2.494–25.681	–	–
collected refl.	46259	44238	–	–
R <sub>int</sub>	0.0687	0.082	–	–
completeness / %	99.9	99.9	–	–
data/restraints/parameters	10284/0/664	10354/1/663	–	–
GOF on F <sup>2</sup>	1.046	1.074	–	–
final R <sub>1</sub> [ <i>I</i> > 2σ( <i>I</i> )]	0.0325	0.0457	–	–
final wR <sub>2</sub> [all data]	0.0762	0.1016	–	–
diff. peak and hole / e·Å <sup>−3</sup>	0.772 and −1.007	1.521 and −1.048	–	–

**Table S5** Crystal data and structure refinement parameters for **Re<sub>2</sub>-bpée**.

compound	Re <sub>2</sub> -bpée			
formula	C <sub>122</sub> H <sub>114</sub> N <sub>12</sub> O <sub>6</sub> P <sub>4</sub> Re <sub>2</sub>			
formula weight / g·mol <sup>-1</sup>	2340.55			
λ / Å	0.71073 Å (Mo Kα)			
T / K	100(2)	120(2)	140(2)	160(2)
crystal system	triclinic			
space group	P -1			
a / Å	9.5573(13)	9.5712(14)	9.5916(13)	9.6037(12)
b / Å	12.3584(17)	12.3730(18)	12.3976(17)	12.4099(16)
c / Å	23.361(3)	23.380(3)	23.419(3)	23.422(3)
α / deg	78.872(4)	78.835(5)	78.791(4)	78.761(4)
β / deg	84.127(5)	84.098(5)	84.065(4)	84.006(4)
γ / deg	84.293(5)	84.282(5)	84.258(5)	84.244(4)
V / Å <sup>3</sup>	2684.1(6)	2692.9(7)	2707.9(6)	2713.8(6)
Z	1	1	1	1
calcd. density / g·cm <sup>-3</sup>	1.448	1.443	1.435	1.432
abs. coeff. / cm <sup>-1</sup>	2.375	2.367	2.354	2.349
F(000)	1188	1188	1188	1188
Θ range / deg	2.396–25.027	2.394–25.026	2.594–25.028	2.388–25.162
collected refl.	43419	43703	44018	44388
R <sub>int</sub>	0.0669	0.0694	0.0723	0.0738
completeness / %	99.9	99.9	99.9	99.9
data/restraints/parameters	9490/18/662	9517/18/662	9569/18/662	9706/20/662
GOF on F <sup>2</sup>	1.069	1.052	1.047	1.030
final R <sub>1</sub> [ <i>I</i> > 2σ( <i>I</i> )]	0.0394	0.0388	0.0403	0.0413
final wR <sub>2</sub> [all data]	0.0787	0.0762	0.0779	0.0801
diff. peak and hole / e·Å <sup>-3</sup>	1.009 and -1.394	0.948 and -1.221	0.864 and -1.231	0.867 and -0.918

**Table S5** (continuation) Crystal data and structure refinement parameters for **Re<sub>2</sub>-bpée**.

compound	Re <sub>2</sub> -bpée			
formula	C <sub>122</sub> H <sub>114</sub> N <sub>12</sub> O <sub>6</sub> P <sub>4</sub> Re <sub>2</sub>			
formula weight / g·mol <sup>-1</sup>	2340.55			
λ / Å	0.71073 Å (Mo Kα)			
T / K	180(2)	200(2)	220(2)	240(2)
crystal system	triclinic			
space group	P -1			
a / Å	9.6152(10)	9.6328(9)	9.6471(6)	9.6629(3)
b / Å	12.4253(13)	12.4485(12)	12.4635(8)	12.4880(4)
c / Å	23.423(2)	23.435(2)	23.4541(14)	23.4479(7)
α / deg	78.727(3)	78.678(3)	78.592(2)	78.5560(10)
β / deg	83.954(4)	83.875(3)	83.817(2)	83.8000(10)
γ / deg	84.253(4)	84.252(3)	84.265(2)	84.2540(10)
V / Å <sup>3</sup>	2720.0(5)	2730.7(4)	2739.3(3)	2747.99(15)
Z	1	1	1	1
calcd. density / g·cm <sup>-3</sup>	1.429	1.423	1.419	1.414
abs. coeff. / cm <sup>-1</sup>	2.344	2.334	2.327	2.320
F(000)	1188	1188	1188	1188
Θ range / deg	2.588–25.040	2.582–25.027	2.382–25.026	2.574–25.025
collected refl.	44139	44484	44687	44744
R <sub>int</sub>	0.0745	0.0764	0.0797	0.0816
completeness / %	99.9	99.9	99.9	99.9
data/restraints/parameters	9607/20/662	9639/20/662	9669/20/662	9693/20/662
GOF on F <sup>2</sup>	1.020	1.007	1.007	1.005
final R <sub>1</sub> [ <i>I</i> > 2σ( <i>I</i> )]	0.0419	0.0422	0.0446	0.0458
final wR <sub>2</sub> [all data]	0.0813	0.0908	0.0947	0.0973
diff. peak and hole / e·Å <sup>-3</sup>	0.811 and -0.997	0.940 and -0.936	0.936 and -0.909	0.823 and -0.725

**Table S5** (continuation) Crystal data and structure refinement parameters for **Re<sub>2</sub>-bppe**.

compound	Re <sub>2</sub> -bppe			
formula	C <sub>122</sub> H <sub>114</sub> N <sub>12</sub> O <sub>6</sub> P <sub>4</sub> Re <sub>2</sub>	–	–	–
formula weight / g·mol <sup>−1</sup>	2340.55	–	–	–
λ / Å	0.71073 Å (Mo Kα)	–	–	–
T / K	260(2)	280(2)	–	–
crystal system	triclinic	–	–	–
space group	P −1	–	–	–
a / Å	9.6797(3)	9.6925(3)	–	–
b / Å	12.5068(4)	12.5233(4)	–	–
c / Å	23.4499(7)	23.4573(7)	–	–
α / deg	78.5340(10)	78.4650(10)	–	–
β / deg	83.7880(10)	83.7870(10)	–	–
γ / deg	84.2650(10)	84.2340(10)	–	–
V / Å <sup>3</sup>	2756.93(15)	2764.31(15)	–	–
Z	1	1	–	–
calcd. density / g·cm <sup>−3</sup>	1.410	1.406	–	–
abs. coeff. / cm <sup>−1</sup>	2.312	2.306	–	–
F(000)	1188	1188	–	–
Θ range / deg	2.570–25.026	2.566–25.059	–	–
collected refl.	44845	44949	–	–
R <sub>int</sub>	0.0853	0.0540	–	–
completeness / %	99.9	99.9	–	–
data/restraints/parameters	9724/20/662	9788/20/662	–	–
GOF on F <sup>2</sup>	1.005	1.004	–	–
final R <sub>1</sub> [ <i>I</i> > 2σ( <i>I</i> )]	0.0456	0.0396	–	–
final wR <sub>2</sub> [all data]	0.0966	0.0884	–	–
diff. peak and hole / e·Å <sup>−3</sup>	0.843 and −0.949	1.142 and −0.945	–	–

**Table S6** Crystal data and structure refinement parameters for **Re<sub>2</sub>-bpn**.

compound	Re <sub>2</sub> -bpn			
formula	C <sub>122</sub> H <sub>116</sub> N <sub>12</sub> O <sub>6</sub> P <sub>4</sub> Re <sub>2</sub>			
formula weight / g·mol <sup>-1</sup>	2342.57			
λ / Å	0.71073 Å (Mo Kα)			
T / K	100(2)	120(2)	140(2)	160(2)
crystal system	triclinic			
space group	P -1			
a / Å	9.5411(6)	9.5542(5)	9.5678(4)	9.5832(4)
b / Å	12.7965(8)	12.8117(7)	12.8266(5)	12.8427(6)
c / Å	22.1542(13)	22.1590(11)	22.1700(9)	22.1842(10)
α / deg	81.158(2)	81.182(2)	81.2230(10)	81.257(2)
β / deg	84.896(2)	84.868(2)	84.8480(10)	84.811(2)
γ / deg	88.548(2)	88.528(2)	88.5270(10)	88.523(2)
V / Å <sup>3</sup>	2661.9(3)	2669.4(2)	2677.83(19)	2687.3(2)
Z	1	1	1	1
calcd. density / g·cm <sup>-3</sup>	1.461	1.457	1.453	1.447
abs. coeff. / cm <sup>-1</sup>	2.395	2.388	2.380	2.372
F(000)	1190	1190	1190	1190
Θ range / deg	2.646–25.681	2.643–25.682	2.64–25.68	2.655–25.682
collected refl.	45452	45542	45564	45728
R <sub>int</sub>	0.0613	0.0620	0.0621	0.0623
completeness / %	99.9	99.9	99.9	99.9
data/restraints/parameters	10110/38/721	10138/38/721	10163/38/721	10195/38/721
GOF on F <sup>2</sup>	1.059	1.062	1.059	1.060
final R <sub>1</sub> [ <i>I</i> > 2σ( <i>I</i> )]	0.0249	0.0254	0.0264	0.0267
final wR <sub>2</sub> [all data]	0.0587	0.0602	0.0622	0.0643
diff. peak and hole / e·Å <sup>-3</sup>	0.946 and -0.895	1.166 and -0.851	1.382 and -0.747	1.549 and -0.785

**Table S6** (continuation) Crystal data and structure refinement parameters for **Re<sub>2</sub>-bpn**.

compound	Re <sub>2</sub> -bpn			
formula	C <sub>122</sub> H <sub>116</sub> N <sub>12</sub> O <sub>6</sub> P <sub>4</sub> Re <sub>2</sub>			
formula weight / g·mol <sup>-1</sup>	2342.57			
λ / Å	0.71073 Å (Mo Kα)			
T / K	180(2)	200(2)	220(2)	240(2)
crystal system	triclinic			
space group	P -1			
a / Å	9.5974(4)	9.6163(4)	9.6355(3)	9.6516(2)
b / Å	12.8567(5)	12.8719(6)	12.8834(4)	12.8920(3)
c / Å	22.1999(9)	22.2145(9)	22.2248(7)	22.2379(5)
α / deg	81.2830(10)	81.316(2)	81.3450(10)	81.3610(10)
β / deg	84.7490(10)	84.7100(10)	84.6760(10)	84.6330(10)
γ / deg	88.5030(10)	88.485(2)	88.4590(10)	88.4360(10)
V / Å <sup>3</sup>	2696.05(19)	2706.4(2)	2715.52(15)	2723.39(10)
Z	1	1	1	1
calcd. density / g·cm <sup>-3</sup>	1.443	1.437	1.432	1.428
abs. coeff. / cm <sup>-1</sup>	2.364	2.355	2.347	2.341
F(000)	1190	1190	1190	1190
Θ range / deg	2.651–25.682	2.646–25.681	2.641–25.681	2.65–25.681
collected refl.	45989	46355	46494	46576
R <sub>int</sub>	0.0637	0.0663	0.0370	0.0374
completeness / %	99.9	99.9	99.9	99.9
data/restraints/parameters	10234/38/721	10271/39/721	10308/39/721	10334/40/721
GOF on F <sup>2</sup>	1.045	1.001	1.024	1.042
final R <sub>1</sub> [ <i>I</i> > 2σ( <i>I</i> )]	0.0272	0.0279	0.0275	0.0280
final wR <sub>2</sub> [all data]	0.0652	0.0705	0.0664	0.0654
diff. peak and hole / e·Å <sup>-3</sup>	1.427 and -0.872	1.424 and -0.928	1.232 and -0.950	1.115 and -0.891

**Table S6** (continuation) Crystal data and structure refinement parameters for **Re<sub>2</sub>-bpn**.

compound	Re <sub>2</sub> -bpn		
formula	C <sub>122</sub> H <sub>116</sub> N <sub>12</sub> O <sub>6</sub> P <sub>4</sub> Re <sub>2</sub>		-
formula weight / g·mol <sup>-1</sup>	2342.57		-
λ / Å	0.71073 Å (Mo Kα)		-
T / K	260(2)	280(2)	300(2)
crystal system	triclinic		
space group	P -1		
a / Å	9.6709(2)	9.6841(3)	9.7001(15)
b / Å	12.9063(3)	12.9157(4)	12.942(2)
c / Å	22.2598(5)	22.2669(7)	22.274(3)
α / deg	81.3760(10)	81.3760(10)	81.412(5)
β / deg	84.5820(10)	84.5410(10)	84.465(5)
γ / deg	88.4190(10)	88.3910(10)	88.367(5)
V / Å <sup>3</sup>	2734.43(11)	2740.83(15)	2760.4(7)
Z	1	1	1
calcd. density / g·cm <sup>-3</sup>	1.423	1.419	1.409
abs. coeff. / cm <sup>-1</sup>	2.331	2.326	2.309
F(000)	1190	1190	1190
Θ range / deg	2.623–25.680	2.622–25.680	2.615–25.681
collected refl.	46830	46856	47207
R <sub>int</sub>	0.0697	0.0725	0.0426
completeness / %	99.9	99.9	99.9
data/restraints/parameters	10381/40/721	10401/40/721	10481/46/721
GOF on F <sup>2</sup>	1.028	1.036	1.051
final R <sub>1</sub> [ <i>I</i> > 2σ( <i>I</i> )]	0.0309	0.0319	0.0339
final wR <sub>2</sub> [all data]	0.0740	0.0750	0.0798
diff. peak and hole / e·Å <sup>-3</sup>	1.064 and -0.843	0.992 and -0.768	1.465 and -0.652

**Table S7** Crystal data and structure refinement parameters for **Re<sub>2</sub>-bpb**.

compound	Re <sub>2</sub> -bpb			
formula	C <sub>126</sub> H <sub>116</sub> N <sub>12</sub> O <sub>6</sub> P <sub>4</sub> Re <sub>2</sub>			
formula weight / g·mol <sup>-1</sup>	2390.61			
λ / Å	0.71073 Å (Mo Kα)			
T / K	100(2)	120(2)	140(2)	160(2)
crystal system	triclinic			
space group	P -1			
a / Å	10.2206(6)	10.2274(6)	10.2379(5)	10.2408(5)
b / Å	12.0308(7)	12.0459(6)	12.0651(6)	12.0766(6)
c / Å	23.5819(13)	23.6107(12)	23.6493(12)	23.6717(11)
α / deg	104.141(2)	104.167(2)	104.175(2)	104.173(2)
β / deg	95.126(2)	95.123(2)	95.136(2)	95.174(2)
γ / deg	100.697(2)	100.704(2)	100.707(2)	100.712(2)
V / Å <sup>3</sup>	2735.2(3)	2743.4(3)	2754.8(2)	2760.6(2)
Z	1	1	1	1
calcd. density / g·cm <sup>-3</sup>	1.451	1.447	1.441	1.438
abs. coeff. / cm <sup>-1</sup>	2.332	2.325	2.316	2.311
F(000)	1214	1214	1214	1214
Θ range / deg	2.639–25.681	2.696–25.679	2.633–25.681	2.631–25.682
collected refl.	45825	45879	46108	46363
R <sub>int</sub>	0.0976	0.0300	0.0303	0.0980
completeness / %	99.9	99.9	99.9	99.9
data/restraints/parameters	10412/0/682	10429/0/682	10458/0/682	10412/0/682
GOF on F <sup>2</sup>	1.071	1.077	1.045	1.069
final R <sub>1</sub> [ <i>I</i> > 2σ( <i>I</i> )]	0.0272	0.0211	0.0221	0.0299
final wR <sub>2</sub> [all data]	0.069	0.0495	0.0512	0.0749
diff. peak and hole / e·Å <sup>-3</sup>	1.783 and -1.363	1.058 and -0.685	1.422 and -0.693	2.010 and -1.255

**Table S7** (continuation) Crystal data and structure refinement parameters for **Re<sub>2</sub>-bpb**.

compound	Re <sub>2</sub> -bpb			
formula	C <sub>126</sub> H <sub>116</sub> N <sub>12</sub> O <sub>6</sub> P <sub>4</sub> Re <sub>2</sub>			
formula weight / g·mol <sup>-1</sup>	2390.61			
λ / Å	0.71073 Å (Mo Kα)			
T / K	180(2)	200(2)	220(2)	240(2)
crystal system	triclinic			
space group	P -1			
a / Å	10.2522(5)	10.2672(6)	10.2841(7)	10.3109(5)
b / Å	12.0974(5)	12.1191(7)	12.1390(7)	12.1652(5)
c / Å	23.6998(10)	23.7322(13)	23.7466(15)	23.7605(10)
α / deg	104.1700(10)	104.192(2)	104.259(2)	104.3890(10)
β / deg	95.193(2)	95.174(2)	95.067(2)	94.819(2)
γ / deg	100.720(2)	100.752(2)	100.800(2)	100.873(2)
V / Å <sup>3</sup>	2771.5(2)	2783.8(3)	2794.0(3)	2808.1(2)
Z	1	1	1	1
calcd. density / g·cm <sup>-3</sup>	1.432	1.426	1.421	1.414
abs. coeff. / cm <sup>-1</sup>	2.302	2.292	2.283	2.272
F(000)	1214	1214	1214	1214
Θ range / deg	2.627–25.682	2.683–25.681	2.682–25.681	2.387–25.682
collected refl.	46542	46664	46995	47705
R <sub>int</sub>	0.0964	0.0326	0.0998	0.1005
completeness / %	99.9	99.9	99.9	99.9
data/restraints/parameters	10534/0/682	10573/0/682	10610/12/677	10534/0/682
GOF on F <sup>2</sup>	1.071	1.053	1.074	1.097
final R <sub>1</sub> [ <i>I</i> > 2σ( <i>I</i> )]	0.0308	0.0257	0.0327	0.0346
final wR <sub>2</sub> [all data]	0.0766	0.0612	0.0835	0.0871
diff. peak and hole / e·Å <sup>-3</sup>	1.808 and -1.115	1.462 and -0.720	1.672 and -0.962	1.368 and -1.037

**Table S7** (continuation) Crystal data and structure refinement parameters for **Re<sub>2</sub>-bpb**.

compound	Re <sub>2</sub> -bpb			
formula	C <sub>126</sub> H <sub>116</sub> N <sub>12</sub> O <sub>6</sub> P <sub>4</sub> Re <sub>2</sub>	–	–	–
formula weight / g·mol <sup>−1</sup>	2390.61	–	–	–
λ / Å	0.71073 Å (Mo Kα)	–	–	–
T / K	260(2)	–	–	–
crystal system	triclinic	–	–	–
space group	P −1	–	–	–
a / Å	10.3477(4)	–	–	–
b / Å	12.1984(4)	–	–	–
c / Å	23.7456(9)	–	–	–
α / deg	104.6500(10)	–	–	–
β / deg	94.3200(10)	–	–	–
γ / deg	101.0150(10)	–	–	–
V / Å <sup>3</sup>	2822.20(18)	–	–	–
Z	1	–	–	–
calcd. density / g·cm <sup>−3</sup>	1.407	–	–	–
abs. coeff. / cm <sup>−1</sup>	2.260	–	–	–
F(000)	1214	–	–	–
Θ range / deg	2.519–25.682	–	–	–
collected refl.	48275	–	–	–
R <sub>int</sub>	0.1065	–	–	–
completeness / %	99.9	–	–	–
data/restraints/parameters	10717/12/682	–	–	–
GOF on F <sup>2</sup>	1.111	–	–	–
final R <sub>1</sub> [ <i>I</i> > 2σ( <i>I</i> )]	0.0382	–	–	–
final wR <sub>2</sub> [all data]	0.0978	–	–	–
diff. peak and hole / e·Å <sup>−3</sup>	1.309 and −1.150	–	–	–

**Table S8** Crystal data and structure refinement parameters for **Re<sub>2</sub>-bpbp**.

compound	Re <sub>2</sub> -bpbp			
formula	C <sub>132</sub> H <sub>120</sub> N <sub>12</sub> O <sub>6</sub> P <sub>4</sub> Re <sub>2</sub>			
formula weight / g·mol <sup>-1</sup>	2466.70			
λ / Å	0.71073 Å (Mo Kα)			
T / K	100(2)	120(2)	140(2)	160(2)
crystal system	monoclinic			
space group	P 2 <sub>1</sub> /n			
a / Å	15.8830(4)	15.8877(5)	15.8949(5)	15.9045(6)
b / Å	22.6871(5)	22.7119(7)	22.7378(8)	22.7639(9)
c / Å	16.5837(3)	16.6046(5)	16.6277(6)	16.6543(6)
α / deg	90	90	90	90
β / deg	106.2840(10)	106.2900(10)	106.3070(10)	106.3160(10)
γ / deg	90	90	90	90
V / Å <sup>3</sup>	5736.0(2)	5751.1(3)	5767.7(3)	5786.8(4)
Z	2	2	2	2
calcd. density / g·cm <sup>-3</sup>	1.428	1.424	1.420	1.416
abs. coeff. / cm <sup>-1</sup>	2.227	2.221	2.214	2.207
F(000)	2508	2508	2508	2508
Θ range / deg	2.238–25.682	2.236–25.681	2.234–25.348	2.232–25.681
collected refl.	44976	72826	71449	73443
R <sub>int</sub>	0.0568	0.0621	0.0839	0.0648
completeness / %	99.9	99.9	99.9	99.9
data/restraints/parameters	10889/56/775	10923/56/775	10550/56/775	10992/56/775
GOF on F <sup>2</sup>	1.027	1.022	1.035	1.013
final R <sub>1</sub> [ <i>I</i> > 2σ( <i>I</i> )]	0.0388	0.0363	0.0377	0.0372
final wR <sub>2</sub> [all data]	0.0836	0.0827	0.0908	0.0897
diff. peak and hole / e·Å <sup>-3</sup>	1.552 and -0.890	1.721 and -1.055	1.832 and -1.008	1.504 and -0.940

**Table S8** (continuation) Crystal data and structure refinement parameters for **Re<sub>2</sub>-bpbp**.

compound	Re <sub>2</sub> -bpbp			
formula	C <sub>132</sub> H <sub>120</sub> N <sub>12</sub> O <sub>6</sub> P <sub>4</sub> Re <sub>2</sub>			
formula weight / g·mol <sup>-1</sup>	2466.70			
λ / Å	0.71073 Å (Mo Kα)			
T / K	180(2)	200(2)	220(2)	240(2)
crystal system	monoclinic			
space group	P 2 <sub>1</sub> /n			
a / Å	15.9113(6)	15.9127(6)	15.9162(7)	15.9273(5)
b / Å	22.7979(8)	22.8416(9)	22.8778(10)	22.9042(7)
c / Å	16.6789(6)	16.7080(7)	16.7402(7)	16.7886(5)
α / deg	90	90	90	90
β / deg	106.3680(10)	106.4460(10)	106.4790(10)	106.4630(10)
γ / deg	90	90	90	90
V / Å <sup>3</sup>	5805.0(4)	5824.4(4)	5845.2(4)	5873.4(3)
Z	2	2	2	2
calcd. density / g·cm <sup>-3</sup>	1.411	1.406	1.401	1.395
abs. coeff. / cm <sup>-1</sup>	2.200	2.193	2.185	2.175
F(000)	2508	2508	2508	2508
Θ range / deg	2.230–25.681	2.542–25.681	2.538–25.681	2.223–25.682
collected refl.	73721	74173	74402	74610
R <sub>int</sub>	0.0646	0.0884	0.0686	0.0718
completeness / %	99.9	99.9	99.9	99.9
data/restraints/parameters	11023/57/775	11052/57/775	11092/63/775	11142/63/775
GOF on F <sup>2</sup>	1.022	1.034	1.018	1.004
final R <sub>1</sub> [ <i>I</i> > 2σ( <i>I</i> )]	0.0380	0.0395	0.0399	0.0411
final wR <sub>2</sub> [all data]	0.0874	0.0945	0.0917	0.0949
diff. peak and hole / e·Å <sup>-3</sup>	1.439 and -0.997	1.355 and -0.985	1.251 and -1.011	1.062 and -0.802

**Table S8** (continuation) Crystal data and structure refinement parameters for **Re<sub>2</sub>-bpbp**.

compound	Re <sub>2</sub> -bpbp			
formula	C <sub>132</sub> H <sub>120</sub> N <sub>12</sub> O <sub>6</sub> P <sub>4</sub> Re <sub>2</sub>			-
formula weight / g·mol <sup>-1</sup>	2466.70			-
λ / Å	0.71073 Å (Mo Kα)			-
T / K	260(2)	280(2)	300(2)	-
crystal system	monoclinic			-
space group	P 2 <sub>1</sub> /n			-
a / Å	15.9295(4)	15.9303(4)	15.9312(14)	-
b / Å	22.9427(6)	22.9953(6)	23.045(2)	-
c / Å	16.8395(4)	16.8945(4)	16.9521(15)	-
α / deg	90	90	90	-
β / deg	106.5070(10)	106.5930(10)	106.691(3)	-
γ / deg	90	90	90	-
V / Å <sup>3</sup>	5900.6(3)	5931.1(3)	5958.0(9)	-
Z	2	2	2	-
calcd. density / g·cm <sup>-3</sup>	1.388	1.381	1.375	-
abs. coeff. / cm <sup>-1</sup>	2.165	2.153	2.144	-
F(000)	2508	2508	2508	-
Θ range / deg	2.220–25.682	2.516–26.371	2.509–25.681	-
collected refl.	75030	79347	75496	-
R <sub>int</sub>	0.0953	0.0826	0.1048	-
completeness / %	99.9	99.9	99.9	-
data/restraints/parameters	11189/63/775	12114/63/775	11293/92/775	-
GOF on F <sup>2</sup>	1.017	1.013	1.006	-
final R <sub>1</sub> [ <i>I</i> > 2σ( <i>I</i> )]	0.0429	0.046	0.0499	-
final wR <sub>2</sub> [all data]	0.1044	0.1081	0.1238	-
diff. peak and hole / e·Å <sup>-3</sup>	0.893 and -0.842	0.888 and -0.782	0.949 and -0.827	-

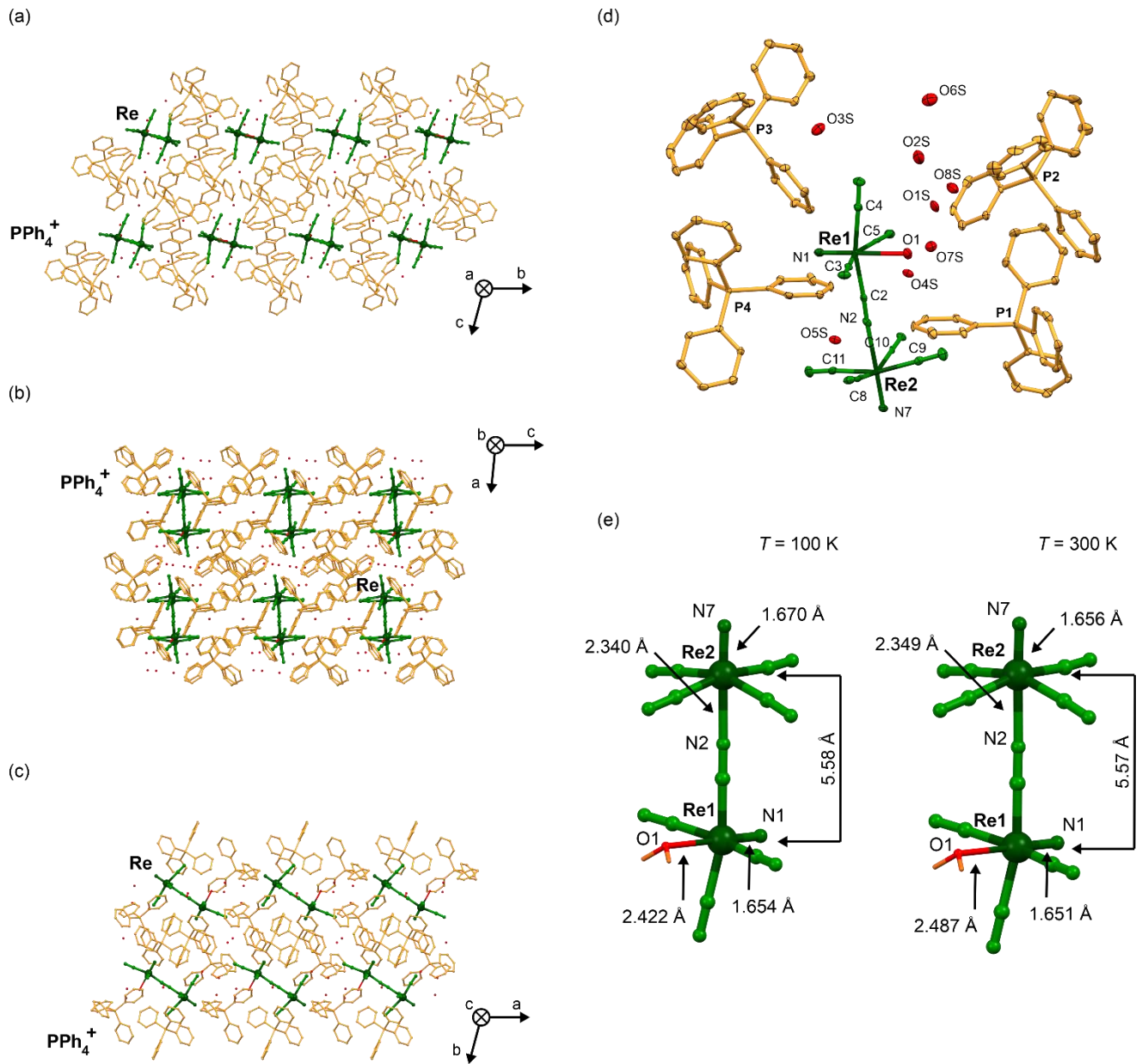


**Fig. S3** Detailed structural views of **Re<sub>2</sub>-CN** material: the crystal structure presented along the main *a*, *b*, and *c* crystallographic axes (*a*, *b*, and *c*, respectively), the asymmetric unit with the labeling scheme for selected symmetrically independent atoms (d), and the comparison of the metric parameters of bimetallic {Re<sup>V<sub>2</sub></sup>}<sup>4-</sup> assemblies at 100(2) and 300(2) K (e). Thermal ellipsoids for the asymmetric unit in (d) are presented at the 50% probability level. Hydrogen atoms in the (a-d) parts views were omitted for clarity. Related detailed structural parameters are presented in Table S9.

**Table S9** Detailed crystal structure parameters of **Re<sub>2</sub>-CN**.

compound	Re <sub>2</sub> -CN					
T / K	100(2)	120(2)	140(2)	160(2)	180(2)	200(2)
Re1/Re2-C / Å	2.092(5) – 2.109(5)	2.094(5) – 2.115(5)	2.094(5) – 2.116(5)	2.093(5) – 2.119(5)	2.098(5) – 2.112(5)	2.090(5) – 2.114(5)
Re1≡N1 / Å	1.654(4)	1.653(4)	1.657(4)	1.654(4)	1.651(4)	1.653(4)
Re1–O1 / Å	2.422(3)	2.420(3)	2.424(3)	2.426(3)	2.426(3)	2.428(4)
Re2≡N7 / Å	1.670(4)	1.668(4)	1.665(4)	1.667(4)	1.665(4)	1.664(4)
Re1–N2 / Å	2.340(4)	2.343(4)	2.344(4)	2.347(4)	2.350(4)	2.348(4)
C-Re1/Re2-C ( <i>cis</i> ) / °	85.43(16) – 91.31(17)	85.18(17) – 91.37(18)	85.07(17) – 91.49(17)	85.27(17) – 91.39(18)	85.38(17) – 91.15(18)	85.40(19) – 91.02(19)
C-Re1/Re2-C ( <i>trans</i> ) / °	159.85(17), 165.85(17)	159.94(18), 165.94(18)	160.03(17), 166.01(18)	160.09(17), 166.04(18)	159.69(18), 165.88(18)	159.54(18), 165.71(19)
N1≡Re1–C / °	96.19(18) – 99.99(17)	96.23(18) – 100.11(18)	96.35(18) – 99.99(18)	96.43(18) – 99.95(18)	95.90(19) – 100.89(18)	96.77(19) – 100.1(2)
N1≡Re1–O1 / °	179.70(15)	179.69(15)	179.51(16)	179.60(16)	179.22(16)	179.52(17)
N7≡Re2–C / °	95.70(18) – 101.09(17)	95.93(19) – 101.08(18)	95.90(18) – 101.03(18)	96.07(19) – 101.03(18)	96.82(19) – 99.94(19)	96.3(2) – 101.07(19)
N7≡Re1–N2 / °	176.99(15)	177.22(16)	177.10(16)	177.08(16)	177.44(16)	177.20(17)
Re1–(L)–Re1 / Å	5.583(7)	5.585(7)	5.588(7)	5.589(7)	5.592(8)	5.591(8)
T / K	220(2)	240(2)	260(2)	280(2)	300(2)	–
Re1/Re2-C / Å	2.095(5) – 2.107(5)	2.084(6) – 2.116(6)	2.089(6) – 2.121(6)	2.092(7) – 2.116(7)	2.085(9) – 2.120(9)	–
Re1≡N1 / Å	1.653(4)	1.657(4)	1.649(5)	1.647(5)	1.651(6)	–
Re1–O1 / Å	2.438(4)	2.437(4)	2.445(4)	2.453(5)	2.487(6)	–
Re2≡N7 / Å	1.658(4)	1.664(4)	1.657(5)	1.652(5)	1.656(6)	–
Re1–N2 / Å	2.346(4)	2.349(4)	2.351(5)	2.349(5)	2.349(7)	–
C-Re1/Re2-C ( <i>cis</i> ) / °	85.51(19) – 90.72(19)	85.4(2) – 90.9(2)	85.4(2) – 90.6(2)	85.5(2) – 90.4(2)	85.5(3) – 90.5(3)	–
C-Re1/Re2-C ( <i>trans</i> ) / °	160.11(19), 165.8(2)	160.4(2), 165.7(2)	160.1(2), 165.5(2)	160.0(2), 165.6(3)	160.2(3), 165.0(4)	–
N1≡Re1–C / °	96.9(2) – 100.1(2)	96.8(2) – 100.0(2)	96.9(2) – 100.0(2)	96.8(3) – 100.4(3)	96.4(4) – 100.6(3)	–
N1≡Re1–O1 / °	179.58(18)	179.37(19)	178.6(2)	179.2(2)	179.8(3)	–
N7≡Re2–C / °	96.4(2) – 100.9(2)	96.6(2) – 100.7(2)	96.5(2) – 100.7(2)	97.1(3) – 100.8(3)	97.5(4) – 100.4(3)	–
N7≡Re1–N2 / °	177.33(17)	177.46(18)	177.5(2)	177.6(2)	177.1(3)	–
Re1–(L)–Re1 / Å	5.590(8)	5.589(9)	5.585(10)	5.58(11)	5.566(14)	–

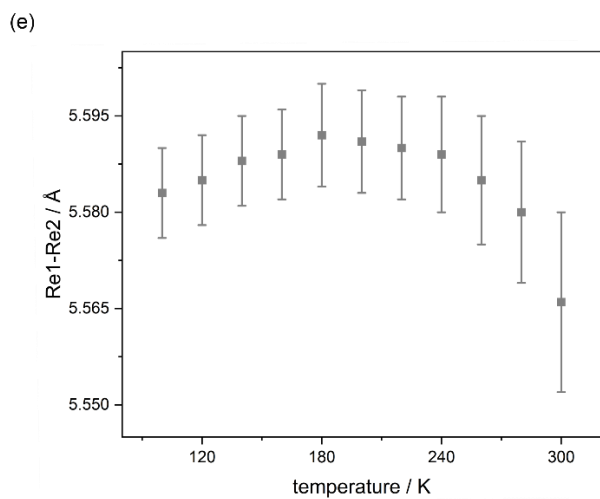
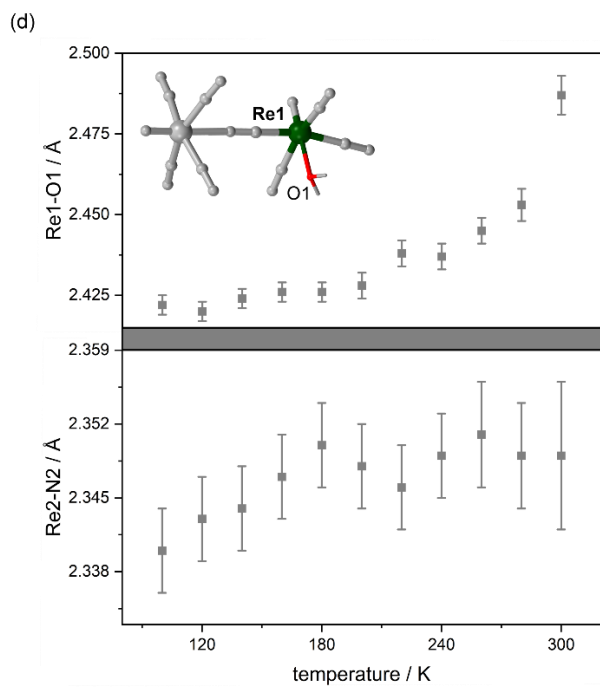
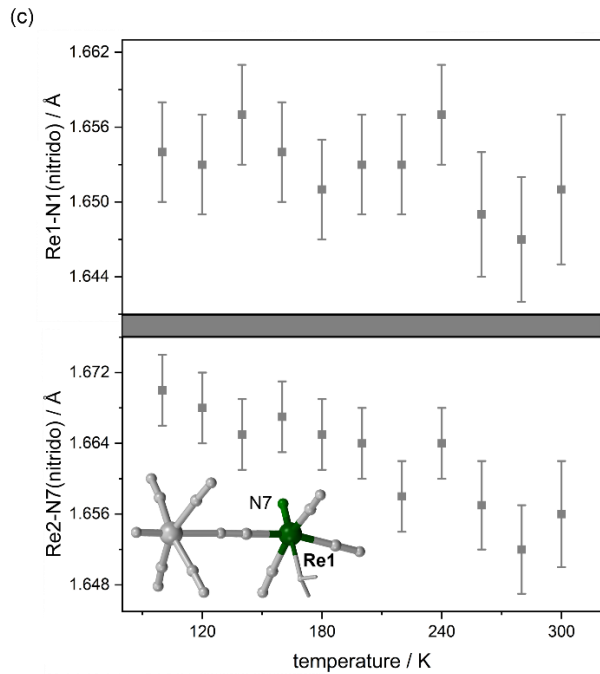
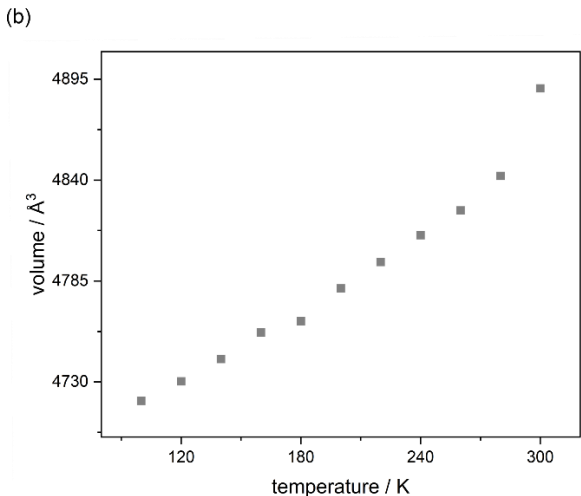
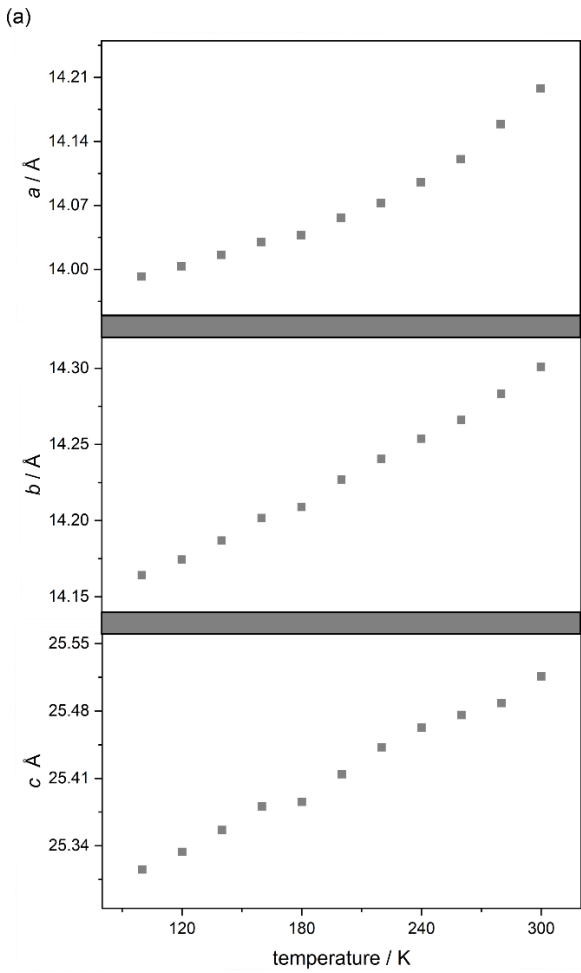
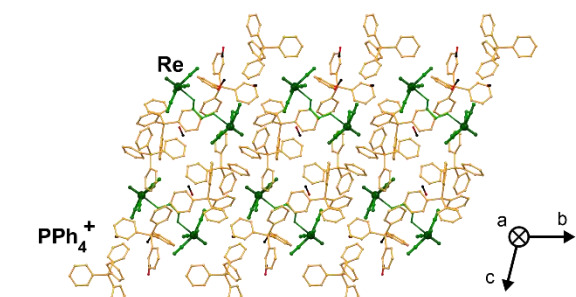
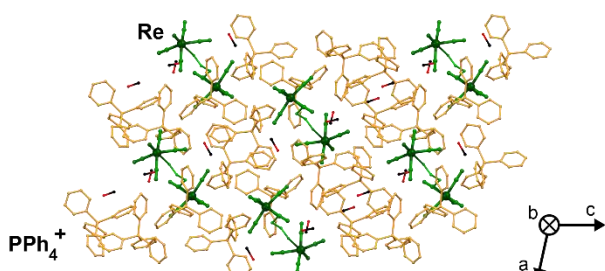


**Fig. S4** The temperature variation of unit cell parameters (a–b), as well as  $\text{Re}\equiv\text{N}(\text{nitrido})$ ,  $\text{Re}-\text{O}1$ ,  $\text{Re}-\text{N}2$ , and  $\text{Re}-\text{Re}$  bond lengths (c–e) within the bimetallic  $\{\text{Re}^{V_2}\}^{4-}$  assemblies in the crystal structure of **Re<sub>2</sub>-CN**.

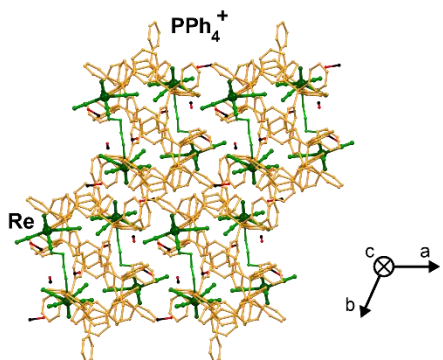
(a)



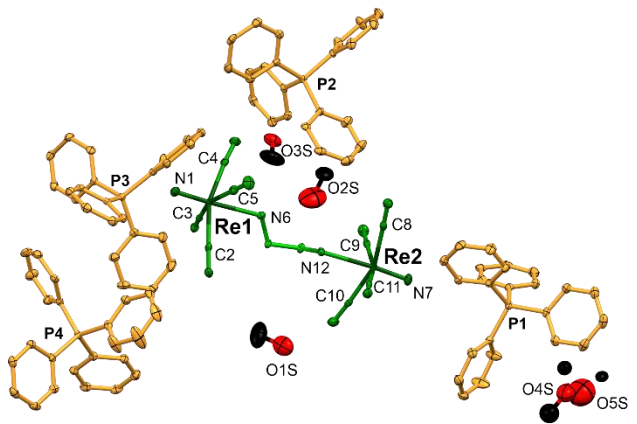
(b)



(c)



(d)



(e)

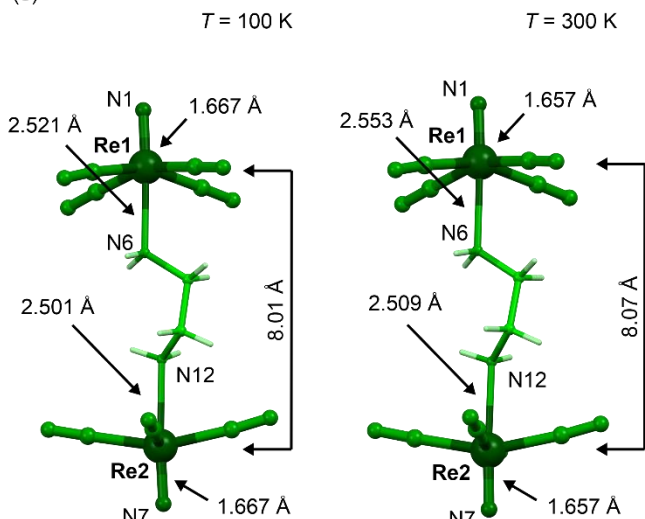


**Fig. S5** Detailed structural views of  $\text{Re}_2\text{-en}$  material: the crystal structure presented along the main  $a$ ,  $b$ , and  $c$  crystallographic axes ( $a$ ,  $b$ , and  $c$ , respectively), the asymmetric unit with the labeling scheme for selected symmetrically independent atoms (d), and the comparison of the metric parameters of bimetallic  $\{\text{Re}^{\text{V}}_2\}^{4-}$  assemblies at  $100(2)$  and  $300(2)$  K (e). Thermal ellipsoids for the asymmetric unit are presented in (d) at the 50% probability level. Hydrogen atoms in the (a-d) parts were omitted for clarity. Related detailed structural parameters are presented in Table S10.

**Table S10** Detailed crystal structure parameters of **Re<sub>2</sub>-en**.

compound	Re <sub>2</sub> -en					
T / K	100(2)	120(2)	140(2)	160(2)	180(2)	200(2)
Re1/Re2-C / Å	2.097(4) – 2.117(4)	2.094(4) – 2.117(4)	2.096(4) – 2.114(4)	2.097(4) – 2.115(4)	2.097(4) – 2.116(4)	2.095(5) – 2.126(5)
Re1≡N1 / Å	1.667(3)	1.666(3)	1.665(3)	1.666(3)	1.667(3)	1.658(4)
Re1–N6 / Å	2.521(3)	2.520(3)	2.523(3)	2.526(3)	2.525(3)	2.523(4)
Re2≡N7 / Å	1.667(3)	1.666(3)	1.668(3)	1.666(3)	1.665(3)	1.654(4)
Re1–N12 / Å	2.501(3)	2.501(3)	2.501(3)	2.505(3)	2.506(3)	2.501(4)
C-Re1/Re2-C ( <i>cis</i> ) / °	85.89(13) – 91.56(13)	85.89(13) – 91.54(13)	86.01(13) – 91.57(14)	86.03(13) – 91.45(14)	86.16(13) – 91.39(14)	85.92(17) – 91.48(18)
C-Re1/Re2-C ( <i>trans</i> ) / °	158.80(13), 163.38(13)	158.81(13), 163.36(13)	158.76(13), 163.34(13)	158.73(13), 163.27(13)	158.86(13), 163.13(13)	158.76(18), 163.02(18)
N1≡Re1–C / °	99.09(14) – 100.81(14)	99.12(14) – 100.90(14)	99.05(14) – 100.92(14)	99.07(14) – 100.96(14)	99.18(15) – 100.92(15)	99.0(2) – 101.0(2)
N1≡Re1–N6 / °	176.83(12)	176.86(12)	176.83(13)	176.86(13)	176.90(13)	177.11(17)
N7≡Re2–C / °	97.50(14) – 101.37(14)	97.52(14) – 101.38(14)	97.49(14) – 101.52(14)	97.58(14) – 101.48(14)	97.67(15) – 101.40(14)	97.9(2) – 101.37(19)
N7≡Re1–N12 / °	176.13(13)	176.18(13)	176.15(13)	176.17(13)	176.34(13)	176.51(18)
Re1–(L)–Re1 / Å	8.014(6)	8.014(6)	8.019(6)	8.027(6)	8.032(6)	8.038(8)
T / K	220(2)	240(2)	260(2)	280(2)	300(2)	–
Re1/Re2-C / Å	2.100(4) – 2.116(4)	2.094(4) – 2.113(4)	2.097(4) – 2.116(4)	2.095(4) – 2.119(4)	2.094(5) – 2.113(5)	–
Re1≡N1 / Å	1.662(3)	1.663(3)	1.658(3)	1.659(3)	1.657(3)	–
Re1–N6 / Å	2.525(3)	2.530(3)	2.531(3)	2.531(3)	2.533(3)	–
Re2≡N7 / Å	1.663(3)	1.666(3)	1.662(3)	1.661(3)	1.657(3)	–
Re1–N12 / Å	2.506(3)	2.509(3)	2.510(3)	2.512(3)	2.509(3)	–
C-Re1/Re2-C ( <i>cis</i> ) / °	86.14(14) – 91.33(15)	86.19(13) – 91.18(15)	86.48(14) – 91.15(16)	86.48(15) – 91.03(16)	86.34(16) – 90.96(17)	–
C-Re1/Re2-C ( <i>trans</i> ) / °	158.64(14), 163.16(14)	158.75(14), 163.09(14)	158.77(15), 163.16(15)	158.65(15), 163.09(15)	158.69(16), 163.16(16)	–
N1≡Re1–C / °	99.12(16) – 100.93(16)	99.15(15) – 100.86(15)	99.20(17) – 100.78(17)	99.10(17) – 100.93(16)	99.10(18) – 100.95(17)	–
N1≡Re1–N6 / °	176.89(14)	176.81(14)	176.81(15)	176.90(15)	176.82(16)	–
N7≡Re2–C / °	97.84(15) – 101.48(15)	97.74(15) – 101.55(15)	97.79(16) – 101.37(16)	97.87(17) – 101.51(16)	97.84(18) – 101.41(17)	–
N7≡Re1–N12 / °	176.44(14)	176.41(14)	176.58(15)	176.61(16)	176.81(17)	–
Re1–(L)–Re1 / Å	8.044(6)	8.05(6)	8.057(7)	8.068(7)	8.068(8)	–

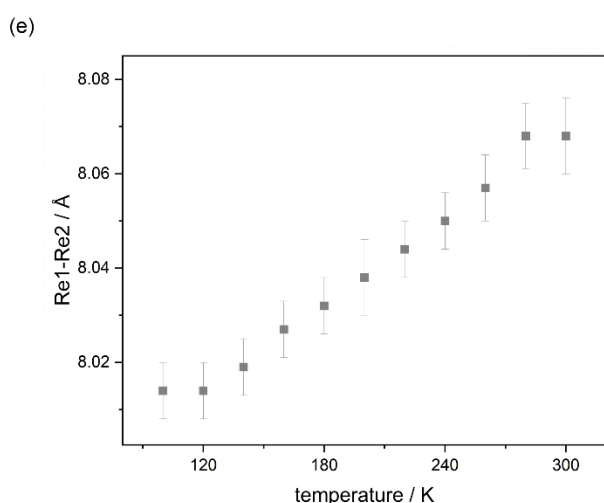
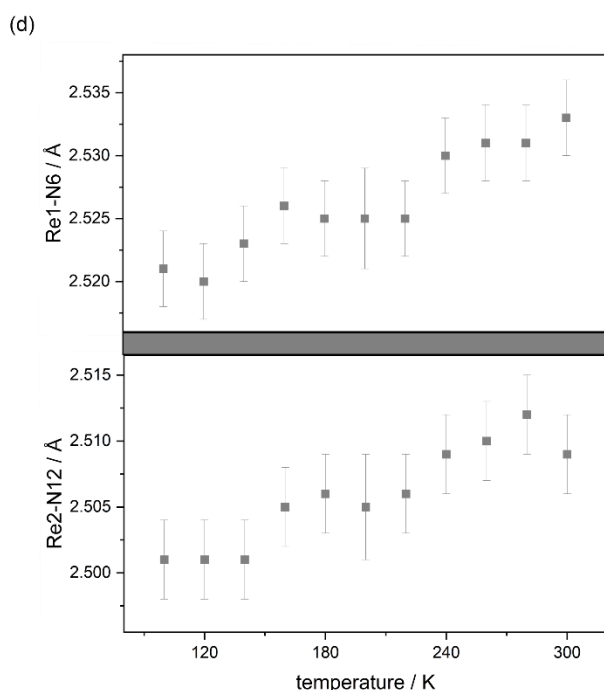
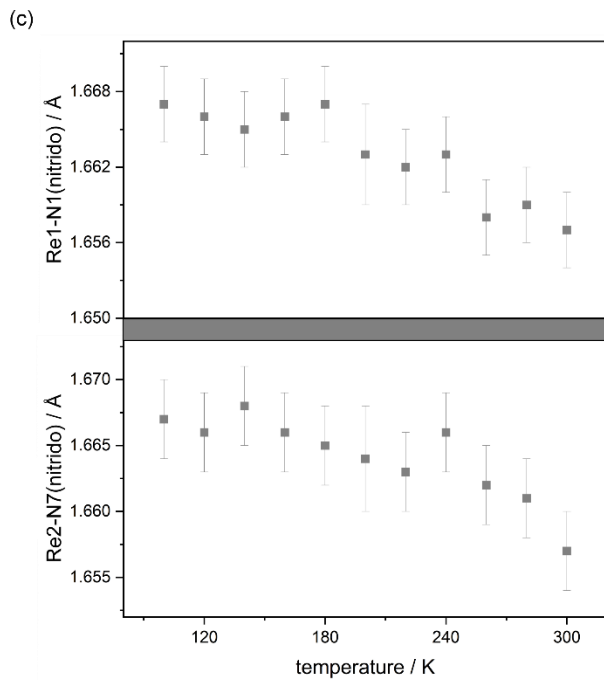
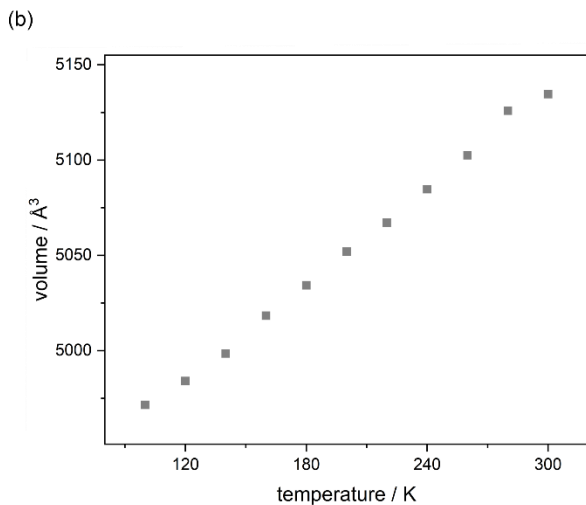
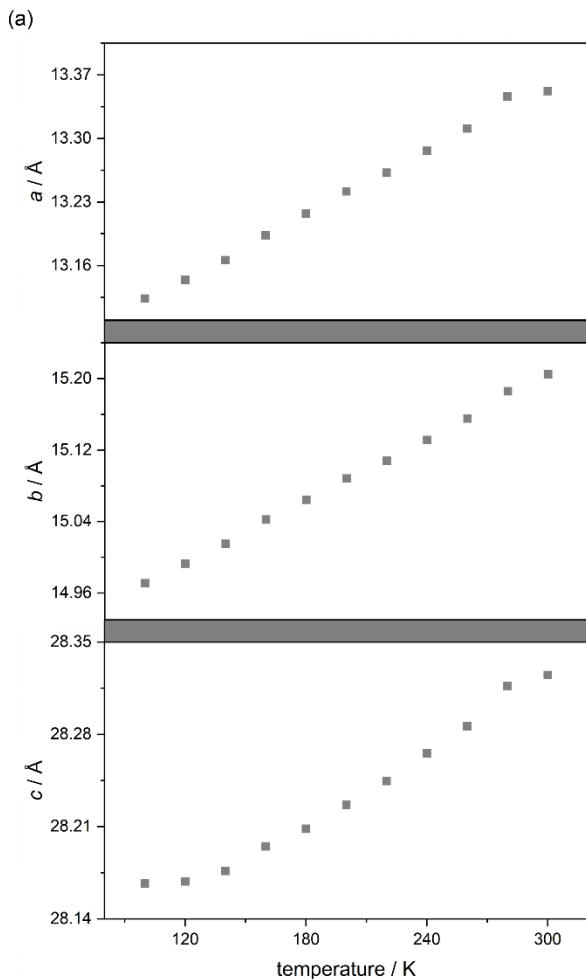


**Fig. S6** The temperature variation of unit cell parameters (a–b), as well as  $\text{Re}\equiv\text{N}(\text{nitrido})$ ,  $\text{Re}_1-\text{N}6$ ,  $\text{Re}_2-\text{N}12$ , and  $\text{Re}-\text{Re}$  bond lengths (c–e) within bimetallic  $\{\text{Re}_2^V\}_2^{4-}$  assemblies in the crystal structure of **Re<sub>2</sub>-en**.

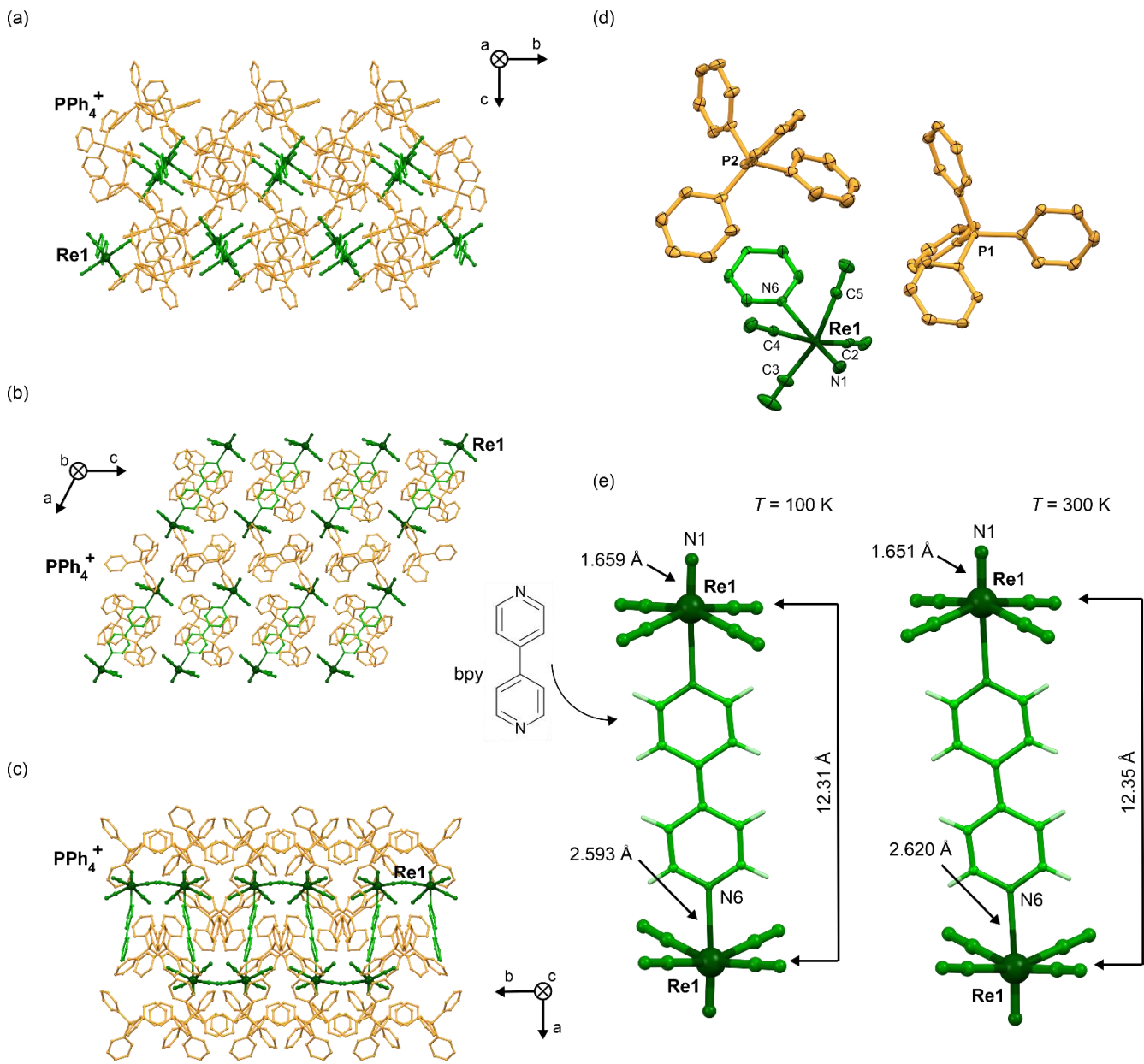


**Fig. S7** Detailed structural views of **Re<sub>2</sub>-bpy** material: the crystal structure presented along the main *a*, *b*, and *c* crystallographic axes (a–c), the asymmetric unit with the labeling scheme for selected symmetrically independent atoms (d), and the comparison of the metric parameters of bimetallic  $\{\text{Re}^{\text{V}_2}\}^{4-}$  assemblies at 100(2) and 300(2) K (e). Thermal ellipsoids for the asymmetric unit are presented in (d) at the 50% probability level. Hydrogen atoms in the (a–d) parts were omitted for clarity. Related detailed structural parameters are presented in Table S11.

**Table S11** Detailed crystal structure parameters of **Re<sub>2</sub>-bpy**.

compound	Re <sub>2</sub> -bpy					
T / K	100(2)	120(2)	140(2)	160(2)	180(2)	200(2)
Re1-C / Å	2.095(3) – 2.108(3)	2.087(4) – 2.109(4)	2.090(4) – 2.106(4)	2.085(4) – 2.109(4)	2.091(3) – 2.103(3)	2.081(4) – 2.104(4)
Re1≡N1 / Å	1.659(2)	1.658(3)	1.658(3)	1.655(3)	1.655(2)	1.654(3)
Re1-N6 / Å	2.593(2)	2.586(3)	2.589(3)	2.593(3)	2.602(2)	2.597(3)
C-Re1-C ( <i>cis</i> ) / °	87.05(11) – 90.14(11)	86.97(14) – 90.19(14)	86.97(14) – 90.09(14)	86.91(14) – 90.20(14)	86.99(12) – 89.95(12)	86.93(14) – 90.21(14)
C-Re1-C ( <i>trans</i> ) / °	161.04(12), 161.22(10)	160.83(16), 161.35(14)	160.88(16), 161.35(14)	160.84(16), 161.24(14)	160.48(12), 161.05(11)	160.59(16), 161.35(13)
N1≡Re1-C / °	98.90(12) – 100.05(12)	99.05(14) – 100.03(16)	99.08(16) – 100.03(16)	99.08(16) – 100.06(17)	99.29(13) – 100.22(13)	98.94(14) – 100.09(17)
N1≡Re1-N6 / °	176.90 (10)	177.02(11)	177.04(11)	177.03(12)	177.02(12)	177.21(13)
Re1-(L)-Re1 / Å	12.306(5)	12.307(5)	12.309(5)	12.312(5)	12.316(5)	12.321(5)
T / K	220(2)	240(2)	260(2)	280(2)	300(2)	–
Re1-C / Å	2.079(4) – 2.104(4)	2.080(4) – 2.099(4)	2.080(4) – 2.102(4)	2.075(4) – 2.101(4)	2.081(4) – 2.101(3)	–
Re1≡N1 / Å	1.654(3)	1.651(3)	1.651(3)	1.646(3)	1.651(3)	–
Re1-N6 / Å	2.603(3)	2.600(3)	2.604(3)	2.612(3)	2.620(3)	–
C-Re1-C ( <i>cis</i> ) / °	87.02(15) – 90.17(14)	87.20(15) – 90.01(15)	87.20(16) – 89.87(15)	87.01(16) – 89.95(15)	86.92(14) – 89.67(14)	–
C-Re1-C ( <i>trans</i> ) / °	160.51(17), 161.35(14)	160.65(17), 1(61.35(14)	160.54(18), 161.39(15)	160.49(18), 161.34(14)	160.28(15), 161.03(12)	–
N1≡Re1-C / °	98.96(15) – 99.99(18)	98.87(15) – 99.99(18)	98.72(16) – 100.08(19)	98.82(16) – 100.08(19)	99.16(13) – 100.23(16)	–
N1≡Re1-N6 / °	177.15(13)	177.39(13)	177.31(15)	177.42(15)	179.55(16)	–
Re1-(L)-Re1 / Å	12.326(5)	12.330(5)	12.334(5)	12.339(5)	12.345(5)	–

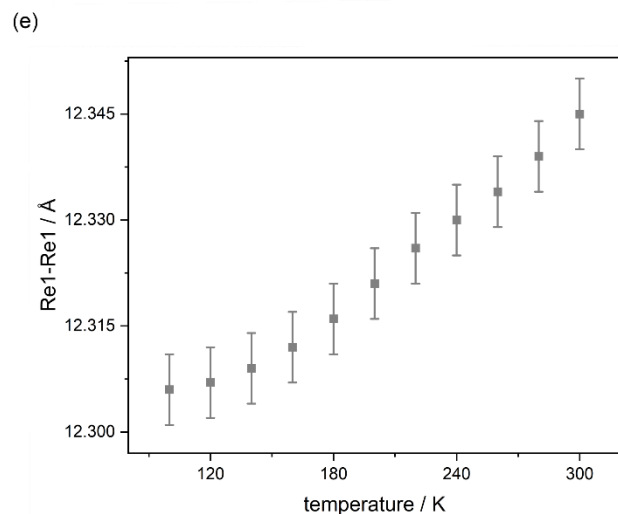
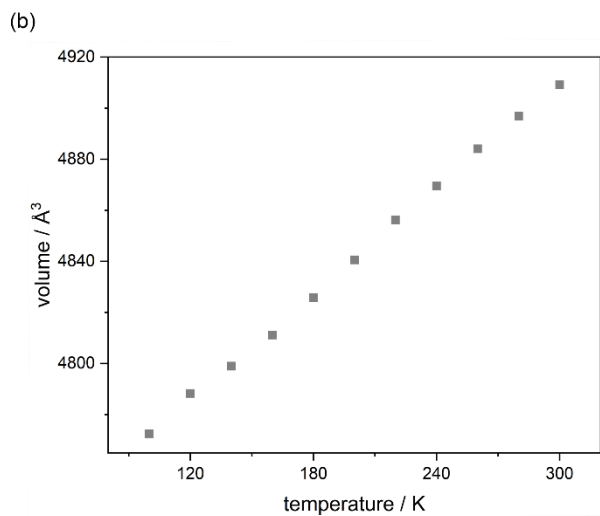
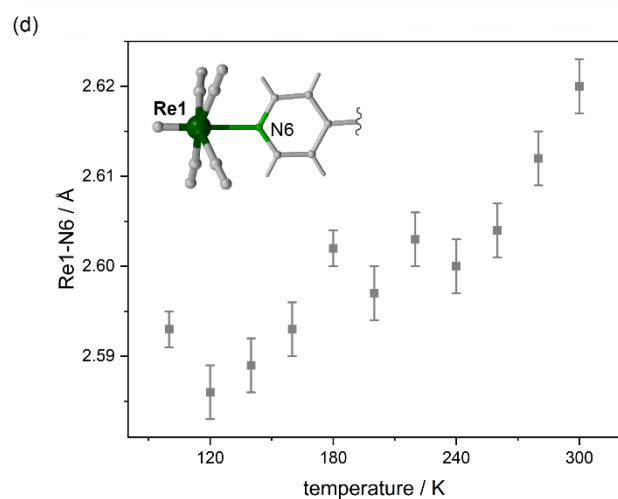
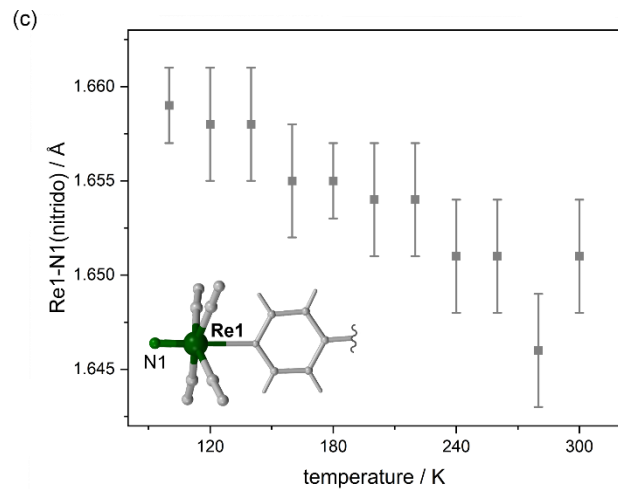
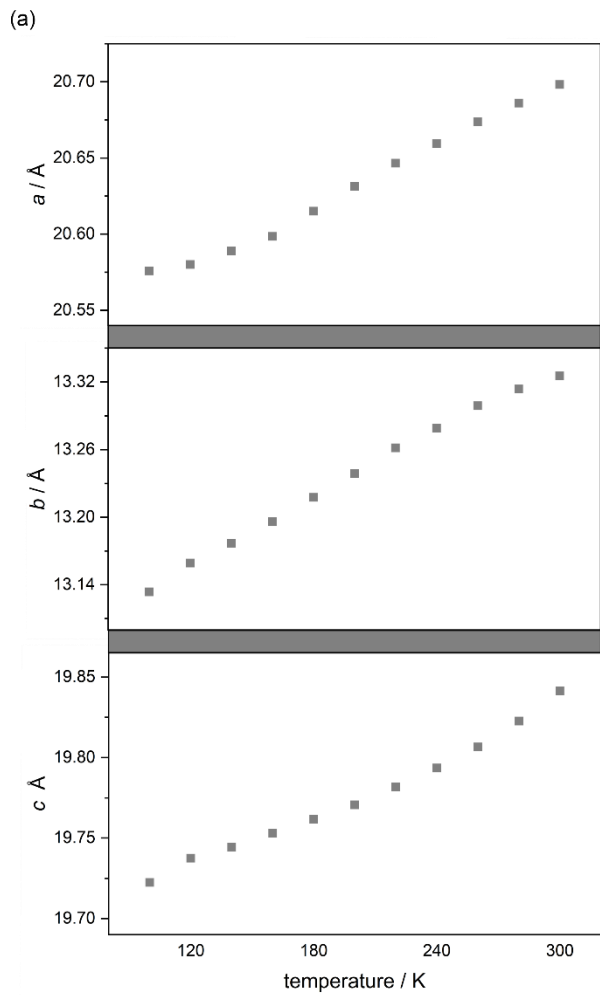


**Fig. S8** The temperature variation of unit cell parameters (a–b), as well as  $\text{Re}\equiv\text{N}(\text{nitrido})$ ,  $\text{Re1-N6}$ , and  $\text{Re1-Re1}$  bond lengths (c–e) within the bimetallic  $\{\text{Re}^{\text{V}_2}\}^{4-}$  assemblies in the crystal structure of **Re<sub>2</sub>-bpy**.

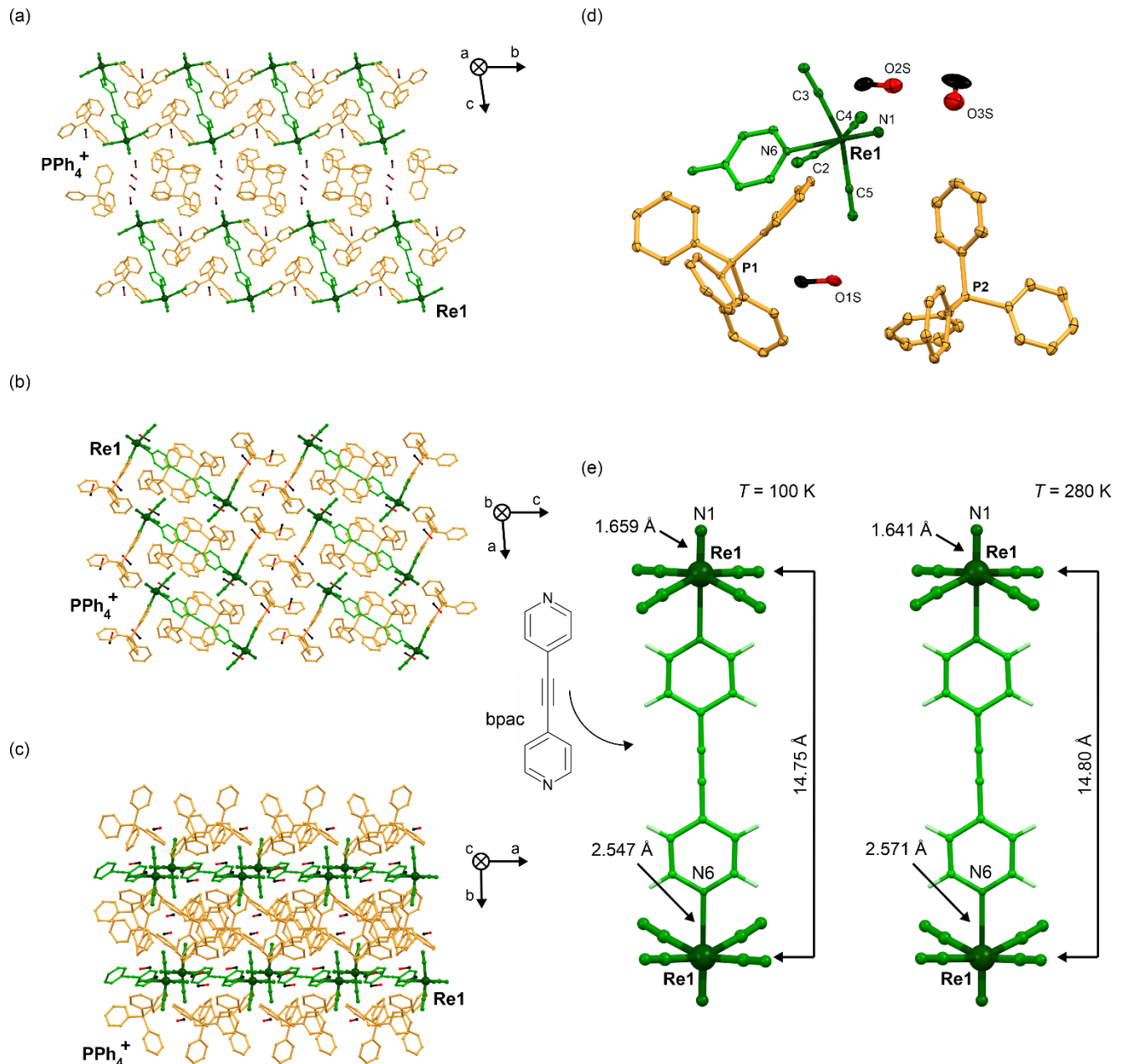


**Fig. S9** Detailed structural views of **Re<sub>2</sub>-bpac** material: the crystal structure presented along the main *a*, *b*, and *c* crystallographic axes (*a*, *b*, and *c*, respectively), the asymmetric unit with the labeling scheme for selected symmetrically independent atoms (d), and the comparison of the metric parameters of bimetallic {Re<sup>V</sup><sub>2</sub>}<sup>4-</sup> assemblies at 100(2) and 300(2) K (e). Thermal ellipsoids for the asymmetric unit in (d) are presented at the 50% probability level. Hydrogen atoms in (a-d) were omitted for clarity. Related detailed structural parameters are presented in Table S12.

**Table S12** Detailed crystal structure parameters of **Re<sub>2</sub>-bpac**.

compound	Re <sub>2</sub> -bpac					
T / K	100(2)	120(2)	140(2)	160(2)	180(2)	200(2)
Re1-C / Å	2.103(3) – 2.114(3)	2.100(3) – 2.117(3)	2.095(3) – 2.114(3)	2.093(3) – 2.112(3)	2.098(3) – 2.111(3)	2.097(3) – 2.113(3)
Re1≡N1 / Å	1.659(3)	1.659(3)	1.660(3)	1.663(3)	1.662(3)	1.655(3)
Re1-N6 / Å	2.547(2)	2.548(2)	2.550(2)	2.555(2)	2.557(2)	2.557(2)
C-Re1-C ( <i>cis</i> ) / °	85.57(11) – 90.80(10)	85.65(11) – 90.70(11)	85.66(11) – 90.60(11)	85.43(12) – 90.57(11)	85.54(12) – 90.65(12)	85.80(11) – 90.53(11)
C-Re1-C ( <i>trans</i> ) / °	159.74(11), 161.12(11)	159.65(11), 161.08(11)	159.79(11), 161.34(11)	159.97(12), 161.09(12)	159.95(12), 161.10(12)	159.98(10), 161.14(11)
N1≡Re1-C / °	99.02(12) – 101.01(12)	99.02(13) – 100.95(12)	99.23(12) – 100.98(12)	99.20(14) – 100.78(13)	99.25(15) – 100.64(13)	99.04(13) – 100.76(12)
N1≡Re1-N6 / °	177.99(11)	177.99(11)	177.92(11)	178.16(12)	178.20(12)	177.94(11)
Re1-(L)-Re1 / Å	14.751(4)	14.749(4)	14.757(5)	14.760(5)	14.773(5)	14.77(5)
T / K	220(2)	240(2)	260(2)	280(2)	–	–
Re1-C / Å	2.096(4) – 2.112(4)	2.093(3) – 2.113(3)	2.093(4) – 2.110(4)	2.089(6) – 2.119(6)	–	–
Re1≡N1 / Å	1.660(3)	1.652(3)	1.654(3)	1.641(5)	–	–
Re1-N6 / Å	2.561(2)	2.563(2)	2.565(3)	2.571(3)	–	–
C-Re1-C ( <i>cis</i> ) / °	85.66(12) – 90.49(12)	85.72(11) – 90.40(11)	85.94(14) – 90.27(14)	85.9(2) – 90.3(2)	–	–
C-Re1-C ( <i>trans</i> ) / °	159.94(12), 161.00(13)	160.02(11), 161.03(11)	160.03(14), 161.13(14)	159.94(19), 160.9(2)	–	–
N1≡Re1-C / °	99.24(14) – 100.82(14)	99.13(14) – 100.66(13)	99.22(16) – 100.74(16)	99.3(2) – 100.8(2)	–	–
N1≡Re1-N6 / °	178.20(13)	178.03(12)	178.13(15)	177.88(14)	–	–
Re1-(L)-Re1 / Å	14.770(5)	14.774(5)	14.778(6)	14.800(9)	–	–

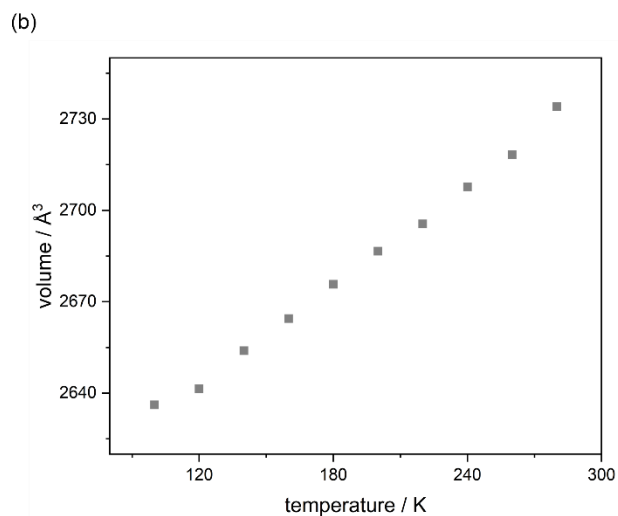
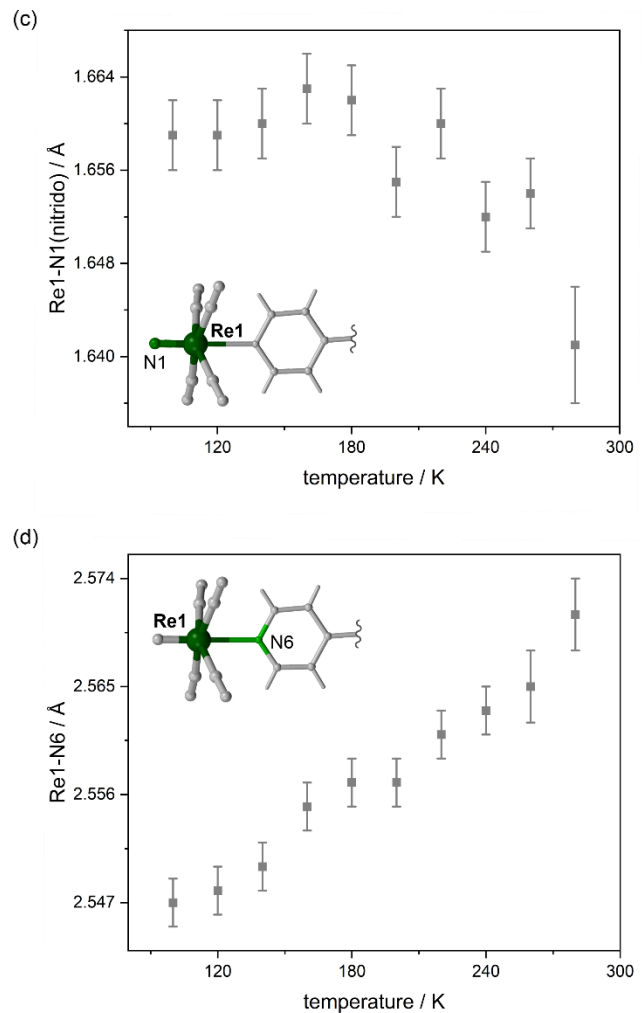
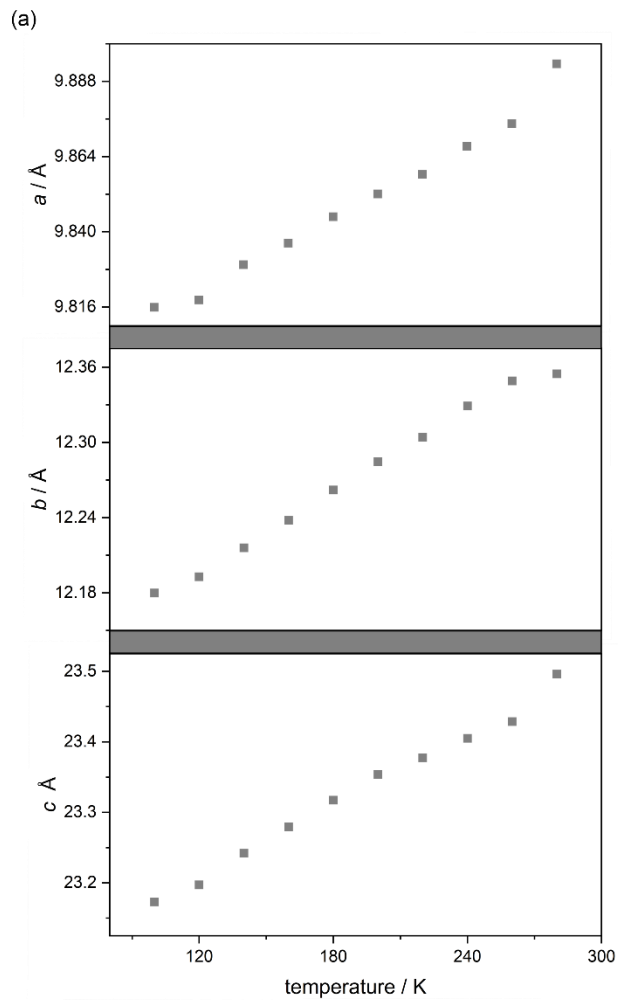


**Fig. S10** The temperature variation of unit cell parameters (a–b), as well as  $\text{Re}\equiv\text{N}(\text{nitrido})$ ,  $\text{Re1-N6}$ , and  $\text{Re1-Re1}$  bond lengths (c–e) within the bimetallic  $\{\text{Re}^{V_2}\}^{4-}$  assemblies in the crystal structure of **Re<sub>2</sub>-bpac**.

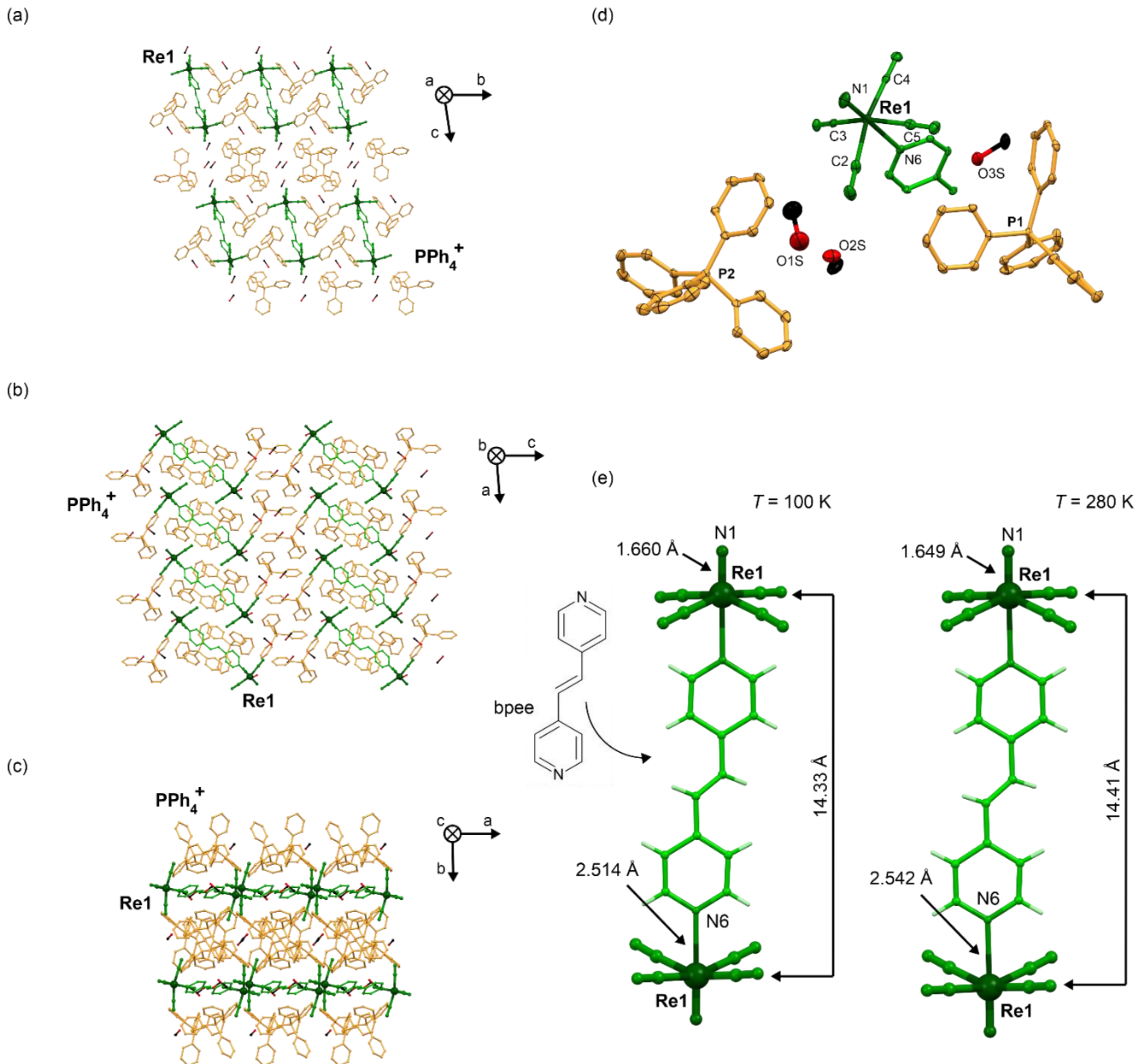


**Fig. S11** Detailed structural views of **Re<sub>2</sub>-bpee** material: the crystal structure presented along the main *a*, *b*, and *c* crystallographic axes (*a*, *b*, and *c*, respectively), the asymmetric unit with the labeling scheme for selected symmetrically independent atoms (d), and the comparison of the metric parameters of bimetallic {Re<sup>V</sup><sub>2</sub>}<sup>4-</sup> assemblies at 100(2) and 300(2) K (e). Thermal ellipsoids for the asymmetric unit in (d) are presented at the 50% probability level. Hydrogen atoms in the (a-d) parts were omitted for clarity. Related detailed structural parameters are presented in Table S13.

**Table S13** Detailed crystal structure parameters of **Re<sub>2</sub>-bpree**.

compound	Re <sub>2</sub> -bpree					
T / K	100(2)	120(2)	140(2)	160(2)	180(2)	200(2)
Re1-C / Å	2.096(5) – 2.109(5)	2.100(5) – 2.108(5)	2.096(5) – 2.120(5)	2.097(6) – 2.113(5)	2.095(6) – 2.116(6)	2.089(6) – 2.118(6)
Re1≡N1 / Å	1.660(4)	1.663(4)	1.660(4)	1.656(4)	1.658(4)	1.649(4)
Re1-N6 / Å	2.514(3)	2.522(3)	2.526(3)	2.521(4)	2.527(4)	2.533(4)
C-Re1-C ( <i>cis</i> ) / °	87.09(17) – 89.66(18)	87.27(17) – 89.78(18)	87.74(18) – 89.08(18)	87.36(18) – 89.74(19)	87.6(2) – 89.6(2)	87.46(19) – 89.4(2)
C-Re1-C ( <i>trans</i> ) / °	159.00(16), 163.01(17)	159.13(16), 163.24(17)	159.43(17), 163.29(17)	159.08(17), 163.04(18)	159.61(17), 163.35(18)	159.13(18), 162.95(19)
N1≡Re1-C / °	98.3(2) – 100.67(19)	98.1(2) – 100.47(18)	98.1(2) – 100.40(19)	98.3(2) – 100.71(19)	98.1(2) – 100.3(2)	98.2(2) – 100.6(2)
N1≡Re1-N6 / °	178.88(18)	178.56(17)	178.49(18)	178.51(18)	178.43(19)	178.4(2)
Re1-(L)-Re1 / Å	14.334(4)	14.344(4)	14.362(5)	14.365(5)	14.365(5)	14.377(5)
T / K	220(2)	240(2)	260(2)	280(2)	–	–
Re1-C / Å	2.090(7) – 2.129(6)	2.085(7) – 2.113(6)	2.096(6) – 2.107(6)	2.093(5) – 2.119(6)	–	–
Re1≡N1 / Å	1.650(5)	1.649(5)	1.647(5)	1.649(4)	–	–
Re1-N6 / Å	2.538(4)	2.542(4)	2.545(4)	2.542(3)	–	–
C-Re1-C ( <i>cis</i> ) / °	87.6(2) – 89.6(2)	87.3(2) – 89.6(2)	87.4(2) – 89.6(2)	87.6(2) – 89.6(2)	–	–
C-Re1-C ( <i>trans</i> ) / °	159.63(19), 163.1(2)	159.7(2), 162.8(2)	159.8(2), 162.9(2)	159.59(18), 162.83(19)	–	–
N1≡Re1-C / °	98.1(3) – 100.2(2)	98.3(3) – 100.3(2)	98.4(3) – 100.4(2)	98.4(2) – 100.4(2)	–	–
N1≡Re1-N6 / °	178.3(2)	178.2(2)	178.4(2)	178.6(2)	–	–
Re1-(L)-Re1 / Å	14.391(5)	14.392(5)	14.399(6)	14.408(9)	–	–

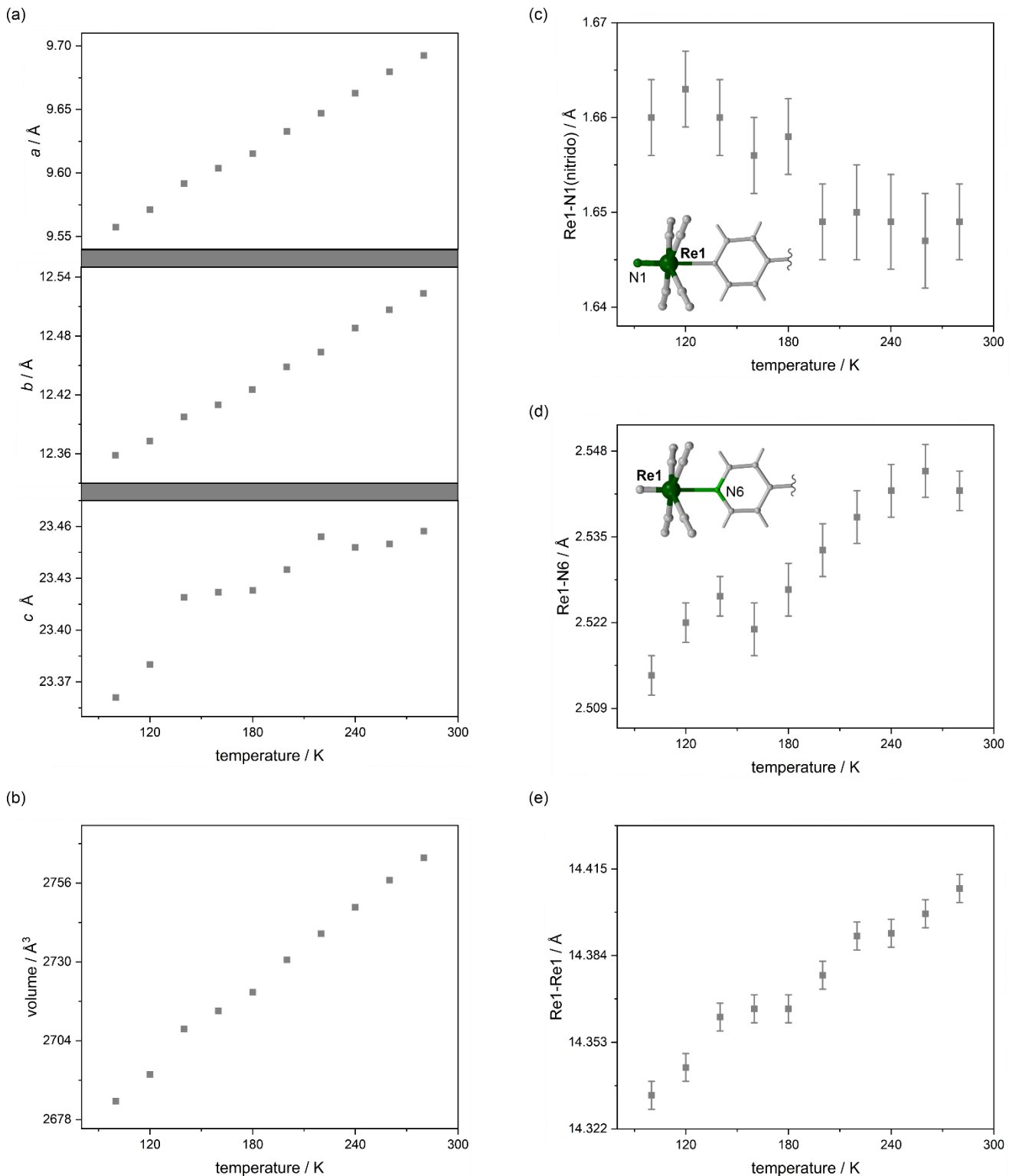


**Fig. S12** The temperature variation of unit cell parameters (a–b), as well as  $\text{Re}\equiv\text{N}(\text{nitrido})$ ,  $\text{Re1-N6}$ , and  $\text{Re1-Re1}$  bond lengths (c–e) within bimetallic  $\{\text{Re}^{V_2}\}^{4-}$  assemblies in the crystal structure of **Re<sub>2</sub>-bppe**.

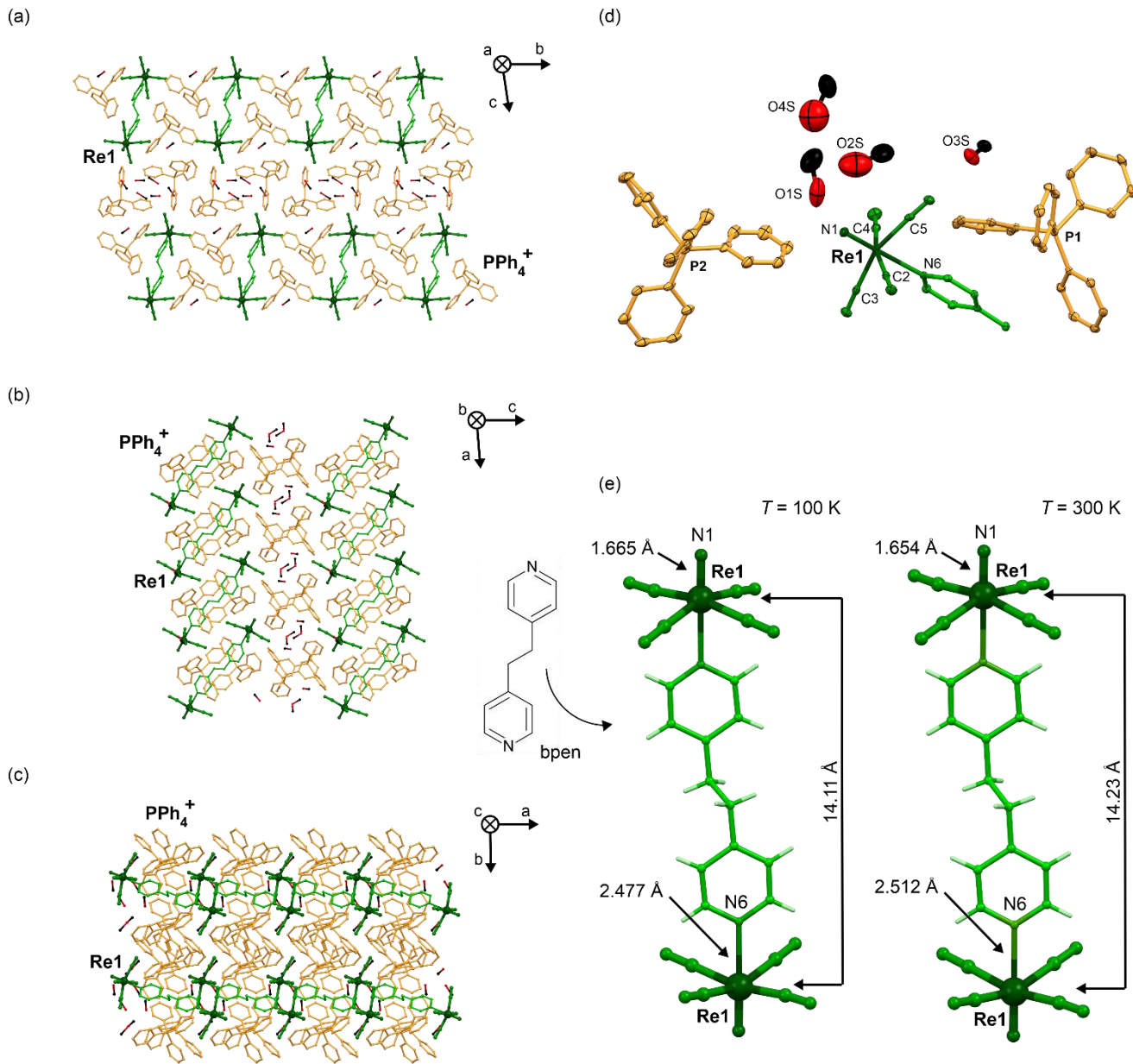


**Fig. S13** Detailed structural views of **Re<sub>2</sub>-bpen** material: the crystal structure presented along the main *a*, *b*, and *c* crystallographic axes (*a*, *b*, and *c*, respectively), the asymmetric unit with the labeling scheme for selected symmetrically independent atoms (d), and the comparison of the metric parameters of bimetallic {Re<sup>V</sup><sub>2</sub>}<sup>4-</sup> assemblies at 100(2) and 300(2) K (e). Thermal ellipsoids for the asymmetric unit in (d) are presented at the 50% probability level. Hydrogen atoms in the (a-d) parts were omitted for clarity. Related detailed structural parameters are presented in Table S14.

**Table S14** Detailed crystal structure parameters of **Re<sub>2</sub>-bpen**.

compound	Re <sub>2</sub> -bpen					
T / K	100(2)	120(2)	140(2)	160(2)	180(2)	200(2)
Re1-C / Å	2.097(3) – 2.121(3)	2.099(3) – 2.119(3)	2.098(3) – 2.120(3)	2.099(3) – 2.118(3)	2.104(3) – 2.118(3)	2.097(3) – 2.118(4)
Re1≡N1 / Å	1.665(2)	1.665(2)	1.663(3)	1.664(3)	1.662(3)	1.661(3)
Re1-N6 / Å	2.477(2)	2.481(2)	2.483(2)	2.485(2)	2.488(2)	2.495(2)
C-Re1-C ( <i>cis</i> ) / °	87.41(11) – 90.15(11)	87.42(11) – 89.99(11)	87.39(11) – 90.12(12)	87.52(12) – 90.07(12)	87.45(12) – 90.18(13)	87.70(13) – 89.92(13)
C-Re1-C ( <i>trans</i> ) / °	159.67(11), 166.21(11)	159.67(11), 166.04(11)	159.80(12), 166.12(11)	159.77(12), 166.05(12)	159.79(12), 165.88(12)	159.89(13), 165.85(12)
N1≡Re1-C / °	95.97(11) – 100.50(12)	96.23(12) – 100.47(12)	96.23(12) – 100.48(13)	96.20(13) – 100.40(13)	96.22(13) – 100.31(13)	96.22(13) – 100.01(14)
N1≡Re1-N6 / °	179.09(10)	179.12(11)	179.02(11)	179.14(12)	179.28(12)	179.33(13)
Re1-(L)-Re1 / Å	14.113(4)	14.120(4)	14.130(4)	14.141(4)	14.150(4)	14.163(4)
T / K	220(2)	240(2)	260(2)	280(2)	300(2)	–
Re1-C / Å	2.100(3) – 2.114(4)	2.102(4) – 2.116(4)	2.102(4) – 2.122(4)	2.097(4) – 2.116(4)	2.104(5) – 2.119(5)	–
Re1≡N1 / Å	1.658(3)	1.655(3)	1.660(3)	1.659(3)	1.654(3)	–
Re1-N6 / Å	2.498(2)	2.499(2)	2.504(3)	2.505(3)	2.512(3)	–
C-Re1-C ( <i>cis</i> ) / °	87.46(13) – 90.02(14)	87.41(13) – 90.07(14)	87.59(14) – 90.04(15)	87.65(15) – 89.85(16)	88.67(17) – 89.85(18)	–
C-Re1-C ( <i>trans</i> ) / °	159.94(13), 165.52(12)	159.85(13), 165.27(13)	159.88(14), 165.31(14)	159.95(15), 165.15(14)	159.74(16), 165.28(15)	–
N1≡Re1-C / °	96.30(14) – 100.05(14)	96.52(14) – 100.04(14)	96.66(15) – 100.10(16)	96.81(16) – 100.19(17)	96.43(17) – 100.26(17)	–
N1≡Re1-N6 / °	179.48(13)	179.44(13)	179.56(15)	179.34(15)	179.55(16)	–
Re1-(L)-Re1 / Å	14.175(4)	14.185(4)	14.199(4)	14.206(4)	14.229(4)	–

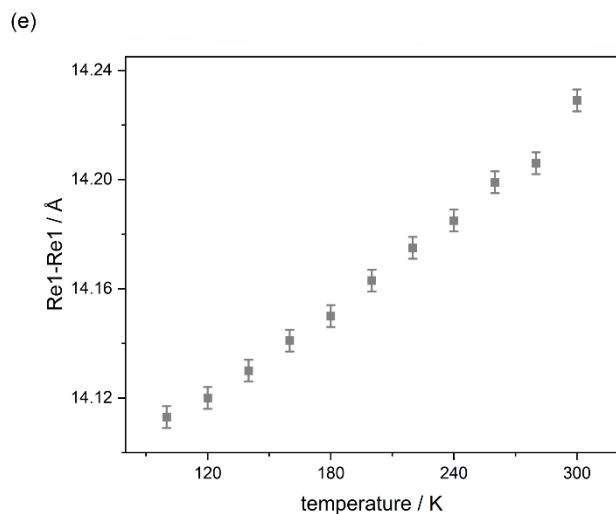
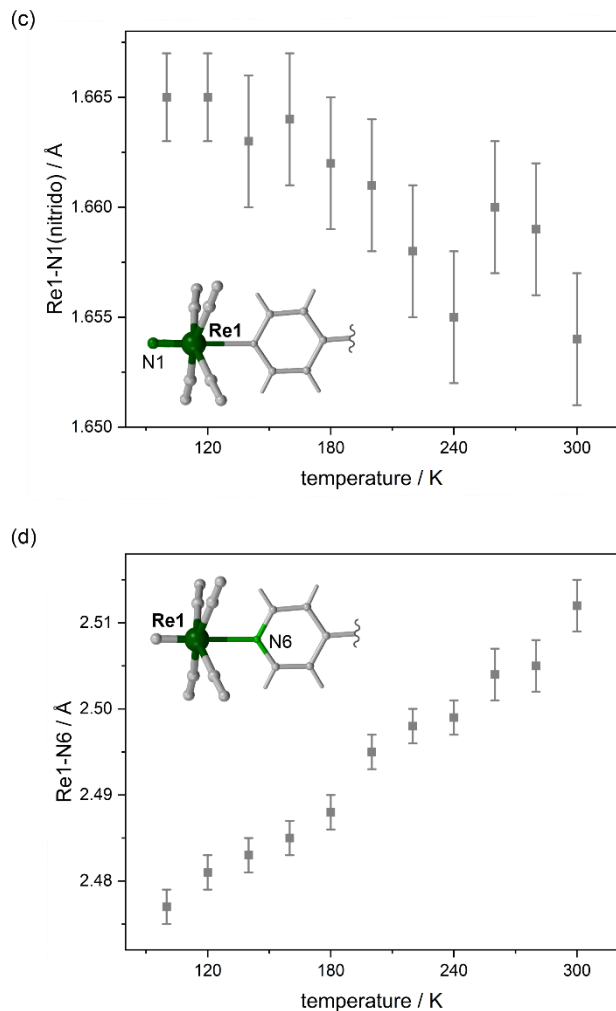
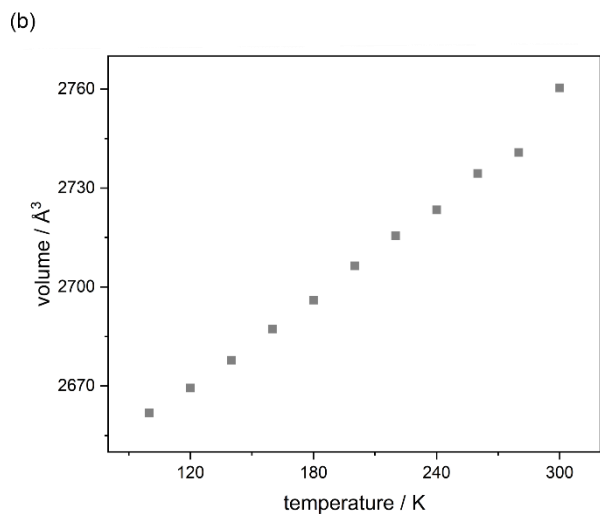
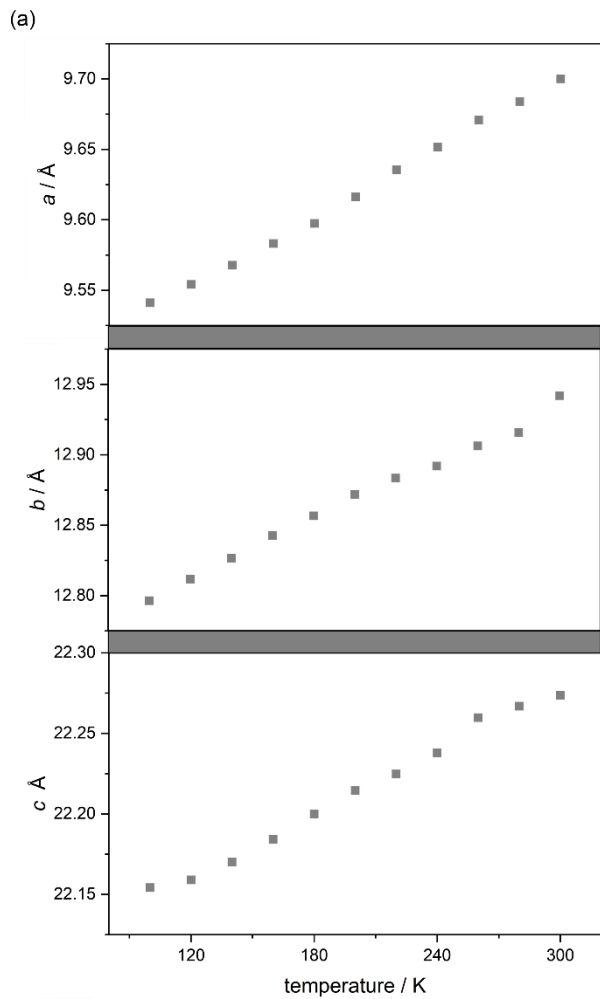


**Fig. S14** The temperature variation of unit cell parameters (a–b), as well as  $\text{Re}\equiv\text{N}(\text{nitrido})$ ,  $\text{Re1-N6}$ , and  $\text{Re1-Re1}$  bond lengths (c–e) within the bimetallic  $\{\text{Re}^{\text{V}_2}\}^{4-}$  assemblies in the crystal structure of **Re<sub>2</sub>-bpen**.

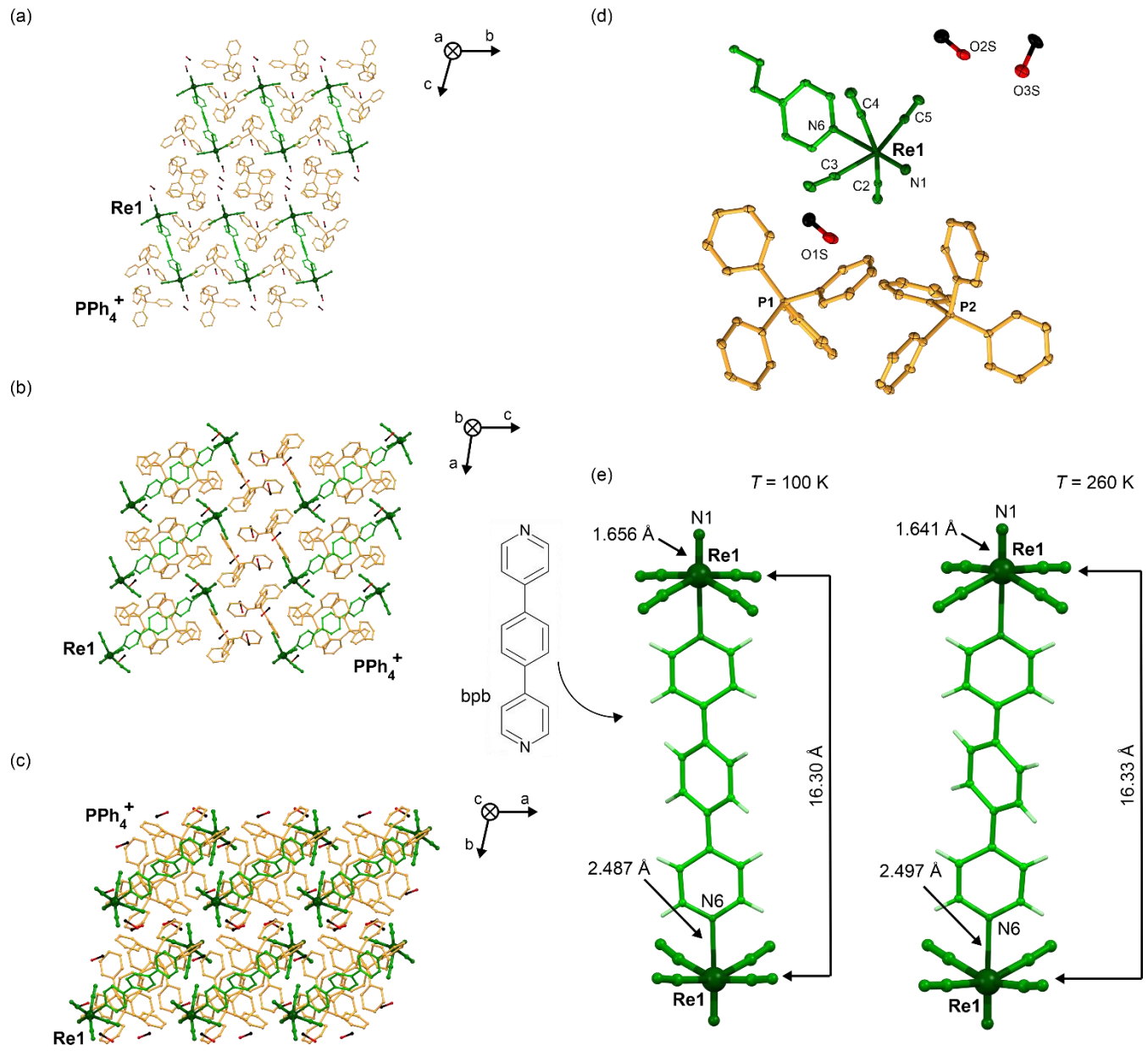


**Fig. S15** Detailed structural views of **Re<sub>2</sub>-bpb** material: the crystal structure presented along the main *a*, *b*, and *c* crystallographic axes (*a*, *b*, and *c*, respectively), the asymmetric unit with the labeling scheme for selected symmetrically independent atoms (d), and the comparison of the metric parameters of bimetallic {Re<sup>V</sup><sub>2</sub>}<sup>4-</sup> assemblies at 100(2) and 300(2) K (e). Thermal ellipsoids for the asymmetric unit in (d) are presented at the 50% probability level. Hydrogen atoms in the (a-d) parts were omitted for clarity. Related detailed structural parameters are presented in Table S15.

**Table S15** Detailed crystal structure parameters of **Re<sub>2</sub>-bpb**.

compound	Re <sub>2</sub> -bpb					
T / K	100(2)	120(2)	140(2)	160(2)	180(2)	200(2)
Re1-C / Å	2.101(3) – 2.111(3)	2.101(3) – 2.115(2)	2.104(3) – 2.113(3)	2.099(4) – 2.113(4)	2.097(4) – 2.110(4)	2.100(3) – 2.112(3)
Re1≡N1 / Å	1.656(3)	1.660(2)	1.659(2)	1.657(3)	1.656(3)	1.657(3)
Re1-N6 / Å	2.487(2)	2.4891(19)	2.4912(19)	2.491(2)	2.494(2)	2.497(2)
C-Re1-C ( <i>cis</i> ) / °	84.32(11) – 90.84(11)	84.43(9) – 90.77(9)	84.44(9) – 90.71(9)	84.53(13) – 90.80(13)	84.70(13) – 90.85(13)	84.93(11) – 90.58(11)
C-Re1-C ( <i>trans</i> ) / °	158.01(11), 158.51(11)	158.00(9), 158.46(9)	157.97(10), 158.60(9)	158.30(13), 158.61(12)	158.31(13), 158.74(13)	158.37(12), 158.80(11)
N1≡Re1-C / °	99.86(12) – 101.69(12)	99.88(10) – 101.65(10)	99.79(10) – 101.49(11)	99.83(14) – 101.62(14)	99.72(15) – 101.54(15)	99.77(13) – 101.43(13)
N1≡Re1-N6 / °	177.57(11)	177.53(8)	177.53(9)	177.60(13)	177.60(14)	177.56(11)
Re1-(L)-Re1 / Å	16.299(5)	16.303(3)	16.311(3)	16.307(5)	16.311(5)	16.316(5)
T / K	220(2)	240(2)	260(2)	–	–	–
Re1-C / Å	2.092(4) – 2.110(4)	2.100(5) – 2.113(4)	2.095(5) – 2.106(5)	–	–	–
Re1≡N1 / Å	1.648(3)	1.650(4)	1.641(4)	–	–	–
Re1-N6 / Å	2.497(3)	2.498(3)	2.497(3)	–	–	–
C-Re1-C ( <i>cis</i> ) / °	84.72(14) – 90.72(14)	85.00(15) – 90.70(15)	85.45(17) – 90.58(18)	–	–	–
C-Re1-C ( <i>trans</i> ) / °	158.61(15), 158.95(14)	158.65(16), 159.29(15)	158.69(19), 159.68(17)	–	–	–
N1≡Re1-C / °	99.68(18) – 101.61(17)	99.5(2) – 101.70(19)	99.0(2) – 102.1(2)	–	–	–
N1≡Re1-N6 / °	177.55(15)	177.50(16)	177.20(19)	–	–	–
Re1-(L)-Re1 / Å	16.315(6)	16.321(6)	16.325(7)	–	–	–

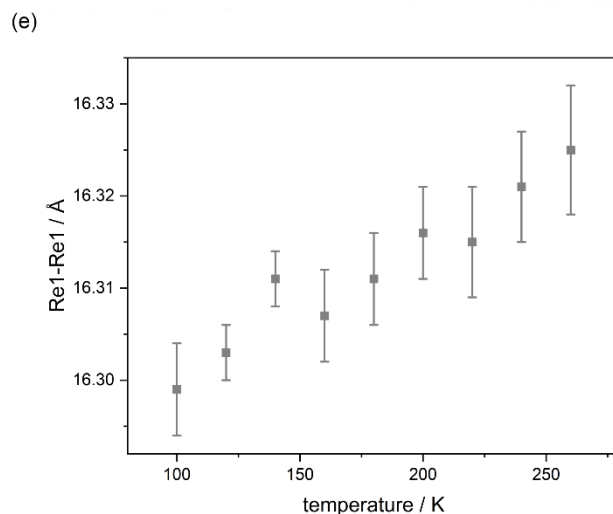
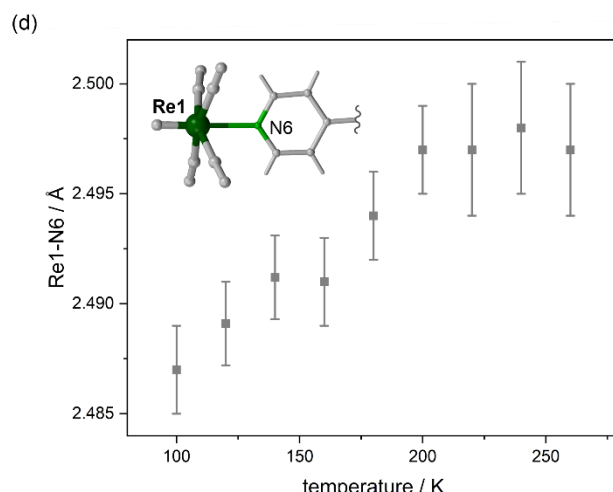
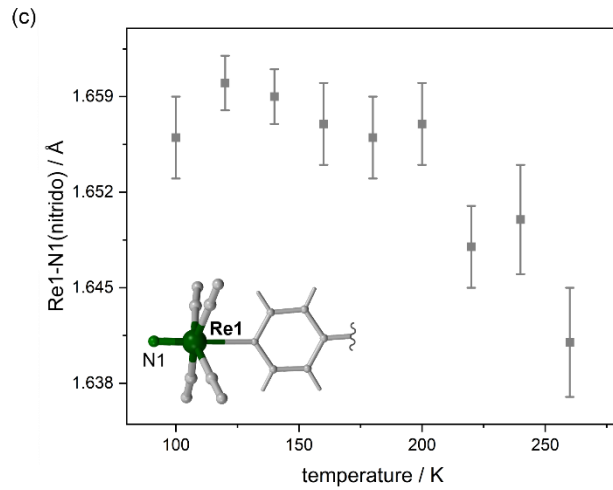
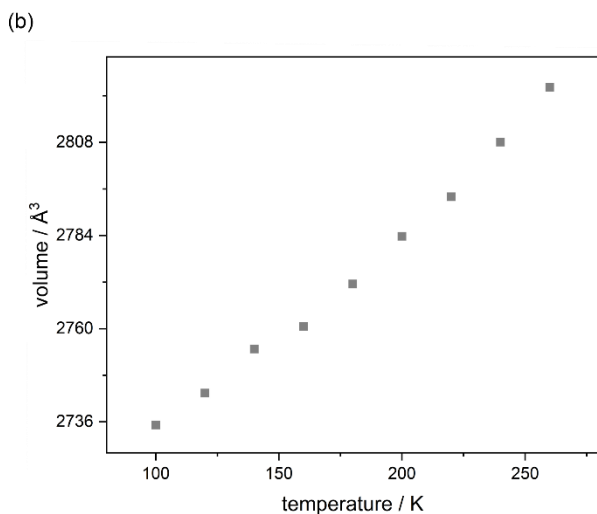
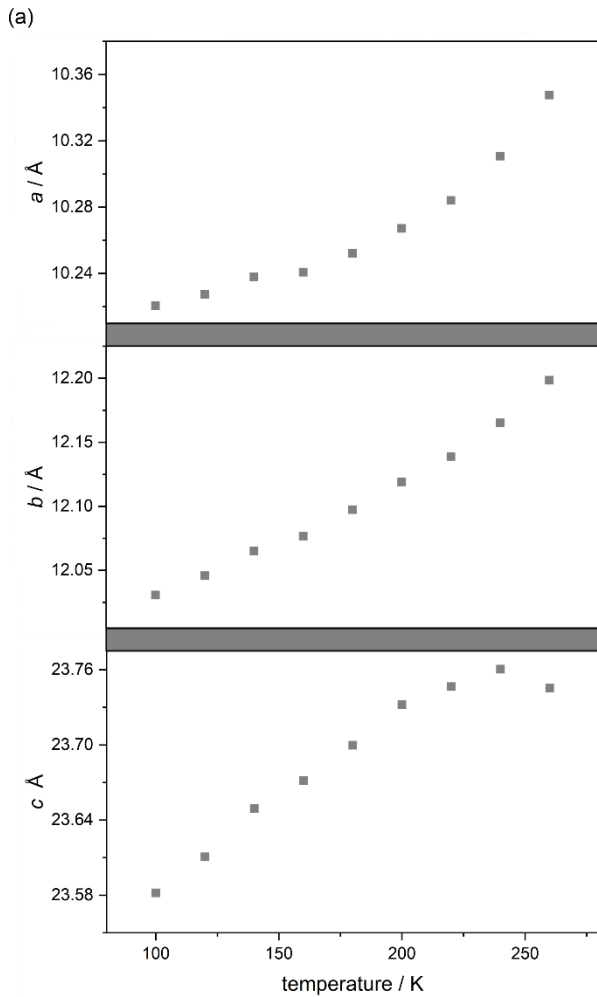


**Fig. S16** The temperature variation of unit cell parameters (a–b), as well as  $\text{Re}\equiv\text{N}(\text{nitrido})$ ,  $\text{Re1-N6}$ , and  $\text{Re1-Re1}$  bond lengths (c–e) within bimetallic  $\{\text{Re}^{V_2}\}^{4-}$  assemblies in the crystal structure of **Re<sub>2</sub>-bpb**.

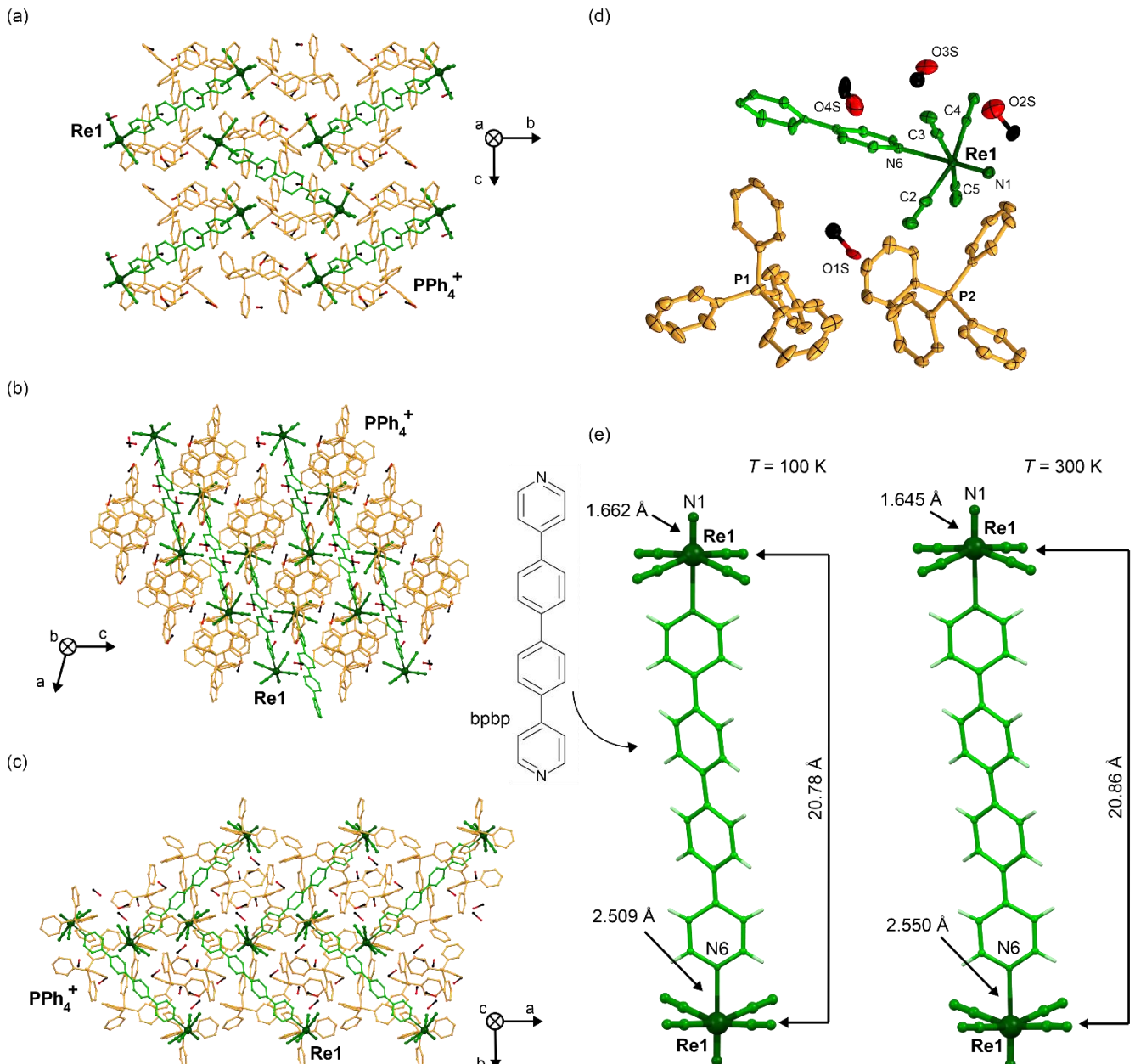


**Fig. S17** Detailed structural views of **Re<sub>2</sub>-bpyp** material: the crystal structure presented along the main *a*, *b*, and *c* crystallographic axes (*a*, *b*, and *c*, respectively), the asymmetric unit with the labeling scheme for selected symmetrically independent atoms (d), and the comparison of the metric parameters of bimetallic {Re<sup>V<sub>2</sub></sup>}<sup>4-</sup> assemblies at 100(2) and 300(2) K (e). Thermal ellipsoids for the asymmetric unit in (d) are presented at the 50% probability level. Hydrogen atoms in the (a-d) parts were omitted for clarity. Related detailed structural parameters are presented in Table S16.

**Table S16** Detailed crystal structure parameters of **Re<sub>2</sub>-bpbp**.

compound	Re <sub>2</sub> -bpbp					
T / K	100(2)	120(2)	140(2)	160(2)	180(2)	200(2)
Re1-C / Å	2.098(5) – 2.112(5)	2.102(4) – 2.113(4)	2.096(5) – 2.110(5)	2.102(5) – 2.111(5)	2.102(5) – 2.109(5)	2.099(5) – 2.109(5)
Re1≡N1 / Å	1.662(4)	1.658(3)	1.659(4)	1.657(4)	1.658(4)	1.654(4)
Re1-N6 / Å	2.509(3)	2.512(3)	2.515(3)	2.523(3)	2.524(3)	2.527(3)
C-Re1-C ( <i>cis</i> ) / °	86.33(17) – 90.96(18)	86.59(16) – 91.01(17)	86.65(17) – 91.09(18)	86.45(17) – 91.03(18)	86.54(17) – 91.07(18)	87.05(18) – 90.96(18)
C-Re1-C ( <i>trans</i> ) / °	161.47(17), 162.32(17)	161.53(16), 162.43(16)	161.47(17), 162.31(17)	161.46(17), 162.52(17)	161.62(17), 162.51(17)	161.69(17), 162.79(17)
N1≡Re1-C / °	98.27(18) – 99.36(18)	98.18(17) – 99.36(17)	98.32(18) – 99.34(18)	98.11(18) – 99.46(18)	97.97(18) – 99.48(18)	97.84(18) – 99.35(18)
N1≡Re1-N6 / °	179.10(16)	178.84(15)	178.78(15)	179.06(15)	178.99(16)	178.65(16)
Re1-(L)-Re1 / Å	20.776(8)	20.781(8)	20.786(8)	20.793(8)	20.800(8)	20.808(8)
T / K	220(2)	240(2)	260(2)	280(2)	300(2)	–
Re1-C / Å	2.098(5) – 2.112(5)	2.101(5) – 2.115(5)	2.098(6) – 2.112(6)	2.097(6) – 2.118(6)	2.098(7) – 2.116(8)	–
Re1≡N1 / Å	1.650(4)	1.656(4)	1.653(4)	1.651(4)	1.646(5)	–
Re1-N6 / Å	2.527(3)	2.530(3)	2.536(3)	2.547(4)	2.550(4)	–
C-Re1-C ( <i>cis</i> ) / °	87.08(19) – 91.02(19)	87.0(2) – 91.0(2)	86.8(2) – 91.0(2)	86.8(2) – 91.0(2)	86.5(2) – 90.9(3)	–
C-Re1-C ( <i>trans</i> ) / °	161.56(17), 162.75(17)	161.73(18), 162.70(18)	161.72(19), 162.73(19)	161.7(2), 163.0(2)	161.7(2), 162.9(2)	–
N1≡Re1-C / °	98.14(19) – 99.16(19)	98.0(2) – 99.3(2)	97.9(2) – 99.4(2)	98.1(2) – 99.2(2)	97.6(3) – 99.5(3)	–
N1≡Re1-N6 / °	178.63(16)	178.65(17)	178.13(17)	178.32(18)	177.9(2)	–
Re1-(L)-Re1 / Å	20.815(9)	20.826(9)	20.834(9)	20.847(9)	20.857(12)	–

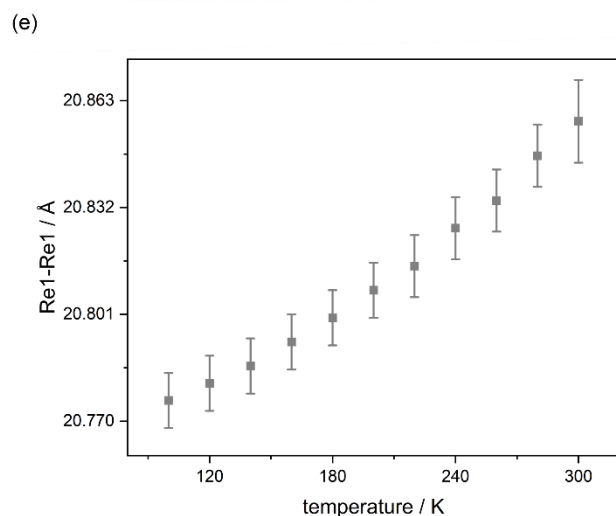
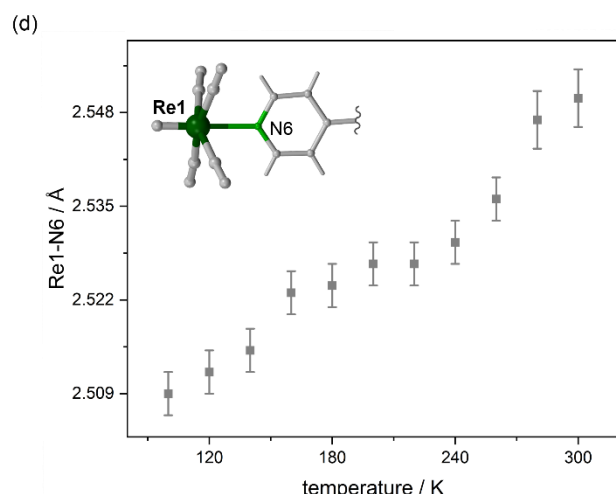
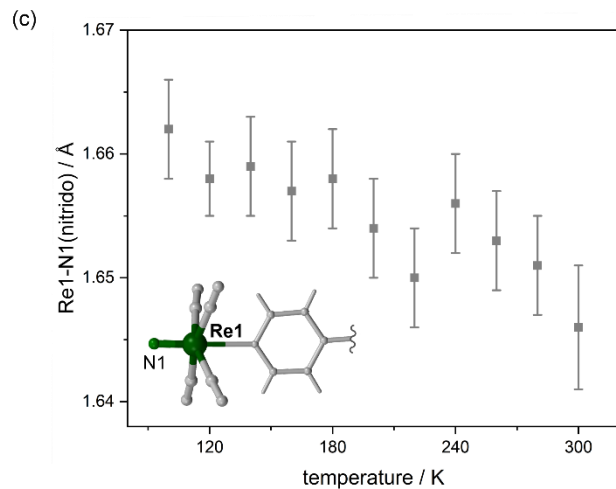
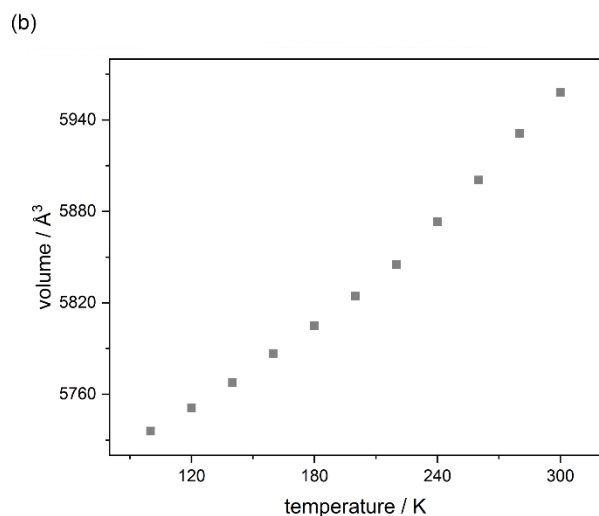
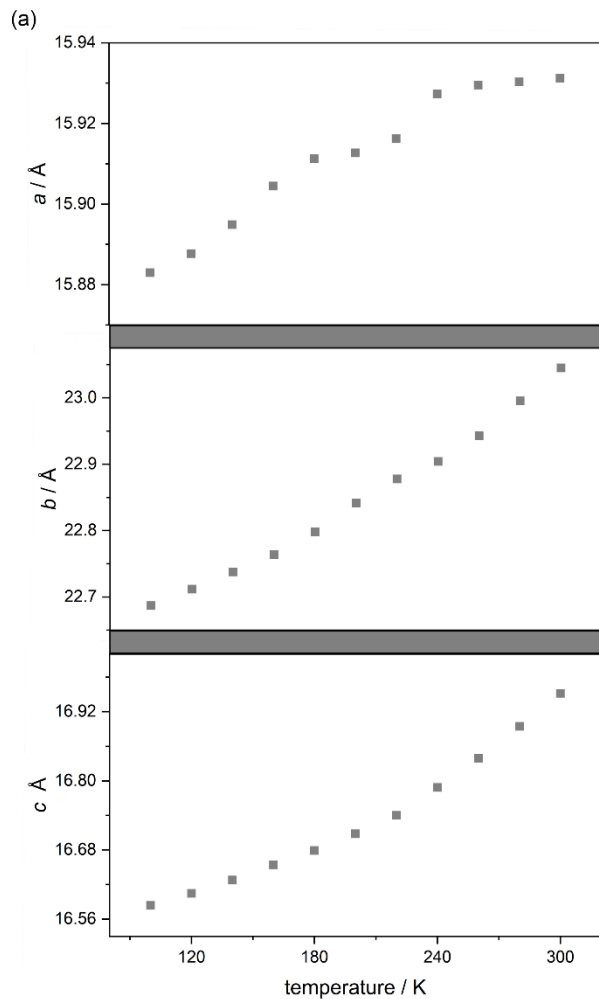


**Fig. S18** The temperature variation of unit cell parameters (a–b), as well as  $\text{Re}\equiv\text{N}(\text{nitrido})$ ,  $\text{Re1-N6}$ , and  $\text{Re1-Re1}$  bond lengths (c–e) within bimetallic  $\{\text{Re}^{V_2}\}^{4-}$  assemblies in the crystal structure of **Re<sub>2</sub>-bpbp**.

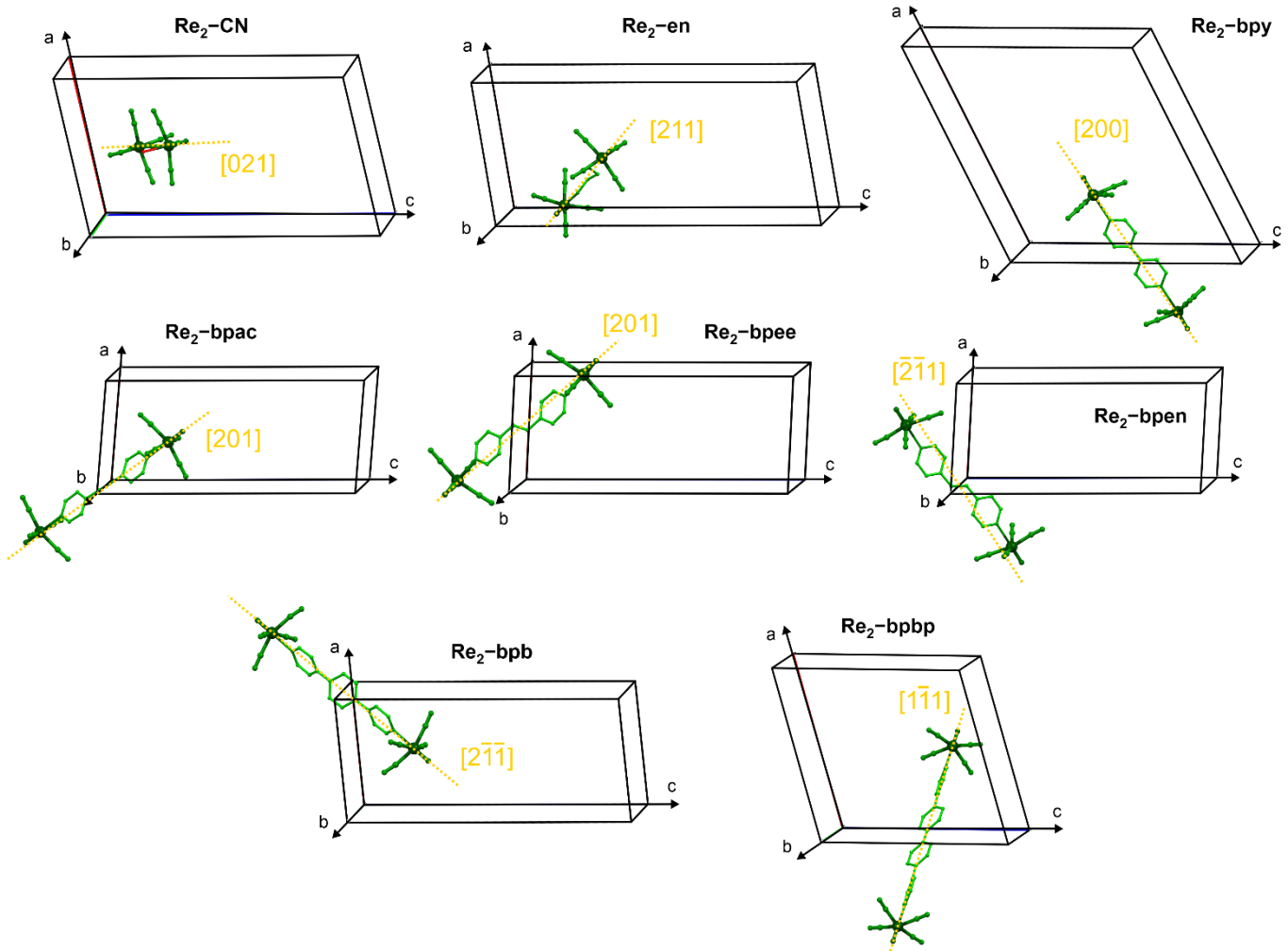


**Fig. S19** Orientation of dinuclear  $\{Re^{V_2}\}^{4-}$  molecular anions in the unit cell of the indicated crystal structures of **Re<sub>2</sub>-CN**, **Re<sub>2</sub>-en**, **Re<sub>2</sub>-bpy**, **Re<sub>2</sub>-bpac**, **Re<sub>2</sub>-bpee**, **Re<sub>2</sub>-bpen**, **Re<sub>2</sub>-bpb**, and **Re<sub>2</sub>-bpbp** materials. The crystallographic directions corresponding to the axis given by the Re-Re connection within the  $\{Re^{V_2}\}^{4-}$  molecular anions were presented in the figure.

**Table S17** Results of Continuous Shape Measure analysis for rhenium(V) complexes in **Re<sub>2</sub>-CN**.<sup>a</sup>

T / K	Continuous Shape Measure parameters for [Re <sup>1V</sup> (CN) <sub>4</sub> (N)(H <sub>2</sub> O)] <sup>2-</sup> complexes in <b>Re<sub>2</sub>-CN</b>		
	PPY-6	OC-6	TPR-6
100(2)	28.854	<b>0.471</b>	15.507
120(2)	28.828	<b>0.470</b>	15.534
140(2)	28.742	<b>0.467</b>	15.441
160(2)	28.793	<b>0.468</b>	15.528
180(2)	28.780	<b>0.466</b>	15.557
200(2)	28.826	<b>0.461</b>	15.612
220(2)	28.807	<b>0.465</b>	15.713
240(2)	28.885	<b>0.462</b>	15.700
260(2)	28.827	<b>0.475</b>	15.649
280(2)	28.893	<b>0.490</b>	15.728
300(2)	29.244	<b>0.506</b>	16.037
T / K	Continuous Shape Measure parameters for [Re <sup>2V</sup> (CN) <sub>4</sub> (N)(μ-NC)] <sup>2-</sup> complexes in <b>Re<sub>2</sub>-CN</b>		
	PPY-6	OC-6	TPR-6
100(2)	28.391	<b>0.510</b>	15.281
120(2)	28.501	<b>0.507</b>	15.304
140(2)	28.336	<b>0.514</b>	15.327
160(2)	28.481	<b>0.508</b>	15.261
180(2)	28.654	<b>0.506</b>	15.262
200(2)	28.728	<b>0.508</b>	15.339
220(2)	28.677	<b>0.493</b>	15.416
240(2)	28.694	<b>0.480</b>	15.507
260(2)	28.693	<b>0.501</b>	15.467
280(2)	28.829	<b>0.487</b>	15.558
300(2)	28.822	<b>0.491</b>	15.830

<sup>a</sup>For details see the comment below Fig. S20.

**Table S18** Results of Continuous Shape Measure analysis for rhenium(V) complexes in **Re<sub>2</sub>-en**.<sup>a</sup>

T / K	Continuous Shape Measure parameters for [Re <sup>V</sup> (CN) <sub>4</sub> (N)(en)] <sup>2-</sup> complexes in <b>Re<sub>2</sub>-en</b>		
	PPY-6	OC-6	TPR-6
100(2)	29.059	<b>0.591</b>	16.218
120(2)	29.064	<b>0.592</b>	16.186
140(2)	29.045	<b>0.590</b>	16.178
160(2)	29.031	<b>0.589</b>	16.192
180(2)	29.053	<b>0.590</b>	16.165
200(2)	28.99	<b>0.593</b>	16.199
220(2)	28.993	<b>0.592</b>	16.121
240(2)	29.088	<b>0.594</b>	16.232
260(2)	29.077	<b>0.596</b>	16.215
280(2)	29.038	<b>0.597</b>	16.251
300(2)	29.041	<b>0.598</b>	16.249
T / K	Continuous Shape Measure parameters for [Re <sup>V</sup> (CN) <sub>4</sub> (N)(en)] <sup>2-</sup> complexes in <b>Re<sub>2</sub>-en</b>		
	PPY-6	OC-6	TPR-6
100(2)	28.841	<b>0.578</b>	15.582
120(2)	28.833	<b>0.579</b>	15.601
140(2)	28.884	<b>0.580</b>	15.534
160(2)	28.868	<b>0.580</b>	15.551
180(2)	28.924	<b>0.579</b>	15.55
200(2)	28.929	<b>0.580</b>	15.589
220(2)	28.989	<b>0.579</b>	15.542
240(2)	28.947	<b>0.577</b>	15.561
260(2)	29.032	<b>0.576</b>	15.554
280(2)	29.054	<b>0.576</b>	15.575
300(2)	29.049	<b>0.575</b>	15.573

<sup>a</sup>For details see the comment below Fig. S20.

**Table S19** Results of Continuous Shape Measure analysis for rhenium(V) complexes in **Re<sub>2</sub>-bpy**.<sup>a</sup>

T / K	Continuous Shape Measure parameters for [Re <sup>V</sup> (CN) <sub>4</sub> (N)(bpy)] <sup>2-</sup> complexes in <b>Re<sub>2</sub>-bpy</b>		
	PPY-6	OC-6	TPR-6
100(2)	29.025	<b>0.620</b>	16.201
120(2)	29.059	<b>0.616</b>	16.158
140(2)	29.103	<b>0.617</b>	16.204
160(2)	29.064	<b>0.629</b>	16.171
180(2)	29.117	<b>0.639</b>	16.196
200(2)	29.124	<b>0.635</b>	16.133
220(2)	29.111	<b>0.645</b>	16.130
240(2)	29.212	<b>0.642</b>	16.206
260(2)	29.231	<b>0.650</b>	16.169
280(2)	29.245	<b>0.663</b>	16.223
300(2)	29.270	<b>0.673</b>	16.254

<sup>a</sup>For details see the comment below Fig. S20.

**Table S20** Results of Continuous Shape Measure analysis for rhenium(V) complexes in **Re<sub>2</sub>-bpac**.<sup>a</sup>

T / K	Continuous Shape Measure parameters for [Re <sup>V</sup> (CN) <sub>4</sub> (N)(bpac)] <sup>2-</sup> complexes in <b>Re<sub>2</sub>-bpac</b>		
	PPY-6	OC-6	TPR-6
100(2)	29.281	<b>0.568</b>	16.551
120(2)	29.348	<b>0.570</b>	16.574
140(2)	29.366	<b>0.568</b>	16.507
160(2)	29.366	<b>0.571</b>	16.574
180(2)	29.411	<b>0.573</b>	16.603
200(2)	29.403	<b>0.576</b>	16.582
220(2)	29.378	<b>0.579</b>	16.618
240(2)	29.456	<b>0.586</b>	16.634
260(2)	29.402	<b>0.582</b>	16.656
280(2)	29.424	<b>0.605</b>	16.685

<sup>a</sup>For details see the comment below Fig. S20.

**Table S21** Results of Continuous Shape Measure analysis for rhenium(V) complexes in **Re<sub>2</sub>-bpee**.<sup>a</sup>

T / K	Continuous Shape Measure parameters for [Re <sup>1V</sup> (CN) <sub>4</sub> (N)(bpee)] <sup>2-</sup> complexes in <b>Re<sub>2</sub>-bpee</b>		
	PPY-6	OC-6	TPR-6
100(2)	29.281	<b>0.568</b>	16.551
120(2)	29.348	<b>0.570</b>	16.574
140(2)	29.366	<b>0.568</b>	16.507
160(2)	29.366	<b>0.571</b>	16.574
180(2)	29.411	<b>0.573</b>	16.603
200(2)	29.403	<b>0.576</b>	16.582
220(2)	29.378	<b>0.579</b>	16.618
240(2)	29.456	<b>0.586</b>	16.634
260(2)	29.402	<b>0.582</b>	16.656
280(2)	29.424	<b>0.605</b>	16.685

<sup>a</sup>For details see the comment below Fig. S20.

**Table S22** Results of Continuous Shape Measure<sup>1</sup> analysis for rhenium(V) complexes in **Re<sub>2</sub>-bpn**.<sup>a</sup>

T / K	Continuous Shape Measure parameters for [Re <sup>1V</sup> (CN) <sub>4</sub> (N)(bpn)] <sup>2-</sup> complexes in <b>Re<sub>2</sub>-bpn</b>		
	PPY-6	OC-6	TPR-6
100(2)	29.001	<b>0.504</b>	15.961
120(2)	29.046	<b>0.504</b>	15.973
140(2)	29.077	<b>0.505</b>	15.991
160(2)	29.093	<b>0.504</b>	16.013
180(2)	29.098	<b>0.508</b>	16.022
200(2)	29.121	<b>0.512</b>	16.008
220(2)	29.170	<b>0.513</b>	16.057
240(2)	29.161	<b>0.515</b>	16.055
260(2)	29.197	<b>0.518</b>	16.094
280(2)	29.309	<b>0.522</b>	16.181
300(2)	29.190	<b>0.527</b>	16.071

<sup>a</sup>For details see the comment below Fig. S20.

**Table S23** Results of Continuous Shape Measure analysis for rhenium(V) complexes in **Re<sub>2</sub>-bpb**.<sup>a</sup>

T / K	Continuous Shape Measure parameters for [Re <sup>V</sup> (CN) <sub>4</sub> (N)(bpb)] <sup>2-</sup> complexes in <b>Re<sub>2</sub>-bpb</b>		
	PPY-6	OC-6	TPR-6
100(2)	28.947	<b>0.601</b>	16.299
120(2)	29.003	<b>0.597</b>	16.274
140(2)	28.993	<b>0.596</b>	16.269
160(2)	29.025	<b>0.593</b>	16.286
180(2)	29.061	<b>0.591</b>	16.309
200(2)	29.118	<b>0.586</b>	16.323
220(2)	29.109	<b>0.585</b>	16.411
240(2)	29.059	<b>0.584</b>	16.332
260(2)	28.905	<b>0.583</b>	16.207

<sup>a</sup>For details see the comment below Fig. S20.

**Table S24** Results of Continuous Shape Measure<sup>1</sup> analysis for rhenium(V) complexes in **Re<sub>2</sub>-bpbp**.<sup>a</sup>

T / K	Continuous Shape Measure parameters for [Re <sup>V</sup> (CN) <sub>4</sub> (N)(bpbp)] <sup>2-</sup> complexes in <b>Re<sub>2</sub>-bpbp</b>		
	PPY-6	OC-6	TPR-6
100(2)	28.939	<b>0.507</b>	16.314
120(2)	28.878	<b>0.512</b>	16.277
140(2)	28.883	<b>0.514</b>	16.294
160(2)	28.902	<b>0.524</b>	16.301
180(2)	28.814	<b>0.521</b>	16.227
200(2)	28.851	<b>0.525</b>	16.315
220(2)	28.871	<b>0.530</b>	16.347
240(2)	28.871	<b>0.530</b>	16.347
260(2)	28.716	<b>0.538</b>	16.247
280(2)	28.890	<b>0.550</b>	16.349
300(2)	28.789	<b>0.562</b>	16.293

<sup>a</sup>For details see the comment below Fig. S20.

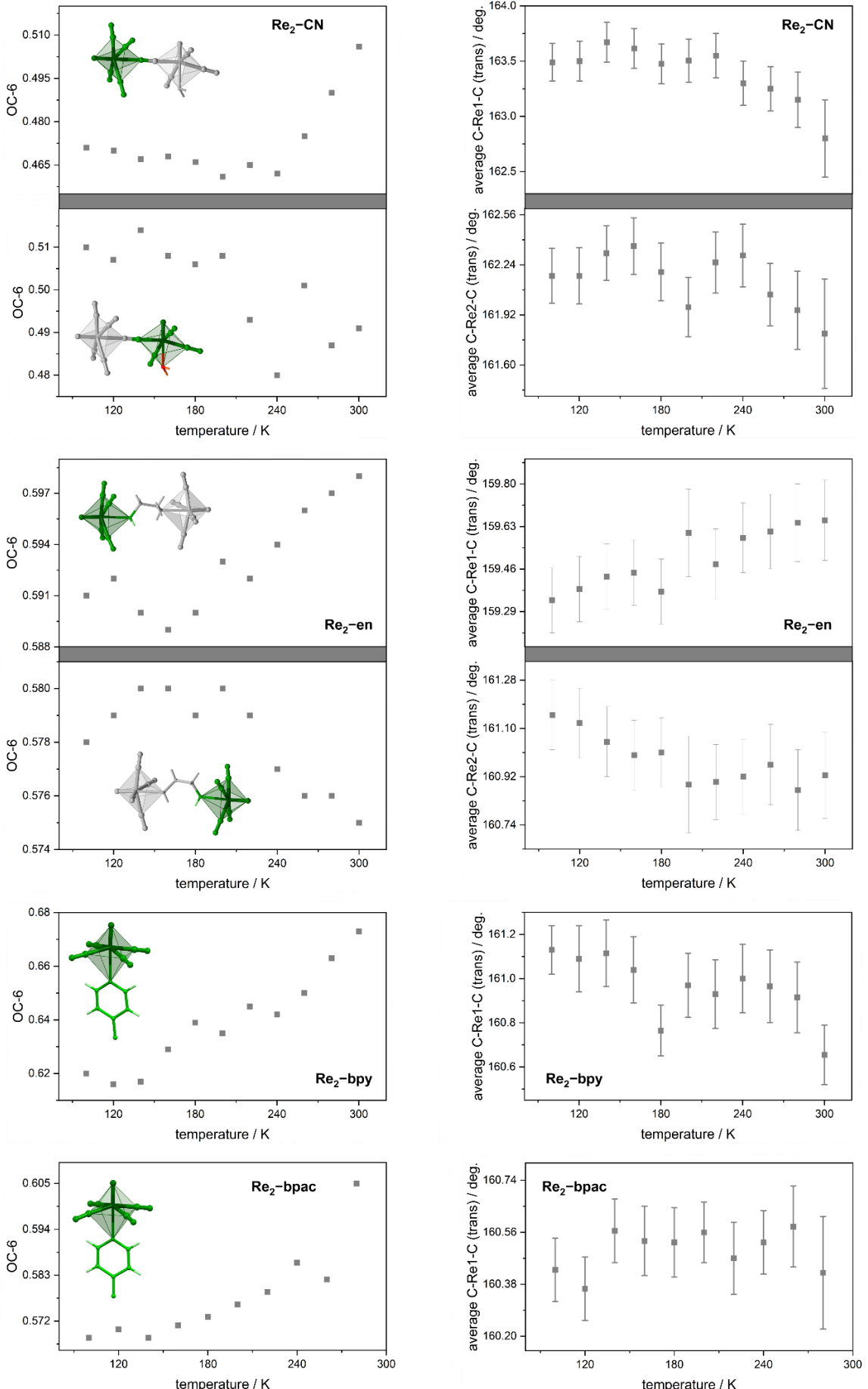


**Fig. S20** Temperature variation of the OC-6 Continuous Shape Measure parameters (which represent the distortion from an ideal octahedral geometry) (a), and an average C-Re-C (*trans*) angle in  $[Re^V(CN)_4(N)(L)]^{2-}$  complexes in **Re<sub>2</sub>-CN**, **Re<sub>2</sub>-en**, **Re<sub>2</sub>-bpy**, **Re<sub>2</sub>-bpac**, **Re<sub>2</sub>-bpac**, **Re<sub>2</sub>-bpac**, **Re<sub>2</sub>-bpac**, **Re<sub>2</sub>-bpac**, and **Re<sub>2</sub>-bpac** materials.

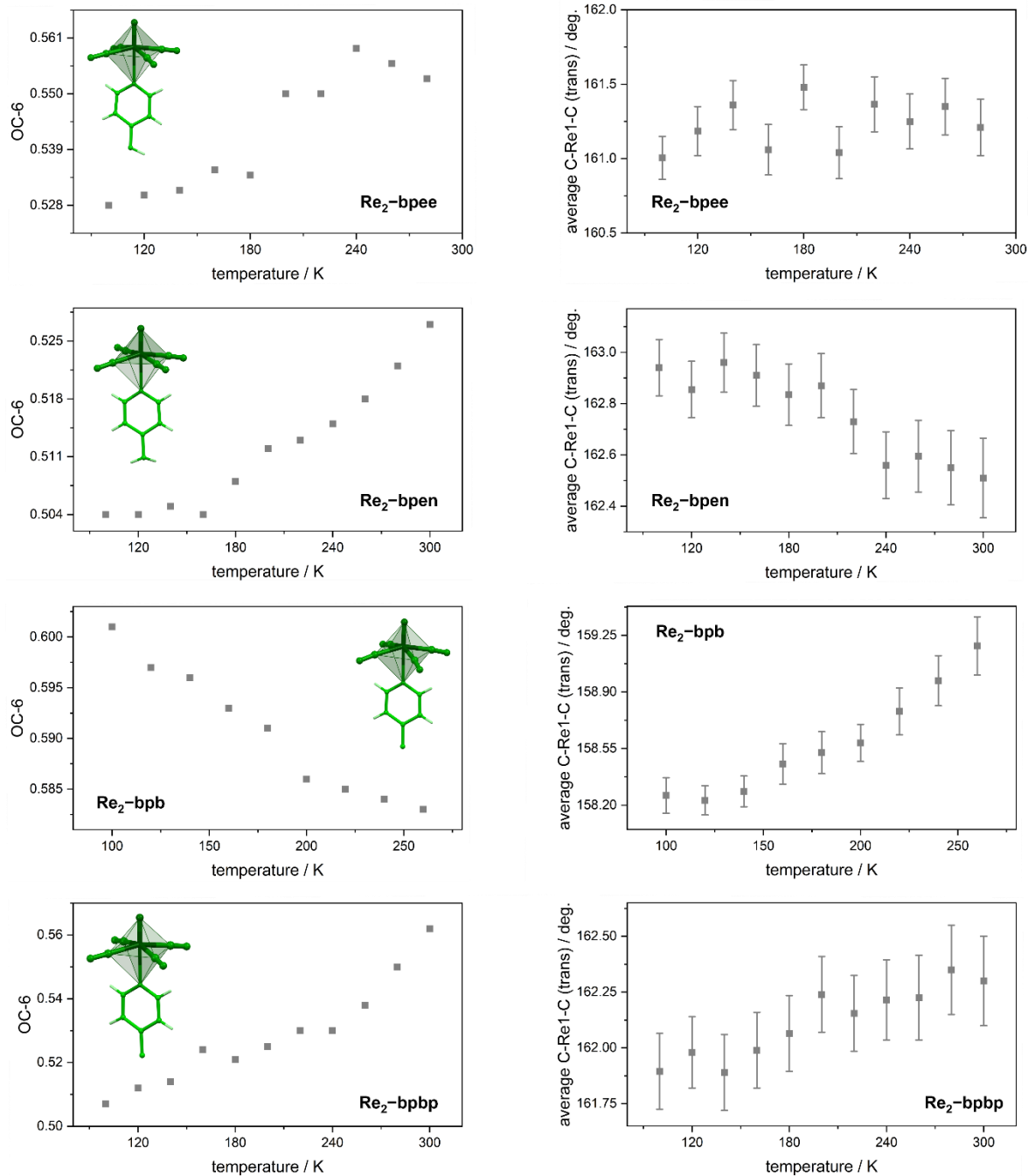


**Fig. S20 (continuation)** Temperature variation of the OC-6 Continuous Shape Measure parameters (which represent the distortion from an ideal octahedral geometry) (a), and an average C-Re1-C (*trans*) angle in [Re<sup>V</sup>(CN)<sub>4</sub>(N)(L)]<sup>2-</sup> complexes in **Re<sub>2</sub>-CN**, **Re<sub>2</sub>-en**, **Re<sub>2</sub>-bpy**, **Re<sub>2</sub>-bpac**, **Re<sub>2</sub>-bpee**, **Re<sub>2</sub>-bpen**, **Re<sub>2</sub>-bpb**, and **Re<sub>2</sub>-bpbp** materials.

**Comment to Fig. S20 and Tables S17–S24:** The Continuous Shape Measure (CShM) parameter represents the distortion from an ideal geometry of the investigated metal complex. It equals 0 for an ideal polyhedron and increases with the increasing distortion.<sup>S3,S4</sup>

The CShM parameters for six-coordinated complexes are as follows:<sup>S3,S4</sup>

- |            |  |
|------------|--|
| CShM PPY-6 | - the parameter related to the pentagonal pyramid ( $C_{5v}$ symmetry) |
| CShM OC-6  | - the parameter related to the octahedron ( $O_h$ )                    |
| CShM TPR-6 | - the parameter related to the trigonal prism ( $D_{3h}$ ).            |

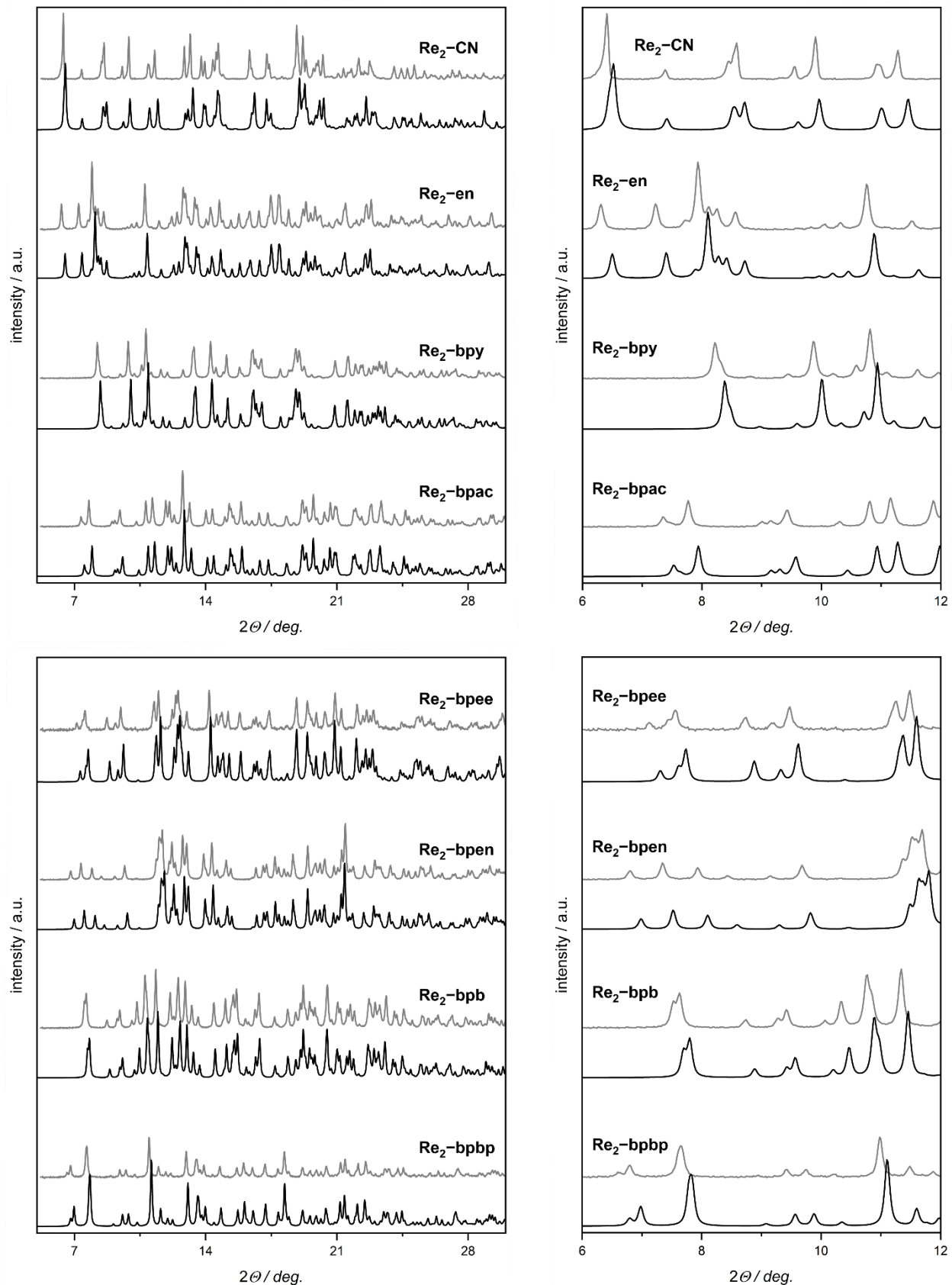


**Fig. S21** Comparison of experimental and calculated powder X-ray diffraction (P-XRD) patterns of **Re<sub>2</sub>-CN**, **Re<sub>2</sub>-en**, **Re<sub>2</sub>-bpy**, **Re<sub>2</sub>-bpac**, **Re<sub>2</sub>-bpee**, **Re<sub>2</sub>-bpen**, **Re<sub>2</sub>-bpb**, and **Re<sub>2</sub>-bpbp** in the broad  $2\theta$  range of 5–30° (left panel) and the limited low-angle region of 6–12° (right panel). Experimental data (gray lines), which were gathered at  $T = 300(2)$  K, were compared with the patterns calculated from the respective structural models obtained from the single-crystal X-ray diffraction (SC-XRD) structural analyses performed at 100(2) K (black lines) which explains the general thermal shift between these P-XRD patterns.

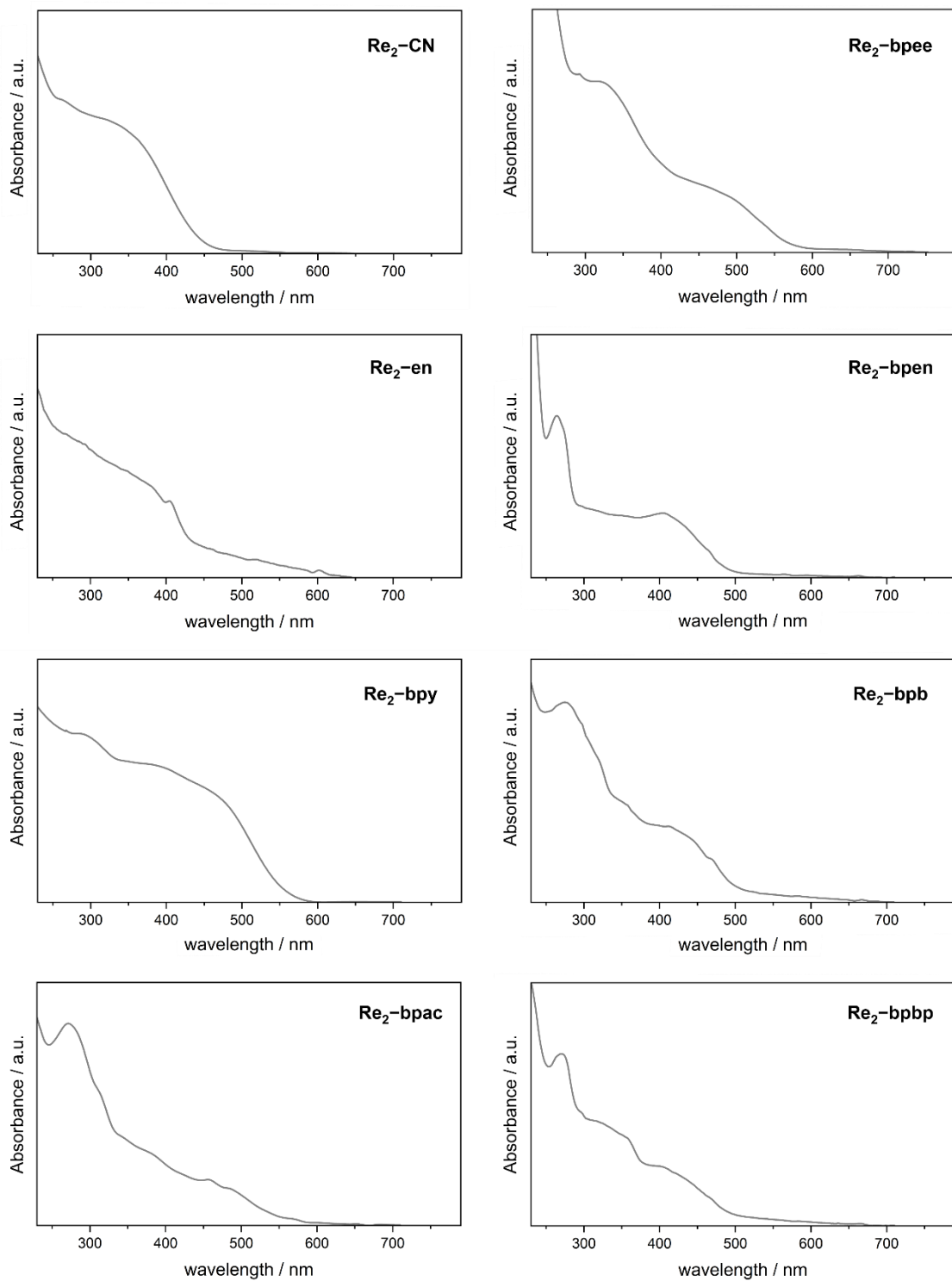


**Fig. S22** Solid-state room-temperature UV-vis absorption spectra of **Re<sub>2</sub>-CN**, **Re<sub>2</sub>-en**, **Re<sub>2</sub>-bpy**, **Re<sub>2</sub>-bpac**, **Re<sub>2</sub>-bpee**, **Re<sub>2</sub>-bpen**, **Re<sub>2</sub>-bpb**, and **Re<sub>2</sub>-bpdp** materials, presented in the 230–790 nm range.

**Table S25** Crystal data, structure refinement, and detailed crystal structure parameters of the reference compound **Re-en**, containing mononuclear Re(V) complexes (see Fig. S23).

crystal data and structure refinement parameters			
formula	C <sub>34</sub> H <sub>45</sub> N <sub>11</sub> P <sub>1</sub> Re <sub>1</sub>	Z	2
formula weight / g·mol <sup>-1</sup>	824.99	calcd. density / g·cm <sup>-3</sup>	1.528
λ / Å	0.71073 Å (Mo Kα)	abs. coeff. / cm <sup>-1</sup>	3.474
T / K	100	F(000)	832
crystal system	triclinic	Θ range / deg	2.346–25.026
space group	P -1	collected refl.	30177
a / Å	9.9423(6)	R <sub>int</sub>	0.0502
b / Å	10.7112(7)	completeness / %	99.9
c / Å	17.5626(11)	data/restraints/ parameters	6322/6/448
α / deg	97.839(2)	GOF on F <sup>2</sup>	1.081
β / deg	91.515(2)	final R <sub>1</sub> [I > 2σ(I)]	0.0274
γ / deg	104.182(2)	final wR <sub>2</sub> [all data]	0.0537
V / Å <sup>3</sup>	1792.9(2)	diff. peak and hole / e·Å <sup>-3</sup>	1.326 and -1.413
detailed crystal structure parameters			
Re1-C / Å	2.093(4) – 2.116(4)	C-Re1-C(trans) / °	161.44(15), 161.98(14)
Re1≡N1 / Å	1.666(3)	N1≡Re1-C / °	98.69(15) – 99.80(15)
Re1-N6 / Å	2.446(3)	N1≡Re1-N6 / °	176.94(13)

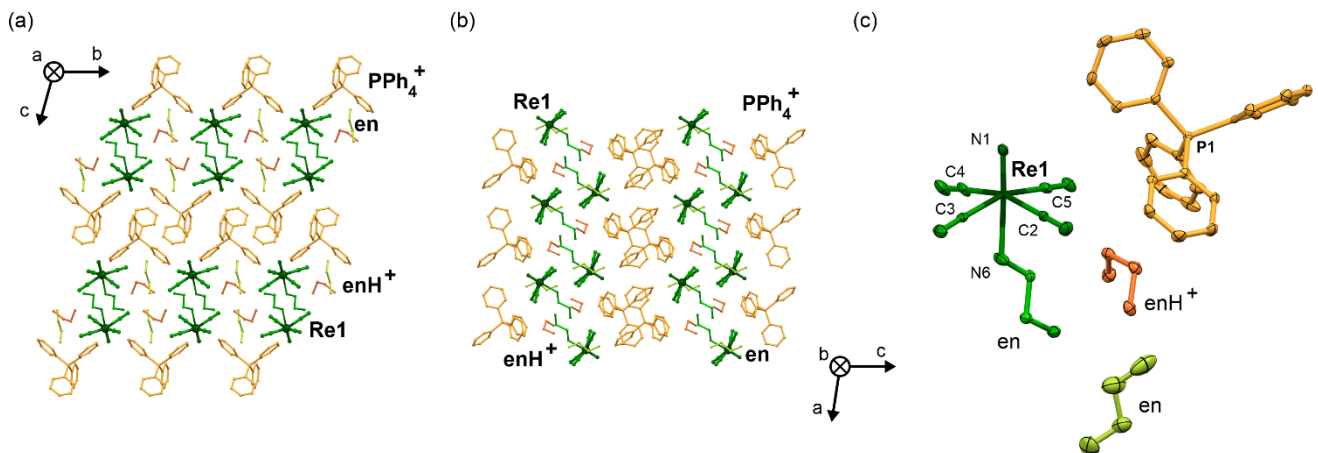


**Fig. S23** Representative structural views of the reference compound **Re-en**, containing mononuclear Re(V) complexes: the crystal structure presented along *a* and *b* crystallographic axes (*a* and *b*, respectively), and the asymmetric unit with the labeling scheme for selected symmetrically independent atoms (*c*). Thermal ellipsoids are presented for the asymmetric unit in (*c*) at the 50% probability level. Hydrogen atoms were omitted for clarity. Related crystal structure parameters are presented in Table S25 (see above).

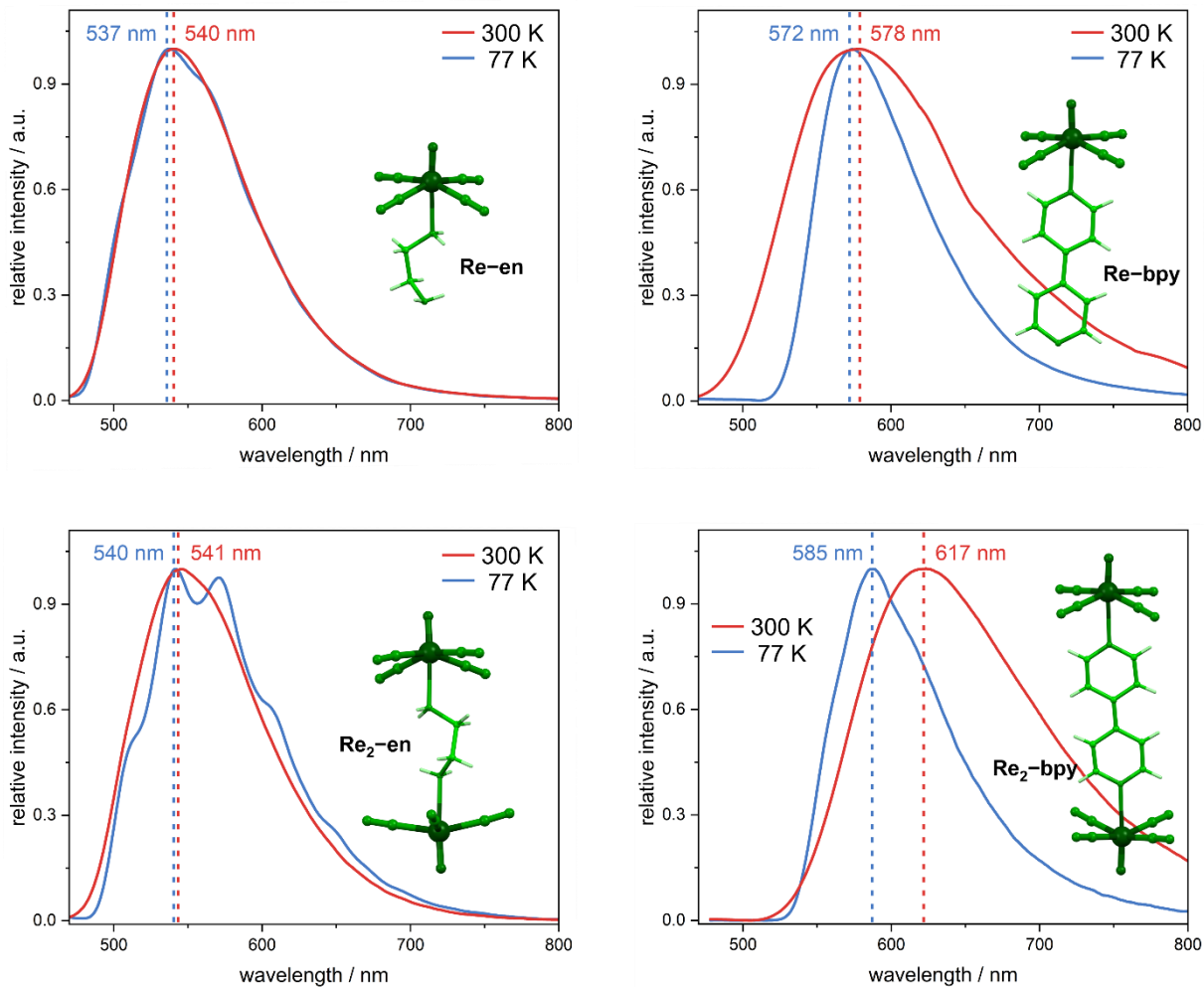


**Fig. S24** Comparison of low- and high-temperature (77 and 300 K, respectively) emission spectra ( $\lambda_{\text{ex}} = 380 \text{ nm}$ ) of indicated monometallic  $[\text{Re}^{\text{V}}(\text{CN})_4(\text{N})(\text{L})]^{2-}$  complexes with en (the reference compound, **Re-en**, see Fig. S23) and bpy (the reference compound, **Re-bpy**) ligands, and their indicated dinuclear analogs,  $\{[\text{Re}^{\text{V}}(\text{CN})_4(\text{N})]_2(\text{L})\}^{4-}$  (**Re<sub>2</sub>-en** and **Re<sub>2</sub>-bpy**). The wavelength positions of the main maxima were depicted on each graph. The set of related spectroscopic parameters of the solid-state photoluminescent properties are gathered in Table S26.<sup>55</sup>

**Table S26** Selected spectroscopic parameters of the solid-state photoluminescent properties of **Re-en**, **Re-bpy**, **Re<sub>2</sub>-en**, and **Re<sub>2</sub>-bpy** at 77 and 300 K (see Fig. S24), including emission pattern maximum ( $\lambda^{\max}$ ), average photoluminescence lifetime ( $\tau_{\text{av.}}$ ), and absolute quantum yield ( $\Phi_{\text{em}}$ ).

compound	selected spectroscopic parameters				
	77 K		300 K		
	$\lambda^{\max} / \text{nm}$	$\tau_{\text{av.}} / \mu\text{s}$	$\lambda^{\max} / \text{nm}$	$\tau_{\text{av.}} / \mu\text{s}$	$\Phi_{\text{em}}$
<b>Re-en</b>	537	127.3	540	20.1	0.73
<b>Re<sub>2</sub>-en</b>	540	57.7	541	19.5	0.67
<b>Re-bpy<sup>55</sup></b>	572	53.9	578	6.8	0.18
<b>Re<sub>2</sub>-bpy</b>	585	73.8	617	9.2	0.31

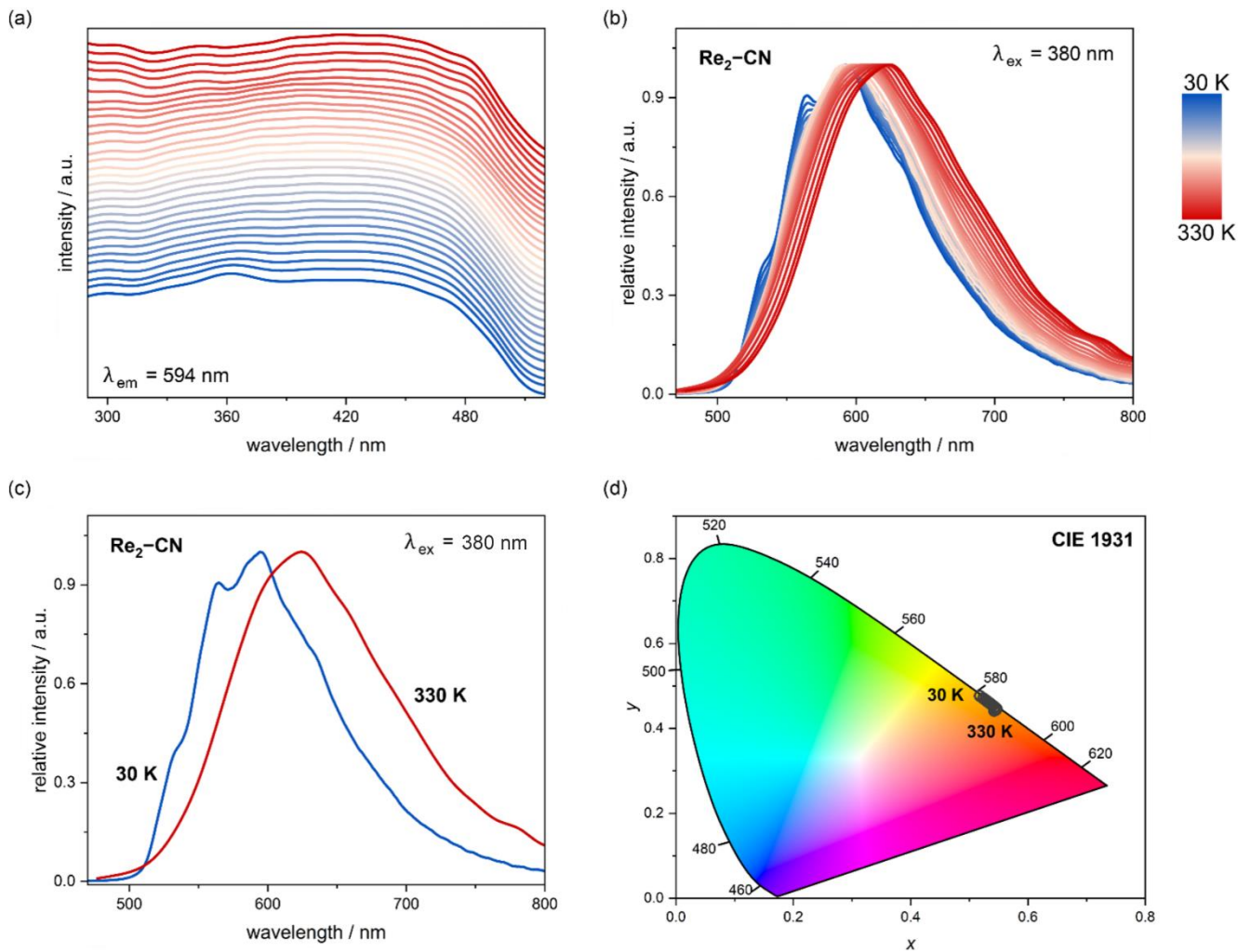


**Fig. S25** Solid-state photoluminescent properties of  $\text{Re}_2\text{-CN}$ : temperature-variable solid-state excitation (a) and emission (b) spectra collected under the indicated excitation and emission wavelengths, gathered in the 30–330 K temperature range, comparison of low- and high-temperature (30 and 330 K, respectively) emission spectra (c), and emission colors presented on the CIE 1931 chromaticity diagram (d). The related spectroscopic parameters of the emission patterns at each temperature are gathered in Table S27. The CIE 1931 chromaticity parameters, also determined at each temperature, are gathered in Table S28.

**Table S27** Selected spectroscopic parameters of the solid-state photoluminescent properties of **Re<sub>2</sub>-CN** material, detected at various indicated temperatures (see Fig. S25), including emission pattern maxima ( $\lambda^{\max}$ ), the integral area under the emission peak ( $I$ ), and full width at half maximum for the emission band ( $FWHM$ ), as well as absolute quantum yield ( $\Phi_{\text{em}}$ , room-temperature value only).

Re <sub>2</sub> -CN							
T / K	selected spectroscopic parameters			T / K	selected spectroscopic parameters		
	$\lambda^{\max}$ / nm <sup>a</sup>	$I$ / a.u.	$FWHM$ / nm		$\lambda^{\max}$ / nm <sup>a</sup>	$I$ / a.u.	$FWHM$ / nm
30	565, <u>595</u>	123.1	109.2	190	596	132.2	120.0
40	565, <u>595</u>	124.1	110.4	200	597	133.2	121.9
50	564, <u>595</u>	125.0	111.3	210	597	134.2	123.8
60	565, <u>595</u>	124.9	111.5	220	600	135.2	124.4
70	565, <u>595</u>	124.7	111.6	230	601	136.2	125.0
80	565, <u>595</u>	125.5	113.5	240	603	137.7	126.2
90	565, <u>593</u>	126.3	115.3	250	606	139.2	127.3
100	565, <u>595</u>	127.0	115.7	260	606	140.1	129.5
110	565, <u>595</u>	127.7	116.1	270	608	140.9	131.6
120	565, <u>595</u>	128.3	117.0	280	610	141.6	132.4
130	565, <u>595</u>	128.8	117.9	290	613	142.3	133.1
140	595	129.1	118.5	300	615	142.5	133.8
150	595	129.4	119.1	310	618	143.3	134.5
160	595	130.0	119.4	320	620	144.5	135.3
170	596	130.6	119.6	330	623	144.9	136.7
180	596	131.4	119.8	$\Phi_{\text{em}}$		0.08	

<sup>a</sup>For the temperature range of 30–130 K, more two well-distinguished maxima on the emission pattern are observed. The position of the main maximum at each temperature was underlined.

**Table S28** The CIE 1931 chromaticity  $x$  and  $y$  parameters of the solid-state photoluminescent properties of **Re<sub>2</sub>-CN** material, detected at various indicated temperatures (see Fig. S25), shown together with one-dimensional CCT and Duv metrics\* representing a chromaticity coordinate system.

parameter		Re <sub>2</sub> -CN						
		30 K	40 K	50 K	60 K	70 K	80 K	90 K
CIE 1931 chromaticity parameters	$x$	0.518	0.521	0.524	0.525	0.527	0.529	0.530
	$y$	0.476	0.474	0.471	0.469	0.468	0.466	0.464
CCT / K		2485	2441	2398	2372	2346	2323	2301
Duv / a.u		0.0182	0.0173	0.0165	0.0160	0.0154	0.0151	0.0146
		100 K	110 K	120 K	130 K	140 K	150 K	160 K
CIE 1931 chromaticity parameters	$x$	0.532	0.533	0.534	0.536	0.533	0.531	0.532
	$y$	0.463	0.461	0.460	0.459	0.461	0.463	0.462
CCT / K		2278	2256	2239	2223	2255	2286	2264
Duv / a.u		0.0142	0.0138	0.0135	0.0132	0.0138	0.0143	0.0139
		170 K	180 K	190 K	200 K	210 K	220 K	230 K
CIE 1931 chromaticity parameters	$x$	0.534	0.532	0.531	0.534	0.537	0.539	0.540
	$y$	0.460	0.462	0.463	0.460	0.457	0.455	0.454
CCT / K		22412	2264	2286	2240	2195	2178	2161
Duv / a.u		0.0135	0.0139	0.0143	0.0134	0.0126	0.0123	0.0120
		240 K	250 K	260 K	270 K	280 K	290 K	300 K
CIE 1931 chromaticity parameters	$x$	0.542	0.543	0.545	0.547	0.546	0.546	0.545
	$y$	0.452	0.450	0.448	0.446	0.445	0.444	0.444
CCT / K		2135	2110	2086	2062	20560	2057	2064
Duv / a.u		0.0116	0.0111	0.0107	0.0102	0.0099	0.0096	0.0094
		310 K	320 K	330 K	-	-	-	-
CIE 1931 chromaticity parameters	$x$	0.544	0.543	0.542	-	-	-	-
	$y$	0.443	0.442	0.441	-	-	-	-
CCT / K		2061	2067	2065	-	-	-	-
Duv / a.u		0.0092	0.0090	0.0087	-	-	-	-

\*The Duv (Delta  $u,v$ ) and CCT (correlated color temperature) quality parameters are one-dimensional metrics that describe the light color point along the black body curve. Typically, they are used in explaining how close to “pure white” light a particular light source is. They are significant whenever discussing color-sensitive lighting applications. Additionally, compared to CIE 1931  $x$  and  $y$  parameters, the one-dimensionality of both parameters can help track temperature changes in the emission spectrum.<sup>56</sup>

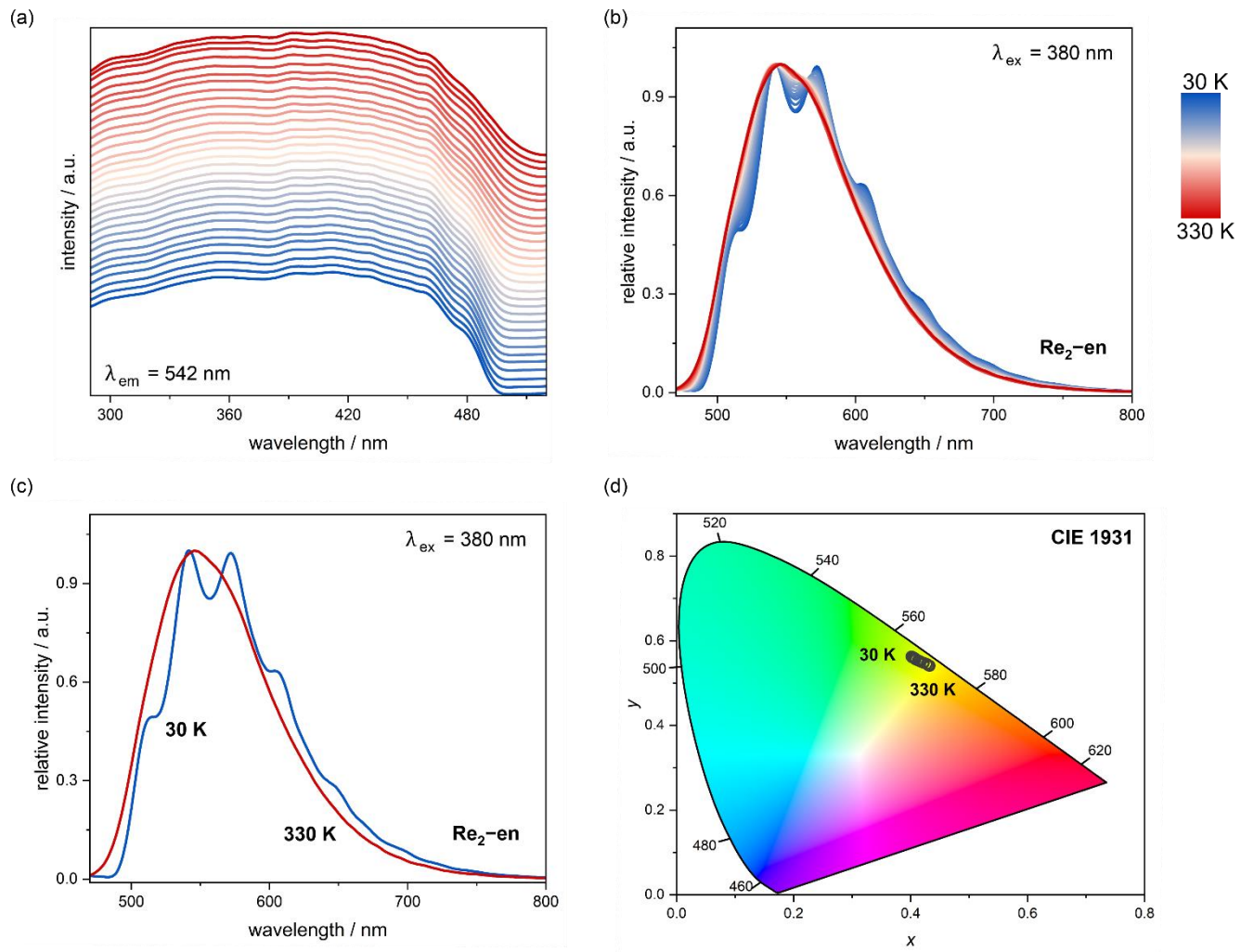


**Fig. S26** Solid-state photoluminescent properties of **Re<sub>2</sub>-en**: temperature-variable solid-state excitation (a) and emission (b) spectra collected under the indicated excitation and emission wavelengths, gathered in the 30–330 K temperature range, comparison of low- and high-temperature (30 and 330 K, respectively) emission spectra (c), and emission colors presented on the CIE 1931 chromaticity diagram (d). The related spectroscopic parameters of the emission patterns at each temperature are gathered in Table S29. The CIE 1931 chromaticity parameters, also determined at each temperature, are gathered in Table S30.

**Table S29** Selected spectroscopic parameters of the solid-state photoluminescent properties of **Re<sub>2</sub>-en** material, detected at various indicated temperatures (see Fig. S26), including emission pattern maxima ( $\lambda^{\max}$ ), the integral area under the emission peak ( $I$ ), and full width at half maximum for the emission band ( $FWHM$ ), as well as absolute quantum yield ( $\Phi_{\text{em}}$ , room-temperature value only).

Re <sub>2</sub> -en							
T / K	selected spectroscopic parameters			T / K	selected spectroscopic parameters		
	$\lambda^{\max}$ / nm <sup>a</sup>	$I$ / a.u.	$FWHM$ / nm		$\lambda^{\max}$ / nm <sup>a</sup>	$I$ / a.u.	$FWHM$ / nm
30	513, <u>540</u> , 571, 605	108.4	97.9	190	540	109.9	103.0
40	513, <u>540</u> , 571, 605	108.4	99.5	200	540	110.0	102.7
50	513, <u>540</u> , 571, 605	108.5	101.2	210	540	109.8	102.4
60	513, <u>540</u> , 570, 605	109.1	103.9	220	540	109.7	102.1
70	<u>540</u> , 569, 605	109.9	105.1	230	539	109.6	101.7
80	<u>540</u> , 571, 605	110.0	105.3	240	539	1094	10.2
90	<u>539</u> , 569, 605	110.1	105.2	250	539	109.1	100.6
100	<u>539</u> , 568, 605	110.1	105.1	260	539	108.7	100.4
110	<u>539</u> , 568, 605	110.2	105.0	270	539	108.4	100.1
120	<u>540</u> , 567	110.2	104.7	280	540	108.9	100.1
130	<u>540</u> , 566	110.3	104.5	290	540	109.3	100.0
140	<u>540</u> , 564	110.2	104.5	300	540	109.5	100.0
150	<u>540</u> , 563	110.1	104.4	310	539	109.7	100.0
160	<u>540</u> , 566	109.6	103.9	320	539	109.9	99.9
170	541	109.4	103.7	330	539	110.2	100.3
180	541	109.7	103.2	$\Phi_{\text{em}}$		0.67	

<sup>a</sup>For the temperature range of 30–160 K, two or more well-distinguished maxima on the emission pattern are observed. The position of the main maximum at each temperature was underlined.

**Table S30** The CIE 1931 chromaticity  $x$  and  $y$  parameters of the solid-state photoluminescent properties of **Re<sub>2</sub>-en** material, detected at various indicated temperatures (see Fig. S26), shown together with one-dimensional CCT (correlated color temperature) and  $D_{uv}$  (Delta  $u,v$ ) metrics\* representing a chromaticity coordinate system.

parameter		Re <sub>2</sub> -en						
		30 K	40 K	50 K	60 K	70 K	80 K	90 K
CIE 1931 chromaticity parameters	$x$	0.432	0.432	0.431	0.429	0.428	0.425	0.422
	$y$	0.541	0.541	0.542	0.543	0.545	0.546	0.548
CCT / K		3854	3866	3877	3906	3934	3978	4021
$D_{uv}$ / a.u		0.0484	0.0487	0.0490	0.0498	0.0506	0.0516	0.0526
		100 K	110 K	120 K	130 K	140 K	150 K	160 K
CIE 1931 chromaticity parameters	$x$	0.420	0.417	0.414	0.413	0.411	0.408	0.408
	$y$	0.549	0.551	0.552	0.553	0.555	0.556	0.558
CCT / K		4068	4115	4148	4180	4215	4251	4263
$D_{uv}$ / a.u		0.0538	0.0549	0.0557	0.0565	0.0574	0.0582	0.0588
		170 K	180 K	190 K	200 K	210 K	220 K	230 K
CIE 1931 chromaticity parameters	$x$	0.407	0.406	0.406	0.406	0.406	0.405	0.404
	$y$	0.559	0.559	0.560	0.560	0.559	0.560	0.561
CCT / K		4277	4289	4301	4301	4301	4313	4325
$D_{uv}$ / a.u		0.0592	0.0596	0.0599	0.0599	0.0598	0.0602	0.0606
		240 K	250 K	260 K	270 K	280 K	290 K	300 K
CIE 1931 chromaticity parameters	$x$	0.403	0.403	0.402	0.402	0.402	0.402	0.402
	$y$	0.561	0.562	0.562	0.563	0.562	0.562	0.562
CCT / K		4339	4353	4361	4370	4366	4363	4356
$D_{uv}$ / a.u		0.0609	0.0613	0.0614	0.0617	0.0616	0.0615	0.0612
		310 K	320 K	330 K	–	–	–	–
CIE 1931 chromaticity parameters	$x$	0.402	0.403	0.403	–	–	–	–
	$y$	0.561	0.561	0.561	–	–	–	–
CCT / K		4348	4343	4343	–	–	–	–
$D_{uv}$ / a.u		0.0609	0.0608	0.0608	–	–	–	–

\*The  $D_{uv}$  and CCT quality parameters are commented on below the Table S28 (see above).

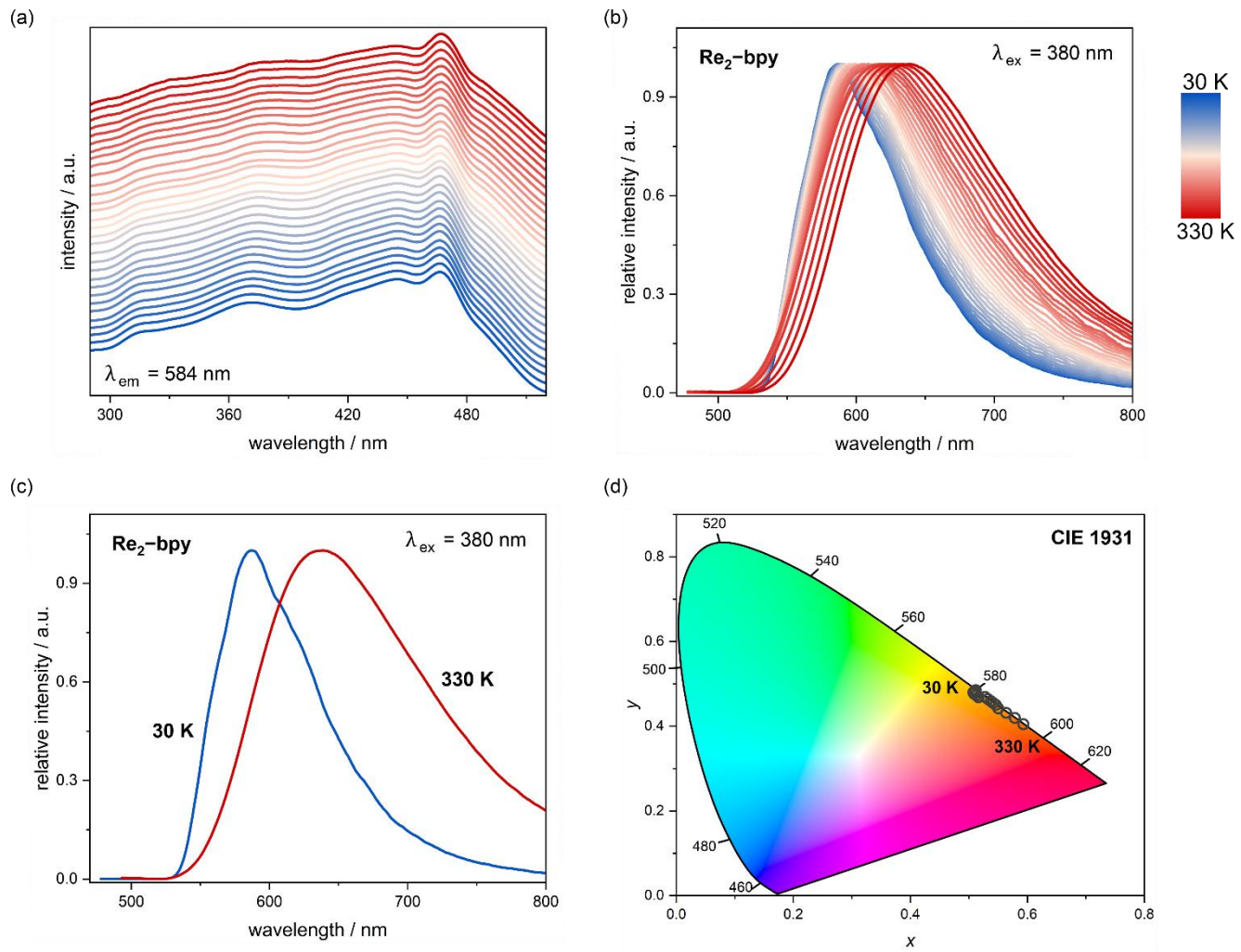


**Fig. S27** Solid-state photoluminescent properties of **Re<sub>2</sub>-bpy**: temperature-variable solid-state excitation (a) and emission (b) spectra collected under the indicated excitation and emission wavelengths, gathered in the 30–330 K temperature range, comparison of low- and high-temperature (30 and 330 K, respectively) emission spectra (c), and emission colors presented on the CIE 1931 chromaticity diagram (d). The related spectroscopic parameters of the emission patterns at each temperature are gathered in Table S31. The CIE 1931 chromaticity parameters, also determined at each temperature, are gathered in Table S32.

**Table S31** Selected spectroscopic parameters of the solid-state photoluminescent properties of **Re<sub>2</sub>-bpy** material, detected at various indicated temperatures (see Fig. S27), including emission pattern maxima ( $\lambda^{\max}$ ), the integral area under the emission peak ( $I$ ), and full width at half maximum for the emission band ( $FWHM$ ), as well as absolute quantum yield ( $\Phi_{\text{em}}$ , room-temperature value only).

Re <sub>2</sub> -bpy							
T / K	selected spectroscopic parameters			T / K	selected spectroscopic parameters		
	$\lambda^{\max}$ / nm	$I$ / a.u.	$FWHM$ / nm		$\lambda^{\max}$ / nm	$I$ / a.u.	$FWHM$ / nm
30	584	96.1	86.0	190	589.5	125.8	108.6
40	584	96.7	86.5	200	589	128.5	111.1
50	584	97.3	87.0	210	590	131.1	113.6
60	585	98.0	87.4	220	591	134.6	116.1
70	585	98.7	87.8	230	591.5	138.0	119.5
80	585	100.1	89.0	240	593.5	140.7	122.9
90	586	101.4	90.2	250	595.5	143.3	126.2
100	586	103.3	91.6	260	599.5	145.3	129.5
110	586	105.1	93.0	270	603.5	147.3	131.4
120	587	107.8	95.2	280	607	151.3	133.3
130	587	110.4	97.4	290	611	155.2	139.1
140	587	113.3	100.1	300	617	157.4	142.8
150	588	116.1	102.7	310	622	159.2	144.8
160	588	118.3	104.4	320	628	162.5	148.6
170	588	120.4	106.1	330	634	167.0	150.1
180	589	123.1	108.6	$\Phi_{\text{em}}$		0.31	

**Table S32** The CIE 1931 chromaticity  $x$  and  $y$  parameters of the solid-state photoluminescent properties of **Re<sub>2</sub>-bpy** material, detected at various indicated temperatures (see Fig. S27), shown together with one-dimensional CCT (correlated color temperature) and  $D_{uv}$  (Delta  $u,v$ ) metrics\* representing a chromaticity coordinate system.

parameter		Re <sub>2</sub> -bpy						
		30 K	40 K	50 K	60 K	70 K	80 K	90 K
CIE 1931 chromaticity parameters	$x$	0.508	0.510	0.512	0.511	0.510	0.512	0.510
	$y$	0.480	0.482	0.485	0.484	0.484	0.483	0.480
CCT / K		2608	2604	2599	2605	2610	2583	2587
$D_{uv}$ / a.u		0.0196	0.0203	0.0209	0.0208	0.0206	0.0204	0.0195
		100 K	110 K	120 K	130 K	140 K	150 K	160 K
CIE 1931 chromaticity parameters	$x$	0.509	0.509	0.511	0.513	0.515	0.517	0.522
	$y$	0.478	0.476	0.474	0.473	0.470	0.468	0.469
CCT / K		2589	2572	2540	2510	2478	2448	2399
$D_{uv}$ / a.u		0.0190	0.0185	0.0179	0.0173	0.0166	0.0159	0.0159
		170 K	180 K	190 K	200 K	210 K	220 K	230 K
CIE 1931 chromaticity parameters	$x$	0.528	0.530	0.533	0.535	0.537	0.540	0.542
	$y$	0.469	0.467	0.464	0.462	0.459	0.457	0.455
CCT / K		2353	2315	2278	2243	22110	2178	2147
$D_{uv}$ / a.u		0.0160	0.0153	0.0146	0.0139	0.0133	0.0128	0.0122
		240 K	250 K	260 K	270 K	280 K	290 K	300 K
CIE 1931 chromaticity parameters	$x$	0.544	0.546	0.548	0.550	0.557	0.564	0.571
	$y$	0.452	0.450	0.446	0.442	0.437	0.431	0.426
CCT / K		2118	2090	2052	2016	1947	1882	1823
$D_{uv}$ / a.u		0.0117	0.0112	0.0103	0.0094	0.0087	0.0082	0.0082
		310 K	320 K	330 K	-	-	-	-
CIE 1931 chromaticity parameters	$x$	0.579	0.586	0.593	-	-	-	-
	$y$	0.419	0.412	0.405	-	-	-	-
CCT / K		1773	1736	1714	-	-	-	-
$D_{uv}$ / a.u		0.0087	0.0098	0.0122	-	-	-	-

\*The  $D_{uv}$  and CCT quality parameters are commented on below the Table S28 (see above).

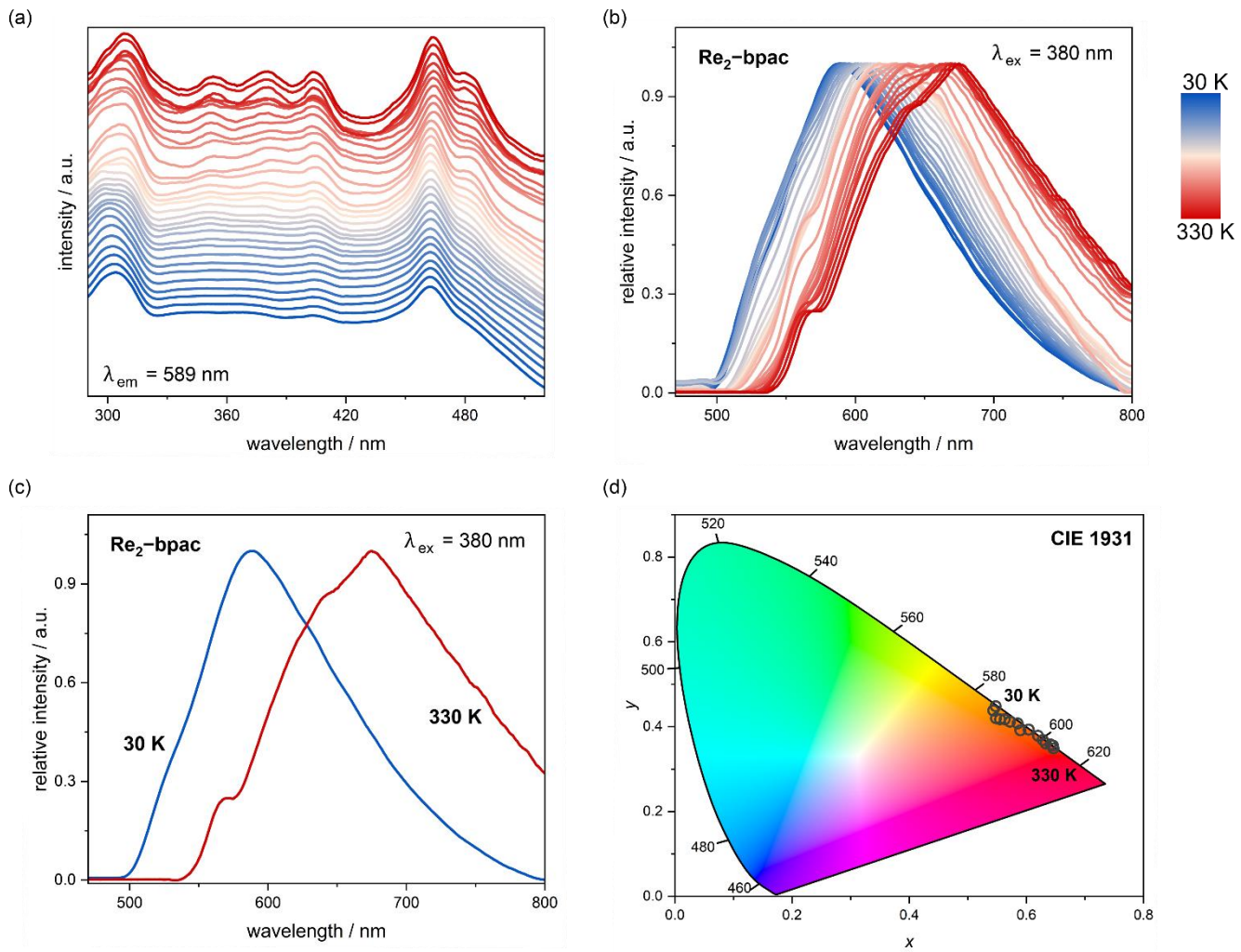


**Fig. S28** Solid-state photoluminescent properties of **Re<sub>2</sub>-bpac**: temperature-variable solid-state excitation (a) and emission (b) spectra collected under the indicated excitation and emission wavelengths, gathered in the 30–330 K temperature range, comparison of low- and high-temperature (30 and 330 K, respectively) emission spectra (c), and emission colors presented on the CIE 1931 chromaticity diagram (d). The related spectroscopic parameters of the emission patterns at each temperature are gathered in Table S33. The CIE 1931 chromaticity parameters, also determined at each temperature, are gathered in Table S34.

**Table S33** Selected spectroscopic parameters of the solid-state photoluminescent properties of **Re<sub>2</sub>-bpac** material, detected at various indicated temperatures (see Fig. S28), including emission pattern maxima ( $\lambda^{\max}$ ), the integral area under the emission peak ( $I$ ), and full width at half maximum for the emission band ( $FWHM$ ), as well as absolute quantum yield ( $\Phi_{\text{em}}$ , room-temperature value only).

Re <sub>2</sub> -bpac							
T / K	selected spectroscopic parameters			T / K	selected spectroscopic parameters		
	$\lambda^{\max}$ / nm	$I$ / a.u.	$FWHM$ / nm		$\lambda^{\max}$ / nm	$I$ / a.u.	$FWHM$ / nm
30	589	133.4	124.2	190	626	152.9	148.1
40	588	135.3	128.3	200	628	151.6	149.7
50	590	141.5	137.9	210	624	149.1	150.2
60	590	142.0	136.4	220	629	150.1	152.3
70	591	145.2	140.1	230	630	155.3	148.4
80	591	147.3	142.9	240	634	–	159.6
90	595	150.3	145.5	250	638	–	165.0
100	600	149.7	147.7	260	654	–	167.7
110	600	150.2	148.0	270	661	–	168.4
120	602	151.2	148.2	280	663	–	169.2
130	604	155.4	148.1	290	664	–	167.1
140	609	150.7	147.2	300	666	–	166.3
150	611	148.4	144.9	310	667	–	164.6
160	616	150.8	146.3	320	672	–	165.6
170	617	151.7	146.1	330	676	–	164.9
180	627	153.0	147.5	$\Phi_{\text{em}}$		0.37	

**Table S34** The CIE 1931 chromaticity  $x$  and  $y$  parameters of the solid-state photoluminescent properties of **Re<sub>2</sub>-bpac** material, detected at various indicated temperatures (see Fig. S28), shown together with one-dimensional CCT (correlated color temperature) and  $D_{uv}$  (Delta  $u,v$ ) metrics\* representing a chromaticity coordinate system.

parameter		Re <sub>2</sub> -bpac						
		30 K	40 K	50 K	60 K	70 K	80 K	90 K
CIE 1931 chromaticity parameters	$x$	0.554	0.552	0.548	0.546	0.543	0.543	0.541
	$y$	0.438	0.440	0.448	0.441	0.441	0.441	0.439
CCT / K		1974	1993	2070	2038	2057	2066	2064
$D_{uv}$ / a.u		0.0087	0.0091	0.0108	0.0089	0.00878	0.0088	0.0080
		100 K	110 K	120 K	130 K	140 K	150 K	160 K
CIE 1931 chromaticity parameters	$x$	0.542	0.543	0.546	0.548	0.558	0.585	0.588
	$y$	0.436	0.431	0.427	0.420	0.413	0.408	0.399
CCT / K		2041	2005	1957	1908	1824	1728	1714
$D_{uv}$ / a.u		0.0074	0.0063	0.0053	0.0038	0.0037	0.0094	0.0104
		170 K	180 K	190 K	200 K	210 K	220 K	230 K
CIE 1931 chromaticity parameters	$x$	0.590	0.603	0.604	0.603	0.604	0.600	0.620
	$y$	0.392	0.395	0.393	0.394	0.393	0.388	0.379
CCT / K		1714	1722	1726	1724	1727	1734	1846
$D_{uv}$ / a.u		0.0116	0.0173	0.0183	0.0179	0.0184	0.0179	0.0340
		240 K	250 K	260 K	270 K	280 K	290 K	300 K
CIE 1931 chromaticity parameters	$x$	0.626	0.628	0.631	0.633	0.636	0.641	0.643
	$y$	0.372	0.369	0.365	0.360	0.360	0.358	0.358
CCT / K		1939	1994	2060	2153	2197	2276	2312
$D_{uv}$ / a.u		0.0431	0.0478	0.0533	0.0601	0.0642	0.0712	0.0743
		310 K	320 K	330 K	-	-	-	-
CIE 1931 chromaticity parameters	$x$	0.645	0.647	0.646	-	-	-	-
	$y$	0.355	0.354	0.349	-	-	-	-
CCT / K		2380	2436	2541	-	-	-	-
$D_{uv}$ / a.u		0.0791	0.0829	0.0885	-	-	-	-

\*The  $D_{uv}$  and CCT quality parameters are commented on below the Table S28 (see above).

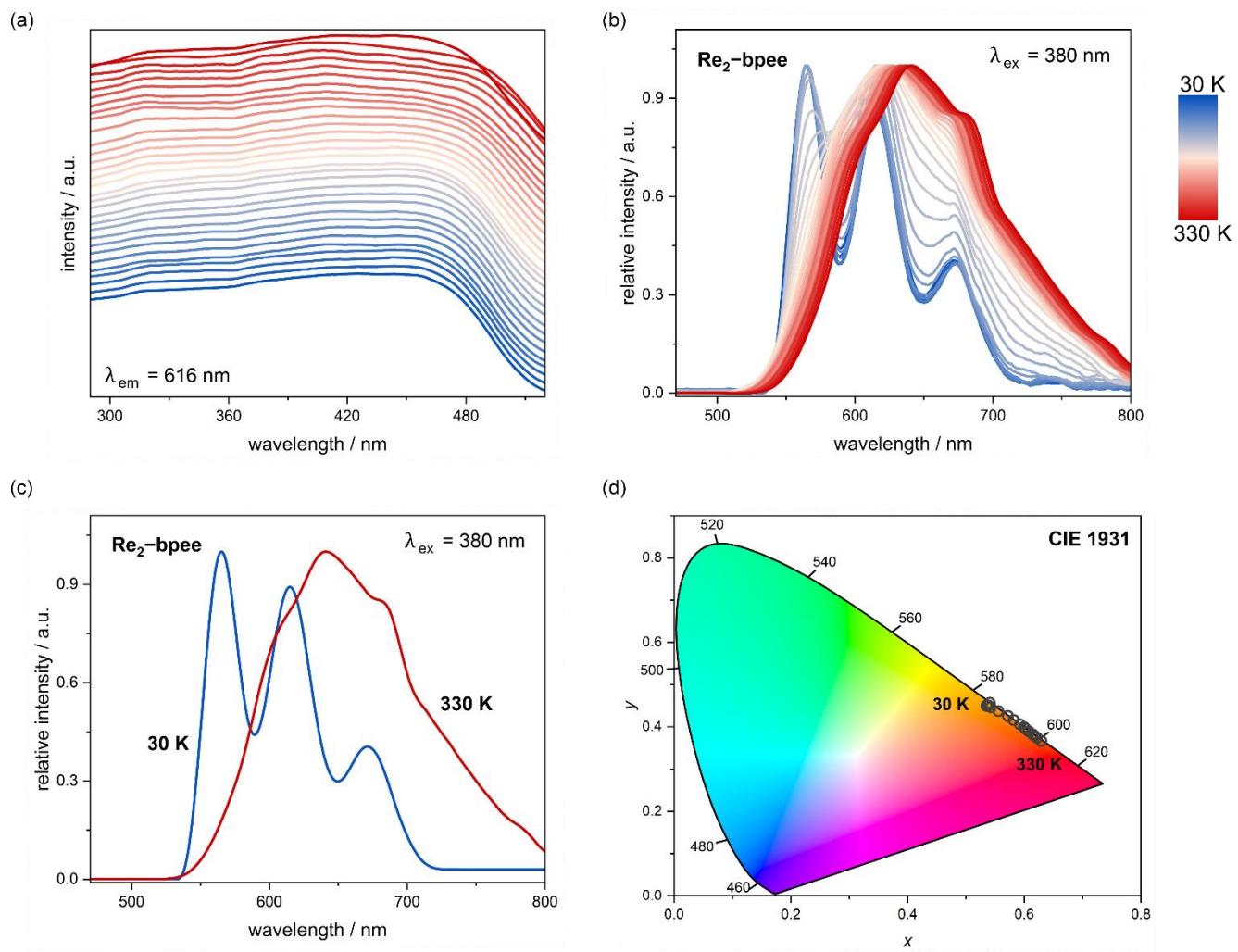


**Fig. S29** Solid-state photoluminescent properties of **Re<sub>2</sub>-bpee**: temperature-variable solid-state excitation (a) and emission (b) spectra collected under the indicated excitation and emission wavelengths, gathered in the 30–330 K temperature range, comparison of low- and high-temperature (30 and 330 K, respectively) emission spectra (c), and emission colors presented on the CIE 1931 chromaticity diagram (d). The related spectroscopic parameters of the emission patterns at each temperature are gathered in Table S35. The CIE 1931 chromaticity parameters, also determined at each temperature, are gathered in Table S36.

**Table S35** Selected spectroscopic parameters of the solid-state photoluminescent properties of **Re<sub>2</sub>-bpree** material, detected at various indicated temperatures (see Fig. S29), including emission pattern maxima ( $\lambda^{\max}$ ), the integral area under the emission peak ( $I$ ), and full width at half maximum for the emission band ( $FWHM$ ), as well as absolute quantum yield ( $\Phi_{\text{em}}$ , room-temperature value only).

Re <sub>2</sub> -bpree							
T / K	selected spectroscopic parameters			T / K	selected spectroscopic parameters		
	$\lambda^{\max}$ / nm <sup>a</sup>	$I$ / a.u.	$FWHM$ / nm		$\lambda^{\max}$ / nm <sup>a</sup>	$I$ / a.u.	$FWHM$ / nm
30	<u>566</u> , 616, 672	86.7	–	190	620	138.2	130.3
40	<u>566</u> , 616, 672	85.4	–	200	622	137.7	129.8
50	<u>566</u> , 616, 672	81.9	–	210	625	137.3	129.2
60	<u>566</u> , 616, 672	81.9	–	220	628	136.8	128.4
70	<u>566</u> , 616, 672	82.0	–	230	630	136.5	127.8
80	<u>566</u> , 616, 672	83.3	–	240	631	136.5	128.0
90	<u>566</u> , 616, 672	84.5	–	250	632	136.4	128.0
100	<u>566</u> , 616, 672	89.2	–	260	633	136.5	128.0
110	<u>567</u> , 616, 672	94.1	–	270	635	136.5	127.8
120	<u>567</u> , 616, 672	104.0	–	280	636	136.5	127.8
130	<u>568</u> , <u>616</u> , 672	114.4	125.1	290	638	136.5	127.9
140	<u>568</u> , <u>616</u> , 672	120.3	125.3	300	638	136.5	127.9
150	<u>568</u> , <u>616</u> , 672	126.4	126.8	310	639	136.5	127.8
160	617	131.7	129.1	320	640	136.4	127.9
170	618	137.1	130.7	330	641	136.4	127.8
180	619	137.5	130.5	$\Phi_{\text{em}}$		0.34	

<sup>a</sup>For the temperature range of 30–150 K, two or more well-distinguished maxima on the emission pattern are observed. The position of the main maximum at each temperature was underlined.

**Table S36** The CIE 1931 chromaticity  $x$  and  $y$  parameters of the solid-state photoluminescent properties of  $\text{Re}_2\text{-bpEE}$  material, detected at various indicated temperatures (see Fig. S29), shown together with one-dimensional CCT (correlated color temperature) and Duv (Delta  $u,v$ ) metrics\* representing a chromaticity coordinate system.

parameter		Re <sub>2</sub> -bpEE						
		30 K	40 K	50 K	60 K	70 K	80 K	90 K
CIE 1931 chromaticity parameters	$x$	0.541	0.538	0.536	0.536	0.5353	0.537	0.538
	$y$	0.457	0.454	0.451	0.450	0.450	0.450	0.451
CCT / K		2165	2168	2172	2170	2169	2159	2151
Duv / a.u		0.0127	0.0119	0.0110	0.0108	0.0107	0.0108	0.011
		100 K	110 K	120 K	130 K	140 K	150 K	160 K
CIE 1931 chromaticity parameters	$x$	0.540	0.543	0.550	0.556	0.564	0.572	0.577
	$y$	0.448	0.447	0.442	0.437	0.431	0.426	0.420
CCT / K		2121	2094	2017	1955	1881	1819	1783
Duv / a.u		0.0105	0.0101	0.0092	0.0087	0.0083	0.0084	0.0080
		170 K	180 K	190 K	200 K	210 K	220 K	230 K
CIE 1931 chromaticity parameters	$x$	0.582	0.587	0.593	0.596	0.600	0.601	0.602
	$y$	0.416	0.411	0.406	0.402	0.399	0.397	0.395
CCT / K		1754	1731	1716	1713	1714	1717	1721
Duv / a.u		0.0091	0.0102	0.0119	0.0134	0.0153	0.0171	0.0185
		240 K	250 K	260 K	270 K	280 K	290 K	300 K
CIE 1931 chromaticity parameters	$x$	0.605	0.608	0.611	0.614	0.615	0.618	0.621
	$y$	0.392	0.389	0.386	0.383	0.381	0.379	0.376
CCT / K		1730	1746	1769	1795	1806	1837	1876
Duv / a.u		0.0209	0.0226	0.0260	0.0281	0.0292	0.0313	0.0337
		310 K	320 K	330 K	-	-	-	-
CIE 1931 chromaticity parameters	$x$	0.622	0.626	0.629	-	-	-	-
	$y$	0.374	0.370	0.366	-	-	-	-
CCT / K		1893	1955	2033	-	-	-	-
Duv / a.u		0.0354	0.0422	0.0499	-	-	-	-

\*The Duv and CCT quality parameters are commented on below the Table S28 (see above).

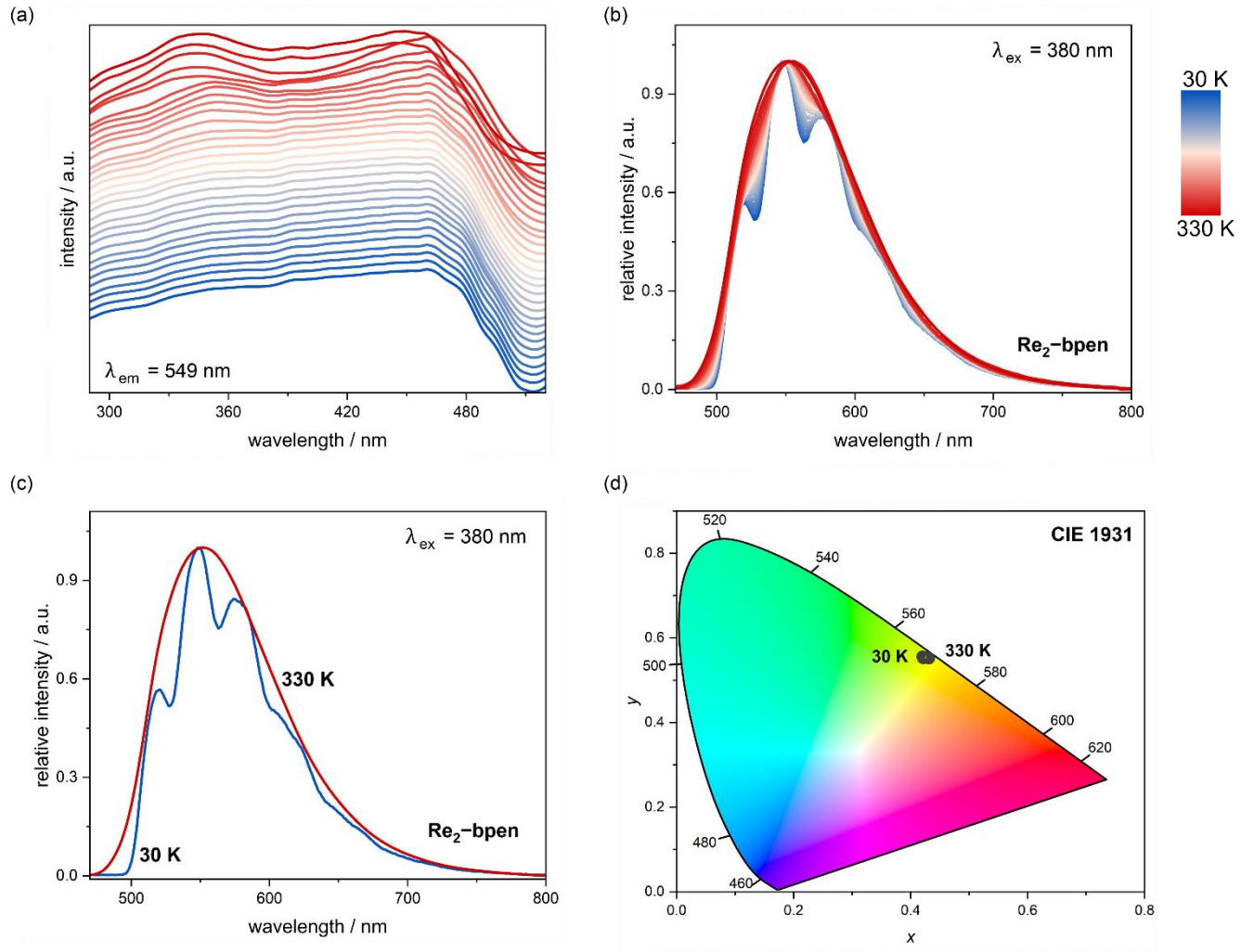


**Fig. S30** Solid-state photoluminescent properties of **Re<sub>2</sub>-bpen**: temperature-variable solid-state excitation (a) and emission (b) spectra collected under the indicated excitation and emission wavelengths, gathered in the 30–330 K temperature range, comparison of low- and high-temperature (30 and 330 K, respectively) emission spectra (c), and emission colors presented on the CIE 1931 chromaticity diagram (d). The related spectroscopic parameters of the emission patterns at each temperature are gathered in Table S37. The CIE 1931 chromaticity parameters, also determined at each temperature, are gathered in Table S38.

**Table S37** Selected spectroscopic parameters of the solid-state photoluminescent properties of **Re<sub>2</sub>-bpen** material, detected at various indicated temperatures (see Fig. S30), including emission pattern maxima ( $\lambda^{\max}$ ), the integral area under the emission peak ( $I$ ), and full width at half maximum for the emission band ( $FWHM$ ), as well as absolute quantum yield ( $\Phi_{\text{em}}$ , room-temperature value only).

Re <sub>2</sub> -bpen							
T / K	selected spectroscopic parameters			T / K	selected spectroscopic parameters		
	$\lambda^{\max}$ / nm <sup>a</sup>	$I$ / a.u.	$FWHM$ / nm		$\lambda^{\max}$ / nm <sup>a</sup>	$I$ / a.u.	$FWHM$ / nm
30	520, <u>549</u> , 576, 603	93.5	90.1	190	<u>549</u> , 576	100.3	93.8
40	520, <u>549</u> , 576, 603	93.4	88.8	200	549	100.8	94.1
50	520, <u>549</u> , 576, 603	93.4	88.3	210	549	101.3	94.5
60	520, <u>549</u> , 576, 603	93.1	88.0	220	549	101.9	94.8
70	520, <u>549</u> , 576, 603	93.1	88.4	230	549	102.1	94.8
80	520, <u>549</u> , 576, 603	93.5	88.8	240	549	101.8	94.9
90	520, <u>549</u> , 576, 603	93.8	88.9	250	549	103.1	95.4
100	520, <u>549</u> , 576	94.1	89.4	260	549	103.7	95.6
110	520, <u>549</u> , 576	94.7	89.8	270	549	104.0	95.6
120	<u>549</u> , 576	95.2	89.9	280	549	103.6	95.8
130	<u>549</u> , 576	96.2	91.2	290	549	103.9	96.4
140	<u>549</u> , 576	96.3	91.5	300	549	105.3	96.7
150	<u>549</u> , 576	97.6	92.0	310	549	105.7	96.5
160	<u>549</u> , 576	98.3	92.8	320	549	106.6	97.0
170	<u>549</u> , 576	99.0	93.1	330	549	108.3	97.7
180	<u>549</u> , 576	99.5	93.2	$\Phi_{\text{em}}$		0.64	

<sup>a</sup>For the temperature range of 30–190 K, two or more well-distinguished maxima on the emission pattern are observed. The position of the main maximum at each temperature was underlined.

**Table S38** The CIE 1931 chromaticity  $x$  and  $y$  parameters of the solid-state photoluminescent properties of **Re<sub>2</sub>-bpn** material, detected at various indicated temperatures (see Fig. S30), shown together with one-dimensional *CCT* (correlated color temperature) and *Duv* (Delta  $u,v$ ) metrics\* representing a chromaticity coordinate system.

parameter		Re <sub>2</sub> -bpn						
		30 K	40 K	50 K	60 K	70 K	80 K	90 K
CIE 1931 chromaticity parameters	<i>x</i>	0.431	0.430	0.429	0.428	0.428	0.428	0.428
	<i>y</i>	0.551	0.552	0.553	0.554	0.554	0.555	0.555
<i>CCT</i> / K		3906	3929	3946	3960	3970	3969	3973
<i>Duv</i> / a.u		0.0517	0.0523	0.0527	0.0532	0.0534	0.0534	0.0535
		100 K	110 K	120 K	130 K	140 K	150 K	160 K
CIE 1931 chromaticity parameters	<i>x</i>	0.428	0.428	0.428	0.428	0.428	0.429	0.429
	<i>y</i>	0.555	0.554	0.554	0.554	0.553	0.554	0.553
<i>CCT</i> / K		3973	3969	3967	3963	3963	3955	3945
<i>Duv</i> / a.u		0.0535	0.0533	0.0533	0.0531	0.0532	0.0530	0.0527
		170 K	180 K	190 K	200 K	210 K	220 K	230 K
CIE 1931 chromaticity parameters	<i>x</i>	0.430	0.429	0.428	0.428	0.427	0.428	0.427
	<i>y</i>	0.553	0.553	0.553	0.553	0.553	0.553	0.553
<i>CCT</i> / K		3937	3942	3957	3957	3970	3968	3977
<i>Duv</i> / a.u		0.0525	0.0526	0.0529	0.0527	0.0530	0.0530	0.0532
		240 K	250 K	260 K	270 K	280 K	290 K	300 K
CIE 1931 chromaticity parameters	<i>x</i>	0.426	0.426	0.425	0.424	0.423	0.424	0.423
	<i>y</i>	0.553	0.553	0.553	0.554	0.553	0.554	0.554
<i>CCT</i> / K		3986	3988	4000	4018	4037	4028	403
<i>Duv</i> / a.u		0.0533	0.0534	0.0536	0.0538	0.0542	0.0543	0.0543
		310 K	320 K	330 K	–	–	–	–
CIE 1931 chromaticity parameters	<i>x</i>	0.421	0.421	0.420	–	–	–	–
	<i>y</i>	0.552	0.554	0.554	–	–	–	–
<i>CCT</i> / K		4050	4061	4075	–	–	–	–
<i>Duv</i> / a.u		0.0545	0.0547	0.0550	–	–	–	–

\*The *Duv* and *CCT* quality parameters are commented on below the Table S28 (see above).

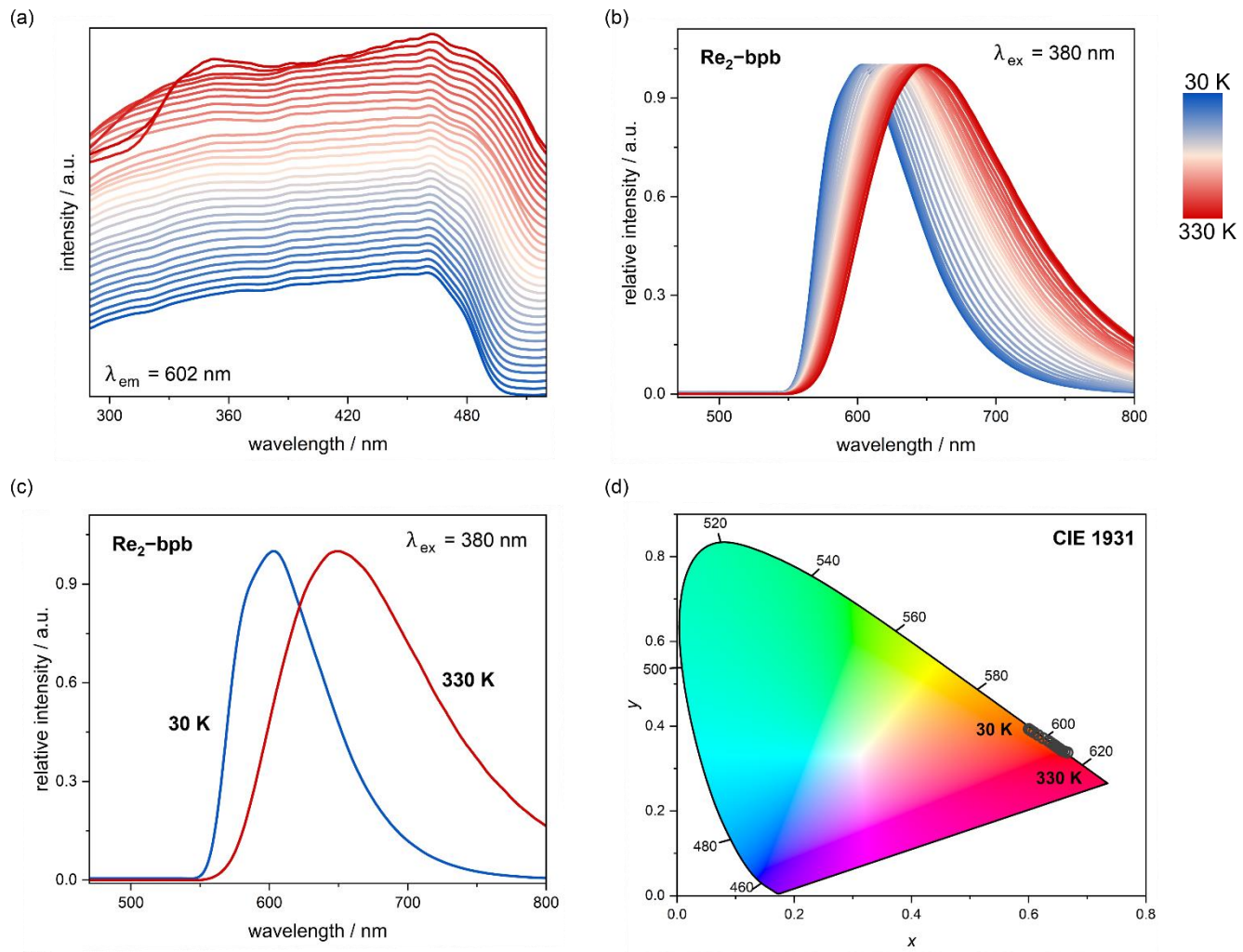


**Fig. S31** Solid-state photoluminescent properties of **Re<sub>2</sub>-bpb**: temperature-variable solid-state excitation (a) and emission (b) spectra collected under the indicated excitation and emission wavelengths, gathered in the 30–330 K temperature range, comparison of low- and high-temperature (30 and 330 K, respectively) emission spectra (c), and emission colors presented on the CIE 1931 chromaticity diagram (d). The related spectroscopic parameters of the emission patterns at each temperature are gathered in Table S39. The CIE 1931 chromaticity parameters, also determined at each temperature, are gathered in Table S40.

**Table S39** Selected spectroscopic parameters of the solid-state photoluminescent properties of **Re<sub>2</sub>-bpb** material, detected at various indicated temperatures (see Fig. S31), including emission pattern maxima ( $\lambda^{\max}$ ), the integral area under the emission peak ( $I$ ), and full width at half maximum for the emission band ( $FWHM$ ), as well as absolute quantum yield ( $\Phi_{\text{em}}$ , room-temperature value only).

Re <sub>2</sub> -bpb							
T / K	selected spectroscopic parameters			T / K	selected spectroscopic parameters		
	$\lambda^{\max}$ / nm	$I$ / a.u.	$FWHM$ / nm		$\lambda^{\max}$ / nm	$I$ / a.u.	$FWHM$ / nm
30	602	84.8	77.8	190	627	119.4	107.9
40	603	85.2	77.8	200	629	121.2	109.6
50	603	85.2	77.8	210	631	122.5	111.1
60	604	85.6	77.9	220	632	124.5	113.3
70	603	86.4	78.6	230	635	126.4	114.8
80	605	87.4	79.3	240	636	128.9	117.2
90	605	89.3	80.6	250	637	131.0	119.4
100	607	92.2	83.0	260	640	132.5	120.6
110	608	95.2	85.7	270	642	133.6	121.7
120	609	98.5	88.6	280	644	135.7	123.9
130	612	102.2	91.9	290	644	137.8	125.3
140	617	105.9	95.4	300	645	140.6	128.1
150	620	109.8	98.8	310	648	143.5	130.9
160	621	112.5	101.2	320	647	147.5	134.7
170	624	115.1	103.8	330	648	151.4	138.3
180	626	117.3	105.7	$\Phi_{\text{em}}$		0.41	

**Table S40** The CIE 1931 chromaticity  $x$  and  $y$  parameters of the solid-state photoluminescent properties of **Re<sub>2</sub>-bpb** material, detected at various indicated temperatures (see Fig. S31), shown together with one-dimensional CCT (correlated color temperature) and  $D_{uv}$  (Delta  $u,v$ ) metrics\* representing a chromaticity coordinate system.

parameter		Re <sub>2</sub> -bpb						
		30 K	40 K	50 K	60 K	70 K	80 K	90 K
CIE 1931 chromaticity parameters	$x$	0.600	0.601	0.602	0.603	0.605	0.607	0.609
	$y$	0.393	0.392	0.391	0.390	0.389	0.387	0.385
CCT / K		1721	1724	1727	1732	1738	1749	1763
$D_{uv}$ / a.u		0.0164	0.0171	0.0177	0.0185	0.0196	0.0214	0.0235
		100 K	110 K	120 K	130 K	140 K	150 K	160 K
CIE 1931 chromaticity parameters	$x$	0.612	0.616	0.620	0.624	0.630	0.634	0.636
	$y$	0.382	0.379	0.376	0.372	0.368	0.365	0.363
CCT / K		1790	1826	1872	1933	2012	2084	2138
$D_{uv}$ / a.u		0.0270	0.0312	0.0361	0.0421	0.0498	0.0560	0.0604
		170 K	180 K	190 K	200 K	210 K	220 K	230 K
CIE 1931 chromaticity parameters	$x$	0.639	0.641	0.643	0.644	0.646	0.648	0.649
	$y$	0.361	0.358	0.356	0.355	0.353	0.352	0.350
CCT / K		2203	2264	2328	2385	2439	2491	2542
$D_{uv}$ / a.u		0.0655	0.0702	0.0750	0.0790	0.0829	0.0865	0.0898
		240 K	250 K	260 K	270 K	280 K	290 K	300 K
CIE 1931 chromaticity parameters	$x$	0.650	0.652	0.653	0.655	0.656	0.658	0.659
	$y$	0.349	0.348	0.346	0.345	0.343	0.342	0.341
CCT / K		2592	2649	2709	2772	2852	2908	2961
$D_{uv}$ / a.u		0.0932	0.0968	0.1007	0.1048	0.1095	0.1130	0.1165
		310 K	320 K	330 K	-	-	-	-
CIE 1931 chromaticity parameters	$x$	0.662	0.663	0.666	-	-	-	-
	$y$	0.340	0.338	0.338	-	-	-	-
CCT / K		3042	3112	3190	-	-	-	-
$D_{uv}$ / a.u		0.1217	0.1256	0.1311	-	-	-	-

\*The  $D_{uv}$  and CCT quality parameters are commented on below the Table S28 (see above).

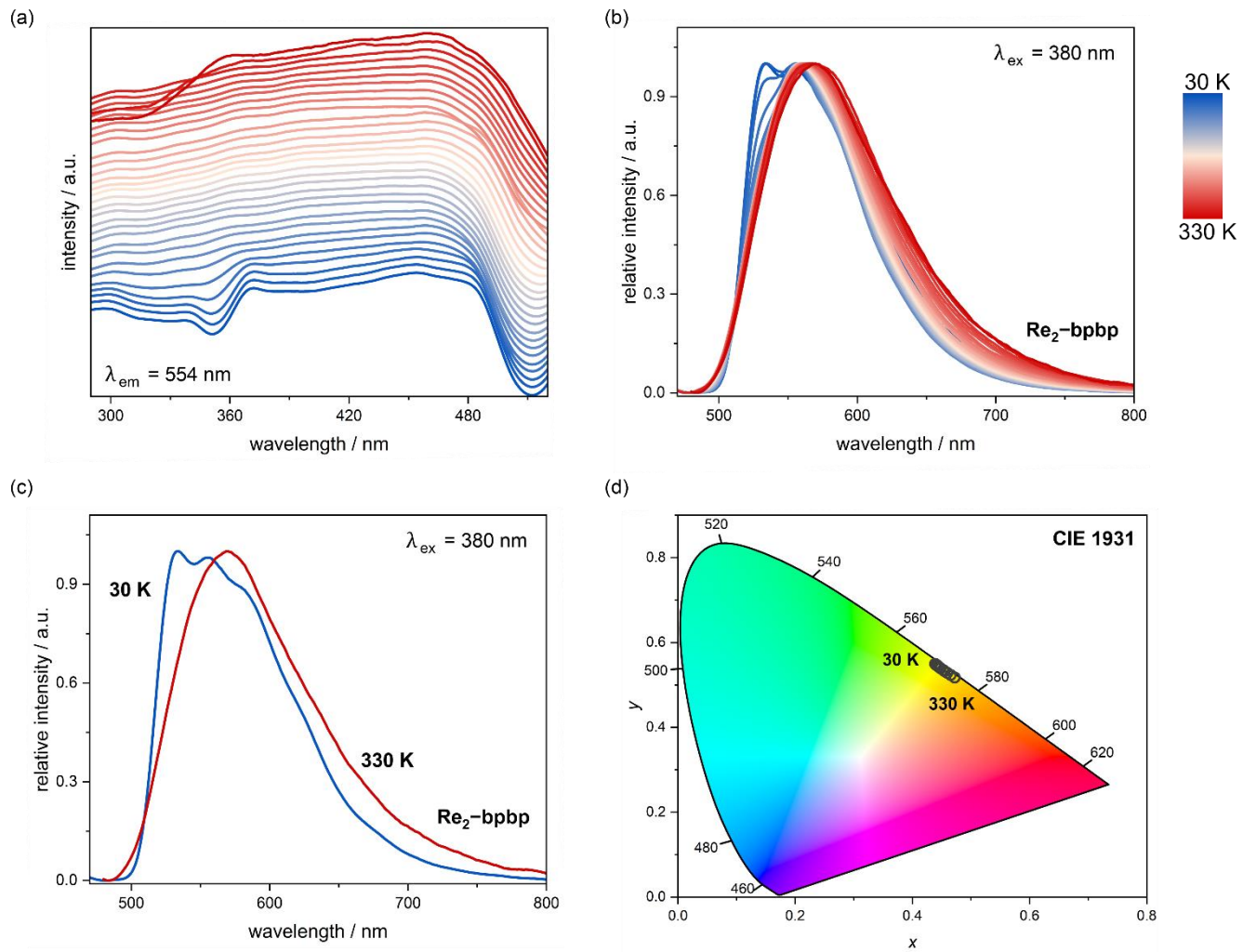


**Fig. S32** Solid-state photoluminescent properties of **Re<sub>2</sub>-bpbbp**: temperature-variable solid-state excitation (a) and emission (b) spectra collected under the indicated excitation and emission wavelengths, gathered in the 30–330 K temperature range, comparison of low- and high-temperature (30 and 330 K, respectively) emission spectra (c), and emission colors presented on the CIE 1931 chromaticity diagram (d). The related spectroscopic parameters of the emission patterns at each temperature are gathered in Table S41. The CIE 1931 chromaticity parameters, also determined at each temperature, are gathered in Table S42.

**Table S41** Selected spectroscopic parameters of the solid-state photoluminescent properties of **Re<sub>2</sub>-bpbp** material, detected at various indicated temperatures (see Fig. S32), including emission pattern maxima ( $\lambda^{\max}$ ), the integral area under the emission peak ( $I$ ), and full width at half maximum for the emission band ( $FWHM$ ), as well as absolute quantum yield ( $\Phi_{\text{em}}$ , room-temperature value only).

Re <sub>2</sub> -bpbp							
T / K	selected spectroscopic parameters			T / K	selected spectroscopic parameters		
	$\lambda^{\max}$ / nm <sup>a</sup>	$I$ / a.u.	$FWHM$ / nm		$\lambda^{\max}$ / nm <sup>a</sup>	$I$ / a.u.	$FWHM$ / nm
30	533, <u>554</u>	113.3	107.7	190	557	103.9	94.4
40	533, <u>554</u>	113.1	107.1	200	557	105.4	95.9
50	533, <u>554</u>	110.1	103.7	210	557	106.8	97.0
60	554.5	102.9	96.2	220	557	107.8	97.9
70	554.5	97.7	91.1	230	558	109.9	99.4
80	555	95.8	89.0	240	558.5	111.1	100.6
90	555	95.2	88.3	250	559	112.4	101.9
100	555	96.3	88.8	260	559	114.5	103.4
110	555	97.1	89.5	270	561	115.6	104.0
120	555.5	97.6	89.8	280	561	117.3	105.4
130	555.5	98.5	90.4	290	562	118.9	107.2
140	556	98.9	90.7	300	564	120.6	108.3
150	556	100.3	91.8	310	565	123.0	110.8
160	556.5	101.2	92.4	320	567	124.3	111.5
170	556.5	101.8	93.0	330	569	124.8	112.5
180	556.5	103.0	93.7	$\Phi_{\text{em}}$		0.71	

<sup>a</sup>For the temperature range of 30–50 K, two well-distinguished maxima on the emission pattern are observed. The position of the main maximum at each temperature was underlined.

**Table S42** The CIE 1931 chromaticity  $x$  and  $y$  parameters of the solid-state photoluminescent properties of  $\text{Re}_2\text{-bpbp}$  material, detected at various indicated temperatures (see Fig. S32), shown together with one-dimensional  $CCT$  (correlated color temperature) and  $D_{uv}$  (Delta  $u,v$ ) metrics\* representing a chromaticity coordinate system.

parameter		Re <sub>2</sub> -bpbp						
		30 K	40 K	50 K	60 K	70 K	80 K	90 K
CIE 1931 chromaticity parameters	$x$	0.442	0.441	0.441	0.440	0.439	0.439	0.439
	$y$	0.546	0.546	0.547	0.548	0.550	0.550	0.549
$CCT$ / K		3747	3755	3764	3785	3802	3805	3797
$D_{uv}$ / a.u		0.0480	0.0483	0.0486	0.0492	0.0497	0.0498	0.0496
		100 K	110 K	120 K	130 K	140 K	150 K	160 K
CIE 1931 chromaticity parameters	$x$	0.441	0.442	0.442	0.443	0.443	0.444	0.444
	$y$	0.547	0.546	0.546	0.545	0.545	0.544	0.544
$CCT$ / K		3761	3743	3738	3727	3721	3704	3706
$D_{uv}$ / a.u		0.0486	0.0481	0.0479	0.0476	0.0474	0.0469	0.0469
		170 K	180 K	190 K	200 K	210 K	220 K	230 K
CIE 1931 chromaticity parameters	$x$	0.445	0.445	0.446	0.447	0.448	0.450	0.453
	$y$	0.543	0.542	0.541	0.540	0.539	0.537	0.535
$CCT$ / K		3694	3687	3673	3653	3634	3607	3555
$D_{uv}$ / a.u		0.0466	0.0463	0.0459	0.0454	0.0448	0.0441	0.0427
		240 K	250 K	260 K	270 K	280 K	290 K	300 K
CIE 1931 chromaticity parameters	$x$	0.453	0.455	0.458	0.460	0.462	0.465	0.469
	$y$	0.534	0.532	0.530	0.528	0.526	0.523	0.520
$CCT$ / K		3547	3514	3474	3438	3391	3342	3277
$D_{uv}$ / a.u		0.0425	0.0416	0.0406	0.0396	0.0384	0.0372	0.0356
		310 K	320 K	330 K	-	-	-	-
CIE 1931 chromaticity parameters	$x$	0.472	0.469	0.472	-	-	-	-
	$y$	0.518	0.520	0.517	-	-	-	-
$CCT$ / K		3232	3278	3223	-	-	-	-
$D_{uv}$ / a.u		0.0345	0.0357	0.0343	-	-	-	-

\*The  $D_{uv}$  and  $CCT$  quality parameters are commented on below the Table S28 (see above).

## Description of the molecular DFT/TD-DFT theoretical calculations

To elucidate and better understand the underlying mechanism of the strong light absorption in the UV-vis range and visible emission, the DFT/TD-DFT methodology was considered. Initially, calculations were performed using the Gaussian 16 software<sup>S7</sup> employing the PBE0 exchange-correlation functional<sup>S8</sup> with a Def2TZVP basis set.<sup>S9</sup> Additionally, for the core electrons of Re(V) centers a suitable pseudo-potential was used (treating 15 valence electrons per Re(V) center), and the pseudopotential was parameterized to include scalar relativistic effects. Only the anionic dinuclear molecular fragments consisting of the two Re(V) centers (with CN<sup>-</sup> and N<sup>3-</sup> ligands) linked by a bridging ligand were studied, completely omitting the counterions present in the crystal structure. To compensate for the lack of a natural crystal matrix in which the considered anions are embedded all computations were done in the presence of solvent within the Polarizable Continuum Model (PCM), using solvation parameters for methanol.<sup>S10</sup>

For geometry optimizations, the PBE0 functional was coupled with the D3 version of Grimme's post-SCF dispersion correction with Becke-Johnson damping included, i.e., GD3BJ.<sup>S11</sup> In the first step, we tried to optimize the geometries from XRD experiments with VeryTight convergence criteria. However, it was found that in general the calculated frequencies from the Hessians were not free of considerable imaginary components connected with twisting of aromatic ring planes within extended ligands. It was checked that in most cases there is effectively negligible energy barrier associated with rotating the rings. Considering this fact it was decided to perform subsequent TD-DFT calculations using the geometry of the ground singlet state taken from the XRD experiments (100 K) where the rings are firmly held in well-defined positions by hydrogen bonds and other intramolecular interactions present in the crystal.

To simulate absorption spectra, the first hundred excited singlets were optimized using TD-DFT<sup>S12</sup> out of which energy and oscillator strengths of the first three were gathered in Tables S44, S46, S48, S50, S52, S54, S56, and S58, and compared with the experimental spectra in Fig. S33–S40. Selected electron transitions between ground and excited states are also presented in Fig. S33–S40. The energy of TD-DFT excitations is comparable with experimental data. It should be noted that our TD-DFT treatment lacks the inclusion of spin-orbit relativistic effects – scalar relativistic effects within the ZORA approximation are included within the employed effective core potential for Re – and the missing relativistic effects should be expected to broaden the spectra, where they completely accounted for.

To identify a possible mechanism of emission, we optimized the geometries of the first excited triplets (T1) and the first excited singles (S1) for all of the molecules and compared the energies to the experimental low-temperature luminescence spectra (Fig. S33–S40) interpreting transitions as vertical ones to the ground state. In all **Re<sub>2</sub>–L** materials, both ground states are of similar topologies and centered on the metal  $d_{xy}$  orbital, with significant contributions from the  $p_{\pi}$  (non-bonding) orbitals of the cyanido ligands.

In **Re<sub>2</sub>–CN**, the triplet excited states consist mainly of a  $p^*$  interaction between the nitrido  $p_{\pi}$  orbitals and the  $d_{xz}$  and  $d_{yz}$  orbitals located on the rhenium(5+) ions or are delocalized on both metal ions and the cyanido bridge between them. Similarly, the excited states in **Re<sub>2</sub>–en** are composed of nitrido  $p_{\pi}$  orbitals and the rhenium  $d_{xz}$  and  $d_{yz}$  orbitals, but with a much larger contribution to the perpendicular cyanido  $p_{\pi}$  orbitals of ligands. The computed emission wavelengths for both compounds are comparable to the experimental value, and they can be assigned to  $(d_{xy})^2 \leftarrow (d_{xy})^1(d_{\pi^*})^1$  ( $d_{\pi^*} = d_{xz}, d_{yz}$ ) transition with  $d_{\pi}-p_{\pi}(L)$  ( $L$  = nitrido and cyanido) overlap (or <sup>3</sup>MLCT+d-d involving the nitrido ligand).

In **Re<sub>2</sub>–bpy**, **Re<sub>2</sub>–bpac**, **Re<sub>2</sub>–bpee**, and **Re<sub>2</sub>–bpb**, there is a remarkable difference in the transition mechanism. In all complexes in this group, the emission transition is reasonably attributed to the  $(d_{xy})^2 \leftarrow \pi^*$  (ligand) charge transfer with small contributions from cyanido ligands to the ground state. The most complex composition of the excited

emissive state was calculated for **Re<sub>2</sub>-bpben** and **Re<sub>2</sub>-bpbp**. Part of their emissive states is located on the  $\pi^*$  orbitals of aromatic fragments of organic ligands, while the others are mainly calculated to be at side fragments of the molecule. These states are mainly delocalized within metal complexes and mostly result from the Re(V)  $d_{xz}$  or  $d_{yz}$  and nitrido  $p_\pi$  orbitals, however small contributions of cyanido ligands and pyridine heterocyclic ring can be also included. It follows that in the case of both these compounds, the luminescence is described by a mixed mechanism, from the rhenium(V)-centered  ${}^3[(d_{xy})^1(d_{\pi^*})^1]$  and  ${}^3\text{MLCT}$  states. It is worth noting, that the calculated transitions from  ${}^3\text{MLCT}$  states in **Re<sub>2</sub>-bpby**, **Re<sub>2</sub>-bpac**, **Re<sub>2</sub>-bpee**, and **Re<sub>2</sub>-bpb**, are much higher in energy (below 400 nm) and significantly differ from the experimentally observed emission bands. In the case of **Re<sub>2</sub>-bpben** and **Re<sub>2</sub>-bpbp**, these states are much closer to the experimental bands, so they were included in the analysis. Moreover, these conclusions are confirmed experimentally (see the main text). The whole postulated path of excitation involving the ca. 380 nm light involves consecutive non-emissive intersystem crossing with geometry relaxation of triplet excited states and final slow phosphorescence emission back to the ground singlet.

Seeking a more refined treatment that would include relativistic vector effects (spin-orbit coupling) we turned our attention to the ORCA 5.0.3 quantum chemistry program package.<sup>S13</sup> Here, the set of new theoretical calculations was carried out for **Re<sub>2</sub>-bpby** and **Re<sub>2</sub>-bpee** once again using the experimental geometry of an anion complex  $\{[\text{Re}^{IV}(\text{CN})_4(\text{N})](\text{L})\}^{2-}$ , consisting of the two Re(V) centers (with CN<sup>-</sup> and N<sup>3-</sup> ligands) linked by a bridging ligand. The counter ions and solvent molecules present in the crystal structure were again completely omitted. This time the B3LYP hybrid exchange-correlation energy functional was employed,<sup>S14,S15</sup> which presented its reasonable performance for predicting the geometry parameters of ground and excited states, as well as, excitation energies for various organic and metal transition compounds.<sup>S16,S17</sup> The def2-TZVP basis set was used together with the charge-dependent atom-pairwise dispersion correction using D4(EEQ)-ATM model.<sup>S9,S18</sup>

For the calculations, the LR-CPCM solvation model was used with chloroform as a solvent.<sup>S19</sup> The restricted KS determinant of a ground state served then as a reference one for the SOC TD-DFT calculations in the next step. To simulate UV-vis spectra, singlet excited states were optimized using TD-DFT and then mixed with calculated triplet excited states for the experimental geometry. Scalar relativistic effects were included using the 0<sup>th</sup> order regular approximation (ZORA)<sup>S20,S21</sup> with a compatible segmented all-electron relativistically contracted basis set SARC-ZORA-TZVP with SARC/J option (general-purpose Coulomb fitting basis set for all-electron calculations which reduces to def2/J for atoms up to Kr and specially implemented auxiliary basis set for atoms beyond Kr, that is Re in this case).<sup>S22,S23</sup> To accelerate the computation of two-electron integrals, in addition to the resolution of identity approximation for the Coulomb part (RIJ), the chain of spheres algorithm for the exchange part (COSX) was used.<sup>S24,S25</sup> The spin-orbit integrals were calculated using the RI-SOMF(1X) approximation that is: using mean-field potential with the inclusion of 1-electron terms together with Coulomb term computed with RI approximation and exchange terms evaluated via one-center exact integrals including the spin-other orbit interaction omitting DFT local correlation terms.<sup>S26</sup> The maximum number of centers to include in the integrals was set to 4.

The list of the selected lowest energy excited singlet states (for the geometry of the ground state optimized in the previous step) is presented in Tables S59 and S61, together with SOC states obtained by mixing singlets and triplets with the calculated SO-coupling. The theoretical UV-vis spectra from Fig. S41 and S44 were simulated using the orca\_mapspc tool with a broadening of 1800 cm<sup>-1</sup> for singlets only (TD-DFT) and spin-orbit states (SOC-corrected) compared to the experimental one. The relevant molecular orbitals with the highest contribution to the first singlet and triplet states (Tables S59 and S61) are presented in Fig. S41 and S44.

To better understand the mechanism of absorption (and later the emission from those levels), difference electron density maps for the first 10 excited SO-states were plotted in Fig. S41 and S44. After the inspection, it can be seen

that the transitions are of rhenium-centered d-d and metal-to-ligand charge transfer (MLCT) character with a slight admixture of cyanido and nitrido ligands.

In the last step, to better elucidate the observed luminescence, we simply performed the geometry optimization of the first excited SO-state taking advantage of the possibility to calculate Hessians for mixed SO states in ORCA software. After the optimization, we presented the first few relevant SOC corrected states for the new geometry in Tables S60 and S62 together with the MOs in Fig. S42 and S45. The computed emission wavelengths for both compounds are comparable to the experimental value and can be reasonably attributed to the  $(d_{xy})^2 \leftarrow \pi^*$  (ligand) charge transfer transition with small contributions from CN ligands to the ground state. The obtained energies of SO-states were compared with the emission spectra of **Re<sub>2</sub>-bpy** and **Re<sub>2</sub>-bpee**. We did not present relative intensities and therefore lifetimes of the simulated emission bands based on calculated dipole-transition moments, because of the significant impact of vibronic coupling and intersystem crossing rates whose simulations are beyond the scope of this work.

The set of representative results of the described molecular DFT/TD-DFT calculations is included in the following Fig. S33–S46 and Tables S43–S62. Next, in this Supporting Information, the periodic theoretical calculations are described (see below Table S62 and the next pages).

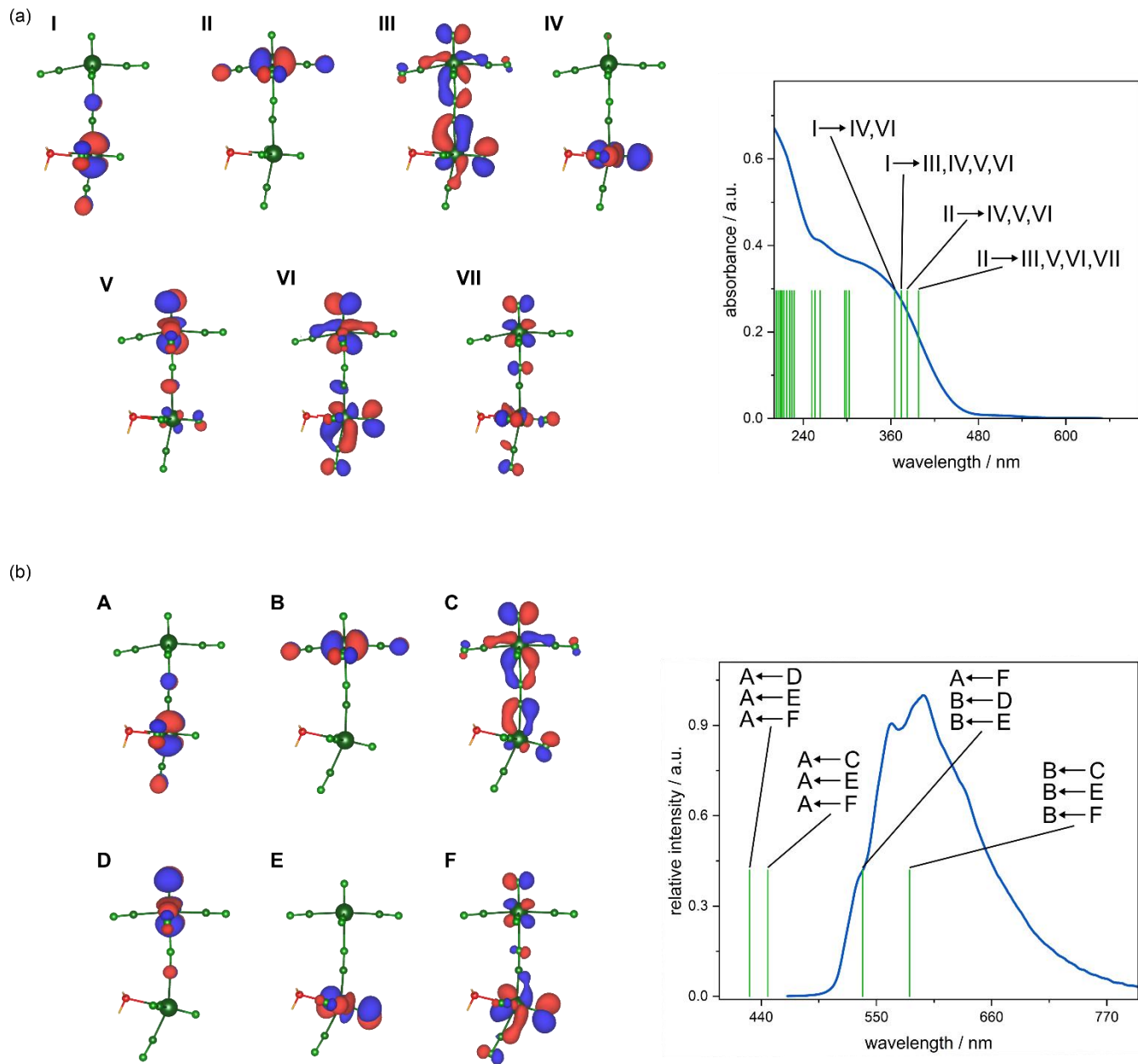


**Fig. S33** Contour plots of chosen MO corresponding to the TD-DFT singlet excitations (a) as well as for optimized excited triplet state geometry (b) in  $\text{Re}_2\text{-CN}$ , together with the comparison of solid-state UV-vis absorption spectra with the excitation energies predicted for the lowest energy excited states and comparison of the low-temperature emission spectrum (30 K) with the emission energies predicted for the lowest energy excited states using the TD-DFT theoretical calculations (green lines). The contours of MO are presented with a 0.05 isovalue level. The transition(s) energies are presented in Table S44.

**Table S43** Selected optimized and experimental bond lengths and angles for complexes in **Re<sub>2</sub>-CN** (see Description of the molecular DFT/TD-DFT theoretical calculations on Page S88 for details).

structure	parameters / Å, °				
	Re1/Re2≡N	Re-C	Re1/Re2-N	N≡Re-C (av.)	N-Re1/Re2≡N
SC-XRD (100 K)	1.654(4)/ 1.670(4)	2.092(5) – 2.109(5)	2.340(4) / 2.422(3)	85.43(16) – 91.31(17)	176.99(15)/ 179.70(15)
ground state	1.654/1.670	2.10 – 2.11	2.422/2.339	95.66 – 101.12	176.83/179.32
excited state	1.748/1.651	2.09 – 2.13	2.572/2.351	92.68 – 99.71	179.32/176.83

**Table S44** The excitation energies of the lowest energy excited states and emission energies predicted for the lowest energy excited states using the TD-DFT calculations in **Re<sub>2</sub>-CN** (green lines in Fig. S33).

<b>Re<sub>2</sub>-CN</b>				
DFT lowest energy singlet excitations				
transition(s) (% contribution)	II → III (61 %) II → V (5 %) II → VI (25 %) II → VII (9 %)	II → IV (5 %) II → V (83 %) II → VI (9 %)	I → III (78 %) I → IV (2 %) I → V (4 %) I → VI (16 %)	I → IV (97 %) I → VI (3 %)
transition(s) energy	398.3 nm (25108.6 cm <sup>-1</sup> )	382.4 nm (26150.6 cm <sup>-1</sup> )	374.5 nm (26705.8 cm <sup>-1</sup> )	365.4 nm (27370.3 cm <sup>-1</sup> )
oscillator strength	<i>f</i> = 0.0015	<i>f</i> = 0.0006	<i>f</i> = 0.0016	<i>f</i> = 0.0015
DFT lowest energy triplet emissions				
transition(s) (% contribution)	B ← C (85 %) B ← E (3 %) B ← F (12 %)	A ← F (4 %) B ← D (93 %) B ← E (3 %)	A ← C (31 %) A ← E (57 %) A ← F (12 %)	A ← D (46 %) A ← E (15 %) A ← F (39 %)
transition(s) energy	581.6 nm (17194.2 cm <sup>-1</sup> )	536.8 nm (18630.3 cm <sup>-1</sup> )	446.6 nm (22390.9 cm <sup>-1</sup> )	429.0 nm (23310.0 cm <sup>-1</sup> )

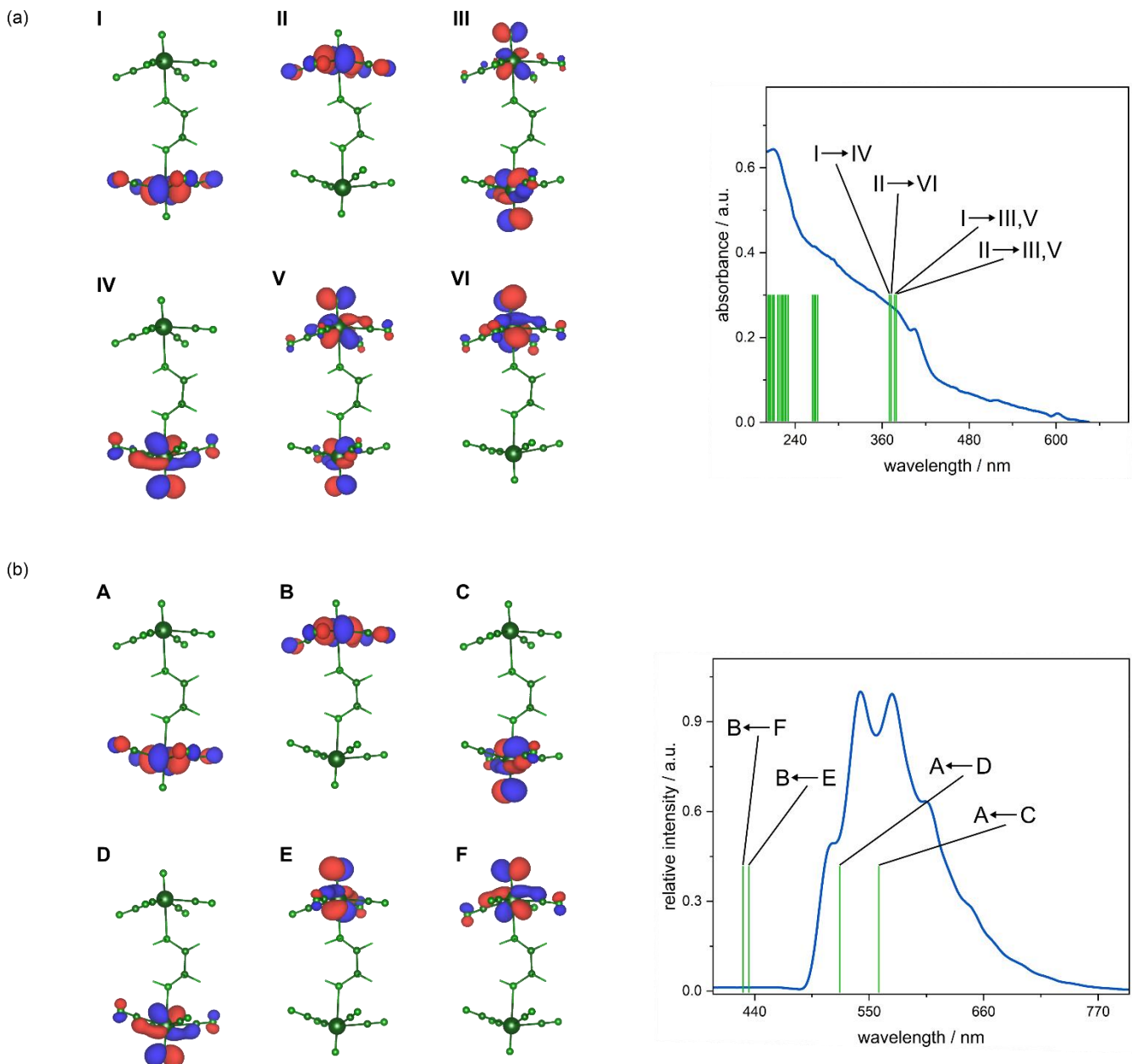


**Fig. S34** Contour plots of chosen MO corresponding to the TD-DFT singlet excitations (a) as well as for optimized triplet state geometry (b) in **Re<sub>2</sub>-en**, together with the comparison of solid-state UV-vis absorption spectra with the excitation energies predicted for the lowest energy excited states and comparison of the low-temperature emission spectrum (30 K) with the emission energies predicted for the lowest energy excited states using the TD-DFT theoretical calculations (green lines). The contours of MO are presented with a 0.05 isovalue level. The transition(s) energies are presented in Table S46.

**Table S45** Selected optimized and experimental bond lengths and angles for complexes in **Re<sub>2</sub>-en** (see Description of the molecular DFT/TD-DFT theoretical calculations on Page S88 for details).

structure	parameters / Å, °				
	Re1/Re2≡N	Re-C	Re1/Re2-N	N≡Re-C (av.)	N-Re1/Re2≡N
SC-XRD (100 K)	1.667(3)/ 1.667(3)	2.097(4) – 2.117(4)	2.521(3)/ 2.501(3)	97.50(14) – 101.37(14)	176.83(12)/ 176.13(13)
ground state	1.667/1.667	2.09 – 2.13	2.521/2.501	89.11 – 100.44	176.83/176.13
excited state	1.661/1.749	2.11 – 2.13	2.575/2.513	89.11 – 100.44	177.71/178.47

**Table S46** The excitation energies of the lowest energy excited states and emission energies predicted for the lowest energy excited states using the TD-DFT calculations in **Re<sub>2</sub>-en** (green lines in Fig. S34).

<b>Re<sub>2</sub>-en</b>				
DFT lowest energy singlet excitations				
transition(s) (% contribution)	II → III (64 %) II → V (36 %)	I → III (37 %) I → V (63 %)	II → VI (100 %)	I → IV (100 %)
transition(s) energy	378.6 nm (26415.2 cm <sup>-1</sup> )	377.1 nm (26520.3 cm <sup>-1</sup> )	373.9 nm (26744.4 cm <sup>-1</sup> )	372.6 nm (26836.3 cm <sup>-1</sup> )
oscillator strength	f = 0.0015	f = 0.0011	f = 0.0006	f = 0.0009
DFT lowest energy triplet emissions				
transition(s) (% contribution)	A ← C (100 %)	A ← D (100 %)	B ← E (100 %)	B ← F (100 %)
transition(s) energy	559.0 nm (17888.1 cm <sup>-1</sup> )	521.6 nm (19173.6 cm <sup>-1</sup> )	429.1 nm (23302.4 cm <sup>-1</sup> )	427.7 nm (23381.4 cm <sup>-1</sup> )

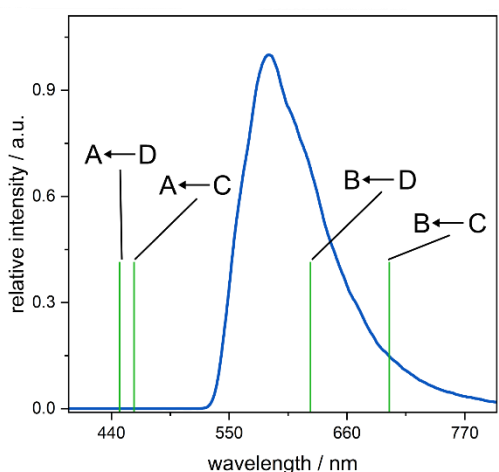
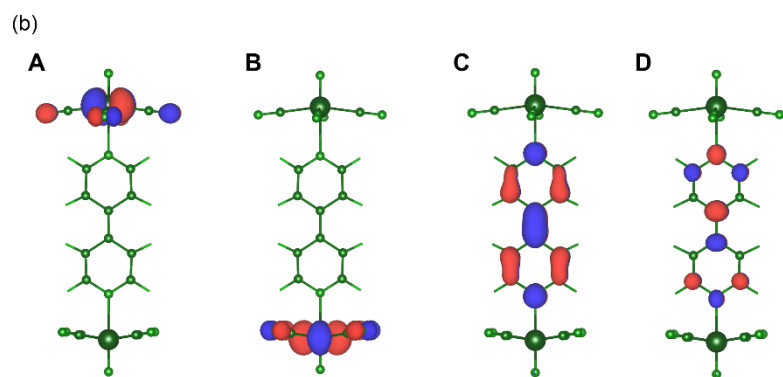
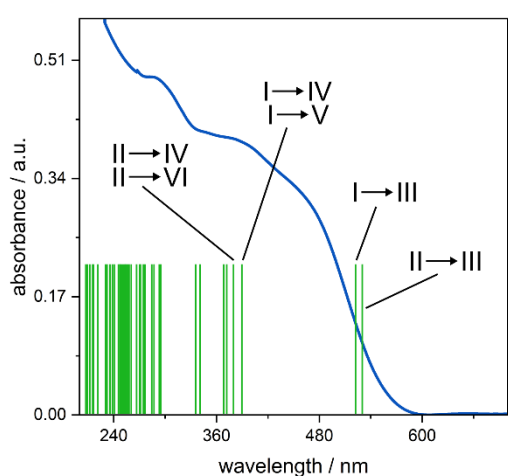
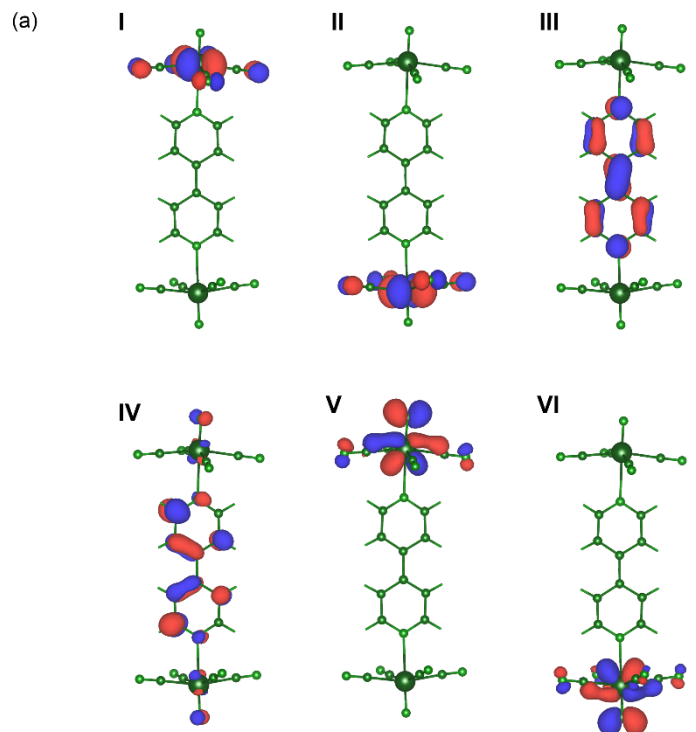


**Fig. S35** Contour plots of chosen MO corresponding to the TD-DFT singlet excitations (a) as well as for optimized excited triplet state geometry (b) in **Re<sub>2</sub>-bpy**, together with the comparison of solid-state UV-vis absorption spectra with the excitation energies predicted for the lowest energy excited states and comparison of the low-temperature emission spectrum (30 K) with the emission energies predicted for the lowest energy excited states using the TD-DFT theoretical calculations (green lines). The contours of MO are presented with a 0.05 isovalue level. The transition(s) energies are presented in Table S48.

**Table S47** Selected optimized and experimental bond lengths and angles for complexes in **Re<sub>2</sub>-bpy** (see Description of the molecular DFT/TD-DFT theoretical calculations on Page S88 for details).

structure	parameters / Å, °				
	Re≡N	Re-C	Re-N	N≡Re-C (av.)	N-Re≡N
SC-XRD (100 K)	1.659(2)	2.095(3) – 2.108(3)	2.593(2)	98.90(12) – 100.05(12)	176.90 (10)
ground state	1.661/1.662	2.10 – 2.12	2.586/2.523	96.13 – 100.70	178.17/179.52
excited state	1.660/1.666	2.11 – 2.12	2.581/2.367	96.73 – 99.72	179.93/179.99

**Table S48** The excitation energies of the lowest energy excited states and emission energies predicted for the lowest energy excited states using the TD-DFT calculations in **Re<sub>2</sub>-bpy** (green lines in Fig. S35).

Re <sub>2</sub> -bpy				
DFT lowest energy singlet excitations				
transition(s) (% contribution)	II → III (100 %)	I → III (100 %)	I → IV (97 %) I → V (3 %)	II → IV (96 %) II → VI (4 %)
transition(s) energy	534.2 nm (18718.5 cm <sup>-1</sup> )	524.6 nm (19064.0 cm <sup>-1</sup> )	390.1 nm (25635.8 cm <sup>-1</sup> )	380.4 nm (26290.9 cm <sup>-1</sup> )
oscillator strength	$f = 0.0001$	$f = 0.0006$	$f = 0.0016$	$f = 0.0013$
DFT lowest energy triplet emissions				
transition(s) (% contribution)	B ← C (100 %)	B ← D (100 %)	A ← C (100 %)	A ← D (100 %)
transition(s) energy	698.4 nm (14319.5 cm <sup>-1</sup> )	627.5 nm (15937.5 cm <sup>-1</sup> )	455.8 nm (23302.4 cm <sup>-1</sup> )	447.9 nm (23381.4 cm <sup>-1</sup> )

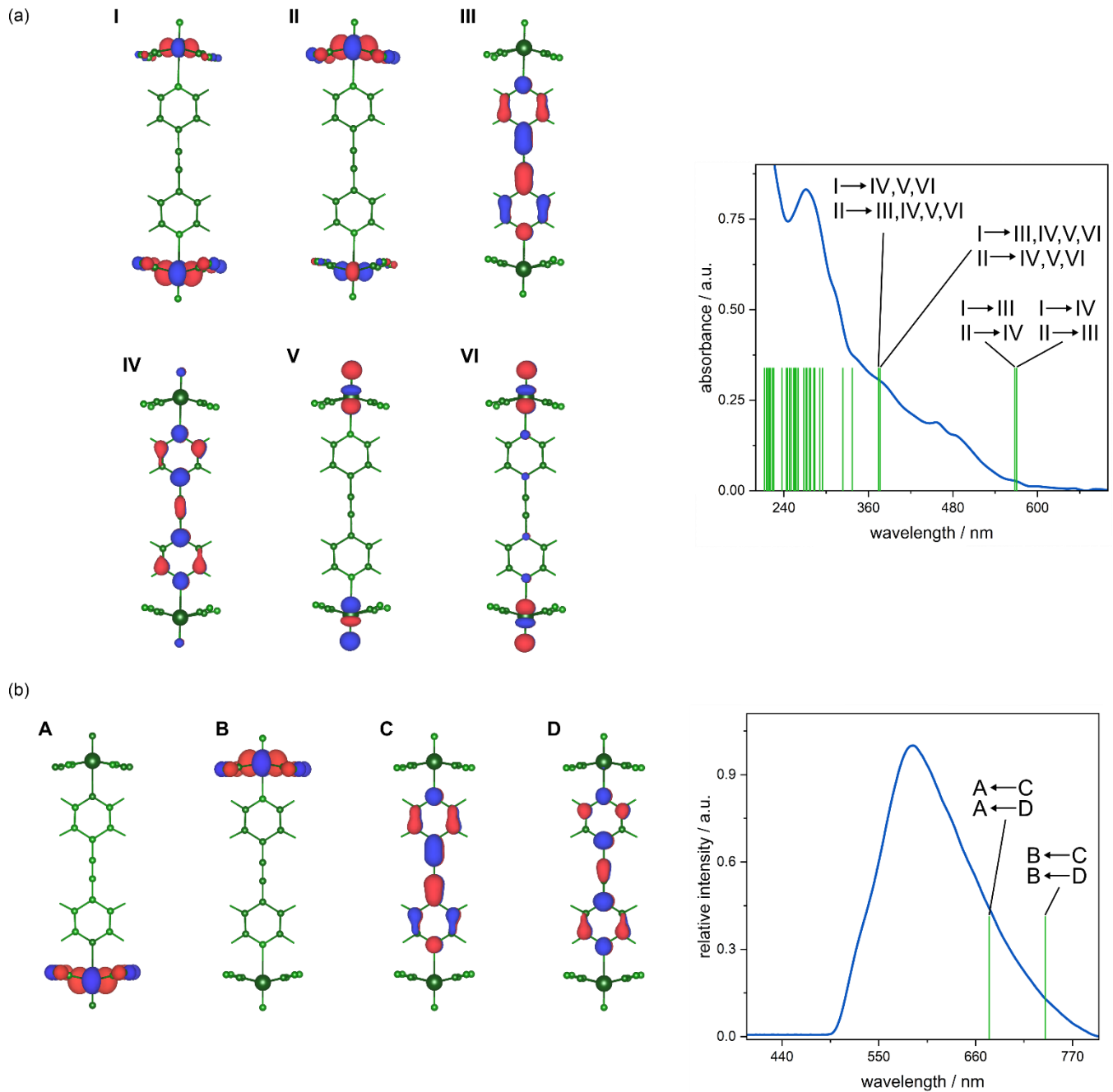


**Fig. S36** Contour plots of chosen MO corresponding to the TD-DFT singlet excitations (a) as well as for optimized excited triplet state geometry (b) in **Re<sub>2</sub>-bpac**, together with the comparison of solid-state UV-vis absorption spectra with the excitation energies predicted for the lowest energy excited states and comparison of the low-temperature emission spectrum (30 K) with the emission energies predicted for the lowest energy excited states using the TD-DFT theoretical calculations (green lines). The contours of MO are presented with a 0.05 isovalue level. The transition(s) energies are presented in Table S50.

**Table S49** Selected optimized and experimental bond lengths and angles for complexes in **Re<sub>2</sub>-bpac** (see **Description of the molecular DFT/TD-DFT theoretical calculations** on Page S88 for details).

structure	parameters / Å, °				
	Re≡N	Re-C	Re-N	N≡Re-C (av.)	N-Re≡N
SC-XRD (100 K)	1.659(3)	2.103(3) – 2.114(3)	2.547(2)	99.02(12) – 101.01(12)	177.99(11)
ground state	1.660/1.660	2.10 – 2.11	2.547/2.547	99.10 – 100.90	178.07/178.07
excited state	1.661/1.662	96.98 – 99.44	2.550/2.387	96.98 – 100.90	179.98/180.00

**Table S50** The excitation energies of the lowest energy excited states and emission energies predicted for the lowest energy excited states using the TD-DFT calculations in **Re<sub>2</sub>-bpac** (green lines in Fig. S36).

<b>Re<sub>2</sub>-bpac</b>				
DFT lowest energy singlet excitations				
transition(s) (% contribution)	I → IV (3 %) II → III (97 %)	I → III (97 %) II → IV (3 %)	I → III (3 %) I → IV (23 %) I → V (29 %) I → VI (16 %) II → IV (14 %) II → V (7 %) II → VI (9 %)	I → IV (14 %) I → V (6 %) I → VI (9 %) II → III (3 %) II → IV (23 %) II → V (28 %) II → VI (16 %)
transition(s) energy	569.8 nm (17550.3 cm <sup>-1</sup> )	569.8 nm (17551.6 cm <sup>-1</sup> )	376.3 nm (26571.7 cm <sup>-1</sup> )	376.3 nm (26574.5 cm <sup>-1</sup> )
oscillator strength	f = 0.0008	f = 0.0000	f = 0.0007	f = 0.0011
DFT lowest energy triplet emissions				
transition(s) (% contribution)	B ← C (97 %) B ← D (3 %)		A ← C (97 %) A ← D (3 %)	
transition(s) energy	743.8 nm (13444.5 cm <sup>-1</sup> )		679.8 nm (14710.6 cm <sup>-1</sup> )	

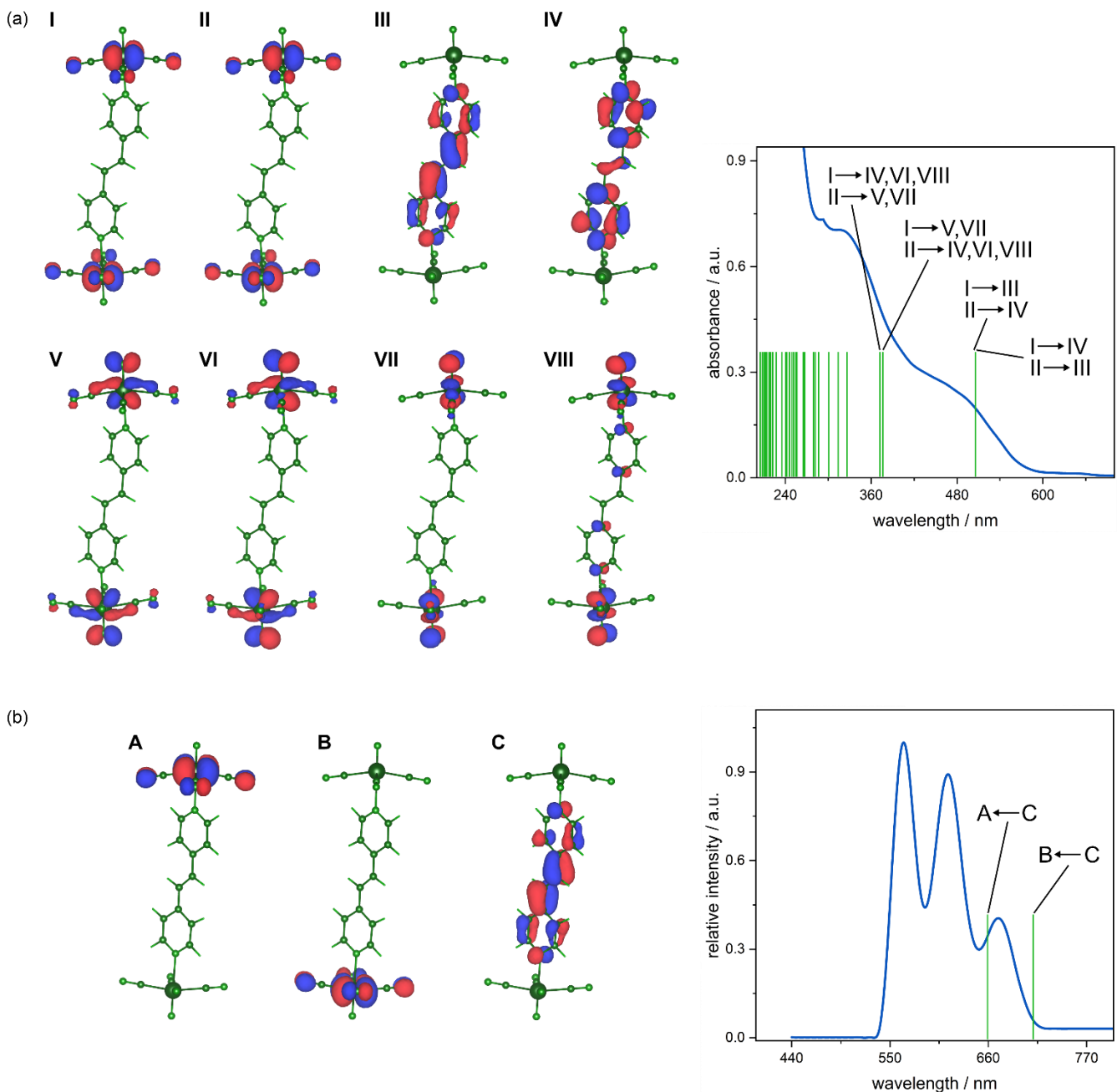


**Fig. S37** Contour plots of chosen MO corresponding to the TD-DFT singlet excitations (a) as well as for optimized excited triplet state geometry (b) in **Re<sub>2</sub>-bpee**, together with the comparison of solid-state UV-vis absorption spectra with the excitation energies predicted for the lowest energy excited states and comparison of the low-temperature emission spectrum (30 K) with the emission energies predicted for the lowest energy excited states using the TD-DFT theoretical calculations (green lines). The contours of MO are presented with a 0.05 isovalue level. The transition(s) energies are presented in Table S52.

**Table S51** Selected optimized and experimental bond lengths and angles for complexes in **Re<sub>2</sub>-bpEE** (see **Description of the molecular DFT/TD-DFT theoretical calculations** on Page S88 for details).

structure	parameters / Å, °				
	Re≡N	Re-C	Re-N	N≡Re-C (av.)	N-Re≡N
SC-XRD (100 K)	1.660(4)	2.096(5) – 2.109(5)	2.514(3)	98.3(2) – 100.67(19)	178.88(18)
ground state	1.660/1.660	2.09 – 2.11	2.514/2.514	98.32 – 100.67	178.89/178.90
excited state	1.662/1.660	2.11 – 2.12	2.534/2.398	97.22 – 99.27	179.94/179.93

**Table S52** The excitation energies of the lowest energy excited states and emission energies predicted for the lowest energy excited states using the TD-DFT calculations in **Re<sub>2</sub>-bpEE** (green lines in Fig. S37).

<b>Re<sub>2</sub>-bpEE</b>				
DFT lowest energy singlet excitations				
transition(s) (% contribution)	I → IV (3 %) II → III (97 %)	I → III (97 %) II → IV (3 %)	I → V (41 %) I → VII (3 %) II → IV (19 %) II → VI (27 %) II → VIII (9 %)	I → IV (19 %) I → VI (27 %) I → VIII (9 %) II → V (41 %) II → VII (3 %)
transition(s) energy	509.2 nm (19637.1 cm <sup>-1</sup> )	509.2 nm (19637.5 cm <sup>-1</sup> )	377.1 nm (26519.6 cm <sup>-1</sup> )	375.1 nm (26661.0 cm <sup>-1</sup> )
oscillator strength	f = 0.0002	f = 0.0000	f = 0.0000	f = 0.0025
DFT lowest energy triplet emissions				
transition(s) (% contribution)	B ← C (100 %)		A ← C (100 %)	
transition(s) energy	707.9 nm (14127.3 cm <sup>-1</sup> )		658.8 nm (15178.2 cm <sup>-1</sup> )	

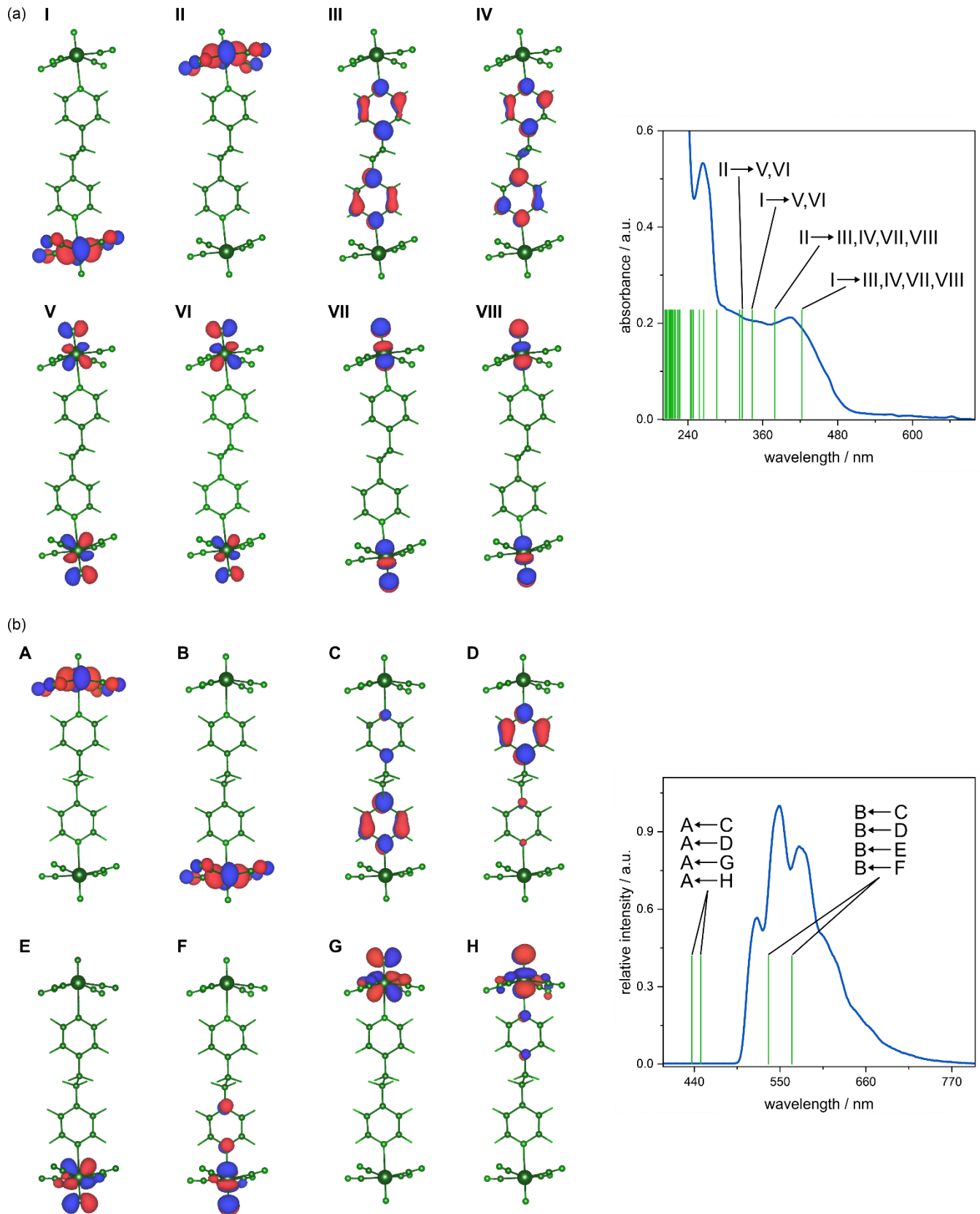


**Fig. S38** Contour plots of chosen MO corresponding to the TD-DFT singlet excitations (a) as well as for optimized excited triplet state geometry (b) in  $\text{Re}_2\text{-bpen}$ , together with the comparison of solid-state UV-vis absorption spectra with the excitation energies predicted for the lowest energy excited states and comparison of the low-temperature emission spectrum (30 K) with the emission energies predicted for the lowest energy excited states using the TD-DFT theoretical calculations (green lines). The contours of MO are presented with a 0.05 isovalue level. The transition(s) energies are presented in Table S54.

**Table S53** Selected optimized and experimental bond lengths and angles for complexes in **Re<sub>2</sub>-bpn** (see **Description of the molecular DFT/TD-DFT theoretical calculations** on Page S88 for details).

structure	parameters / Å, °				
	Re≡N	Re-C	Re-N	N≡Re-C (av.)	N-Re≡N
SC-XRD (100 K)	1.665(2)	2.097(3) – 2.121(3)	2.477(2)	95.97(11) – 100.50(12)	179.09(10)
ground state	1.663/1.664	2.10 – 2.12	2.488/2.478	96.09 – 100.48	179.20/179.20
excited state	1.658/1.742	2.11 – 2.13	2.602/2.460	93.82 – 100.48	179.82/179.70

**Table S54** The excitation energies of the lowest energy excited states and emission energies predicted for the lowest energy excited states using the TD-DFT calculations in **Re<sub>2</sub>-bpn** (green lines in Fig. S38).

<b>Re<sub>2</sub>-bpn</b>				
DFT lowest energy singlet excitations				
transition(s) (% contribution)	I → III (52 %) I → IV (32 %) I → VII (8 %) I → VIII (8 %)	II → III (53 %) II → IV (32 %) II → VII (8 %) II → VIII (8 %)	I → V (61 %) I → VI (39 %)	II → V (40 %) II → VI (60 %)
transition(s) energy	422.5 nm (23669.8 cm <sup>-1</sup> )	422.5 nm (23670.3 cm <sup>-1</sup> )	378.9 nm (26392.2 cm <sup>-1</sup> )	378.9 nm (26393.6 cm <sup>-1</sup> )
oscillator strength	<i>f</i> = 0.0006	<i>f</i> = 0.0010	<i>f</i> = 0.0008	<i>f</i> = 0.0013
DFT lowest energy triplet emissions				
transition(s) (% contribution)	B ← C (32 %) B ← D (13 %) B ← E (35 %) B ← F (20 %)	B ← C (12 %) B ← D (2 %) B ← E (62 %) B ← F (24 %)	A ← C (18 %) A ← D (26 %) A ← G (30 %) A ← H (26 %)	A ← C (3 %) A ← D (11 %) A ← G (58 %) A ← H (28 %)
transition(s) energy	564.5 nm (17715.4 cm <sup>-1</sup> )	534.3 nm (18717.1 cm <sup>-1</sup> )	444.2 nm (22511.4 cm <sup>-1</sup> )	431.7 nm (23166.4 cm <sup>-1</sup> )

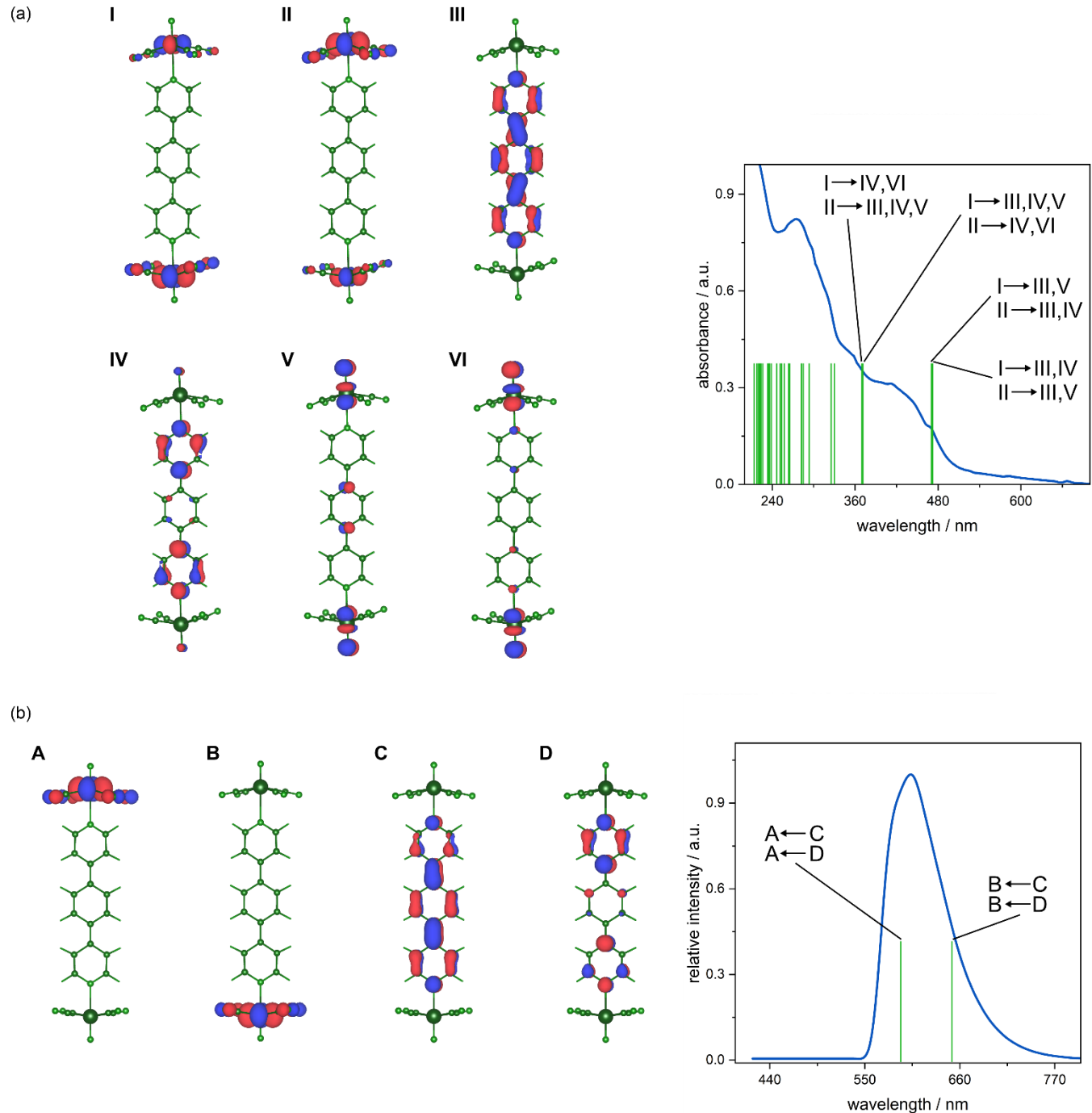


**Fig. S39** Contour plots of chosen MO corresponding to the TD-DFT singlet excitations (a) as well as for optimized excited triplet state geometry (b) in **Re<sub>2</sub>-bpb**, together with the comparison of solid-state UV-vis absorption spectra with the excitation energies predicted for the lowest energy excited states and comparison of the low-temperature emission spectrum (30 K) with the emission energies predicted for the lowest energy excited states using the TD-DFT theoretical calculations (green lines). The contours of MO are presented with a 0.05 isovalue level. The transition(s) energies are presented in Table S56.

**Table S55** Selected optimized and experimental bond lengths and angles for complexes in **Re<sub>2</sub>-bpb** (see Description of the molecular DFT/TD-DFT theoretical calculations on Page S88 for details).

structure	parameters / Å, °				
	Re≡N	Re-C	Re-N	N≡Re-C (av.)	N-Re≡N
SC-XRD (100 K)	1.656(3)	2.101(3) – 2.111(3)	2.487(2)	99.86(12) – 101.69(12)	177.57(11)
ground state	1.656/1.656	2.10 – 2.11	2.487/2.487	99.86 – 101.68	177.57/177.56
excited state	1.666/1.660	2.11 – 2.12	2.377/2.561	96.83 – 99.84	180.00/179.99

**Table S56** The excitation energies of the lowest energy excited states and emission energies predicted for the lowest energy excited states using the TD-DFT calculations in **Re<sub>2</sub>-bpb** (green lines in Fig. S39).

<b>Re<sub>2</sub>-bpb</b>				
DFT lowest energy singlet excitations				
transition(s) (% contribution)	I → III (8 %) I → IV (12 %) II → IV (78 %) II → V (2 %)	I → III (2 %) I → V (78 %) II → III (8 %) II → IV (12 %)	I → III (14 %) I → IV (3 %) I → V (27 %) II → IV (38 %) II → VI (18 %)	I → IV (38 %) I → VI (18 %) II → III (14 %) II → IV (3 %) II → V (27 %)
transition(s) energy	471.9 nm (21191.8 cm <sup>-1</sup> )	471.9 nm (21193.2 cm <sup>-1</sup> )	371.1 nm (26944.0 cm <sup>-1</sup> )	371.1 nm (26944.7 cm <sup>-1</sup> )
oscillator strength	f = 0.0013	f = 0.0000	f = 0.0000	f = 0.0013
DFT lowest energy triplet emissions				
transition(s) (% contribution)	B ← C (95 %) B ← D (5 %)		A ← C (96 %) A ← D (4 %)	
transition(s) energy	652.8 nm (15318.4 cm <sup>-1</sup> )		590.8 nm (16925.1 cm <sup>-1</sup> )	

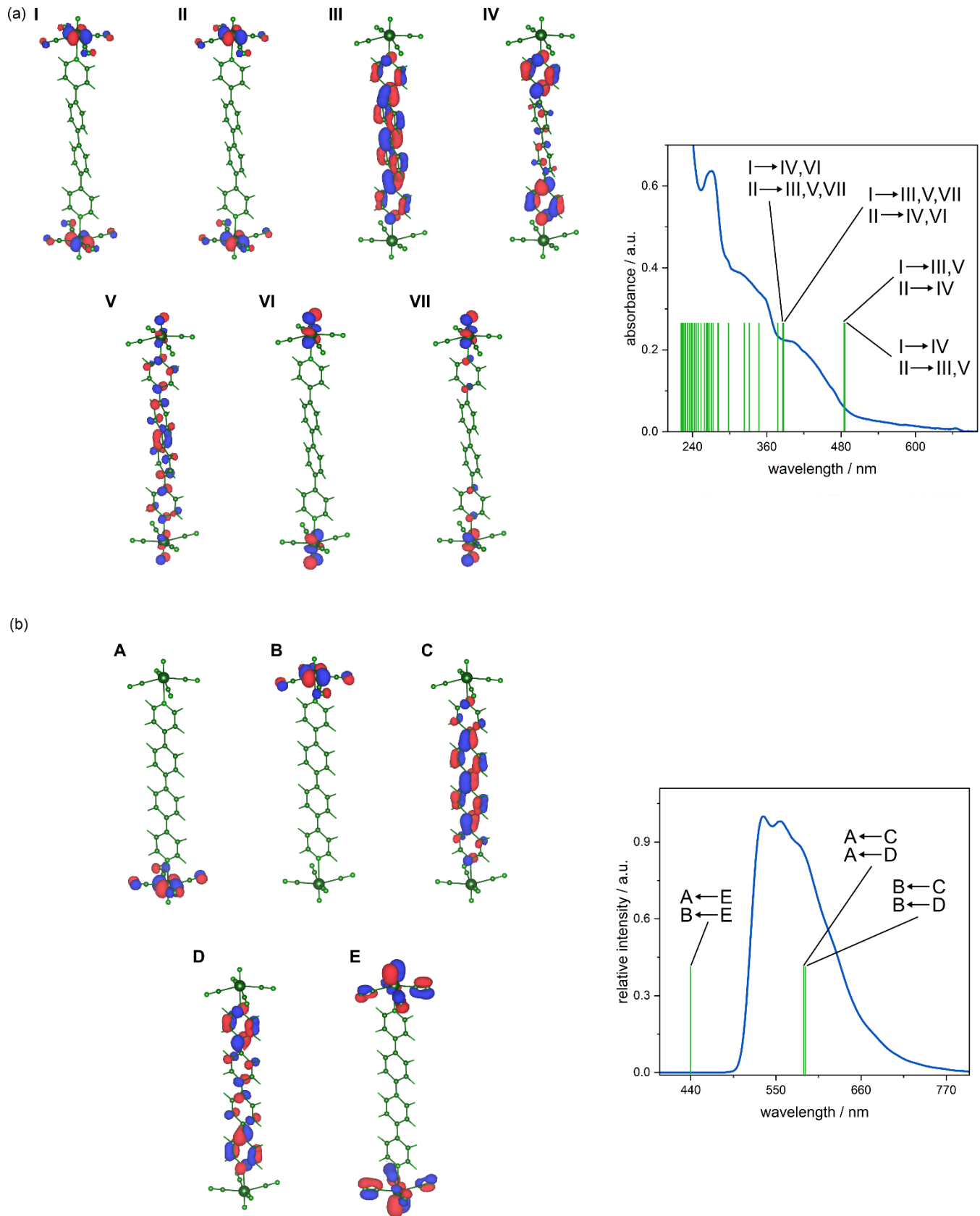


**Fig. S40** Contour plots of chosen MO corresponding to the TD-DFT singlet excitations (a) as well as for optimized excited triplet state geometry (b) in **Re<sub>2</sub>-bpbp**, together with the comparison of solid-state UV-vis absorption spectra with the excitation energies predicted for the lowest energy excited states and comparison of the low-temperature emission spectrum (30 K) with the emission energies predicted for the lowest energy excited states using the TD-DFT theoretical calculations (green lines). The contours of MO are presented with a 0.05 isovalue level. The transition(s) energies are presented in Table S58.

**Table S57** Selected optimized and experimental bond lengths and angles for complexes in **Re<sub>2</sub>-bpbp** (see **Description of the molecular DFT/TD-DFT theoretical calculations** on Page S88 for details).

structure	parameters / Å, °				
	Re≡N	Re-C	Re-N	N≡Re-C (av.)	N-Re≡N
SC-XRD (100 K)	1.662(4)	2.098(5) – 2.112(5)	2.509(3)	98.27(18) – 99.36(18)	179.10(16)
ground state	1.661/1.661	2.09 – 2.11	2.512/2.512	98.27 – 99.41	179.18/179.17
excited state	1.658/1.658	2.11 – 2.12	2.593/2.593	98.63 – 100.02	179.69/179.69

**Table S58** The excitation energies of the lowest energy excited states and emission energies predicted for the lowest energy excited states using the TD-DFT calculations in **Re<sub>2</sub>-bpbp** (green lines in Fig. S40).

<b>Re<sub>2</sub>-bpbp</b>				
DFT lowest energy singlet excitations				
transition(s) (% contribution)	I → IV (14 %) II → III (83 %) II → V (3 %)	I → III (83 %) I → V (3 %) II → IV (14 %)	I → III (18 %) I → V (14 %) I → VII (7 %) II → IV (49 %) II → VI (13 %)	I → IV (49 %) I → VI (13 %) II → III (18 %) II → V (14 %) II → VII (7 %)
transition(s) energy	486.9 nm (20539.4 cm <sup>-1</sup> )	486.9 nm (20539.8 cm <sup>-1</sup> )	387.8 nm (25784.5 cm <sup>-1</sup> )	387.8 nm (25784.5 cm <sup>-1</sup> )
oscillator strength	f = 0.0005	f = 0.0000	f = 0.0000	f = 0.0010
DFT lowest energy triplet emissions				
transition(s) (% contribution)	B ← C (96 %) B ← D (4 %)	A ← C (96 %) A ← D (4 %)	A ← E (48 %) B ← E (52 %)	A ← E (51 %) B ← E (49 %)
transition(s) energy	587.3 nm (17026.8 cm <sup>-1</sup> )	587.3 nm (17028.2 cm <sup>-1</sup> )	439.5 nm (22752.6 cm <sup>-1</sup> )	432.7 nm (23110.7 cm <sup>-1</sup> )

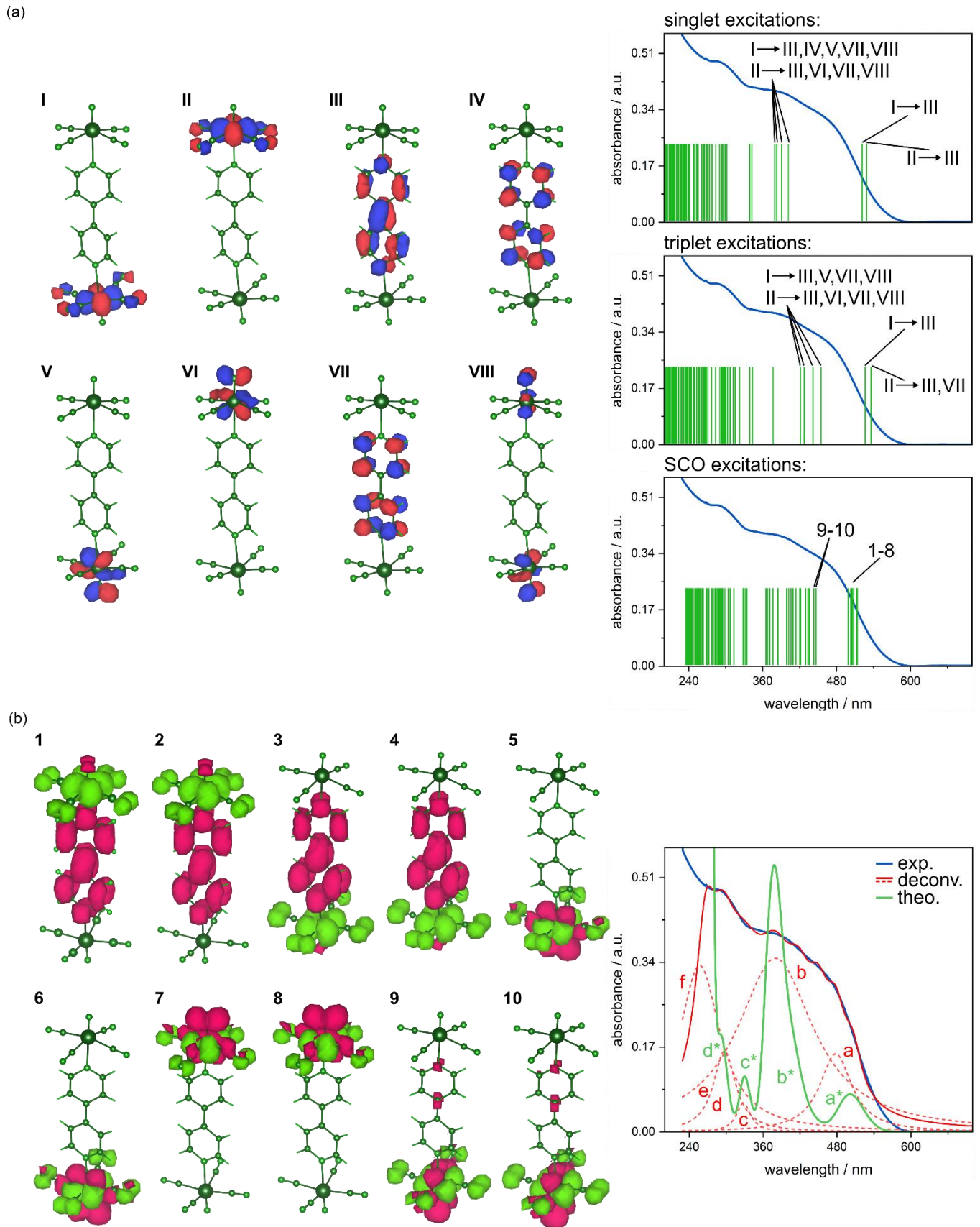


**Fig. S41** Contour plots (with the 0.05 isovalue level) of chosen MO corresponding to the TD-DFT singlet or triplet excitations (a) as well as differential contour plots (b) corresponding to changes in the orbital occupation during the transition between the ground and the respective excited spin-orbit coupled state (green - electron depletion, purple - electron gain) in **Re<sub>2</sub>-bpy**, together with the comparison of absorption spectra with the excitation energies predicted for the lowest energy excited states (a, right panel), and the comparison of the deconvoluted absorption spectra with the theoretically simulated spectrum (b, right panel). The transition(s) energies are presented in Table S59.

**Table S59** The predicted excitation energies of lowest energy singlet, triplet, and spin-orbit corrected excited states using the TD-DFT calculations in **Re<sub>2</sub>-bpy** (see Fig. S41) compared with deconvoluted experimental absorption spectra.

DFT lowest energy singlet excitations						
transition(s)	II → III	I → III	I → IV,V,VII	II → VI,VII	I → III, VIII	II → III, VIII
transition(s) energy	528.8 nm (18911 cm <sup>-1</sup> )	520.9 nm (19198 cm <sup>-1</sup> )	400.8 nm (24950 cm <sup>-1</sup> )	390.5 nm (25608 cm <sup>-1</sup> )	382.8 nm (26123 cm <sup>-1</sup> )	379.2 nm (26371 cm <sup>-1</sup> )
oscillator strength	<i>f</i> = 0.0002	<i>f</i> = 0.0006	<i>f</i> = 0.0024	<i>f</i> = 0.0024	<i>f</i> = 0.0010	<i>f</i> = 0.0012
DFT lowest energy triplet excitations						
transition(s)	II → III, VII	I → III II → VII	I → V, VII	II → VI, VII	I → III, VIII	II → III, VIII
transition(s) energy	536.2 nm (18650 cm <sup>-1</sup> )	526.9 nm (18979 cm <sup>-1</sup> )	454.4 nm (22007 cm <sup>-1</sup> )	440.9 nm (22681 cm <sup>-1</sup> )	427.2 nm (23408 cm <sup>-1</sup> )	421.2 nm (23742 cm <sup>-1</sup> )
DFT lowest energy spin-orbit corrected excitations						
state no.	1	2	3	4	5	
state energy	514.1 nm (19451 cm <sup>-1</sup> )	514.0 nm (19455 cm <sup>-1</sup> )	513.6 nm (19470 cm <sup>-1</sup> )	506.6 nm (19739 cm <sup>-1</sup> )	505.6 nm (19778 cm <sup>-1</sup> )	
oscillator strength	<i>f</i> = 0.0000	<i>f</i> = 0.0000	<i>f</i> = 0.0000	<i>f</i> = 0.0002	<i>f</i> = 0.0000	
composition	100 % triplet	100 % triplet	100 % triplet	100 % singlet	100 % triplet	
state no.	6	7	8	9	10	
state energy	505.5 nm (19782 cm <sup>-1</sup> )	505.3 nm (19790 cm <sup>-1</sup> )	499.3 nm (20028 cm <sup>-1</sup> )	446.3 nm (22406 cm <sup>-1</sup> )	446.2 nm (22411 cm <sup>-1</sup> )	
oscillator strength	<i>f</i> = 0.0000	<i>f</i> = 0.0000	<i>f</i> = 0.0006	<i>f</i> = 0.0000	<i>f</i> = 0.0001	
composition	100 % triplet	100 % triplet	100 % singlet	100 % triplet	100 % triplet	
comparison of deconvoluted experimental absorption spectra with DFT-predicted absorption bands						
transition	a	b	c	d	e	f
experimental absorption spectra	478 nm (20921 cm <sup>-1</sup> )	380 nm (26316 cm <sup>-1</sup> )	326 nm (30675 cm <sup>-1</sup> )	298 nm (33557 cm <sup>-1</sup> )	286 nm (34965 cm <sup>-1</sup> )	260 nm (38462 cm <sup>-1</sup> )
transition	a*	b*	c*	d*	-	-
DFT predicted absorption bands	501 nm (19960 cm <sup>-1</sup> )	378 nm (26455 cm <sup>-1</sup> )	329 nm (30395 cm <sup>-1</sup> )	291 nm (34364 cm <sup>-1</sup> )	-	-

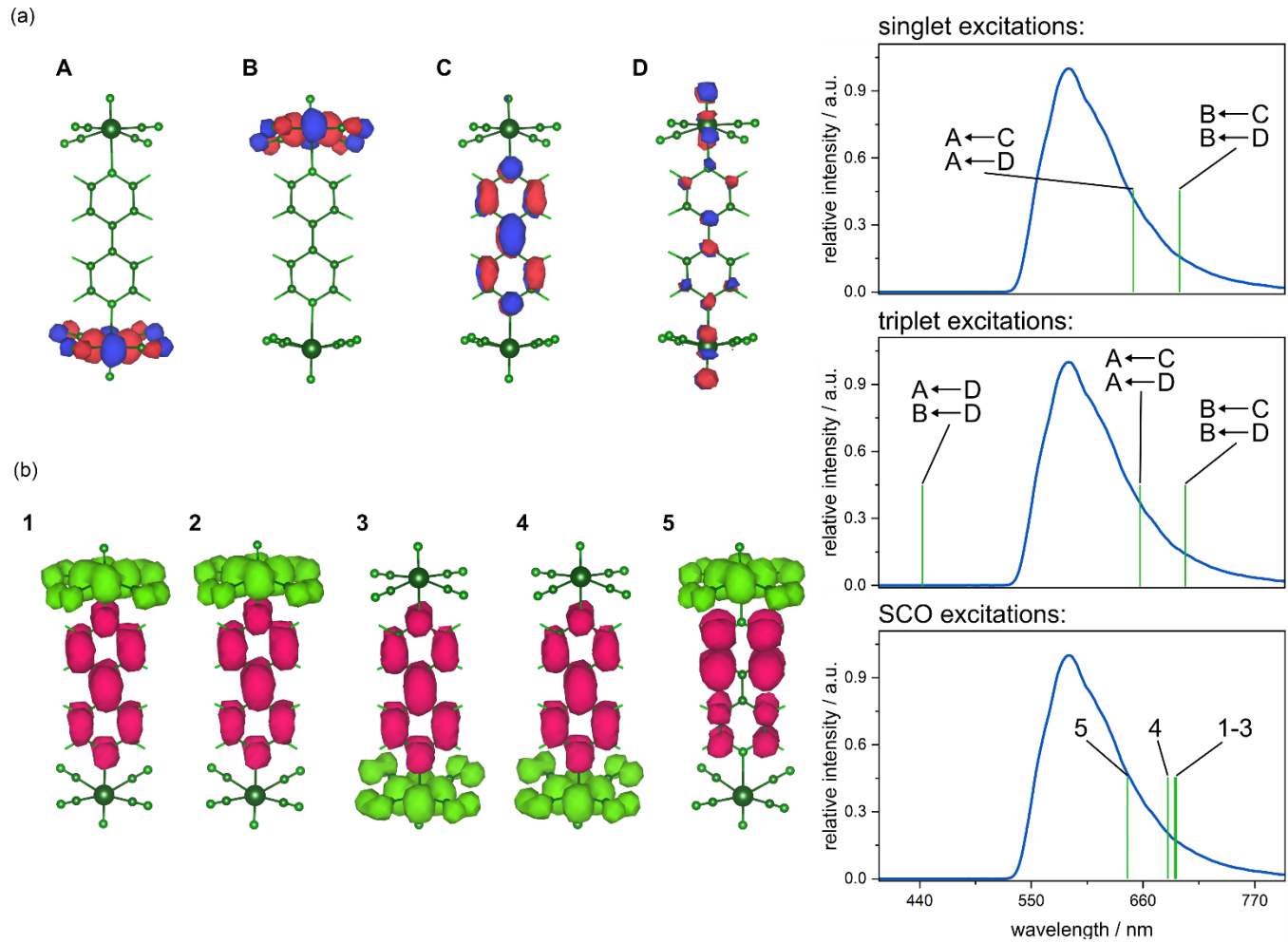


**Fig. S42** Contour plots (with the 0.05 isovalue level) of chosen MO corresponding to the TD-DFT singlet or triplet emissions (a) as well as differential contour plots (b) corresponding to changes in the orbital occupation during the transition between the respective excited spin-orbit coupled state and ground state (green - electron depletion, purple - electron gain) in **Re<sub>2</sub>-bpy**, together with the comparison of the low-temperature emission spectrum (30 K) with the emission energies predicted for the lowest energy excited states using the TD-DFT theoretical calculations (green lines, right panel). The transition(s) energies are presented in Table S60.

**Table S60** The predicted emission energies predicted for the lowest energy excited states using the TD-DFT calculations in **Re<sub>2</sub>-bpy** (green lines in Fig. S42).

DFT lowest energy singlet emissions					
transition(s)	B ← C B ← D	A ← C A ← D	-	-	-
transition(s) energy	698.8 nm (14310 cm <sup>-1</sup> )	653.4 nm (15305 cm <sup>-1</sup> )	-	-	-
oscillator strength	$f = 0.0003$	$f = 0.0002$	-	-	-
DFT lowest energy triplet emissions					
transition(s)	B ← C B ← D	A ← C A ← D	A ← D B ← D	-	-
transition(s) energy	705.9 nm (14166 cm <sup>-1</sup> )	657.4 nm (15211 cm <sup>-1</sup> )	441.3 nm (22660 cm <sup>-1</sup> )	-	-
DFT lowest energy spin-orbit corrected emissions					
state no.	1	2	3	4	5
state energy	691.9 nm (14453 cm <sup>-1</sup> )	691.8 nm (14455 cm <sup>-1</sup> )	691.7 nm (14457 cm <sup>-1</sup> )	684.9 nm (14601 cm <sup>-1</sup> )	645.1 nm (15501 cm <sup>-1</sup> )
oscillator strength	$f = 0.0000$	$f = 0.0000$	$f = 0.0001$	$f = 0.0003$	$f = 0.0000$
composition	100 % triplet	100 % triplet	100 % triplet	100 % singlet	100 % triplet

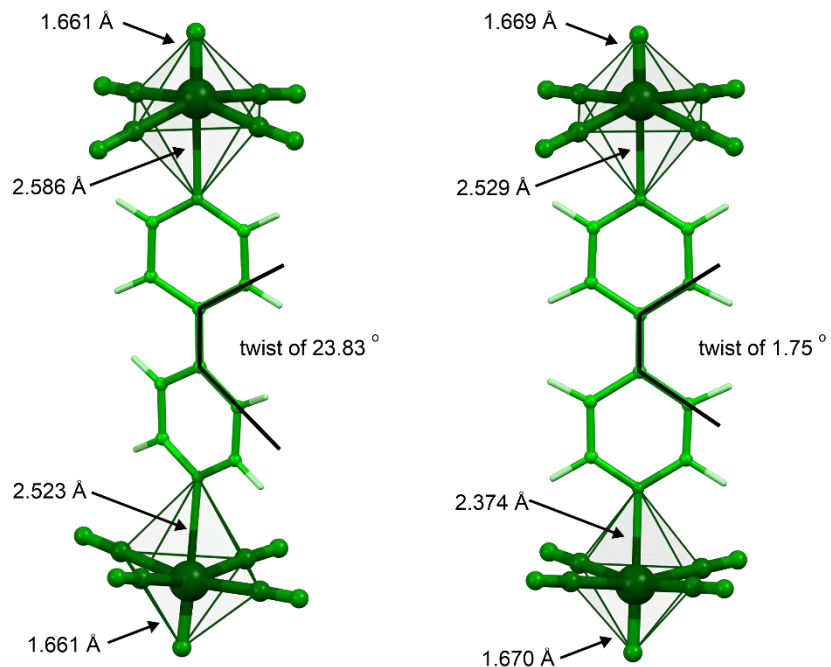


**Fig. S43** Comparison of selected bond lengths and angles of initial (experimental SC-XRD, left) and final (DFT optimized excited state, right) structure of dinuclear molecular anions in **Re<sub>2</sub>-bpy**.

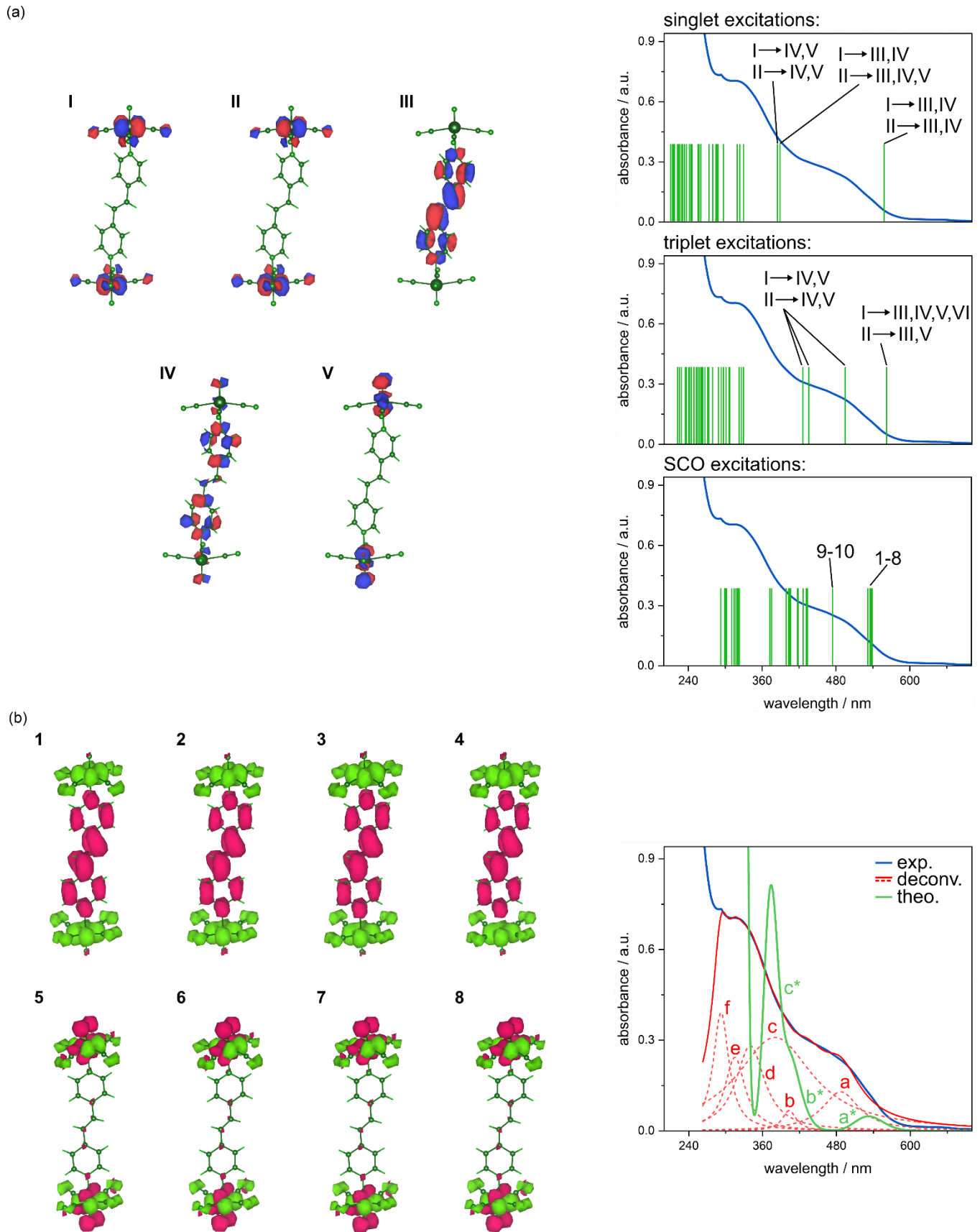


**Fig. S44** Contour plots (with the 0.05 isovalue level) of chosen MO corresponding to the TD-DFT singlet or triplet excitations (a) as well as differential contour plots (b) corresponding to changes in the orbital occupation during the transition between the ground and the respective excited spin-orbit coupled state (green - electron depletion, purple - electron gain) in **Re<sub>2</sub>-bphee**, together with the comparison of absorption spectra with the excitation energies predicted for the lowest energy excited states (a, right panel), and comparison of the deconvoluted absorption spectra with the theoretically simulated spectrum (b, right panel). The transition(s) energies are presented in Table S61.

**Table S61** The predicted excitation energies of lowest energy singlet, triplet, and spin-orbit corrected excited states using the TD-DFT calculations in **Re<sub>2</sub>-bpEE** (see Fig. S44) compared with deconvoluted experimental absorption spectra.

DFT lowest energy singlet excitations						
transition(s)	I → IV II → III	I → III II → IV	I → IV II → III, V	I → III II → IV	I → IV II → V	I → V II → IV
transition(s) energy	557.7 nm (17931 cm <sup>-1</sup> )	557.7 nm (17931 cm <sup>-1</sup> )	388.3 nm (25753 cm <sup>-1</sup> )	388.3 nm (25753 cm <sup>-1</sup> )	383.9 nm (26048 cm <sup>-1</sup> )	383.9 nm (26048 cm <sup>-1</sup> )
oscillator strength	f = 0.0000	f = 0.0004	f = 0.0000	f = 0.0043	f = 0.0000	f = 0.0026
DFT lowest energy triplet excitations						
transition(s)	I → III, V, IV II → III,V	I → IV II → V	I → V II → IV	I → V II → IV	I → IV II → V	I → IV,V II → IV,V
transition(s) energy	562.4 nm (17781 cm <sup>-1</sup> )	562.3 nm (17784 cm <sup>-1</sup> )	494.6 nm (20218 cm <sup>-1</sup> )	436.0 nm (22936 cm <sup>-1</sup> )	436.0 nm (22935 cm <sup>-1</sup> )	426.2 nm (23463 cm <sup>-1</sup> )
DFT lowest energy spin-orbit corrected excitations						
state no.	1	2	3	4	5	
state energy	536.5 nm (18639 cm <sup>-1</sup> )	536.5 nm (18639 cm <sup>-1</sup> )	536.3 nm (18646 cm <sup>-1</sup> )	536.3 nm (18646 cm <sup>-1</sup> )	536.2 nm (18650 cm <sup>-1</sup> )	
oscillator strength	f = 0.0000					
composition	100 % triplet					
state no.	6	7	8	9	10	
state energy	535.9 nm (18660 cm <sup>-1</sup> )	531.6 nm (18811 cm <sup>-1</sup> )	531.6 nm (18811 cm <sup>-1</sup> )	473.4 nm (21124 cm <sup>-1</sup> )	473.4 nm (21124 cm <sup>-1</sup> )	
oscillator strength	f = 0.0000	f = 0.0004	f = 0.0000	f = 0.0000	f = 0.0000	
composition	100 % triplet	100 % singlet	100 % singlet	100 % triplet	100 % triplet	
comparison of deconvoluted experimental absorption spectra with DFT-predicted absorption bands						
transition	a	b	c	d	e	f
experimental absorption spectra	485 nm (20619 cm <sup>-1</sup> )	406 nm (24631 cm <sup>-1</sup> )	378 nm (26455 cm <sup>-1</sup> )	339 nm (29499 cm <sup>-1</sup> )	315 nm (31746 cm <sup>-1</sup> )	291 nm (34364 cm <sup>-1</sup> )
transition	a*	b*	c*	-	-	-
DFT predicted absorption bands	526 nm (19011 cm <sup>-1</sup> )	402 nm (24876 cm <sup>-1</sup> )	374 nm (26738 cm <sup>-1</sup> )	-	-	-

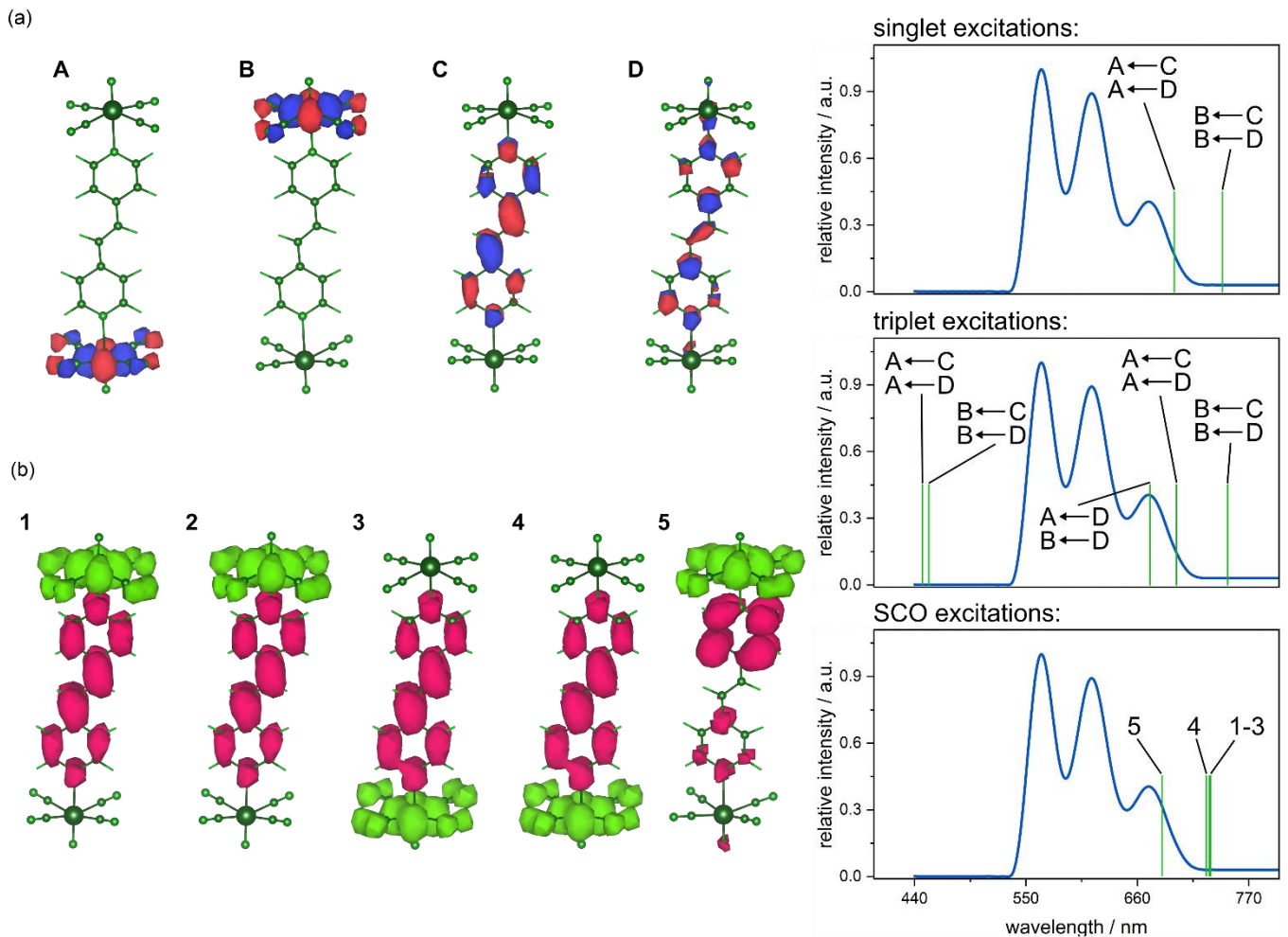


**Fig. S45** Contour plots (with the 0.05 isovalue level) of chosen MO corresponding to the TD-DFT singlet or triplet emissions (a) as well as differential contour plots (b) corresponding to changes in the orbital occupation during the transition between the respective excited spin-orbit coupled state and ground state (green - electron depletion, purple - electron gain) in **Re<sub>2</sub>-bpEE**, together with the comparison of the low-temperature emission spectrum (30 K) with the emission energies predicted for the lowest energy excited states using the TD-DFT theoretical calculations (green lines, right panel). The transition(s) energies are presented in Table S62.

**Table S62** The predicted emission energies predicted for the lowest energy excited states using the TD-DFT calculations in **Re<sub>2</sub>-bpEE** (green lines in Fig. S45).

DFT lowest energy singlet emissions					
transition(s)	B ← C B ← D	A ← C A ← D	-	-	-
transition(s) energy	744.4 nm (13434 cm <sup>-1</sup> )	696.3 nm (14362 cm <sup>-1</sup> )	-	-	-
oscillator strength	$f = 0.0001$	$f = 0.0001$	-	-	-
DFT lowest energy triplet emissions					
transition(s)	B ← C B ← D	A ← C A ← D	A ← D B ← D	A ← C A ← D	A ← C A ← D
transition(s) energy	748.9 nm (13353 cm <sup>-1</sup> )	698.8 nm (14310 cm <sup>-1</sup> )	673.2 nm (14854 cm <sup>-1</sup> )	446.8 nm (22381 cm <sup>-1</sup> )	443.5 nm (22548 cm <sup>-1</sup> )
DFT lowest energy spin-orbit corrected emissions					
state no.	1	2	3	4	5
state energy	733.6 nm (13631 cm <sup>-1</sup> )	733.6 nm (13631 cm <sup>-1</sup> )	733.5 nm (13633 cm <sup>-1</sup> )	729.2 nm (13714 cm <sup>-1</sup> )	685.4 nm (14590 cm <sup>-1</sup> )
oscillator strength	$f = 0.0000$	$f = 0.0000$	$f = 0.0001$	$f = 0.0001$	$f = 0.0001$
composition	100 % triplet	100 % triplet	100 % triplet	100 % singlet	100 % triplet

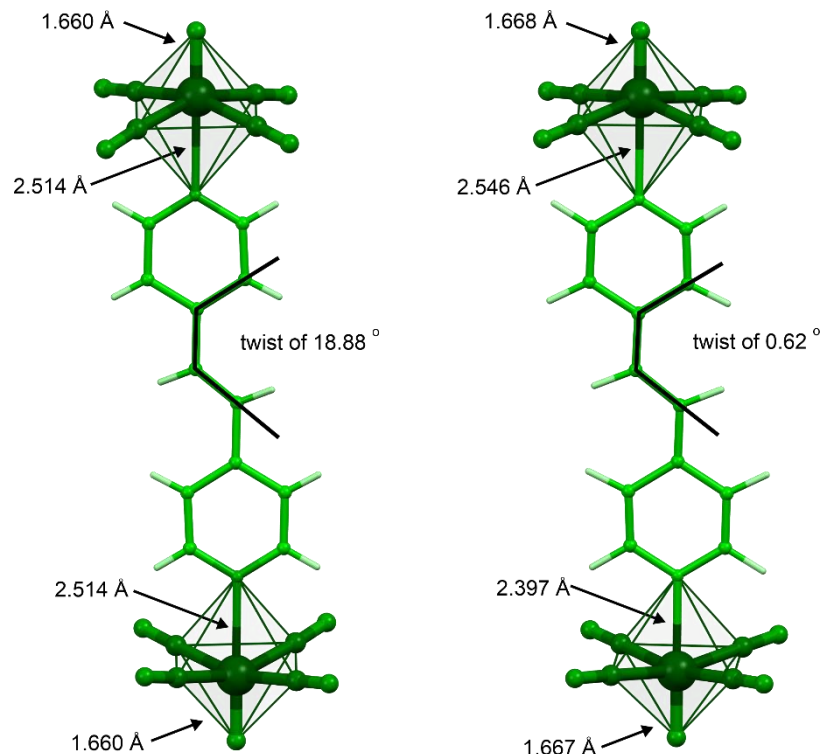


**Fig. S46** Comparison of selected bond lengths and angles of initial (experimental SC-XRD, left) and final (DFT optimized excited state, right) structure of dinuclear molecular anions in **Re<sub>2</sub>-bppe**.

## Description of the periodic DFT theoretical calculations

The crystal structures of the **Re<sub>2</sub>-bpac**, **Re<sub>2</sub>-bpb**, **Re<sub>2</sub>-bpbp**, and **Re<sub>2</sub>-bpen** materials were modeled at the DFT level of theory using periodic boundary conditions as implemented in the VASP program. These four systems create a meaningful set to analyze because two of them (**Re<sub>2</sub>-bpbp** and **Re<sub>2</sub>-bpen**) were assigned to the A group (see Fig. 4 and the main text) while **Re<sub>2</sub>-bpac** and **Re<sub>2</sub>-bpb** were assigned to the B group.

The calculations on periodic crystal structures were performed using density functional theory (DFT) methods within the Vienna Ab-Initio Simulation Package (VASP).<sup>S27</sup> Given the importance of non-covalent interactions between molecules and the intent to use the periodic models to complement the results on molecular clusters, the experimentally determined lattice constants at room temperature were used and kept fixed during geometry optimizations. The PBE<sup>S28</sup> exchange-correlation functional with a D3-generation post-SCF dispersion correction (PBE+D3; including Becke-Johnson dampening)<sup>S11</sup> was used to optimize the first set of geometries. The hybrid HSE06 functional was used to compare with the PBE+D3 method and assess any potential problems that the expected electron delocalization error within PBE may have on the Re(V) metal-organic complexes.<sup>S29</sup> The electronic structure plots shown in the main text (Fig. 6) used the DFT+U method to separate the energy levels of one of the organic linker molecules from the other (see text for description).

The plane-wave basis set cutoff was set to 500 eV, and the Re(6s/5d), P(3s/3p), O/N/C (2s/2p), and H (1s) valence electrons were treated explicitly and used in conjunction with PAW potentials that were supplied with the standard VASP package - version 5.4.<sup>S30</sup> The VESTA program was used to generate the electron density plots.<sup>S31</sup> Benchmarking calculations showed that including only the Gamma k-point was sufficient to obtain converged band energies and interaction energies, and so the geometries were optimized with Gamma-point-only calculations and the total energies and interaction energies were computed with an automatically generated k-point grid wherein the length parameter (Rk, as implemented in the VASP program) is set to 20 Å. The set of supporting results from these calculations together with the detailed comments is gathered in Fig. S47 and Tables S63–S65 (see below).

**Table S63** Computed bond distances (Å) in optimized geometries of selected dinuclear {Re<sup>V<sub>2</sub></sup>}<sup>4-</sup> molecular anions of **Re<sub>2</sub>-bpac**, **Re<sub>2</sub>-bpb**, and **Re<sub>2</sub>-bpen** materials (see Fig. 1, S9, S13, and S15 for comparison) at two levels of DFT theory using periodic boundary conditions: PBE+D3 and HSE06. The room-temperature experimental values (Exp.) are provided for comparison.

Functional	<b>Re<sub>2</sub>-bpac</b>		<b>Re<sub>2</sub>-bpen</b>		<b>Re<sub>2</sub>-bpb</b>	
	Re1–N6	Re1–N6	Re1–N6	Re1≡N1	Re1≡N1	Re1≡N1
PBE+D3	2.586	2.535	2.529	1.690	1.693	1.690
HSE06	2.566	2.508	2.507	1.668	1.668	1.662
Exp.	2.571	2.512	2.497	1.641	1.654	1.641

**Comment to Table S63:** Table S63 shows the computed Re≡N and Re–L distances from the optimized geometries with two types of DFT functionals (PBE+D3 and HSE06). Note that the simulation cell was kept fixed at the 298K parameters that were deduced from the experiment and the solvent molecules were removed from the simulation cell in this set of calculations. Both functionals agree well qualitatively with the crystal data in the sense that the Re–L distances are longest in **Re<sub>2</sub>-bpac** by >0.05 Å. It is also seen that the experimental values of Re–L and Re≡N are better reproduced by the HSE06 method, which agrees with the expectation that the treatment electron correlation within the hybrid (HSE06) DFT methodology is better suited for the metal-to-ligand bonding.

**Table S64** Computed interaction energies ( $\Delta E_{\text{int}}$ ) for the **Re<sub>2</sub>-bpac**, **Re<sub>2</sub>-bpb**, and **Re<sub>2</sub>-bpen** materials. The  $\Delta E_{\text{int}}$  was calculated from the difference between the total energy of the crystal structure and the sum of the total energies of the crystal without the ligand and the ligand alone. The  $\Delta E_{\text{int,disp}}$  is the portion of the interaction energy that comes from the post-SCF dispersion correction in the PBE+D3 method.

PBE + D3	$\Delta E_{\text{int}} / \text{eV}$	$\Delta E_{\text{int,disp}} / \text{eV}$	$\Delta E_{\text{int}} - \Delta E_{\text{int,disp}} / \text{eV}$
<b>Re<sub>2</sub>-bpac</b>	-2.890	-2.252	-0.644
<b>Re<sub>2</sub>-bpen</b>	-3.355	-2.148	-1.186
<b>Re<sub>2</sub>-bpb</b>	-3.242	-2.711	-0.533
HSE06	$\Delta E_{\text{int}} / \text{eV}$	$\Delta E_{\text{int,disp}} / \text{eV}$	$\Delta E_{\text{int}} - \Delta E_{\text{int,disp}} / \text{eV}$
<b>Re<sub>2</sub>-bpac</b>	-0.893	0.000	-0.893
<b>Re<sub>2</sub>-bpen</b>	-1.464	0.000	-1.464
<b>Re<sub>2</sub>-bpb</b>	-0.812	0.000	-0.812

**Comment to Table S64:** A quantitative analysis of the Re–ligand interactions was performed by computing the ligands' interaction energies ( $\Delta E_{\text{int}}$ ) within the crystal, calculated as:

$$\Delta E_{\text{int}} = E_{\text{xtal}} - E_{\text{xtal\_noL}} - E_L,$$

where  $E_{\text{xtal}}$  is the total energy of the optimized crystal structure,  $E_{\text{xtal\_noL}}$  is the single-point energy of the crystal with the ligand removed, and  $E_L$  is the single-point energy of the crystal with the metal complex and cations removed. The computed  $\Delta E_{\text{int}}$  values are shown in Table S64 (at both the PBE+D3 and HSE06 levels of theory). Also shown for the PBE+D3 method is a decomposition of  $\Delta E_{\text{int}}$  into the contribution that comes from the post-SCF dispersion correction ( $\Delta E_{\text{int,disp}}$ ).

The PBE+D3 results in Table S64 show that the total ligand/environment interactions calculations all have comparable strengths to one another (between -2.8 and -3.4 eV per unit cell). The large contribution of the dispersion energy, as could be expected from the prevalence of non-covalent contacts between molecules, amounts to 66.1% for **Re<sub>2</sub>-bpac**, 54.9% for **Re<sub>2</sub>-bpb**, and 35.5% for **Re<sub>2</sub>-bpen**. If it is assumed that the remainder of the interaction energy is dominated by the ligand/metal-complex interaction, then it can be seen that the interaction between the ligand and the metal complexes seems weaker for **Re<sub>2</sub>-bpac/Re<sub>2</sub>-bpb** than for **Re<sub>2</sub>-bpen**. This clear separation of **Re<sub>2</sub>-bpen** from **Re<sub>2</sub>-bpb/Re<sub>2</sub>-bpac** aligns with their division into groups A and B in the main text; which corroborates that the main feature that defines the two groups is the nature of the Re...L contact. The strength of the non-dispersion contribution to the interaction is reproduced with the HSE06 functional, even somewhat enhanced.

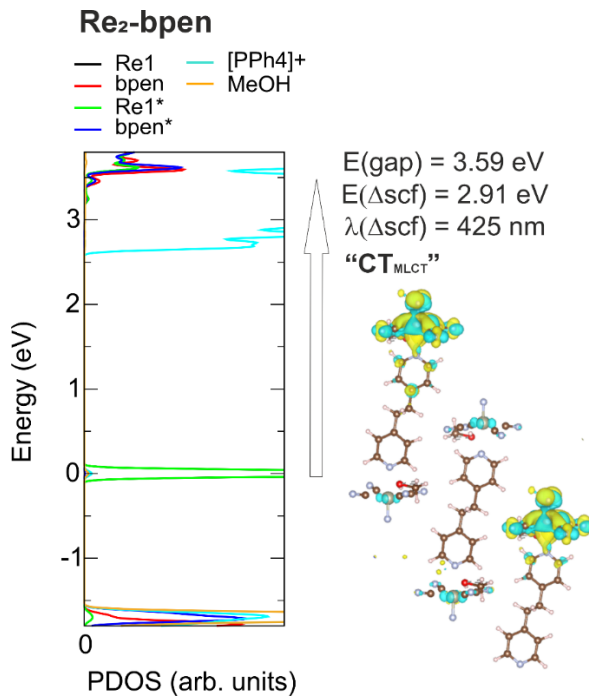


**Fig. S47** Computed molecule-projected densities of states (PDOS) for the **Re<sub>2</sub>-bpen** material, computed with the HSE06 functional at the PBE+D3 optimized geometry. The figure to the right shows the redistribution of electron density that is seen when generating a low-energy intermolecular CT excited state, CT<sub>MLCT</sub>, using a ΔSCF approach, wherein blue/yellow indicates a loss/gain in electron density relative to the ground state. E(gap) is an (estimated) energy difference between ground-state energy levels, and E(Δscf)/λ(Δscf) are differences between the total DFT energies of the ground and model CT<sub>MLCT</sub> excited state.

**Comment to Fig. S47:** Fig. S47 shows the analogous results for **Re<sub>2</sub>-bpen** as those which are shown for **Re<sub>2</sub>-bpac**, **Re<sub>2</sub>-bpb**, and **Re<sub>2</sub>-bpbp** in Fig. 6 of the main text. The CT<sub>MLCT</sub> state was generated in two steps: *i*) the first step generated the analogous CT1 state that is described in Figure 6 of the main text (i.e., the occupancies of the highest occupied and lowest unoccupied ground-state spin-orbitals were swapped), and *ii*) the second step was to change the orbital occupancies in the CT1 state in a way that reassigns the “excited” electron to the lowest unoccupied spin-orbital with Re1/bpen character (as identified by the site-projected densities of states that are written by the VASP program).

**Table S65** Computed energy spacings between the (ground-state) energy levels that best correspond to the p<sub>π</sub>→d<sub>xy</sub>+p<sub>CN</sub> and d<sub>xz</sub>+d<sub>yz</sub>+p<sub>CN</sub>+p<sub>N</sub>→d<sub>xy</sub>+p<sub>CN</sub> emission processes that were characterized in the main manuscript.

light-induced emission events	<b>Re<sub>2</sub>-bpac</b>	<b>Re<sub>2</sub>-bpen</b>	<b>Re<sub>2</sub>-bpb</b>
p <sub>π</sub> →d <sub>xy</sub> +p <sub>CN</sub> / eV	2.2	3.6	2.6
d <sub>xz</sub> +d <sub>yz</sub> +p <sub>CN</sub> +p <sub>N</sub> →d <sub>xy</sub> +p <sub>CN</sub> / eV	4.4	4.3	4.4

**Comment to Table S65:** Table S65 shows the energy spacings between the ground-state orbitals that best characterize the p<sub>π</sub>→d<sub>xy</sub>+p<sub>CN</sub> and d<sub>xz</sub>+d<sub>yz</sub>+p<sub>CN</sub>+p<sub>N</sub>→d<sub>xy</sub>+p<sub>CN</sub> emission processes, and it is seen that the differences between them are much smaller in **Re<sub>2</sub>-bpen** than in **Re<sub>2</sub>-bpb** and **Re<sub>2</sub>-bpac** materials. This qualitative agreement of solid-state models with the TD-DFT results from the molecular clusters (see the main manuscript and the detailed results of the molecular DFT/TD-DFT calculations above) further confirms that the molecular models are properly capturing the essential chemistry that occurs in the periodic crystals of investigated emissive solids.

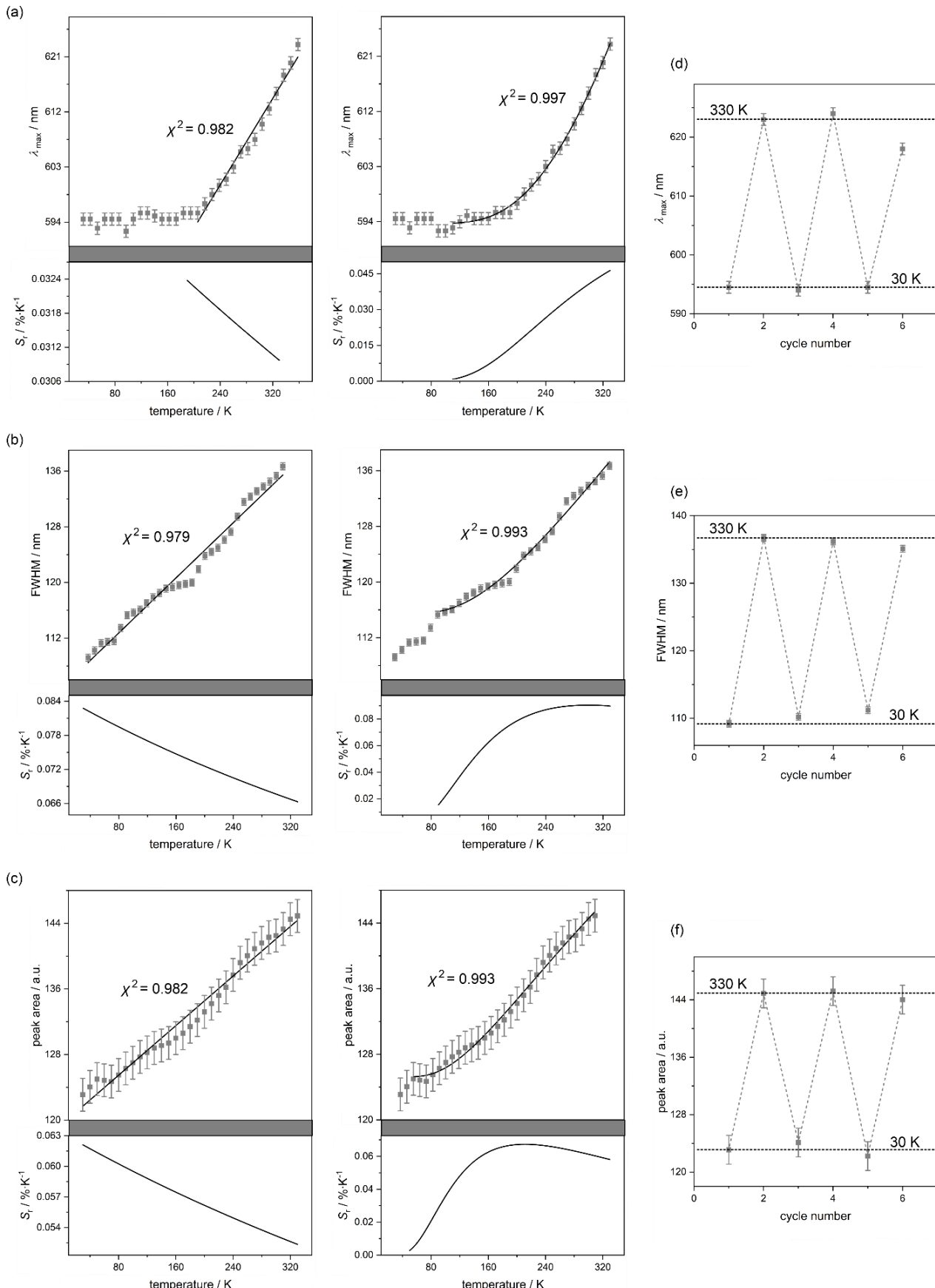


**Fig. S48** Temperature dependencies of the wavelength position of the emission maximum ( $\lambda_{\max}$ , a), the full width at half maximum of the emission band (FWHM, b), and the integrated emission intensity (peak area, c) for  $\text{Re}_2\text{-CN}$  (see Fig. S25 and Table S27), presented with the best-fit curves (solid lines) obtained using the linear (left panel) and Mott-Seitz equations (right panel), together with the relative thermal sensitivity ( $S_r$ ) parameters (under the corresponding fits), and thermal repeatability of each of three discussed parameters along six consecutive measurements (d-f, corresponding to the a-c parts, respectively). The resulting best-fit parameters and used equations are gathered in Tables S66-S68.

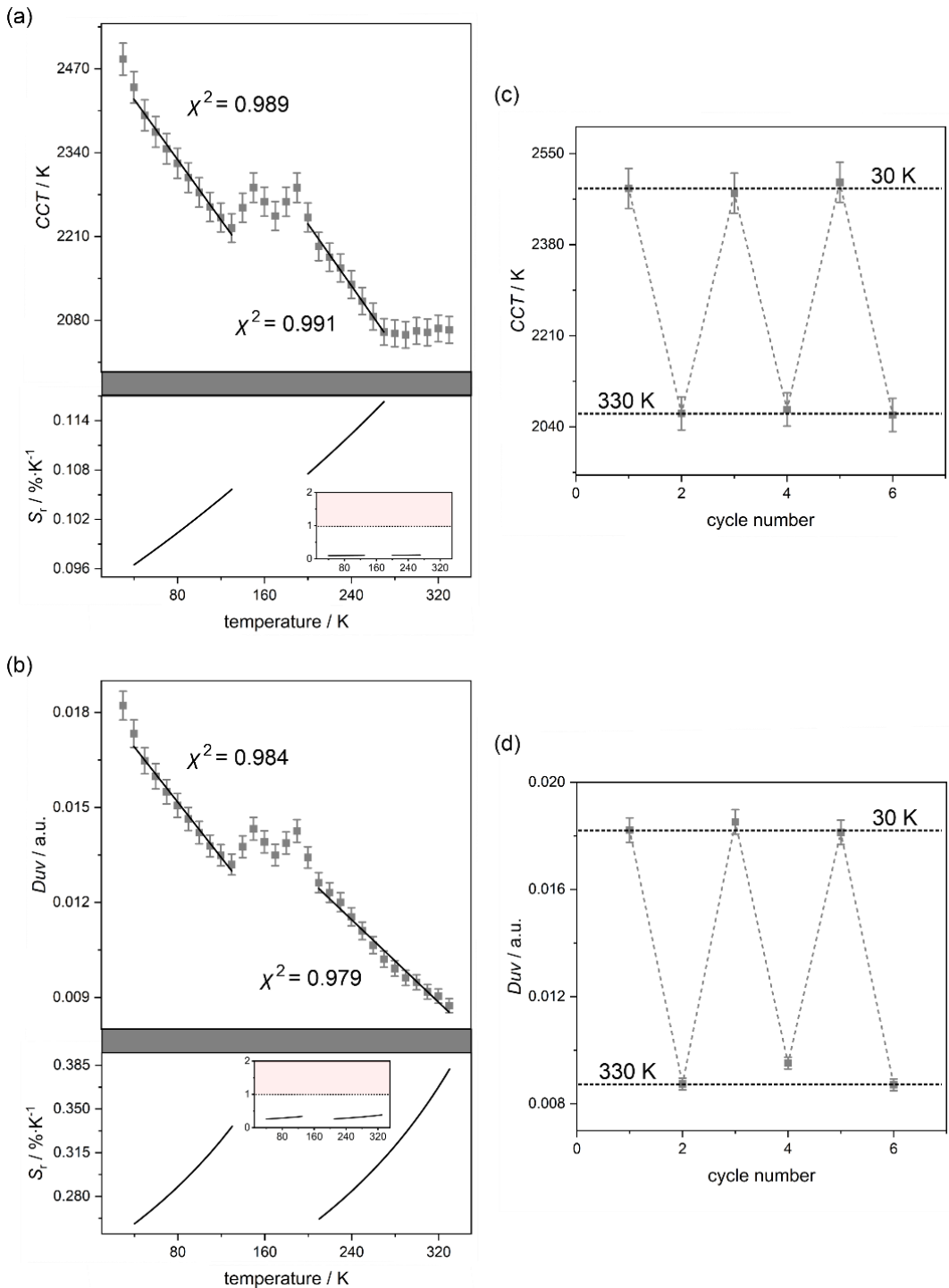


**Fig. S49** Temperature dependencies of the correlated color temperature ( $CCT$ , a) and  $D_{uv}$  value (b) calculated from the CIE 1931 chromaticity  $x$  and  $y$  parameters of the solid-state photoluminescent properties of  $\text{Re}_2\text{-CN}$  (see Fig. S25 and Table S28), shown with the best-fit curves (solid lines) obtained using the linear fitting, together with the relative thermal sensitivity ( $S_r$ ) parameters (under the corresponding fits), and thermal repeatability of each parameter of two discussed parameters along six consecutive measurements (c and d, corresponding to the a and b parts, respectively). The resulting best-fit parameters and employed equations are collected in Tables S69 and S70.

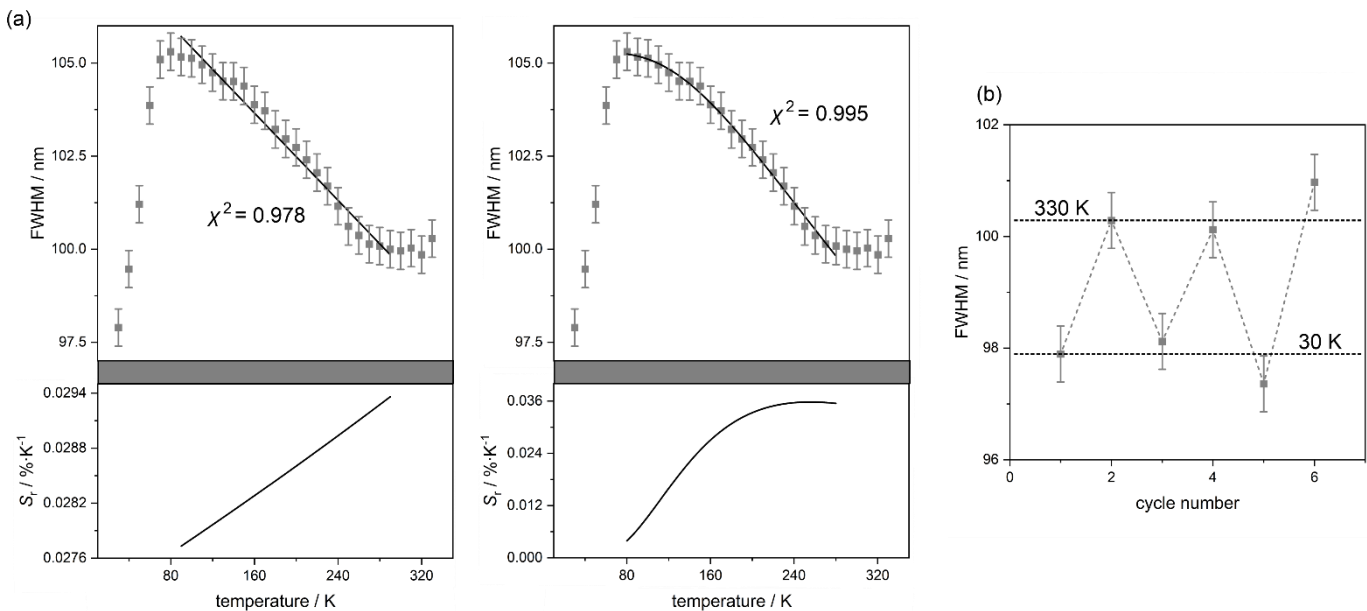


**Fig. S50** Temperature dependence of the full width at half maximum of the emission band (FWHM, a) for **Re<sub>2</sub>-en** (see Fig. S26 and Table S29), presented with the best-fit curves (solid lines) obtained using the linear (left panel) and Mott-Seitz equations (right panel), together with the relative thermal sensitivity ( $S_r$ ) parameters (under the corresponding fits), and thermal repeatability along six consecutive measurements (b). The resulting best-fit parameters and used equations are gathered in Table S67.

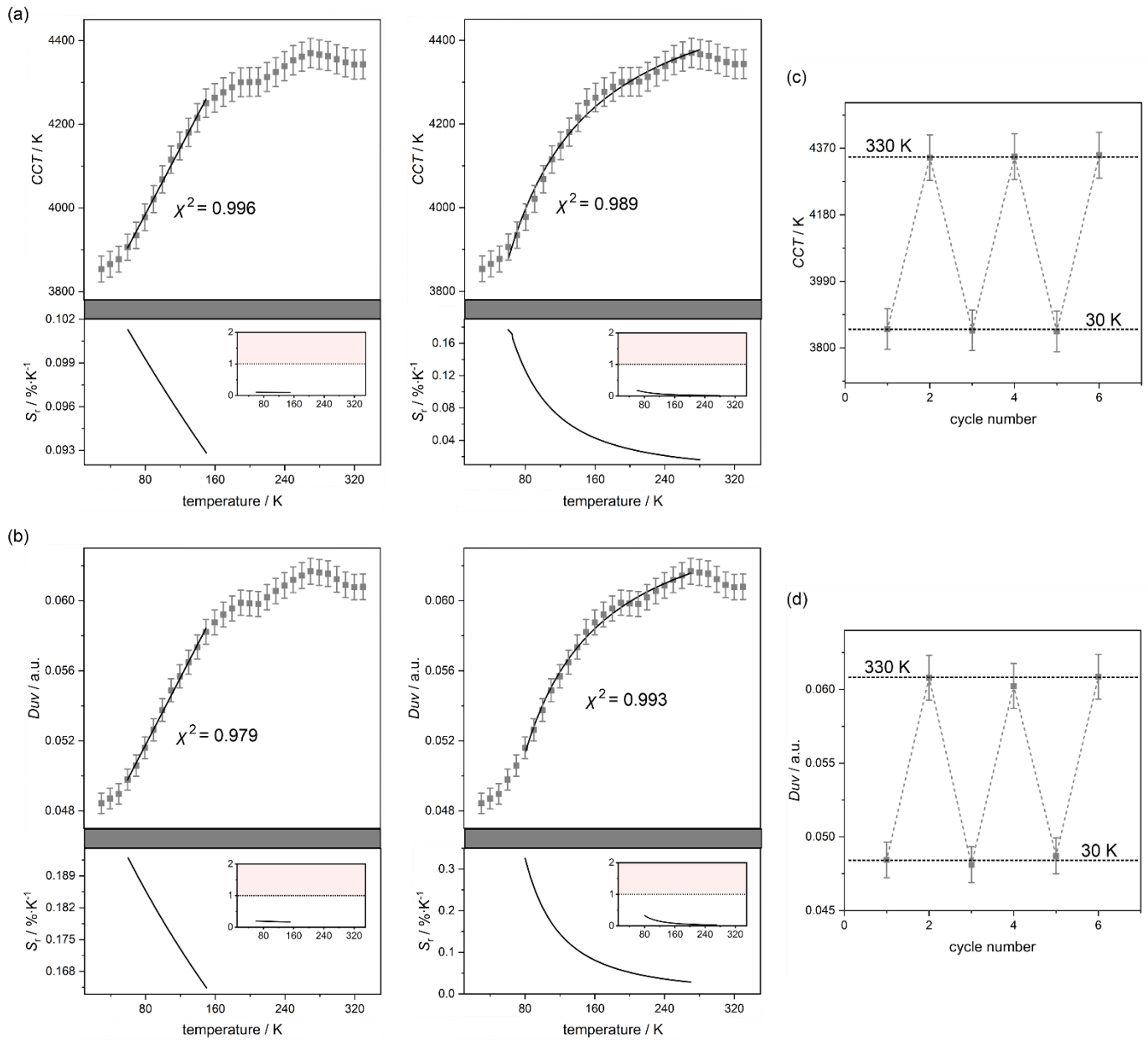


**Fig. S51** Temperature dependencies of the correlated color temperature (CCT, a) and  $D_{uv}$  value (b) calculated from the CIE 1931 chromaticity  $x$  and  $y$  parameters of the solid-state photoluminescent properties of **Re<sub>2</sub>-en** (see Fig. S26 and Table S30), shown with the best-fit curves (solid lines) obtained using the linear (left panel) and Mott-Seitz equations (right panel), together with the relative thermal sensitivity ( $S_r$ ) parameters (under the corresponding fits), and thermal repeatability of each parameter of two discussed parameters along six consecutive measurements (c and d, corresponding to the a and b parts, respectively). The resulting best-fit parameters and employed equations are gathered in Tables S69 and S70.

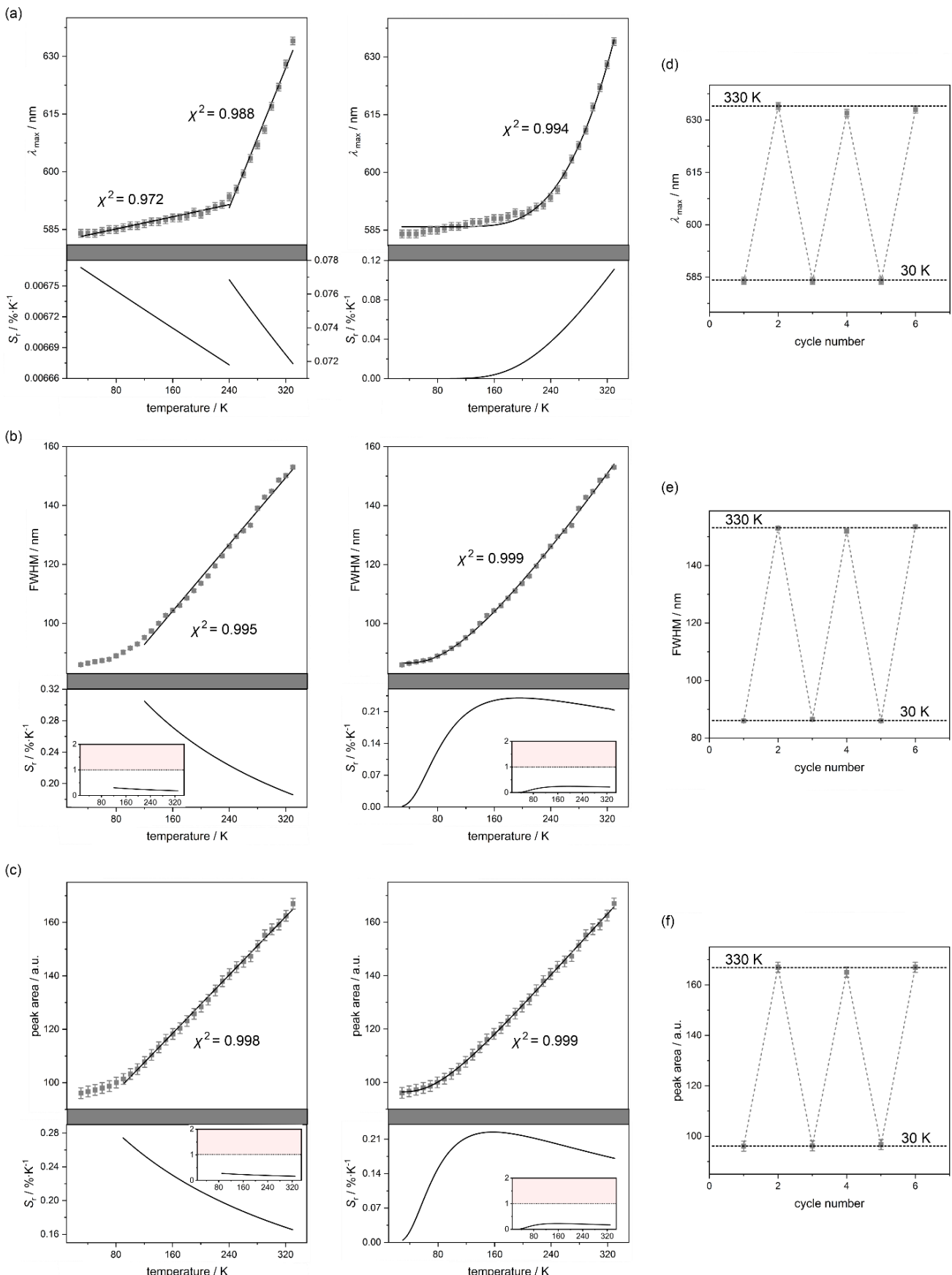


**Fig. S52** Temperature dependencies of the wavelength position of the emission maximum ( $\lambda_{\max}$ , a), the full width at half maximum of the emission band (FWHM, b), and the integrated emission intensity (peak area, c) for **Re<sub>2</sub>-bpy** (see Fig. S27 and Table S31), presented with the best-fit curves (solid lines) obtained using the linear (left panel) and Mott-Seitz equations (right panel), together with the relative thermal sensitivity ( $S_r$ ) parameters (under the corresponding fits), and thermal repeatability of each of three discussed parameters along six consecutive measurements (d–f, corresponding to the a–c parts, respectively). The resulting best-fit parameters and used equations are gathered in Tables S66–S68.

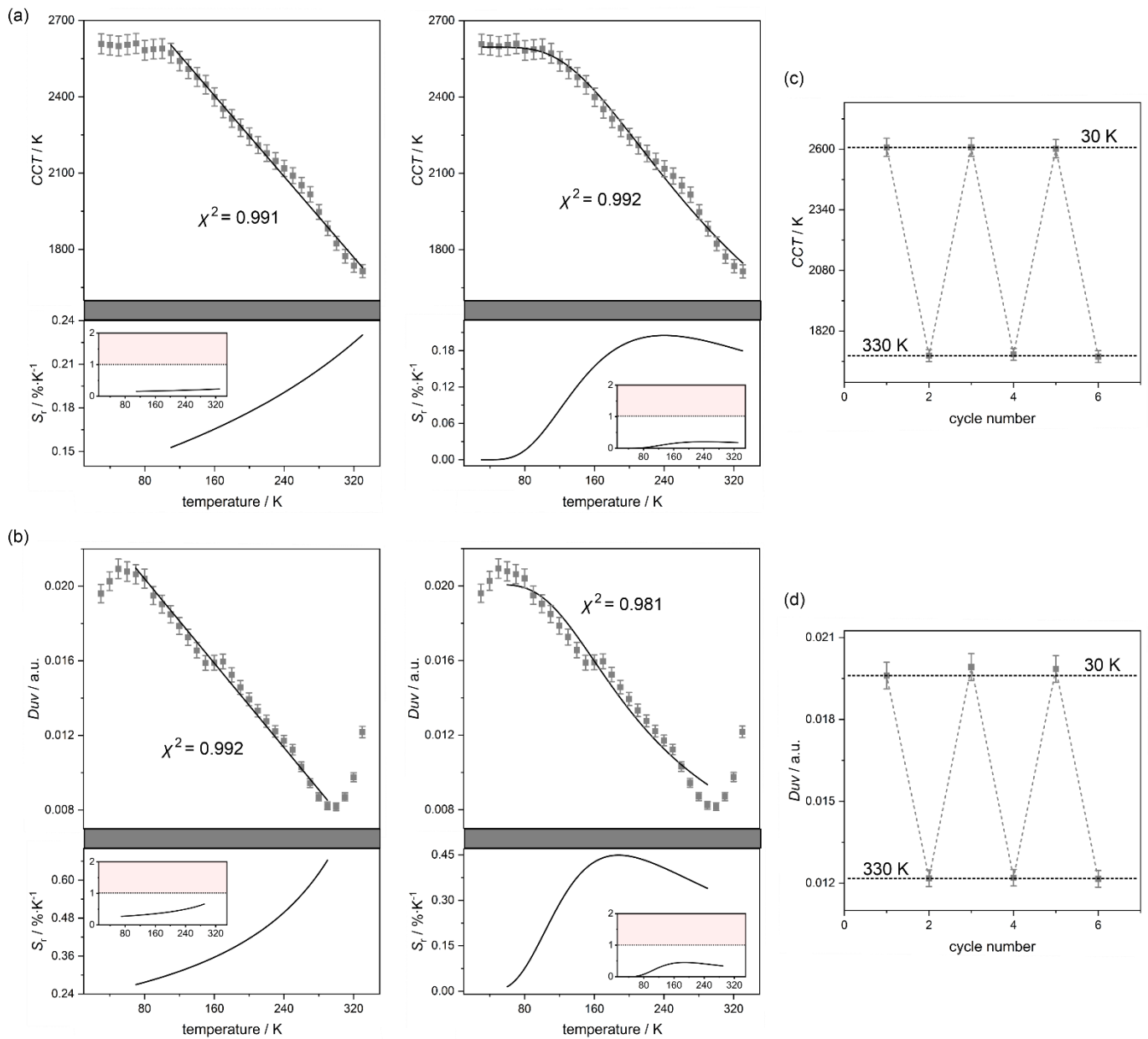


**Fig. S53** Temperature dependencies of the correlated color temperature (CCT, a) and  $D_{uv}$  value (b) calculated from the CIE 1931 chromaticity  $x$  and  $y$  parameters of the solid-state photoluminescent properties of **Re<sub>2</sub>-bpy** (see Fig. S27 and Table S32), shown with the best-fit curves (solid lines) obtained using the linear (left panel) and Mott-Seitz equations (right panel), together with the relative thermal sensitivity ( $S_r$ ) parameters (under the corresponding fits), and thermal repeatability of each of two discussed parameters along six consecutive measurements (c and d, corresponding to the a and b parts, respectively). The resulting best-fit parameters and employed equations are gathered in Tables S69 and S70.

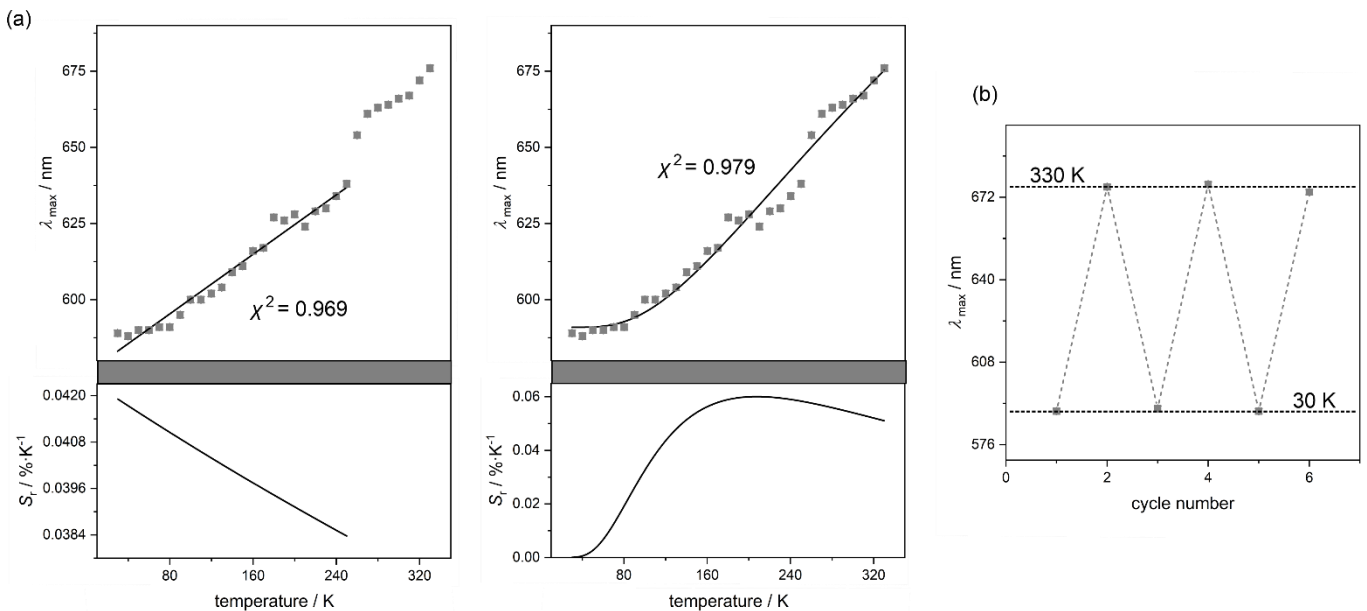


**Fig. S54** Temperature dependence of the wavelength position of the emission maximum ( $\lambda_{\text{max}}$ , a) for **Re<sub>2</sub>-bpac** (see Fig. S28 and Table S33), presented with the best-fit curves (solid lines) obtained using the linear (left panel) and Mott-Seitz equations (right panel), together with the relative thermal sensitivity ( $S_r$ ) parameters (under the corresponding fits), and thermal repeatability of each of two discussed parameters along six consecutive measurements (b). The resulting best-fit parameters and used equations are gathered in Table S66.

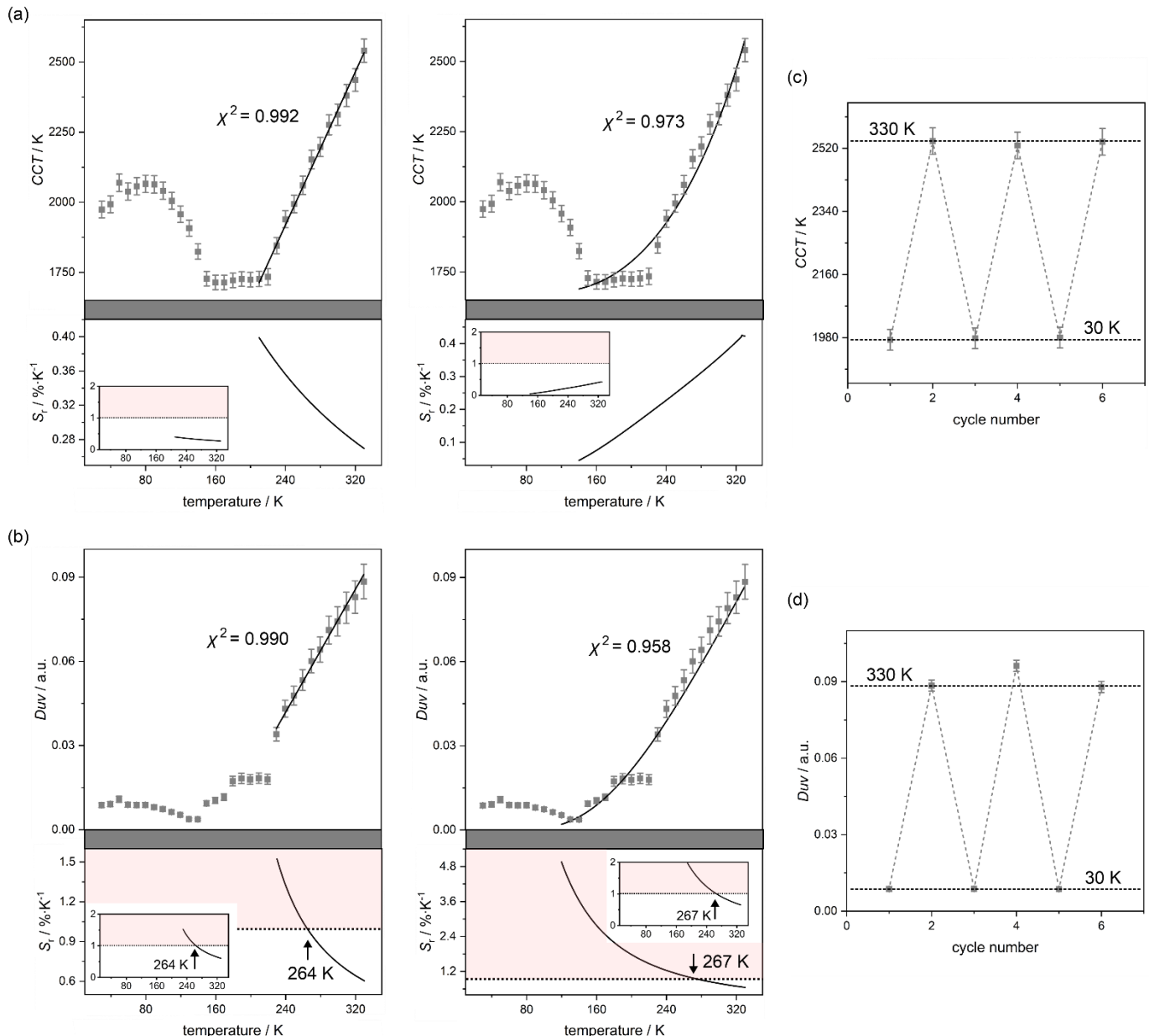


**Fig. S55** Temperature dependencies of the correlated color temperature (CCT, a) and  $D_{uv}$  value (b) calculated from the CIE 1931 chromaticity  $x$  and  $y$  parameters of the solid-state photoluminescent properties of **Re<sub>2</sub>-bpac** (see Fig. S28 and Table S34), shown with the best-fit curves (solid lines) obtained using the linear (left panel) and Mott-Seitz equations (right panel), together with the relative thermal sensitivity ( $S_r$ ) parameters (under the corresponding fits), and thermal repeatability of each of two discussed parameters along six consecutive measurements (c and d, corresponding to the a and b parts, respectively). The resulting best-fit parameters and employed equations are gathered in Tables S69 and S70.

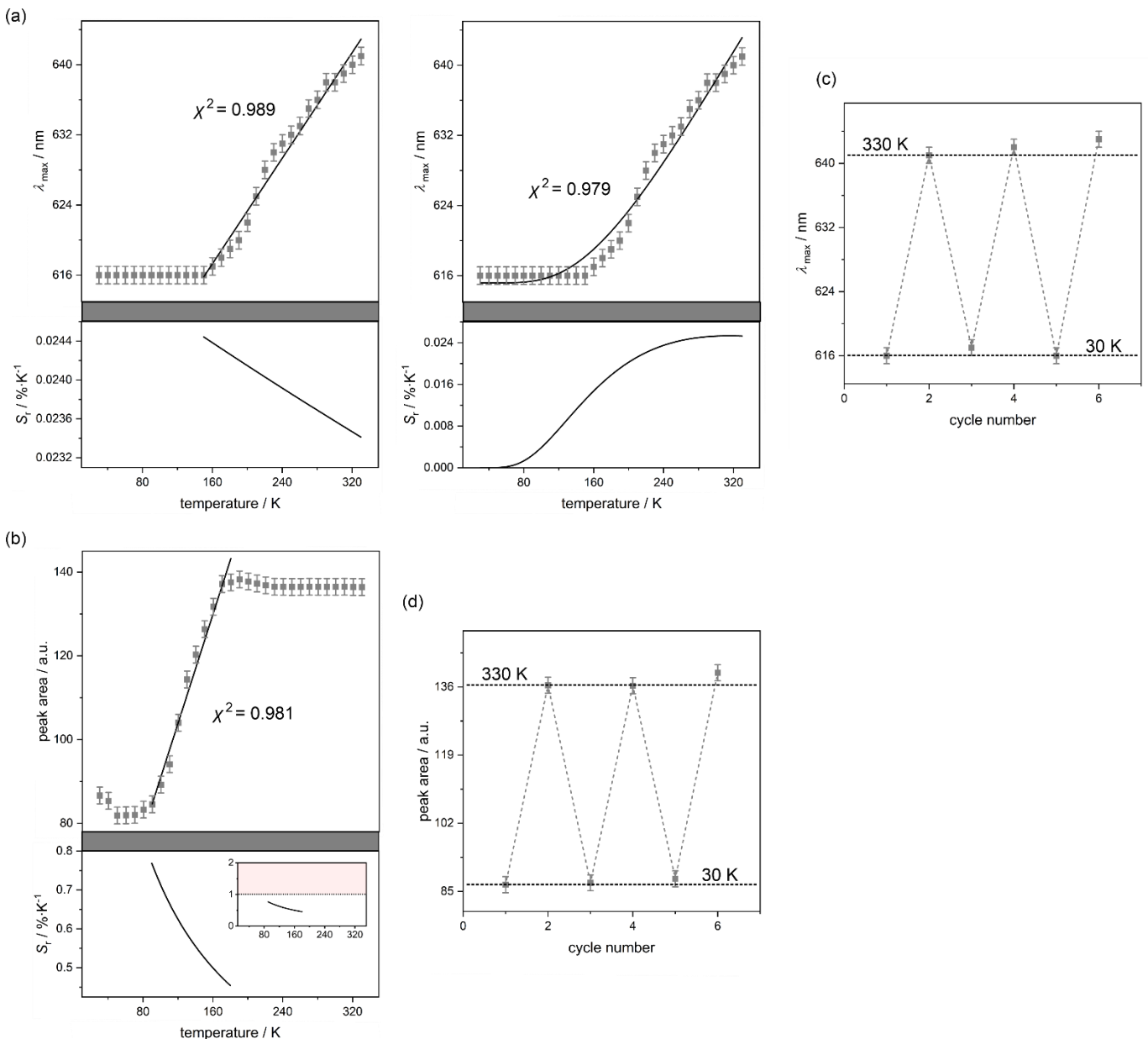


**Fig. S56** Temperature dependencies of the wavelength position of the emission maximum ( $\lambda_{\max}$ , a), and the integrated emission intensity (peak area, b) for **Re<sub>2</sub>-bpee** (see Fig. S29 and Table S35), presented with the best-fit curves (solid lines) obtained using the linear (left panel) and Mott-Seitz equations (right panel, only for the b part), together with the relative thermal sensitivity ( $S_r$ ) parameters (under the corresponding fits), and thermal repeatability of each of two discussed parameters along six consecutive measurements (c and d, corresponding to the a and b parts, respectively). The resulting best-fit parameters and used equations are gathered in Tables S66 and S68.

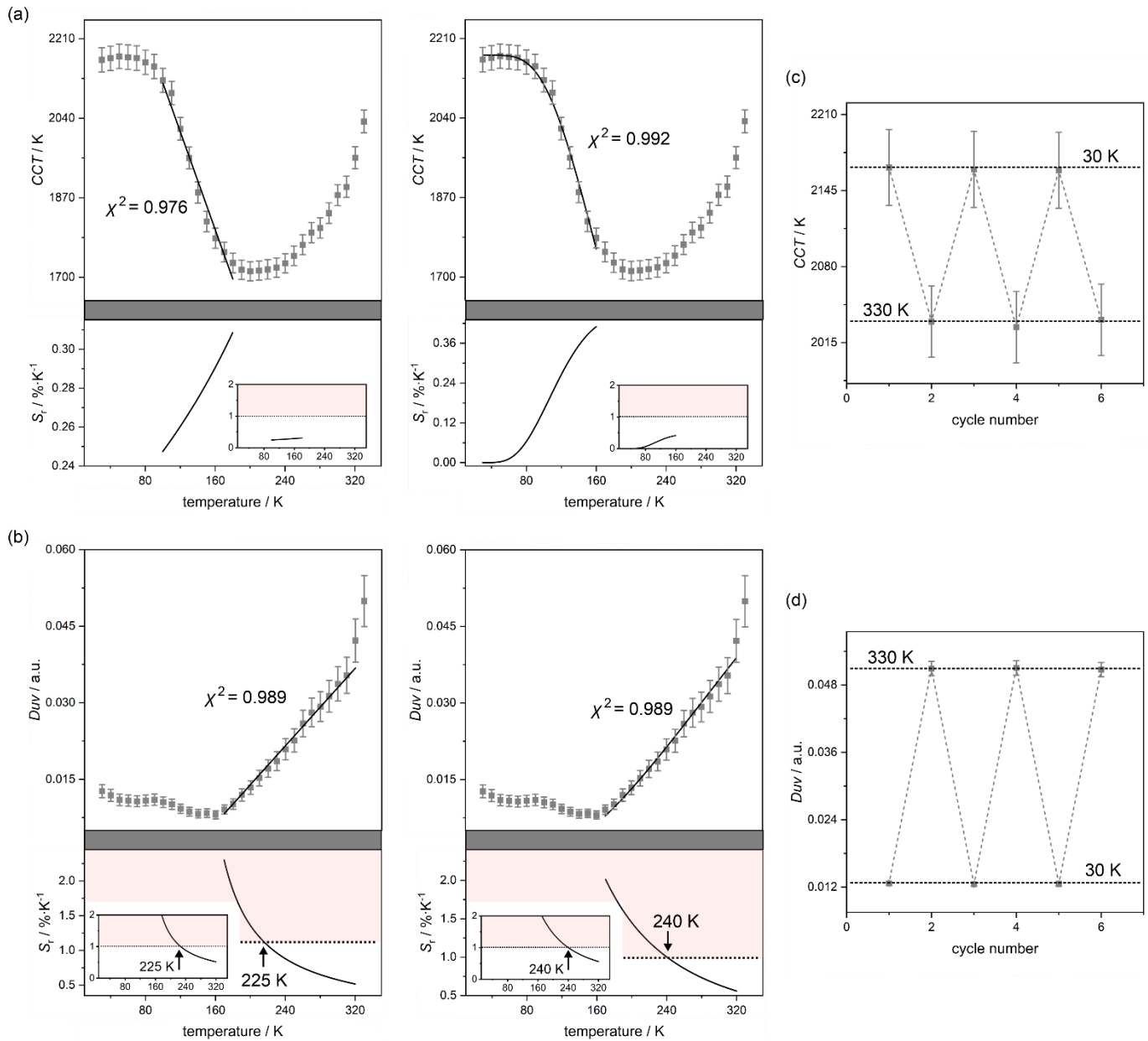


**Fig. S57** Temperature dependencies of the correlated color temperature (CCT, a) and  $D_{uv}$  value (b) calculated from the CIE 1931 chromaticity  $x$  and  $y$  parameters of the solid-state photoluminescent properties of **Re<sub>2</sub>-bpee** (see Fig. S29 and Table S36), shown with the best-fit curves (solid lines) obtained using the linear (left panel) and Mott-Seitz equations (right panel), together with the relative thermal sensitivity ( $S_r$ ) parameters (under the corresponding fits), and thermal repeatability of each of two discussed parameters along six consecutive measurements (c and d, corresponding to the a and b parts, respectively). The resulting best-fit parameters and employed equations are gathered in Tables S69 and S70.

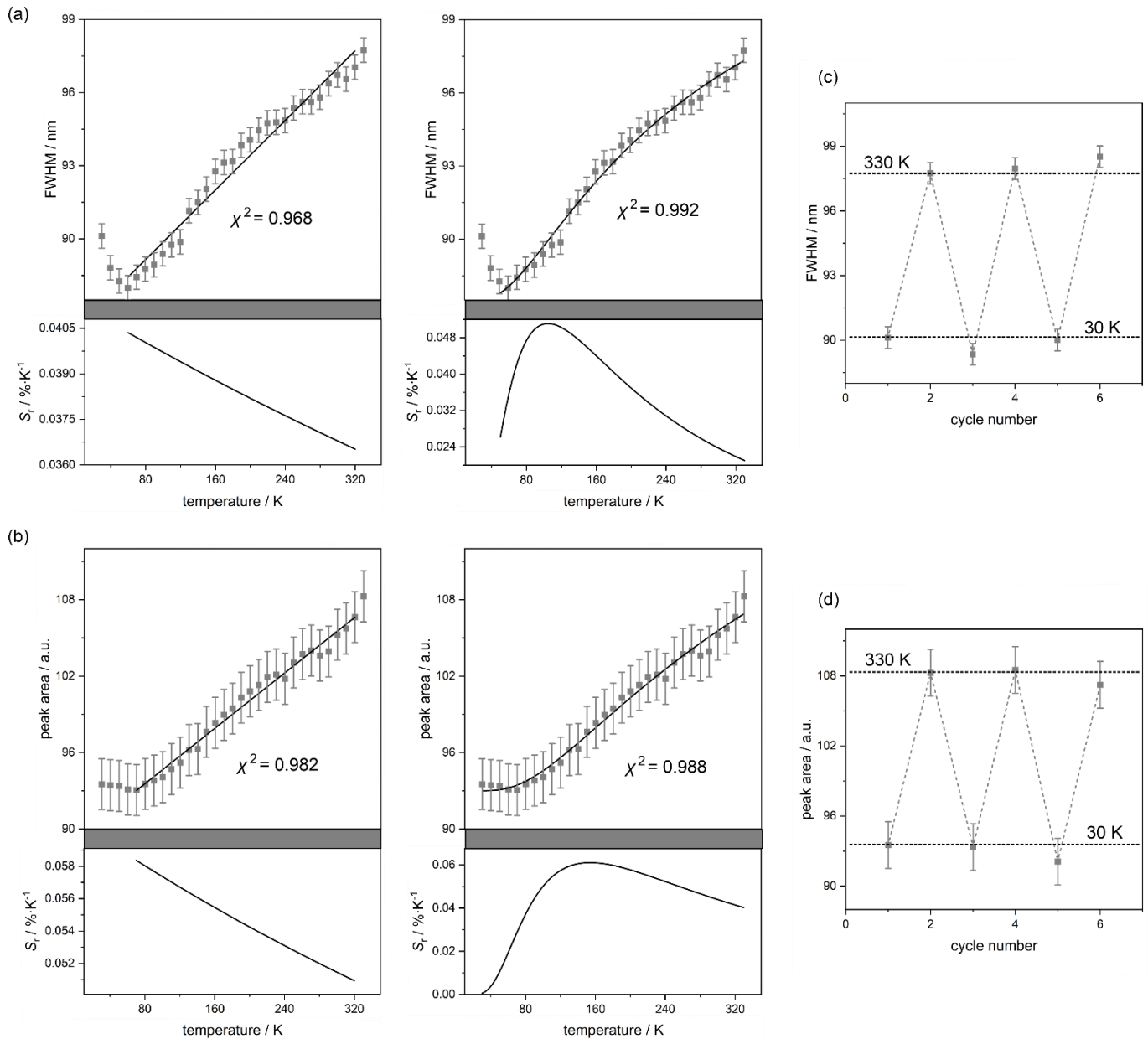


**Fig. S58** Temperature dependencies of the full width at half maximum of the emission band ( $FWHM$ , a), and the integrated emission intensity (peak area, b) for **Re<sub>2</sub>-bpn** (see Fig. S30 and Table S37), presented with the best-fit curves (solid lines) obtained using the linear (left panel) and Mott-Seitz equations (right panel), together with the relative thermal sensitivity ( $S_t$ ) parameters (under the corresponding fits), and thermal repeatability of each of two discussed parameters along six consecutive measurements (c and d, corresponding to the a and b parts, respectively). The resulting best-fit parameters and used equations are gathered in Tables S67 and S68.

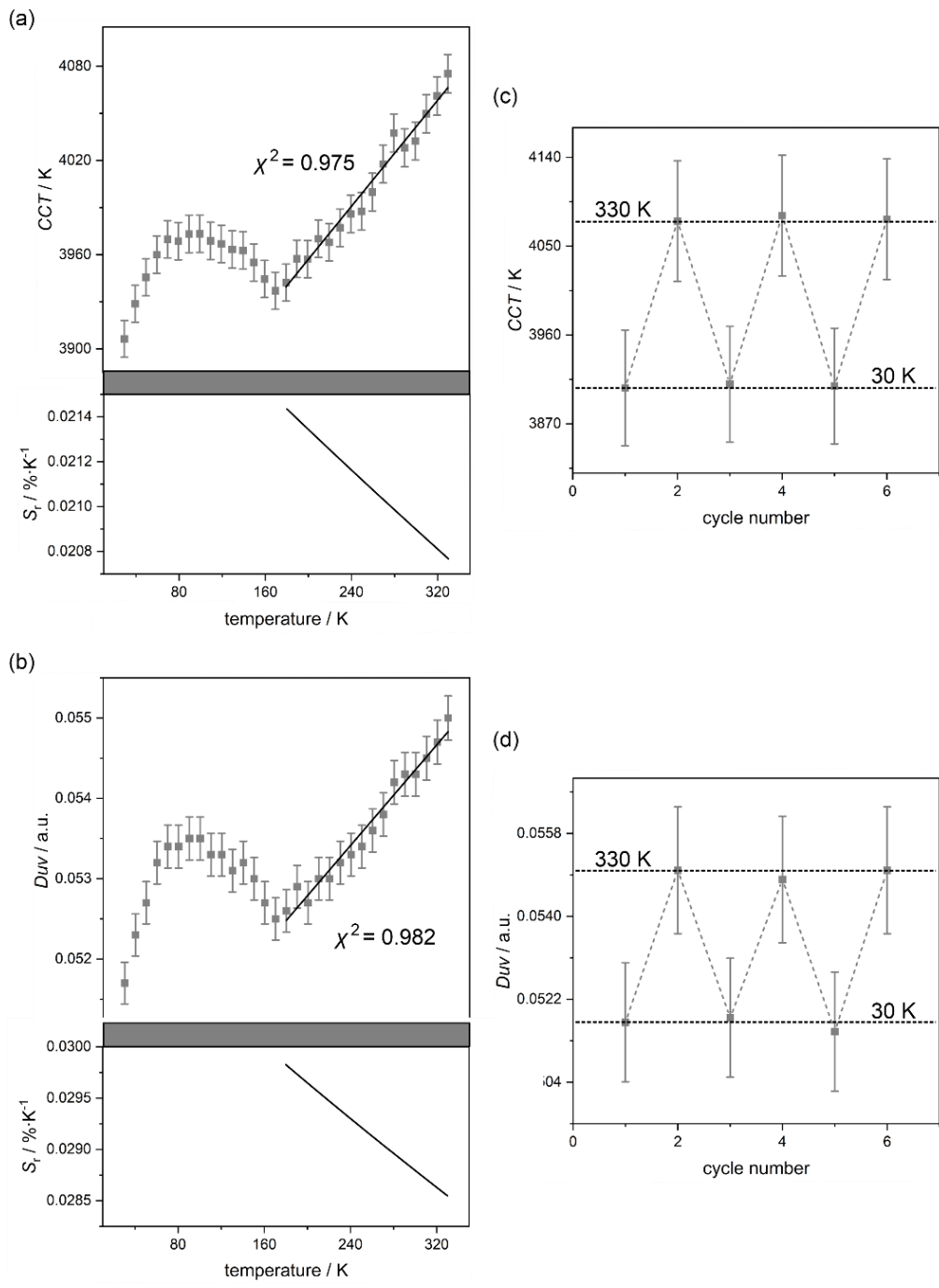


**Fig. S59** Temperature dependencies of the correlated color temperature (CCT, a) and  $D_{uv}$  value (b) calculated from the CIE 1931 chromaticity  $x$  and  $y$  parameters of the solid-state photoluminescent properties of **Re<sub>2</sub>-bpn** (see Fig. S30 and Table S38), shown with the best-fit curves (solid lines) obtained using the linear fitting, together with the relative thermal sensitivity ( $S_r$ ) parameters (under the corresponding fits), and thermal repeatability of each parameter along six consecutive measurements (c and d, corresponding to the a and b parts, respectively). The resulting best-fit parameters and employed equations are gathered in Tables S69 and S70.

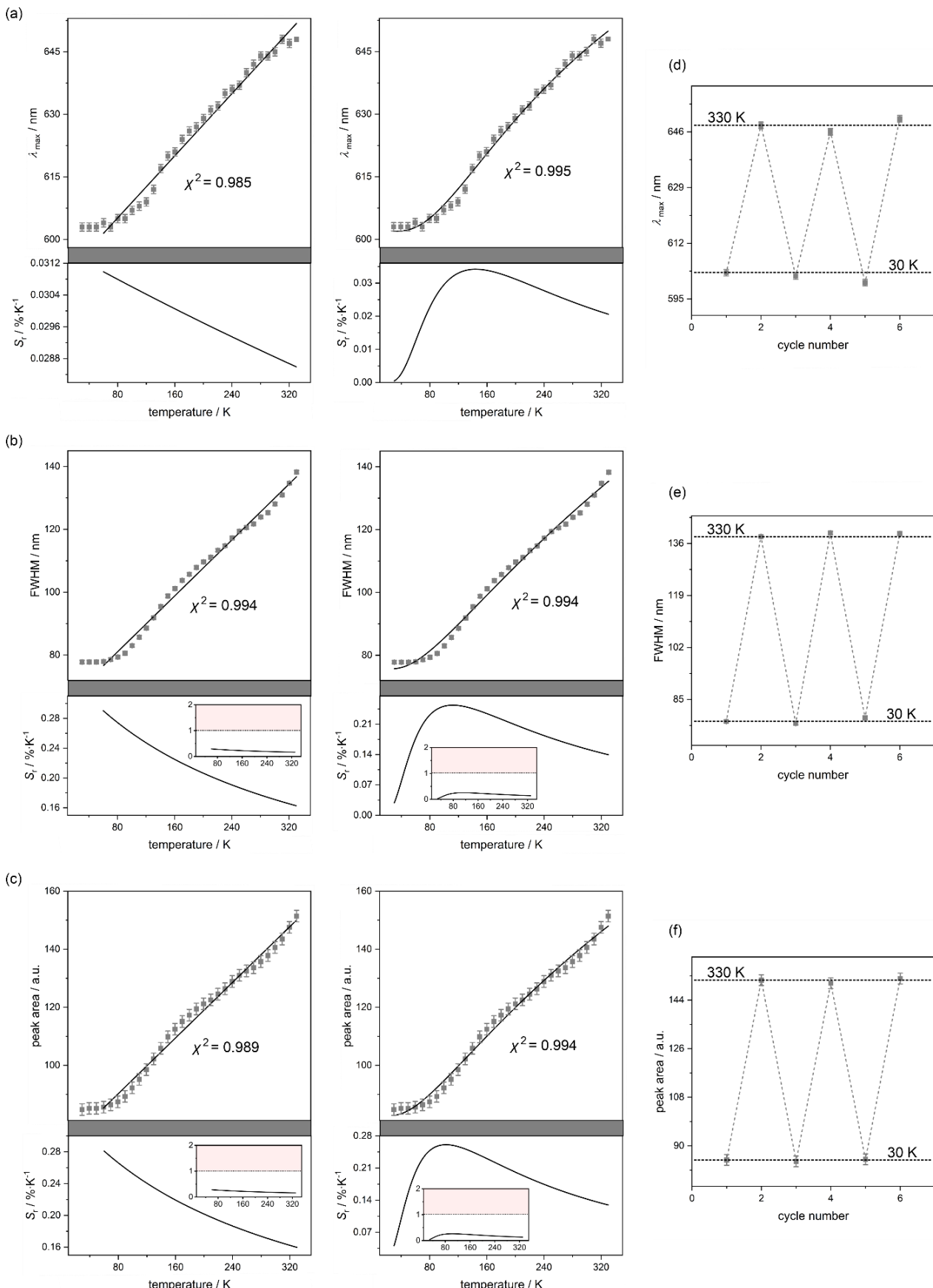


**Fig. S60** Temperature dependencies of the wavelength position of the emission maximum ( $\lambda_{\text{max}}$ , a), the full width at half maximum of the emission band (FWHM, b), and the integrated emission intensity (peak area, c) for **Re<sub>2</sub>-bpb** (see Fig. S31 and Table S39), presented with the best-fit curves (solid lines) obtained using the linear (left panel) and Mott-Seitz equations (right panel), together with the relative thermal sensitivity ( $S_r$ ) parameters (under the corresponding fits), and thermal repeatability of each of three discussed parameters along six consecutive measurements (d–f, corresponding to the a–c parts, respectively). The resulting best-fit parameters and used equations are gathered in Tables S66–S68.

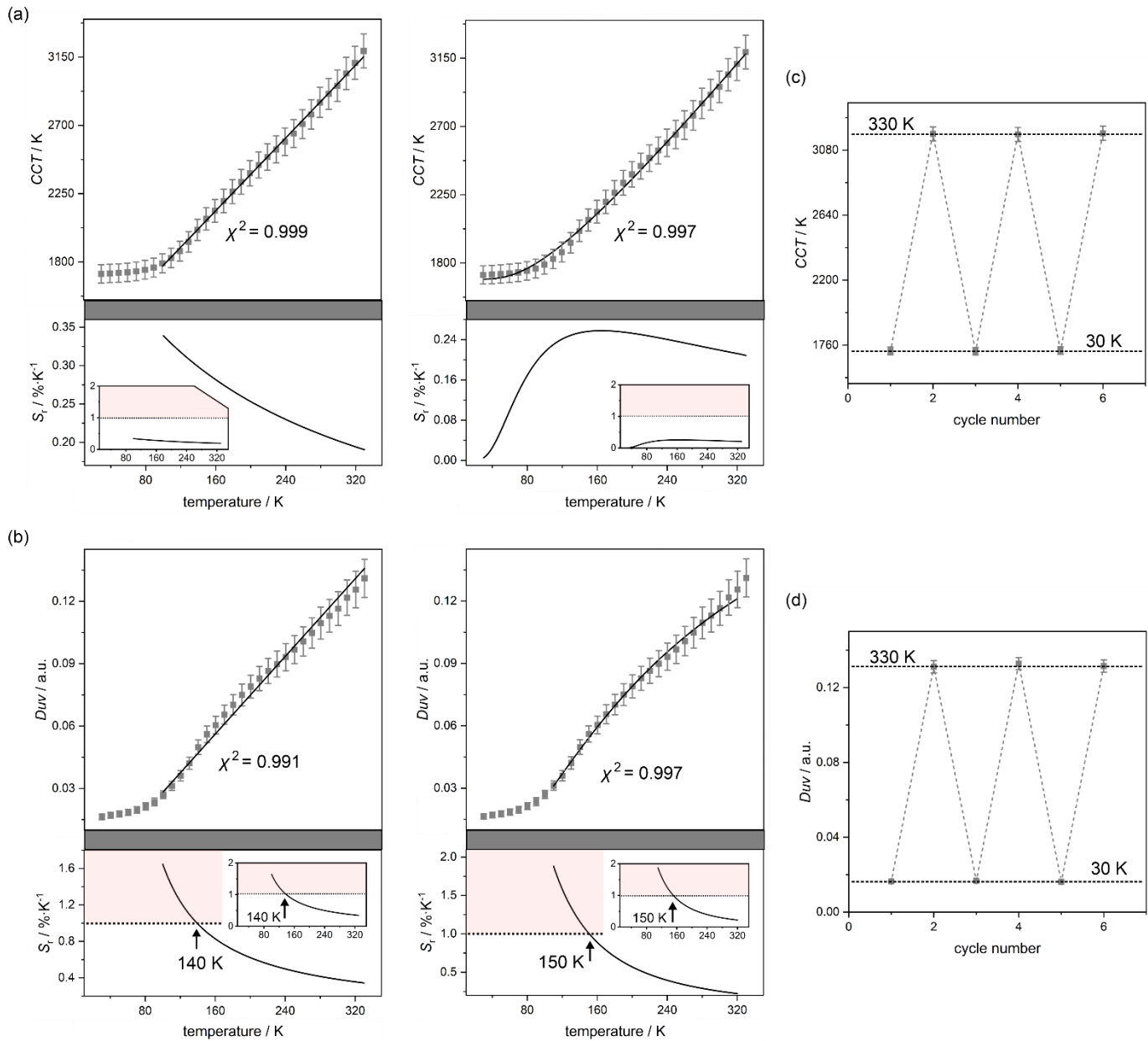


**Fig. S61** Temperature dependencies of the correlated color temperature (CCT, a) and  $D_{uv}$  value (b) calculated from the CIE 1931 chromaticity  $x$  and  $y$  parameters of the solid-state photoluminescent properties of **Re<sub>2</sub>-bpb** (see Fig. S31 and Table S40), shown with the best-fit curves (solid lines) obtained using the linear (left panel) and Mott-Seitz equations (right panel), together with the relative thermal sensitivity ( $S_r$ ) parameters (under the corresponding fits), and thermal repeatability of each of two discussed parameters along six consecutive measurements (c and d, corresponding to the a and b parts, respectively). The resulting best-fit parameters and employed equations are gathered in Tables S69 and S70.

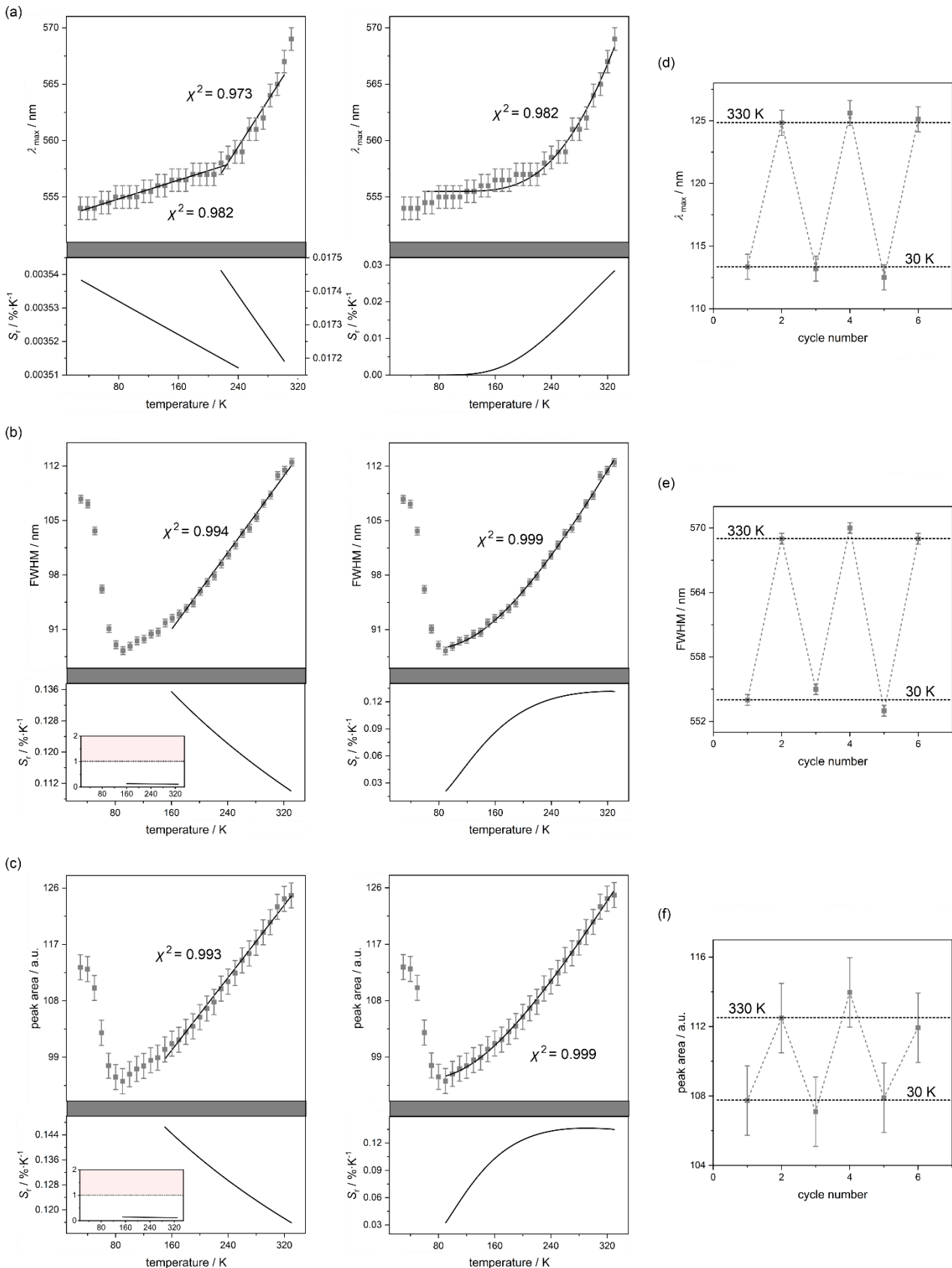


**Fig. S62** Temperature dependencies of the wavelength position of the emission maximum ( $\lambda_{\max}$ , a), the full width at half maximum of the emission band (FWHM, b), and the integrated emission intensity (peak area, c) for **Re<sub>2</sub>-bpbp** (see Fig. S32 and Table S41), presented with the best-fit curves (solid lines) obtained using the linear (left panel) and Mott-Seitz equations (right panel), together with the relative thermal sensitivity ( $S_r$ ) parameters (under the corresponding fits), and thermal repeatability of each of three discussed parameters along six consecutive measurements (d–f, corresponding to the a–c parts, respectively). The resulting best-fit parameters and used equations are gathered in Tables S66–S68.

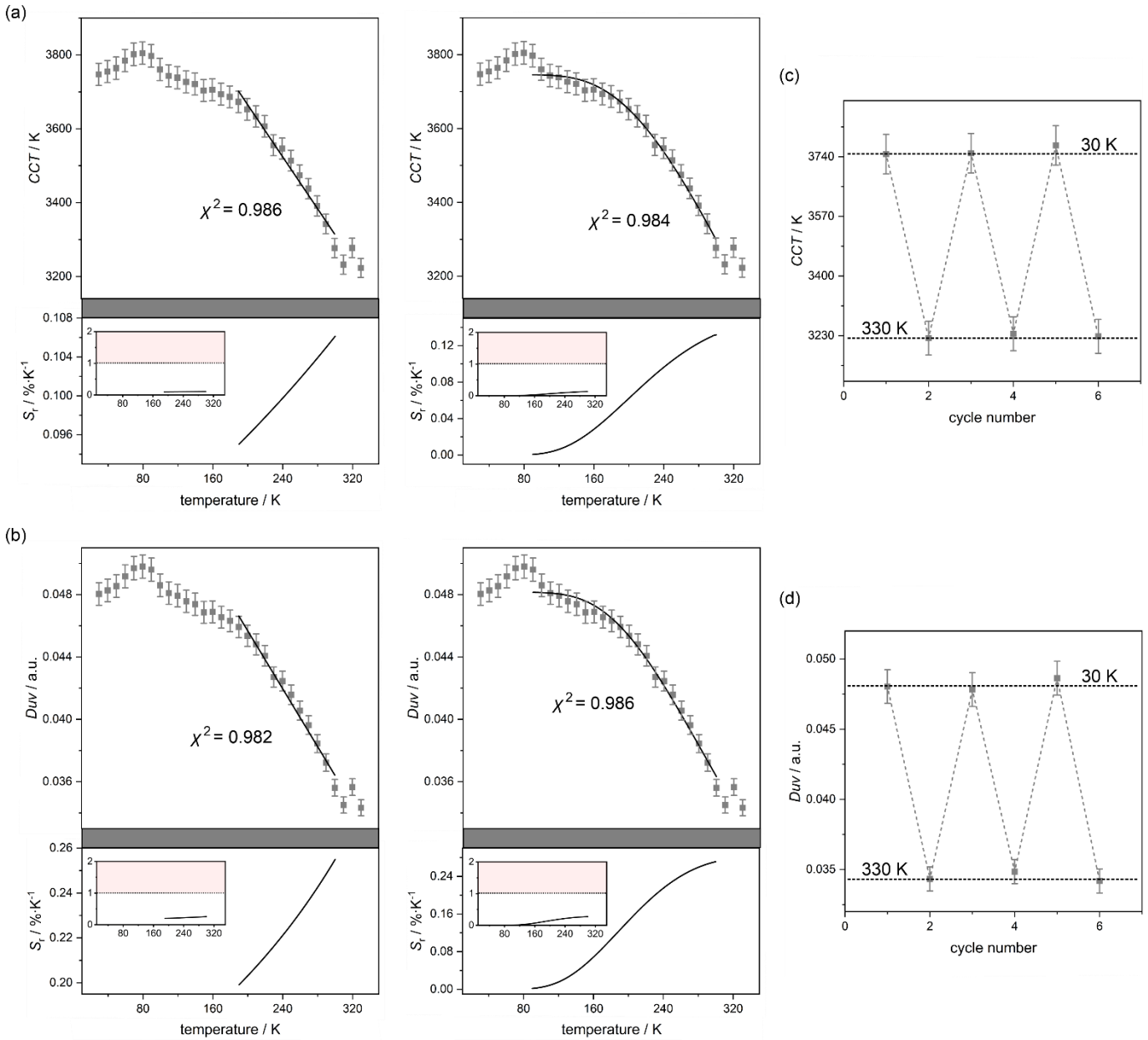


**Fig. S63** Temperature dependencies of the correlated color temperature (CCT, a) and Duv value (b) calculated from the CIE 1931 chromaticity  $x$  and  $y$  parameters of the solid-state photoluminescent properties of **Re<sub>2</sub>-bpfp** (see Fig. S32 and Table S42), shown with the best-fit curves (solid lines) obtained using the linear (left panel) and Mott-Seitz equations (right panel), together with the relative thermal sensitivity ( $S_r$ ) parameters (under the corresponding fits), and thermal repeatability of each of two discussed parameters along six consecutive measurements (c and d, corresponding to the a and b parts, respectively). The resulting best-fit parameters and employed equations are gathered in Tables S69 and S70.

**Table S66** Best-fit parameters for the linear and Mott-Seitz fittings of the temperature dependencies of the wavelength position of the emission maximum ( $\lambda_{\max}$ ) for **Re<sub>2</sub>-CN**, **Re<sub>2</sub>-bpy**, **Re<sub>2</sub>-bpac**, **Re<sub>2</sub>-bpee**, **Re<sub>2</sub>-bpb**, and **Re<sub>2</sub>-bpbp**, investigated within the indicated temperature ranges (see Fig. S48, S52, S54, S56, S60, and S62). Note that **Re<sub>2</sub>-en** and **Re<sub>2</sub>-bpn** do not appear here as the related temperature dependencies of the  $\lambda_{\max}$  values were too weak to be employed for optical thermometry.

Material	Temp. range / K	Equation: $\lambda^{\max} = A + B \cdot T$			$\chi^2 / \%$	$S_r^{\max} / \text{m}^2 \cdot \text{K}^{-1}$	$T$ for $S_r^{\max} / \text{K}$
		A / nm	B / nm·K <sup>-1</sup>				
<b>Re<sub>2</sub>-CN</b>	190–330	557.5(1.90)	0.192(0.007)		98.2	0.03	190
<b>Re<sub>2</sub>-bpy</b>	30–240	582.0(0.31)	0.039(0.002)		97.2	<0.01	–
	240–330	481.7(5.67)	0.454(0.020)		98.8	0.08	240
<b>Re<sub>2</sub>-bpac</b>	30–250	575.7(1.51)	0.244(0.010)		96.9	0.04	30
<b>Re<sub>2</sub>-bpee</b>	150–330	593.2(1.34)	0.151(0.005)		98.9	0.02	150
<b>Re<sub>2</sub>-bpb</b>	60–330	590.3(0.95)	0.186(0.004)		98.5	0.03	60
<b>Re<sub>2</sub>-bpbp</b>	30–240	553.2(0.13)	0.020(0.001)		98.2	<0.01	–
	230–320	534.7(2.45)	0.097(0.009)		97.3	0.02	230
Material	Temp. range / K	Mott-Seitz equation: <sup>S32</sup> $\lambda^{\max} = A / (1 + B \cdot \exp(C/T))$			$\chi^2 / \%$	$S_r^{\max} / \text{m}^2 \cdot \text{K}^{-1}$	$T$ for $S_r^{\max} / \text{K}$
		A / nm	B	C / K			
<b>Re<sub>2</sub>-CN</b>	110–330	593.7(0.24)	-1.0(0.07)	-1021.3(31.67)	99.7	0.05	330
<b>Re<sub>2</sub>-bpy</b>	30–330	585.9(0.28)	-6.4(1.01)	-1461.9(49.00)	99.4	0.11	330
<b>Re<sub>2</sub>-bpac</b>	30–330	590.9(1.69)	-0.4(0.03)	-389.4(28.67)	97.9	0.06	210
<b>Re<sub>2</sub>-bpee</b>	30–330	615.2(0.48)	-0.3(0.01)	-605.1(43.23)	97.7	0.03	310
<b>Re<sub>2</sub>-bpb</b>	30–330	601.9(0.59)	-0.2(0.01)	-281.2(11.15)	99.5	0.03	145
<b>Re<sub>2</sub>-bpbp</b>	60–330	555.5(0.17)	-1.3(0.37)	-1337.6(52.12)	98.2	0.03	330

**Table S67** Best-fit parameters for the linear and Mott-Seitz fittings of the temperature dependencies of the full width at half maximum of emission band (*FWHM*) for **Re<sub>2</sub>-CN**, **Re<sub>2</sub>-en**, **Re<sub>2</sub>-bpy**, **Re<sub>2</sub>-bpb**, and **Re<sub>2</sub>-bpbp**, investigated within the indicated temperature ranges (see Fig. S48, S50, S52, S58, S60, and S62). Note that **Re<sub>2</sub>-bpac** and **Re<sub>2</sub>-bpee** do not appear here as the related temperature dependencies of the *FWHM* values were too weak to be employed for optical thermometry.

Material	Temp. range / K	Equation: $FWHM = A + B \cdot T$		$\chi^2 / \%$	$S_r^{\max} / \text{m}^2 \cdot \text{K}^{-1}$	$T$ for $S_r^{\max} / \text{K}$
		A / nm	B / nm·K <sup>-1</sup>			
<b>Re<sub>2</sub>-CN</b>	30–330	105.8(0.49)	0.090(0.002)	97.9	0.08	30
<b>Re<sub>2</sub>-en</b>	90–290	108.4(0.20)	-0.029(0.001)	97.8	0.03	290
<b>Re<sub>2</sub>-bpy</b>	120–330	58.9(1.18)	0.283(0.005)	99.5	0.30	120
<b>Re<sub>2</sub>-bpn</b>	60–320	86.3(0.27)	0.036(0.001)	96.8	0.04	60
<b>Re<sub>2</sub>-bpb</b>	60–330	63.3(0.87)	0.223(0.004)	99.4	0.29	60
<b>Re<sub>2</sub>-bpbp</b>	160–330	71.4(0.68)	0.123(0.003)	99.4	0.14	160
Material	Temp. range / K	Mott-Seitz equation: <sup>S32</sup> $FWHM = A / (1 + B \cdot \exp(C/T))$			$\chi^2 / \%$	$T$ for $S_r^{\max} / \text{K}$
		A / nm	B	C / K		
<b>Re<sub>2</sub>-CN</b>	90–330	115.5(0.43)	-0.8(0.07)	-518.0(33.8)	99.3	0.09
<b>Re<sub>2</sub>-en</b>	80–280	105.3(0.08)	0.4(0.03)	-534.3(23.56)	99.5	0.04
<b>Re<sub>2</sub>-bpy</b>	30–330	86.6(0.31)	-1.1(0.02)	-299.2(5.60)	99.9	0.24
<b>Re<sub>2</sub>-bpn</b>	50–330	87.5(0.24)	-0.2(0.01)	-203.8(13.02)	99.2	0.05
<b>Re<sub>2</sub>-bpb</b>	30–330	75.6(0.89)	-0.8(0.02)	-192.2(10.4)	99.4	0.25
<b>Re<sub>2</sub>-bpbp</b>	90–330	88.4(0.18)	-1.0(0.03)	-518.5(12.92)	99.9	0.13

**Table S68** Best-fit parameters for the linear and Mott-Seitz fittings of the temperature dependencies of the integrated emission intensity (peak area,  $I$ ) for **Re<sub>2</sub>-CN**, **Re<sub>2</sub>-bpy**, **Re<sub>2</sub>-bpee**, **Re<sub>2</sub>-bpen**, **Re<sub>2</sub>-bpb**, and **Re<sub>2</sub>-bpbp**, investigated within the indicated temperature ranges (see Fig. S48, S52, S56, S58, S60, and S62). Note that **Re<sub>2</sub>-en** and **Re<sub>2</sub>-bpac** do not appear here as the related temperature dependencies of the  $I$  values were too weak to be employed for optical thermometry.

Material	Temp. range / K	Equation: $I = A + B \cdot T$			$\chi^2 / \%$	$S_r^{\max} / \text{mV}\cdot\text{K}^{-1}$	$T$ for $S_r^{\max} / \text{K}$
		A	$B / \text{K}^{-1}$				
<b>Re<sub>2</sub>-CN</b>	30–330	119.4(0.42)		0.076(0.002)	98.2	0.06	30
<b>Re<sub>2</sub>-bpy</b>	90–330	74.9(0.55)		0.273(0.003)	99.8	0.27	90
<b>Re<sub>2</sub>-bpee</b>	90–180	26.1(1.84)		0.651(0.035)	98.1	0.77	90
<b>Re<sub>2</sub>-bpen</b>	70–320	89.2(0.29)		0.054(0.001)	98.2	0.06	70
<b>Re<sub>2</sub>-bpb</b>	60–330	70.9(1.05)		0.240(0.005)	98.9	0.28	60
<b>Re<sub>2</sub>-bpbp</b>	150–330	77.0(0.76)		0.145(0.003)	99.3	0.15	150
Material	Temp. range / K	Mott-Seitz equation: <sup>S32</sup> $I = A / (1 + B \cdot \exp(C/T))$			$\chi^2 / \%$	$S_r^{\max} / \text{mV}\cdot\text{K}^{-1}$	$T$ for $S_r^{\max} / \text{K}$
		A	B	C / K			
<b>Re<sub>2</sub>-CN</b>	50–330	125.2(0.26)	-0.5(0.01)	-392.5(17.43)	99.3	0.07	210
<b>Re<sub>2</sub>-bpy</b>	30–330	96.5(0.25)	-0.9(0.01)	-259.3(3.67)	99.9	0.22	160
<b>Re<sub>2</sub>-bpen</b>	30–330	93.0(0.24)	-0.3(0.01)	-293.5(16.89)	98.8	0.06	150
<b>Re<sub>2</sub>-bpb</b>	30–330	82.6(1.03)	-0.8(0.02)	-178.1(10.13)	99.4	0.26	100
<b>Re<sub>2</sub>-bpbp</b>	90–330	95.4(0.24)	-1.0(0.03)	-465.7(12.07)	99.9	0.14	290

**Table S69** Best-fit parameters for the linear and Mott-Seitz fittings of the temperature dependencies of the correlated color temperature (*CCT*) for **Re<sub>2</sub>-CN**, **Re<sub>2</sub>-en**, **Re<sub>2</sub>-bpy**, **Re<sub>2</sub>-bpac**, **Re<sub>2</sub>-bpee**, **Re<sub>2</sub>-bpen**, **Re<sub>2</sub>-bpb**, and **Re<sub>2</sub>-bpbp**, investigated within the indicated temperature ranges (see Fig. S49, S51, S53, S55, S57, S59, S61, and S63).

Material	Temp. range / K	Equation: $\text{CCT} = A + B \cdot T$		$\chi^2 / \%$	$S_r^{\max} / \text{mV} \cdot \text{K}^{-1}$	$T$ for $S_r^{\max} / \text{K}$	
		A / K	B				
<b>Re<sub>2</sub>-CN</b>	40–130	2516.5(8.6)	-2.3(0.1)	98.9	0.11	130	
	220–270	2709.2(23.0)	-2.4(0.1)	99.1	0.12	280	
<b>Re<sub>2</sub>-en</b>	60–150	3666.5(9.3)	4.0 (0.1)	99.6	0.10	60	
<b>Re<sub>2</sub>-bpy</b>	110–330	3041.1(20.6)	-4.0(0.1)	99.1	0.23	330	
<b>Re<sub>2</sub>-bpac</b>	210–330	278.6(46.5)	6.8(0.2)	99.2	0.40	210	
<b>Re<sub>2</sub>-bpee</b>	100–180	2638.2(48.5)	-5.2(0.3)	97.6	0.31	180	
<b>Re<sub>2</sub>-bpen</b>	180–330	3787.6(10.2)	0.8(0.01)	97.5	0.02	180	
<b>Re<sub>2</sub>-bpb</b>	100–330	1171.1(9.8)	6.0(0.1)	99.9	0.34	100	
<b>Re<sub>2</sub>-bpbp</b>	190–300	4370.5( $\pm 43.9$ )	-3.5( $\pm 0.2$ )	98.6	0.11	300	
Material	Temp. range / K	Mott-Seitz equation: $\text{CCT} = A / (1 + B \cdot \exp(C/T))$			$\chi^2 / \%$	$T$ for $S_r^{\max} / \text{K}$	
		A / K	B	C / K			
<b>Re<sub>2</sub>-en</b>	60–280	3319.0(222.4)	-0.3(0.01)	-39.5(13.4)	98.9	0.18	60
<b>Re<sub>2</sub>-bpy</b>	30–330	2595.7(9.2)	3.0(0.3)	-598.5(23.7)	99.2	0.21	240
<b>Re<sub>2</sub>-bpac</b>	140–330	1672.2(39.0)	-4.8(0.8)	-864.0(14.2)	97.3	0.42	330
<b>Re<sub>2</sub>-bpee</b>	30–160	2174.2(5.9)	7.4(1.6)	-551.0(29.6)	99.2	0.41	160
<b>Re<sub>2</sub>-bpb</b>	30–330	1693.1(11.1)	-1.0(0.1)	-259.4(7.4)	99.7	0.26	165
<b>Re<sub>2</sub>-bpbp</b>	90–300	3745.9(6.9)	3.8(0.8)	-1000.0(60.3)	98.4	0.13	300

**Table S70** Best-fit parameters for the linear and Mott-Seitz fittings of the temperature dependencies of the Delta  $u,v$  ( $D_{UV}$ ) value for **Re<sub>2</sub>-CN**, **Re<sub>2</sub>-en**, **Re<sub>2</sub>-bpy**, **Re<sub>2</sub>-bpac**, **Re<sub>2</sub>-bpee**, **Re<sub>2</sub>-bpen**, **Re<sub>2</sub>-bpb**, and **Re<sub>2</sub>-bpbp**, investigated within the indicated temperature ranges (see Fig. S49, S51, S53, S55, S57, S59, S61, and S63).

Material	Temp. range / K	Equation: $D_{UV} = A + B \cdot T$		$\chi^2 / \%$	$S_r^{\max} / \text{mV}\cdot\text{K}^{-1}$	$T$ for $S_r^{\max} / \text{K}$	
		A	B / $10^{-5} \text{ K}^{-1}$				
<b>Re<sub>2</sub>-CN</b>	40–130	0.019(0.0002)	-4.368(0.192)	98.4	0.34	130	
	210–330	0.019(0.0004)	-3.258(0.148)	97.9	0.38	330	
<b>Re<sub>2</sub>-en</b>	60–150	0.044(0.0001)	9.604(0.180)	99.7	0.19	60	
<b>Re<sub>2</sub>-bpy</b>	70–290	0.025(0.0003)	-5.654(0.117)	99.2	0.66	290	
<b>Re<sub>2</sub>-bpac</b>	230–330	-0.090(0.005)	54.941(1.822)	99.0	1.52	230	
<b>Re<sub>2</sub>-bpee</b>	170–320	-0.024(0.001)	26.178(1.240)	98.9	2.29	170	
<b>Re<sub>2</sub>-bpen</b>	180–330	0.050(0.0002)	1.565(0.072)	98.2	0.03	180	
<b>Re<sub>2</sub>-bpb</b>	100–330	-0.018(0.002)	46.702(0.973)	99.1	1.65	100	
<b>Re<sub>2</sub>-bpbp</b>	190–300	0.064( $\pm 0.001$ )	-9.285( $\pm 0.405$ )	98.2	0.25	300	
Material	Temp. range / K	Mott-Seitz equation: $D_{UV} = A / (1 + B \cdot \exp(C/T))$			$\chi^2 / \%$	$T$ for $S_r^{\max} / \text{K}$	
		A	B	C / K			
<b>Re<sub>2</sub>-en</b>	80–270	1.213 (0.03)	17.2(1.2)	21.80353(1.2)	99.3	0.33	80
<b>Re<sub>2</sub>-bpy</b>	60–290	0.020(0.001)	7.2(0.91)	-534.4(23.1)	98.1	0.45	190
<b>Re<sub>2</sub>-bpac</b>	120–320	416718.3(1.1)	554346.3(1.5)	711.5(42.2)	95.8	4.96	120
<b>Re<sub>2</sub>-bpee</b>	170–320	2.0(0.1)	0.717(0.03)	674.0(12.0)	98.9	2.02	170
<b>Re<sub>2</sub>-bpb</b>	110–320	26580.6(6.6)	107694.4(2.6)	227.7(10.2)	99.7	1.88	110
<b>Re<sub>2</sub>-bpbp</b>	90–300	0.048(0.0002)	8.9(0.8)	-993.98(63.8)	98.6	0.27	300

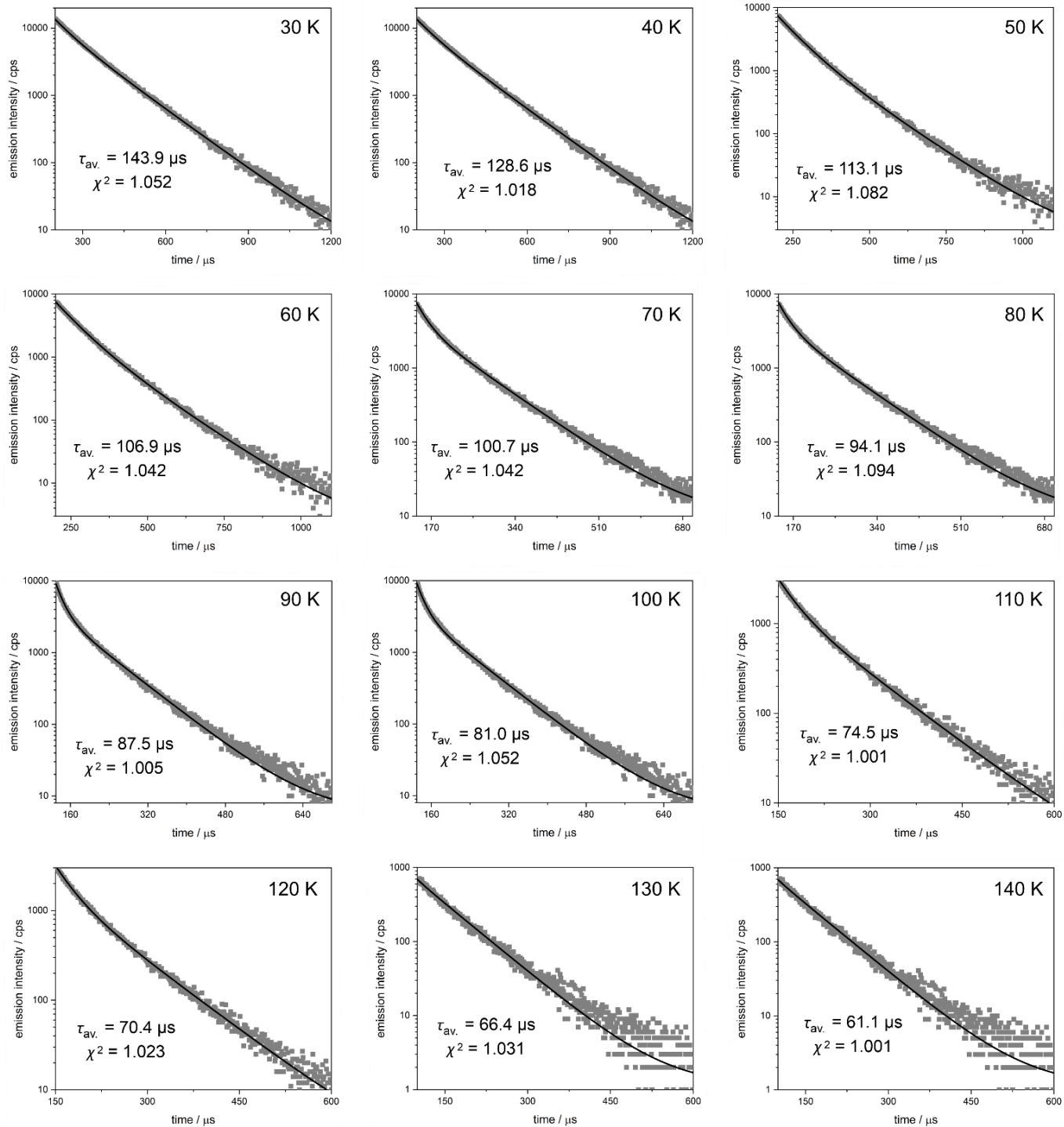


**Fig. S64 (part 1 of 2)** Temperature-variable emission decay profiles for **Re<sub>2</sub>-CN** under  $\lambda_{\text{ex}} = 430$  nm and  $\lambda_{\text{em}} = 595$  nm, collected for the indicated temperatures from the 30–230 K range (in this part, the region of 30–140 K is shown). The double exponential fitting was applied for each temperature; the related best-fit curve is illustrated by a solid line. The best-fit parameters are roughly presented on the graphs while the detailed values are gathered in Table S71.

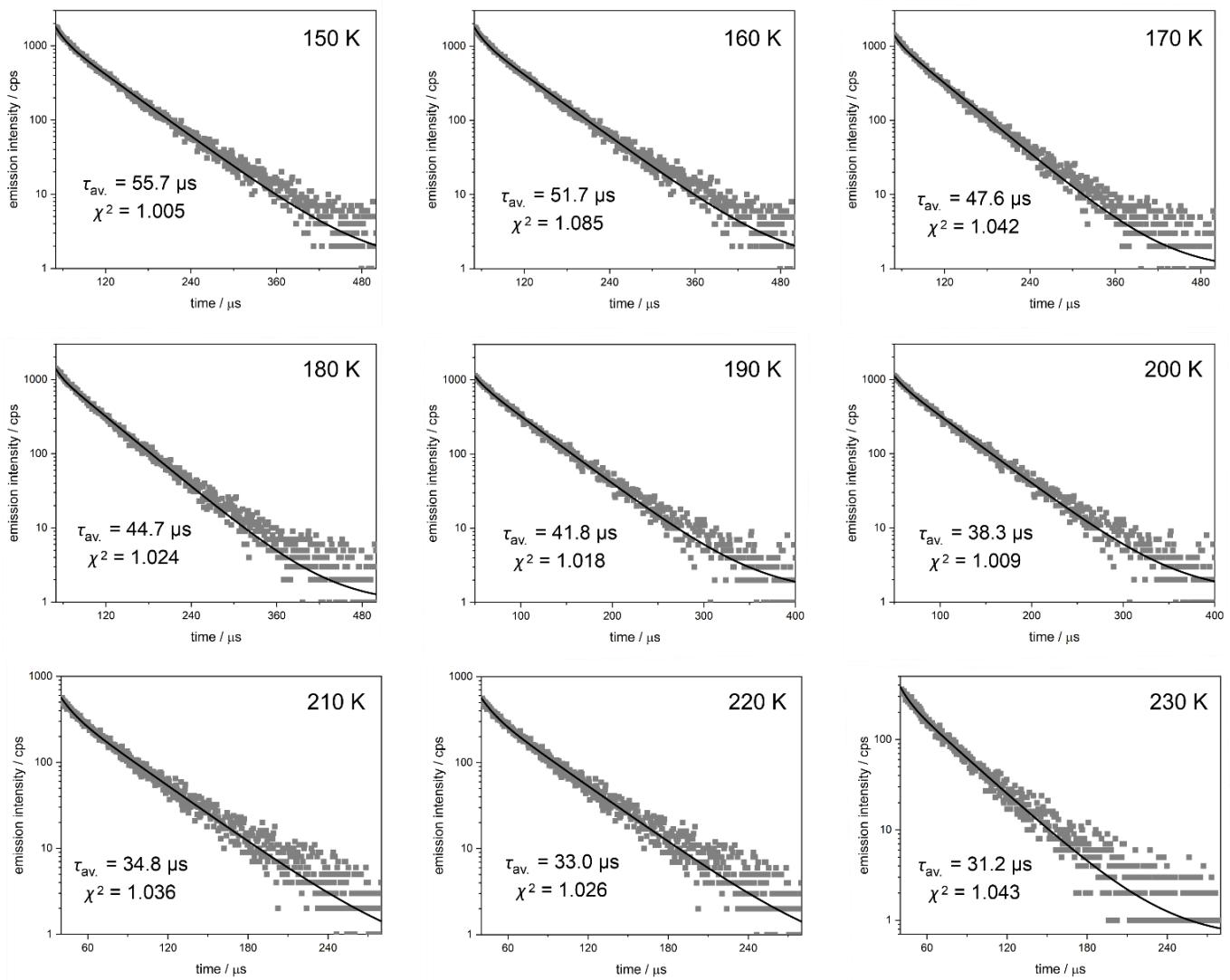


**Fig. S64** (part 2 of 2) Temperature-variable emission decay profiles for **Re<sub>2</sub>-CN** under  $\lambda_{ex} = 430$  nm and  $\lambda_{em} = 595$  nm, collected for the indicated temperatures from the 30–230 K range (in this part, the region of 150–230 K is shown). The double exponential fitting was applied for each temperature; the related best-fit curve is illustrated by a solid line. The best-fit parameters are roughly presented on the graphs while the detailed values are gathered in Table S71.

**Table S71** Best-fit parameters for the emission decay profiles of **Re<sub>2</sub>-CN** to the double exponential decay function (represented by the  $\tau_1$  and  $\tau_2$  values of emission lifetime components, with the respective contributions given in the brackets next to the lifetime values), and the calculated weighted-average emission lifetime ( $\tau_{\text{av.}}$ ), all presented for the 30–230 K temperature range (see Fig. S64 for the respective emission decay profiles).

parameter	<b>Re<sub>2</sub>-CN</b>					
	30 K	40 K	50 K	60 K	70 K	80 K
$\tau_1$ (%) / $\mu\text{s}$	98.4 (42.79)	85.0 (41.38)	71.6 (39.98)	64.4 (37.23)	57.1 (34.48)	52.6 (33.39)
$\tau_2$ (%) / $\mu\text{s}$	177.9 (57.21)	159.4 (58.62)	140.8 (60.02)	132.2 (62.77)	123.6 (65.52)	115.0 (66.61)
$\tau_{\text{av.}}$ / $\mu\text{s}$	143.9	128.6	113.1	106.9	100.7	94.1
$\chi^2$	1.052	1.018	1.082	1.042	1.038	1.094
	90 K	100 K	110 K	120 K	130 K	140 K
$\tau_1$ (%) / $\mu\text{s}$	48.1 (32.29)	42.5 (30.55)	36.9 (28.81)	33.8 (27.64)	30.7 (26.47)	24.5 (23.17)
$\tau_2$ (%) / $\mu\text{s}$	106.3 (67.71)	98.0 (69.45)	89.7 (71.19)	84.4 (72.36)	79.2 (73.53)	72.1 (76.83)
$\tau_{\text{av.}}$ / $\mu\text{s}$	87.5	81.0	74.5	70.4	66.4	61.1
$\chi^2$	1.005	1.052	1.001	1.023	1.031	1.001
	150 K	160 K	170 K	180 K	190 K	200 K
$\tau_1$ (%) / $\mu\text{s}$	18.3 (19.87)	14.6 (18.94)	11.0 (18.00)	10.6 (16.84)	10.1 (15.68)	9.4 (15.28)
$\tau_2$ (%) / $\mu\text{s}$	65.0 (80.13)	60.3 (81.06)	55.6 (82.00)	51.7 (83.16)	47.7 (84.32)	43.5 (84.72)
$\tau_{\text{av.}}$ / $\mu\text{s}$	55.7	51.7	47.6	44.7	41.8	38.3
$\chi^2$	1.001	1.085	1.042	1.024	1.018	1.009
	210 K	220 K	230 K	–	–	–
$\tau_1$ (%) / $\mu\text{s}$	8.7 (14.89)	8.8 (14.07)	8.9 (13.24)	–	–	–
$\tau_2$ (%) / $\mu\text{s}$	39.4 (85.11)	37.0 (85.93)	34.6 (86.76)	–	–	–
$\tau_{\text{av.}}$ / $\mu\text{s}$	34.8	33.0	31.2	–	–	–
$\chi^2$	1.036	1.026	1.043	–	–	–

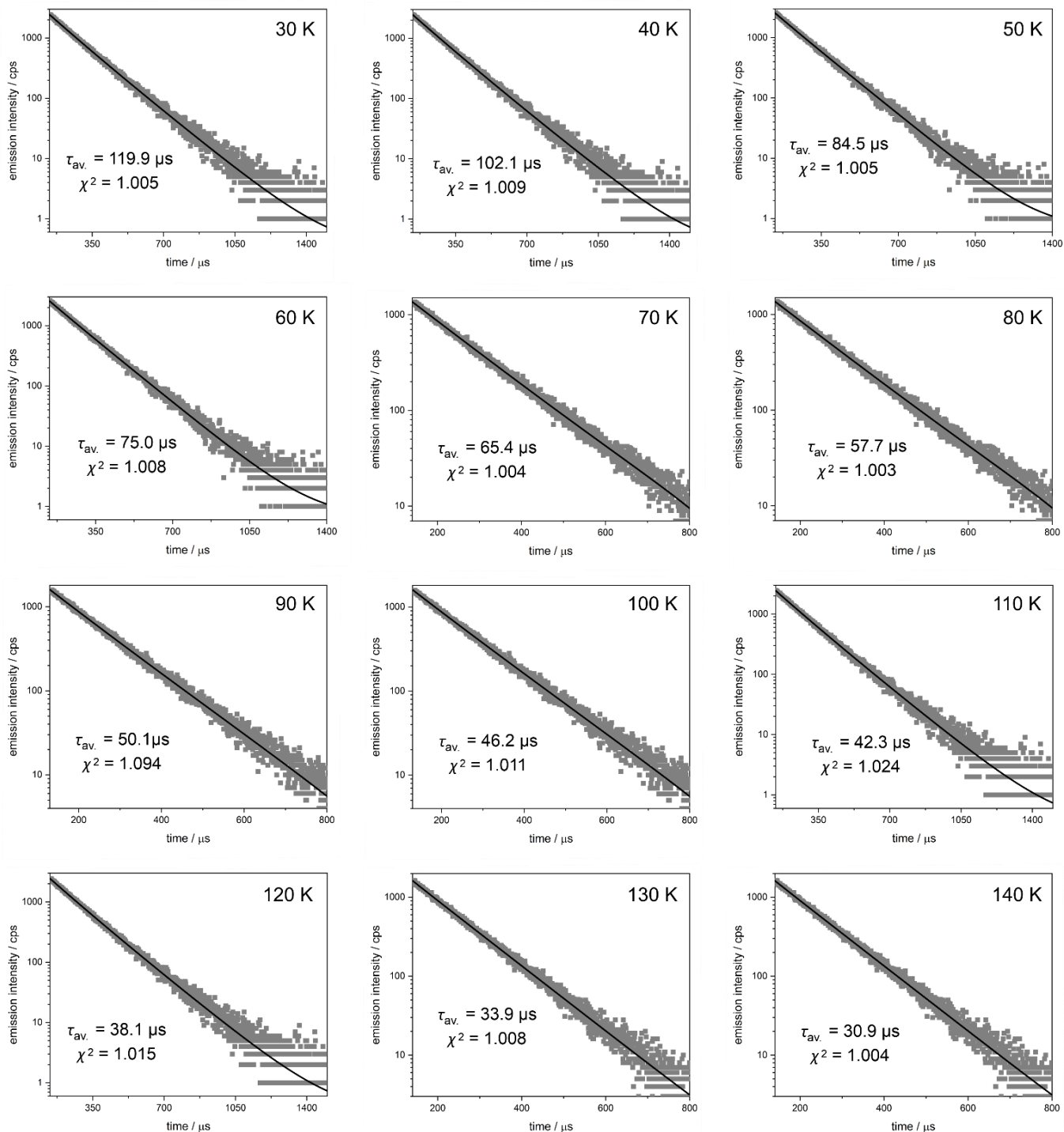


**Fig. S65 (part 1 of 3)** Temperature-variable emission decay profiles for **Re<sub>2</sub>-en** under  $\lambda_{ex} = 430$  nm and  $\lambda_{em} = 542$  nm, collected for the indicated temperatures from the 30–330 K range (in this part, the region of 30–140 K is shown). The double exponential fitting was applied for each temperature; the related best-fit curve is illustrated by a solid line. The best-fit parameters are roughly presented on the graphs while the detailed values are gathered in Table S72.

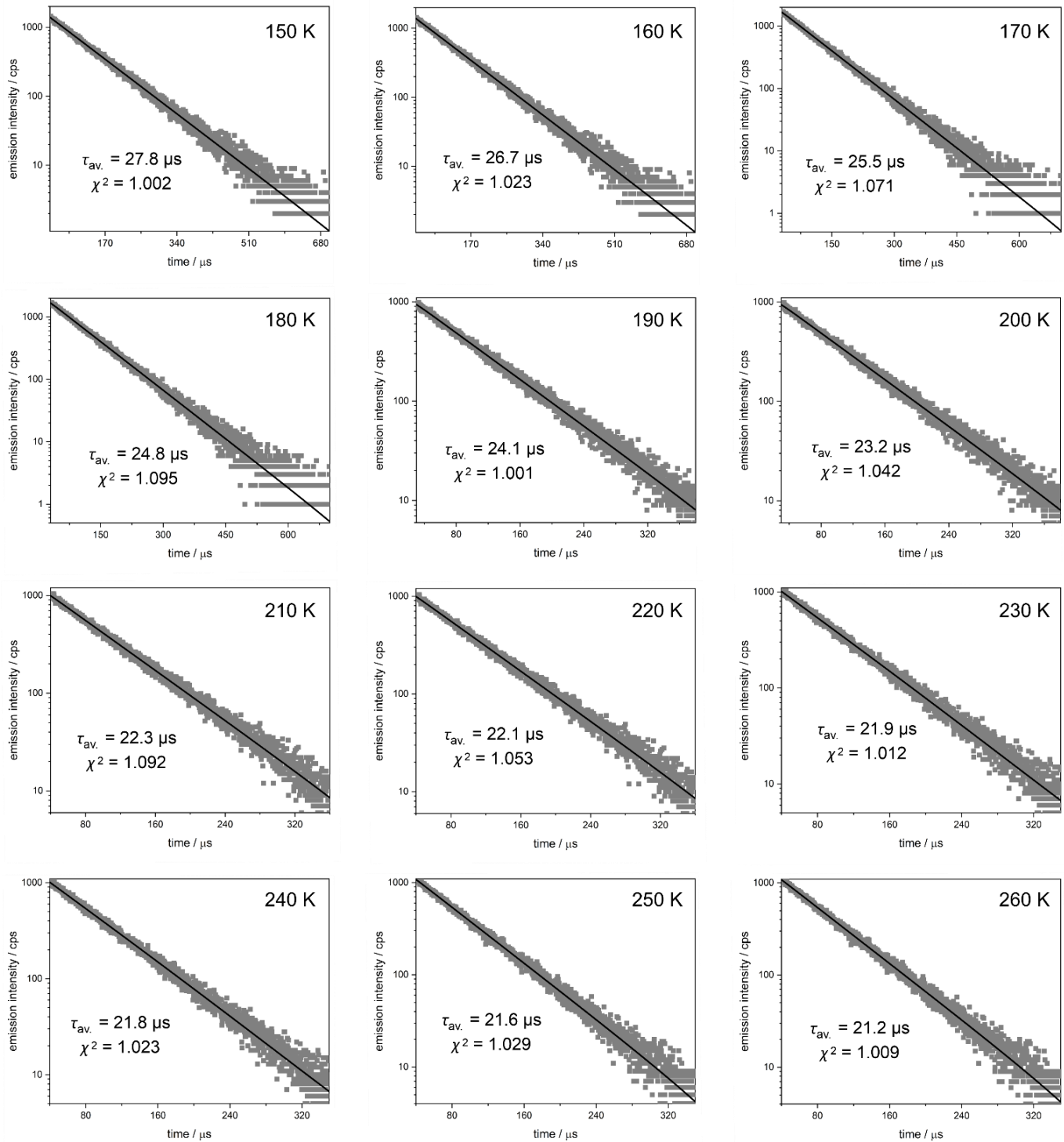


**Fig. S65** (part 2 of 3) Temperature-variable emission decay profiles for **Re<sub>2</sub>-en** under  $\lambda_{\text{ex}} = 430 \text{ nm}$  and  $\lambda_{\text{em}} = 542 \text{ nm}$ , collected for the indicated temperatures from the 30–330 K range (in this part, the region of 150–260 K is shown). The double exponential fitting was applied for each temperature; the related best-fit curve is illustrated by a solid line. The best-fit parameters are roughly presented on the graphs while the detailed values are gathered in Table S72.

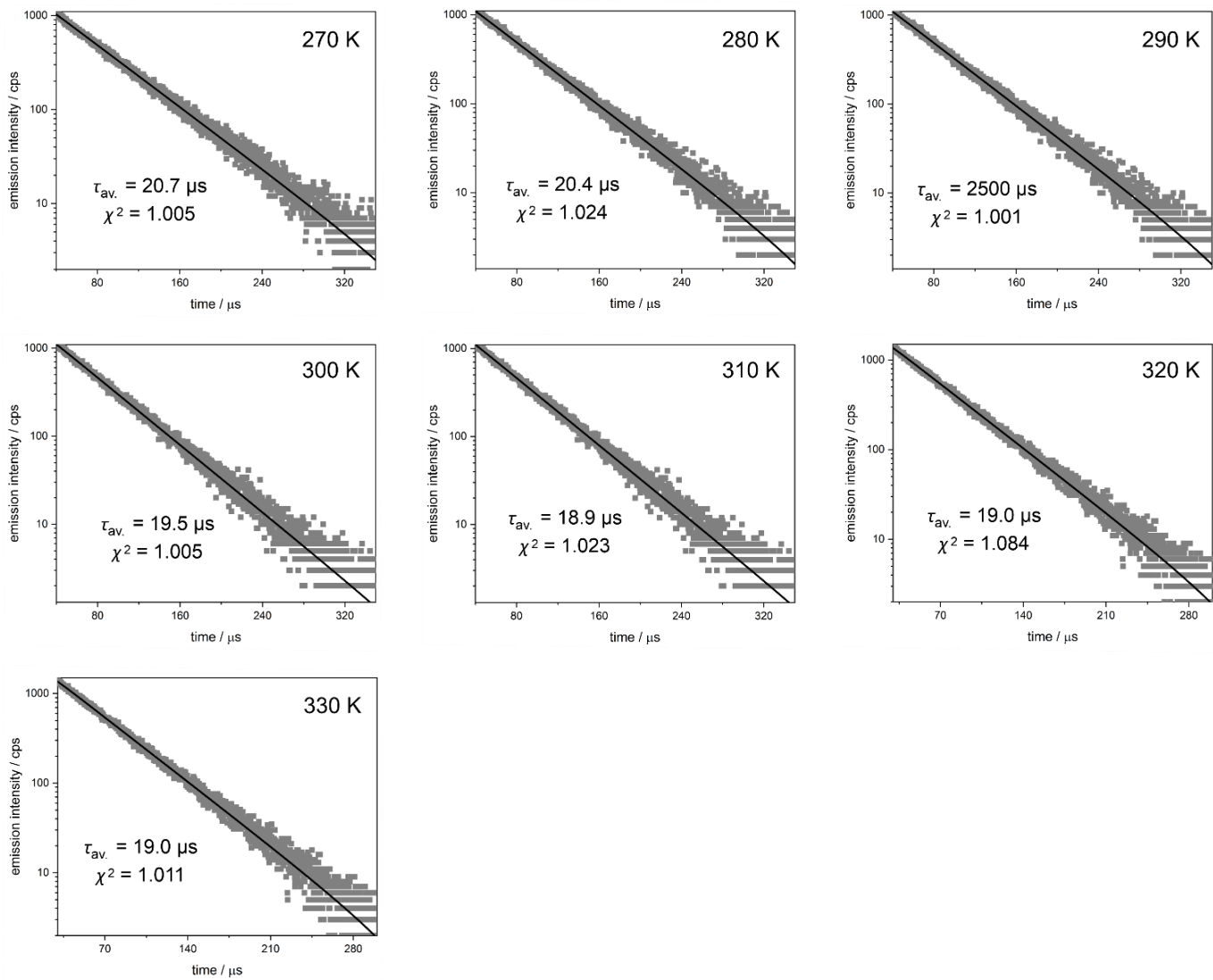


**Fig. S65** (part 3 of 3) Temperature-variable emission decay profiles for **Re<sub>2</sub>-en** under  $\lambda_{\text{ex}} = 430 \text{ nm}$  and  $\lambda_{\text{em}} = 542 \text{ nm}$ , collected for the indicated temperatures from the 30–330 K range (in this part, the region of 270–330 K is shown). The double exponential fitting was applied for each temperature; the related best-fit curve is illustrated by a solid line. The best-fit parameters are roughly presented on the graphs while the detailed values are gathered in Table S72.

**Table S72** Best-fit parameters for the emission decay profiles of **Re<sub>2</sub>-en** to the double exponential decay function (represented by the  $\tau_1$  and  $\tau_2$  values of emission lifetime components, with the respective contributions given in the brackets next to the lifetimes values), and the calculated weighted-average emission lifetime ( $\tau_{\text{av.}}$ ), all presented for the 30–330 K temperature range (see Fig. S65 for the respective emission decay profiles).

parameter	<b>Re<sub>2</sub>-en</b>					
	30 K	40 K	50 K	60 K	70 K	80 K
$\tau_1$ (%) / $\mu\text{s}$	114.1 (88.02)	94.1 (86.82)	74.0 (85.62)	63.4 (84.80)	52.8 (83.98)	43.9 (82.79)
$\tau_2$ (%) / $\mu\text{s}$	162.7 (11.98)	154.9 (13.18)	147.0 (14.38)	139.3 (15.20)	131.5 (16.02)	124.5 (17.21)
$\tau_{\text{av.}}$ / $\mu\text{s}$	119.9	102.1	84.5	75.0	65.4	57.7
$\chi^2$	1.005	1.009	1.005	1.008	1.004	1.003
	90 K	100 K	110 K	120 K	130 K	140 K
$\tau_1$ (%) / $\mu\text{s}$	34.9 (81.6)	29.7 (79.71)	24.4 (77.82)	19.4 (76.57)	14.4 (75.31)	11.5 (74.83)
$\tau_2$ (%) / $\mu\text{s}$	117.4 (18.4)	111.3 (20.29)	105.2 (22.18)	99.2 (23.43)	93.2 (24.69)	88.5 (25.17)
$\tau_{\text{av.}}$ / $\mu\text{s}$	50.1	46.2	42.3	38.1	33.9	30.9
$\chi^2$	1.094	1.011	1.024	1.015	1.008	1.014
	150 K	160 K	170 K	180 K	190 K	200 K
$\tau_1$ (%) / $\mu\text{s}$	8.5 (74.35)	8.3 (74.04)	8.1 (73.73)	7.8 (73.17)	7.5 (72.61)	7.2 (72.30)
$\tau_2$ (%) / $\mu\text{s}$	83.8 (25.65)	79.0 (25.96)	74.3 (26.27)	71.2 (26.83)	68.1 (27.39)	65.1 (27.70)
$\tau_{\text{av.}}$ / $\mu\text{s}$	27.8	26.7	25.5	24.8	24.1	23.2
$\chi^2$	1.002	1.023	1.071	1.095	1.001	1.042
	210 K	220 K	230 K	240 K	250 K	260 K
$\tau_1$ (%) / $\mu\text{s}$	6.8 (71.99)	6.8 (71.12)	6.9 (70.24)	7.3 (69.72)	7.8 (69.21)	7.9 (69.11)
$\tau_2$ (%) / $\mu\text{s}$	62.1 (28.01)	59.7 (28.88)	57.4 (29.76)	55.1 (30.28)	52.8 (30.79)	51.0 (30.89)
$\tau_{\text{av.}}$ / $\mu\text{s}$	22.3	22.1	21.9	21.8	21.6	21.2
$\chi^2$	1.092	1.053	1.012	1.023	1.029	1.009
	270 K	280 K	290 K	300 K	310 K	320 K
$\tau_1$ (%) / $\mu\text{s}$	8.0 (69.01)	8.1 (68.64)	8.2 (68.27)	7.8 (67.74)	7.4 (67.21)	7.4 (65.66)
$\tau_2$ (%) / $\mu\text{s}$	49.1 (30.99)	47.3 (31.36)	45.5 (31.73)	44.0 (32.26)	42.5 (32.79)	41.1 (34.34)
$\tau_{\text{av.}}$ / $\mu\text{s}$	20.7	20.4	20.0	19.5	18.9	19.0
$\chi^2$	1.005	1.024	1.001	1.005	1.023	1.084
	330 K	–	–	–	–	–
$\tau_1$ (%) / $\mu\text{s}$	7.4 (64.11)	–	–	–	–	–
$\tau_2$ (%) / $\mu\text{s}$	39.8 (35.89)	–	–	–	–	–
$\tau_{\text{av.}}$ / $\mu\text{s}$	19.0	–	–	–	–	–
$\chi^2$	1.011	–	–	–	–	–

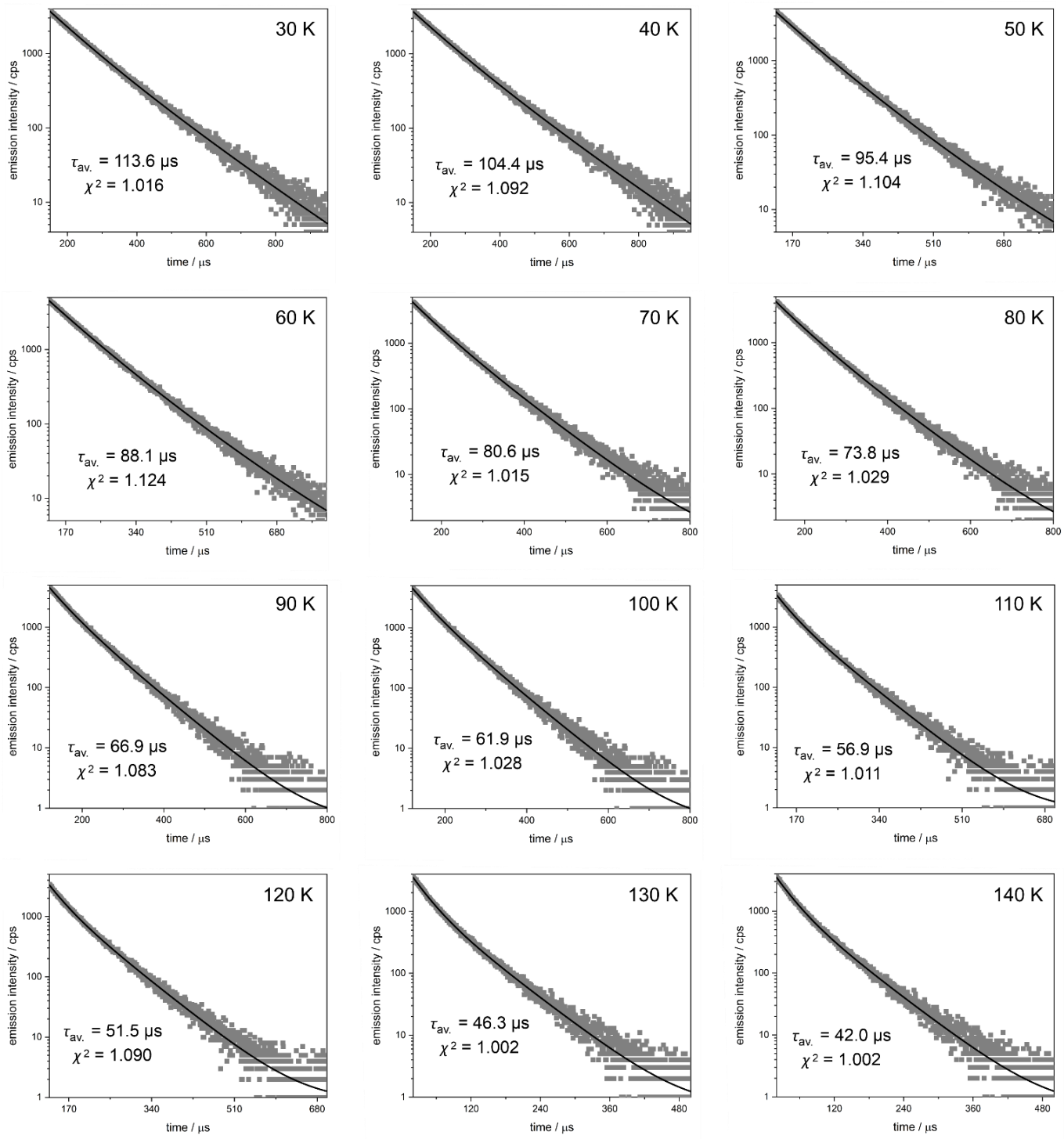


**Fig. S66** (part 1 of 3) Temperature-variable emission decay profiles for **Re<sub>2</sub>-bpy** under  $\lambda_{\text{exc}} = 430$  nm and  $\lambda_{\text{em}} = 584$  nm, collected for the indicated temperatures from the 30–330 K range (in this part, the region of 30–140 K is shown). The double exponential fitting was applied for each temperature; the related best-fit curve is illustrated by a solid line. The best-fit parameters are roughly presented on the graphs while the detailed values are gathered in Table S73.

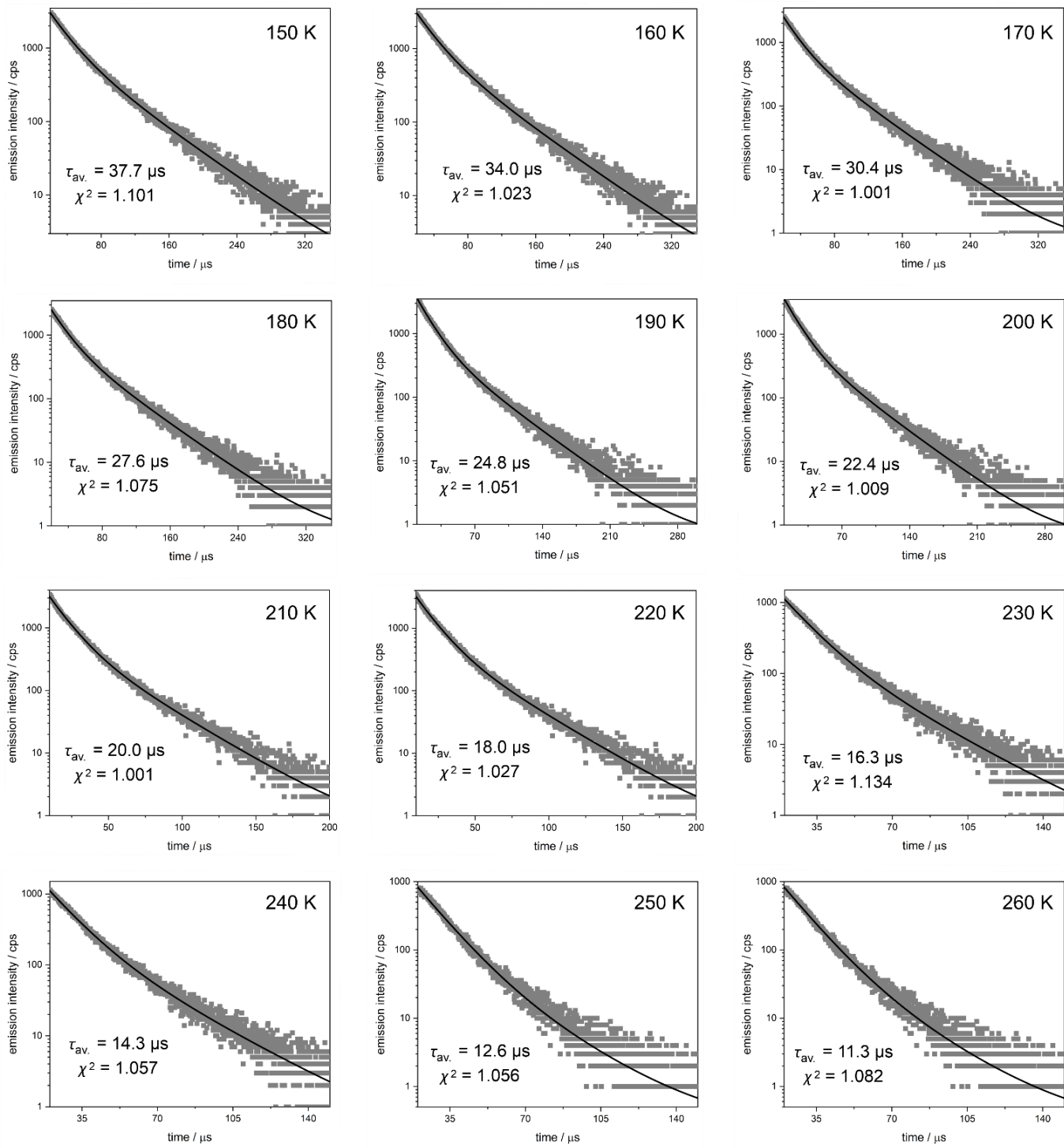


**Fig. S66** (part 2 of 3) Temperature-variable emission decay profiles for **Re<sub>2</sub>-bpy** under  $\lambda_{\text{exc}} = 430 \text{ nm}$  and  $\lambda_{\text{em}} = 584 \text{ nm}$ , collected for the indicated temperatures from the 30–330 K range (in this part, the region of 150–260 K is shown). The double exponential fitting was applied for each temperature; the related best-fit curve is illustrated by a solid line. The best-fit parameters are roughly presented on the graphs while the detailed values are gathered in Table S73.

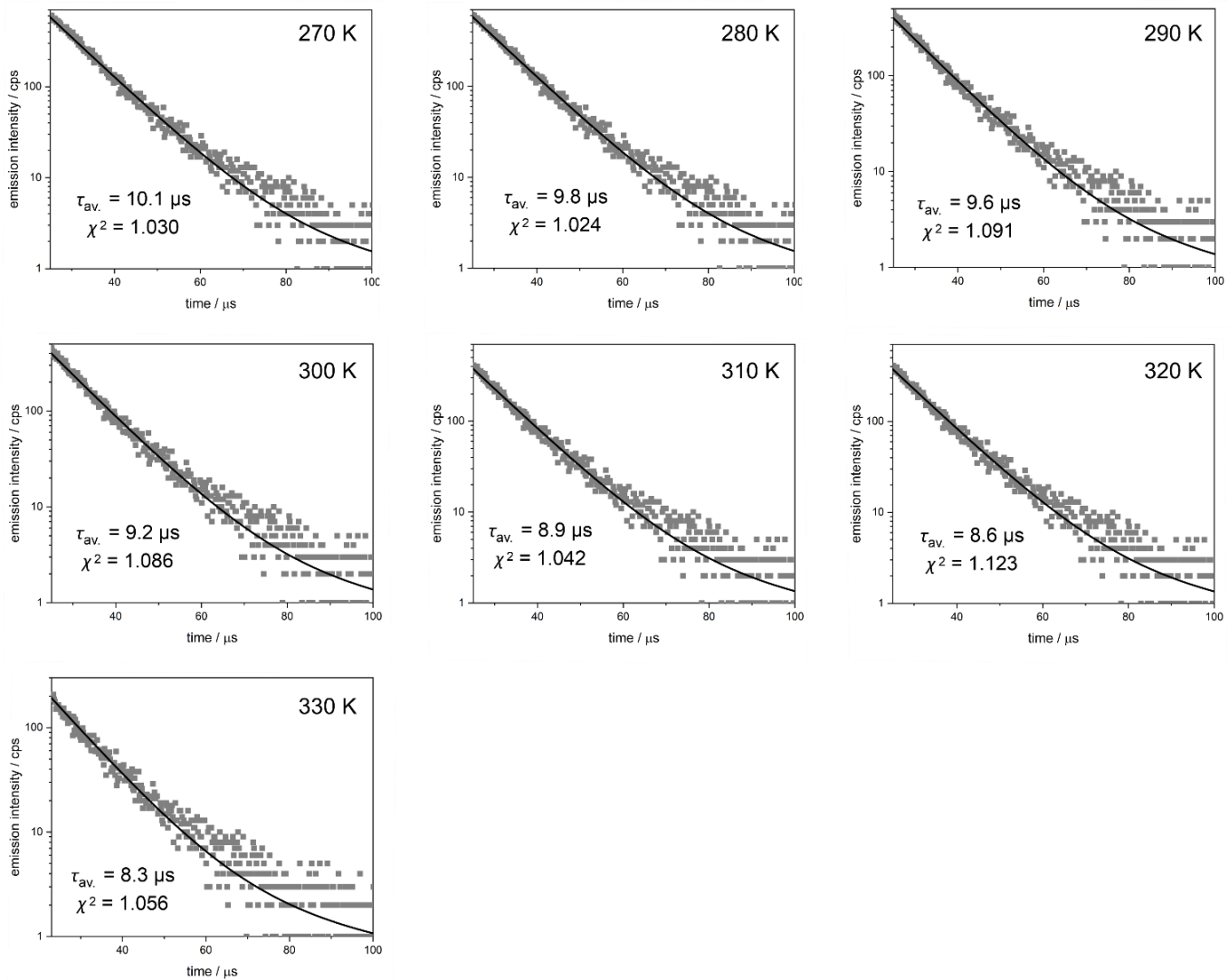


**Fig. S66** (part 3 of 3) Temperature-variable emission decay profiles for **Re<sub>2</sub>-bpy** under  $\lambda_{exc} = 430$  nm and  $\lambda_{em} = 584$  nm, collected for the indicated temperatures from the 30–330 K range (in this part, the region of 270–330 K is shown). The double exponential fitting was applied for each temperature; the related best-fit curve is illustrated by a solid line. The best-fit parameters are roughly presented on the graphs while the detailed values are gathered in Table S73.

**Table S73** Best-fit parameters for the emission decay profiles of **Re<sub>2</sub>-bpy** to the double exponential decay function (represented by the  $\tau_1$  and  $\tau_2$  values of emission lifetime components, with the respective contributions given in the brackets next to the lifetime values), and the calculated weighted-average emission lifetime ( $\tau_{\text{av.}}$ ), all presented for the 30–330 K temperature range (see Fig. S66 for the respective emission decay profiles).

parameter	<b>Re<sub>2</sub>-bpy</b>					
	30 K	40 K	50 K	60 K	70 K	80 K
$\tau_1$ (%) / $\mu\text{s}$	84.3 (42.94)	78.8 (44.86)	73.3 (46.78)	64.2 (40.98)	55.1 (35.18)	48.1 (32.89)
$\tau_2$ (%) / $\mu\text{s}$	135.6 (57.06)	125.2 (55.14)	114.8 (53.22)	104.6 (59.02)	94.5 (64.82)	86.4 (67.11)
$\tau_{\text{av.}}$ / $\mu\text{s}$	113.6	104.4	95.4	88.1	80.6	73.8
$\chi^2$	1.016	1.092	1.104	1.124	1.015	1.029
	90 K	100 K	110 K	120 K	130 K	140 K
$\tau_1$ (%) / $\mu\text{s}$	41.0 (30.60)	35.4 (29.80)	29.8 (29.00)	27.9 (35.67)	25.9 (42.35)	23.5 (45.19)
$\tau_2$ (%) / $\mu\text{s}$	78.4 (69.40)	73.2 (70.20)	68.0 (71.00)	64.6 (64.33)	61.3 (57.65)	57.2 (54.81)
$\tau_{\text{av.}}$ / $\mu\text{s}$	66.9	61.9	56.9	51.5	46.3	42.0
$\chi^2$	1.083	1.028	1.011	1.090	1.002	1.002
	150 K	160 K	170 K	180 K	190 K	200 K
$\tau_1$ (%) / $\mu\text{s}$	21.0 (48.03)	18.9 (50.54)	16.7 (53.04)	15.2 (54.06)	13.7 (55.09)	12.6 (55.78)
$\tau_2$ (%) / $\mu\text{s}$	53.2 (51.97)	49.5 (49.46)	45.9 (46.96)	42.2 (45.94)	38.6 (44.91)	34.7 (44.22)
$\tau_{\text{av.}}$ / $\mu\text{s}$	37.7	34.0	30.4	27.6	24.8	22.4
$\chi^2$	1.101	1.023	1.001	1.075	1.051	1.009
	210 K	220 K	230 K	240 K	250 K	260 K
$\tau_1$ (%) / $\mu\text{s}$	11.6 (56.47)	11.2 (60.76)	10.8 (65.05)	10.4 (73.56)	10.1 (82.07)	9.9 (89.30)
$\tau_2$ (%) / $\mu\text{s}$	30.9 (43.53)	28.7 (39.24)	26.5 (34.95)	25.1 (26.44)	23.7 (17.93)	22.8 (10.70)
$\tau_{\text{av.}}$ / $\mu\text{s}$	20.0	18.0	16.3	14.3	12.6	11.3
$\chi^2$	1.001	1.027	1.134	1.057	1.056	1.082
	270 K	280 K	290 K	300 K	310 K	320 K
$\tau_1$ (%) / $\mu\text{s}$	9.7 (96.53)	9.5 (97.03)	9.3 (97.54)	9.0 (97.98)	8.7 (98.42)	8.4 (98.68)
$\tau_2$ (%) / $\mu\text{s}$	21.8 (3.47)	20.8 (2.97)	19.8 (2.46)	19.3 (2.02)	18.8 (1.58)	18.1 (1.32)
$\tau_{\text{av.}}$ / $\mu\text{s}$	10.1	9.8	9.6	9.2	8.9	8.6
$\chi^2$	1.030	1.024	1.091	1.086	1.042	1.123
	330 K	–	–	–	–	–
$\tau_1$ (%) / $\mu\text{s}$	8.2 (98.95)	–	–	–	–	–
$\tau_2$ (%) / $\mu\text{s}$	17.4 (1.05)	–	–	–	–	–
$\tau_{\text{av.}}$ / $\mu\text{s}$	8.3	–	–	–	–	–
$\chi^2$	1.056	–	–	–	–	–

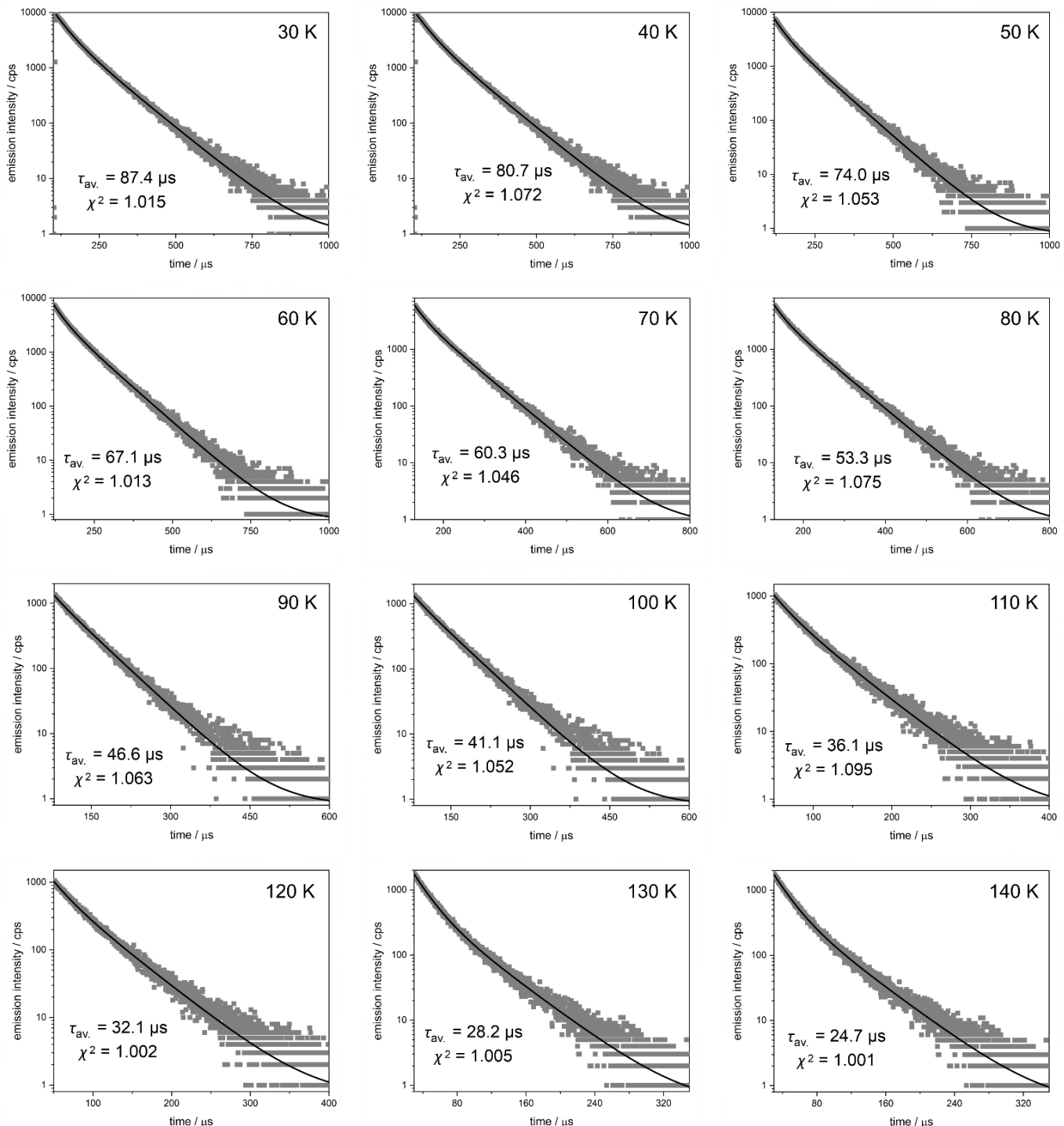


**Fig. S67** (part 1 of 2) Temperature-variable emission decay profiles for **Re<sub>2</sub>-bpac** under  $\lambda_{exc} = 430$  nm and  $\lambda_{em} = 598$  nm, collected for the indicated temperatures from the 30–240 K range (in this part, the region of 30–140 K is shown). The double exponential fitting was applied for each temperature; the related best-fit curve is illustrated by a solid line. The best-fit parameters are roughly presented on the graphs while the detailed values are gathered in Table S74.

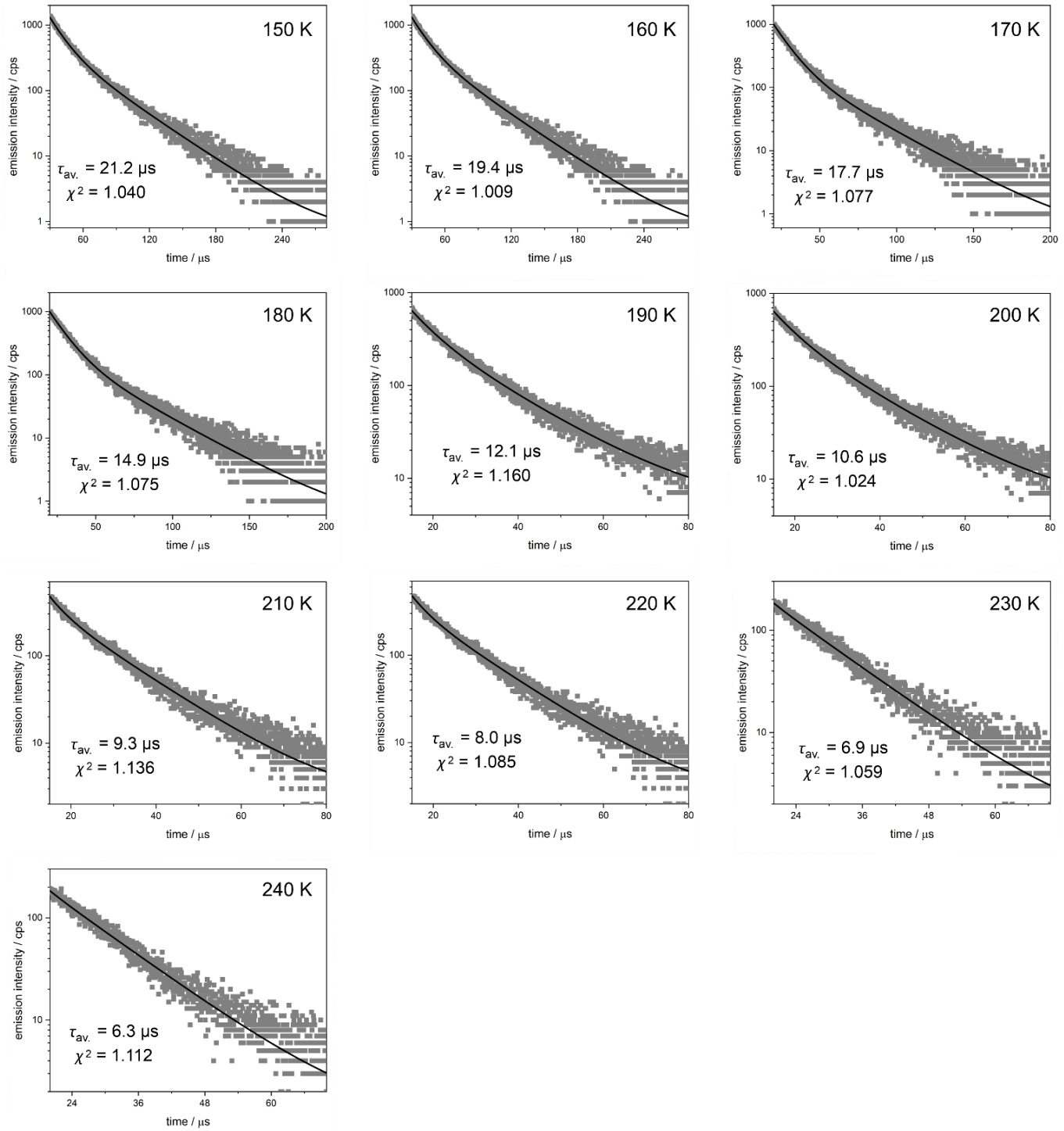


**Fig. S67** (part 2 of 2) Temperature-variable emission decay profiles for **Re<sub>2</sub>-bpac** under  $\lambda_{exc} = 430$  nm and  $\lambda_{em} = 598$  nm, collected for the indicated temperatures from the 30–240 K range (in this part, the region of 150–240 K is shown). The double exponential fitting was applied for each temperature; the related best-fit curve is illustrated by a solid line. The best-fit parameters are roughly presented on the graphs while the detailed values are gathered in Table S74.

**Table S74** Best-fit parameters for the emission decay profiles of **Re<sub>2</sub>-bpac** to the double exponential decay function (represented by the  $\tau_1$  and  $\tau_2$  values of emission lifetime components, with the respective contributions given in the brackets next to the lifetime values), and the calculated weighted-average emission lifetime ( $\tau_{\text{av.}}$ ), all presented for the 30–240 K temperature range (see Fig. S67 for the respective emission decay profiles).

parameter	<b>Re<sub>2</sub>-bpac</b>					
	30 K	40 K	50 K	60 K	70 K	80 K
$\tau_1$ (%) / $\mu\text{s}$	40.4 (16.85)	35.6 (18.57)	30.7 (20.30)	27.4 (22.28)	24.0 (24.27)	22.1 (26.53)
$\tau_2$ (%) / $\mu\text{s}$	96.9 (83.15)	91.0 (81.43)	85.0 (79.70)	78.5 (77.72)	71.9 (75.73)	64.6 (73.47)
$\tau_{\text{av.}}$ / $\mu\text{s}$	87.4	80.7	74.0	67.1	60.3	53.3
$\chi^2$	1.015	1.072	1.053	1.013	1.046	1.075
	90 K	100 K	110 K	120 K	130 K	140 K
$\tau_1$ (%) / $\mu\text{s}$	20.2 (28.79)	19.8 (34.88)	19.4 (40.97)	18.2 (49.91)	16.9 (58.85)	14.6 (61.83)
$\tau_2$ (%) / $\mu\text{s}$	57.3 (71.21)	52.5 (65.12)	47.7 (59.03)	46.1 (50.09)	44.5 (41.15)	41.1 (38.17)
$\tau_{\text{av.}}$ / $\mu\text{s}$	46.6	41.1	36.1	32.1	28.2	24.7
$\chi^2$	1.063	1.052	1.095	1.002	1.005	1.001
	150 K	160 K	170 K	180 K	190 K	200 K
$\tau_1$ (%) / $\mu\text{s}$	12.2 (64.81)	11.1 (65.24)	10.1 (65.68)	7.8 (66.29)	5.5 (66.91)	4.6 (67.89)
$\tau_2$ (%) / $\mu\text{s}$	37.7 (35.19)	35.0 (34.76)	32.2 (34.32)	28.9 (33.71)	25.7 (33.09)	23.5 (32.11)
$\tau_{\text{av.}}$ / $\mu\text{s}$	21.2	19.4	17.7	14.9	12.1	10.6
$\chi^2$	1.040	1.009	1.077	1.075	1.160	1.024
	210 K	220 K	230 K	240 K	–	–
$\tau_1$ (%) / $\mu\text{s}$	3.7 (68.88)	3.0 (69.13)	2.3 (69.37)	2.1 (69.87)	–	–
$\tau_2$ (%) / $\mu\text{s}$	21.4 (31.12)	19.3 (30.87)	17.2 (30.63)	15.9 (30.13)	–	–
$\tau_{\text{av.}}$ / $\mu\text{s}$	9.3	8.0	6.9	6.3	–	–
$\chi^2$	1.136	1.085	1.059	1.112	–	–

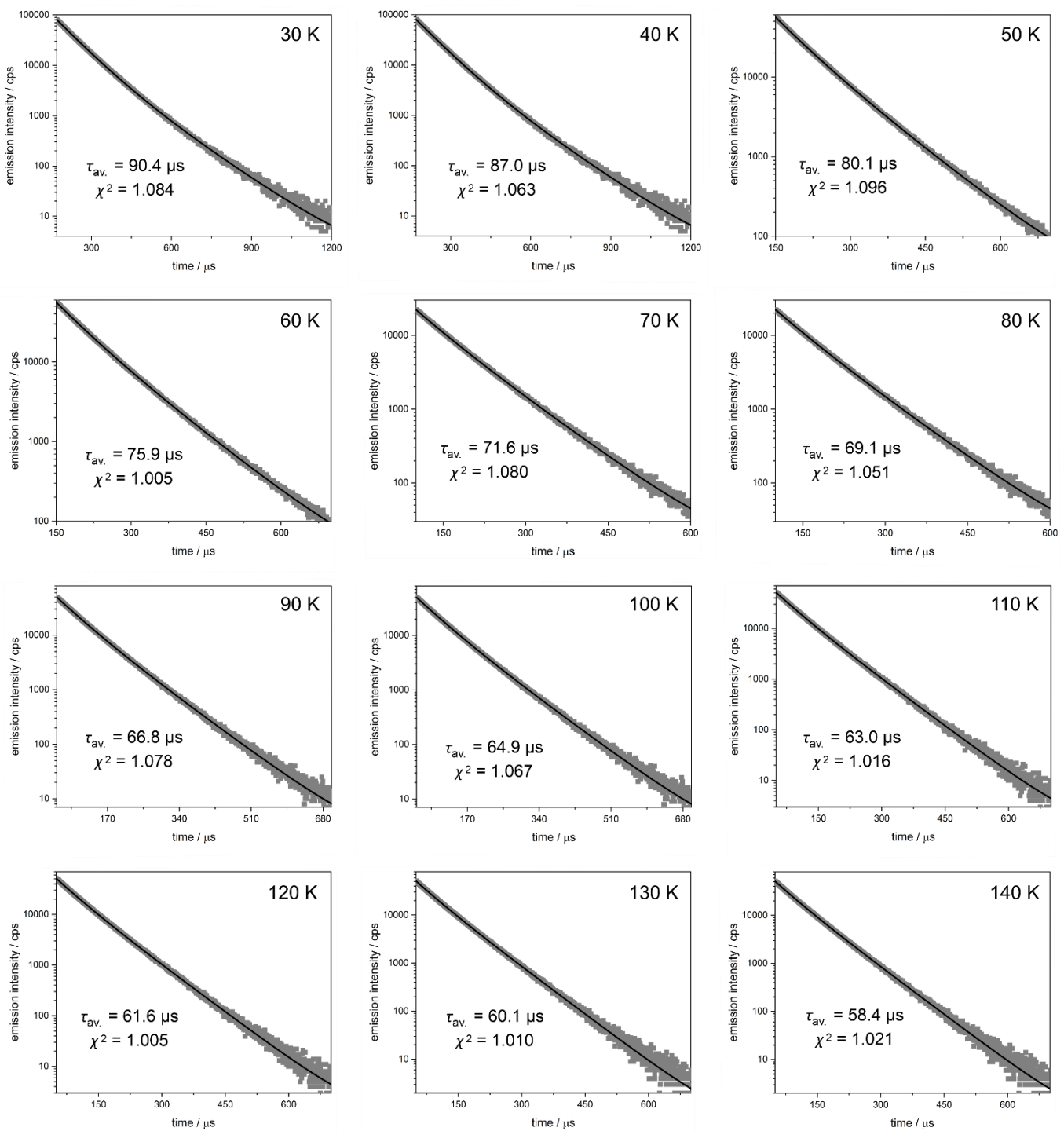


**Fig. S68** (part 1 of 3) Temperature-variable emission decay profiles for **Re<sub>2</sub>-bpen** under  $\lambda_{\text{exc}} = 430 \text{ nm}$  and  $\lambda_{\text{em}} = 616 \text{ nm}$ , collected for the indicated temperatures from the 30–330 K range (in this part, the region of 30–140 K is shown). The double exponential fitting was applied for each temperature; the related best-fit curve is illustrated by a solid line. The best-fit parameters are roughly presented on the graphs while the detailed values are gathered in Table S75.

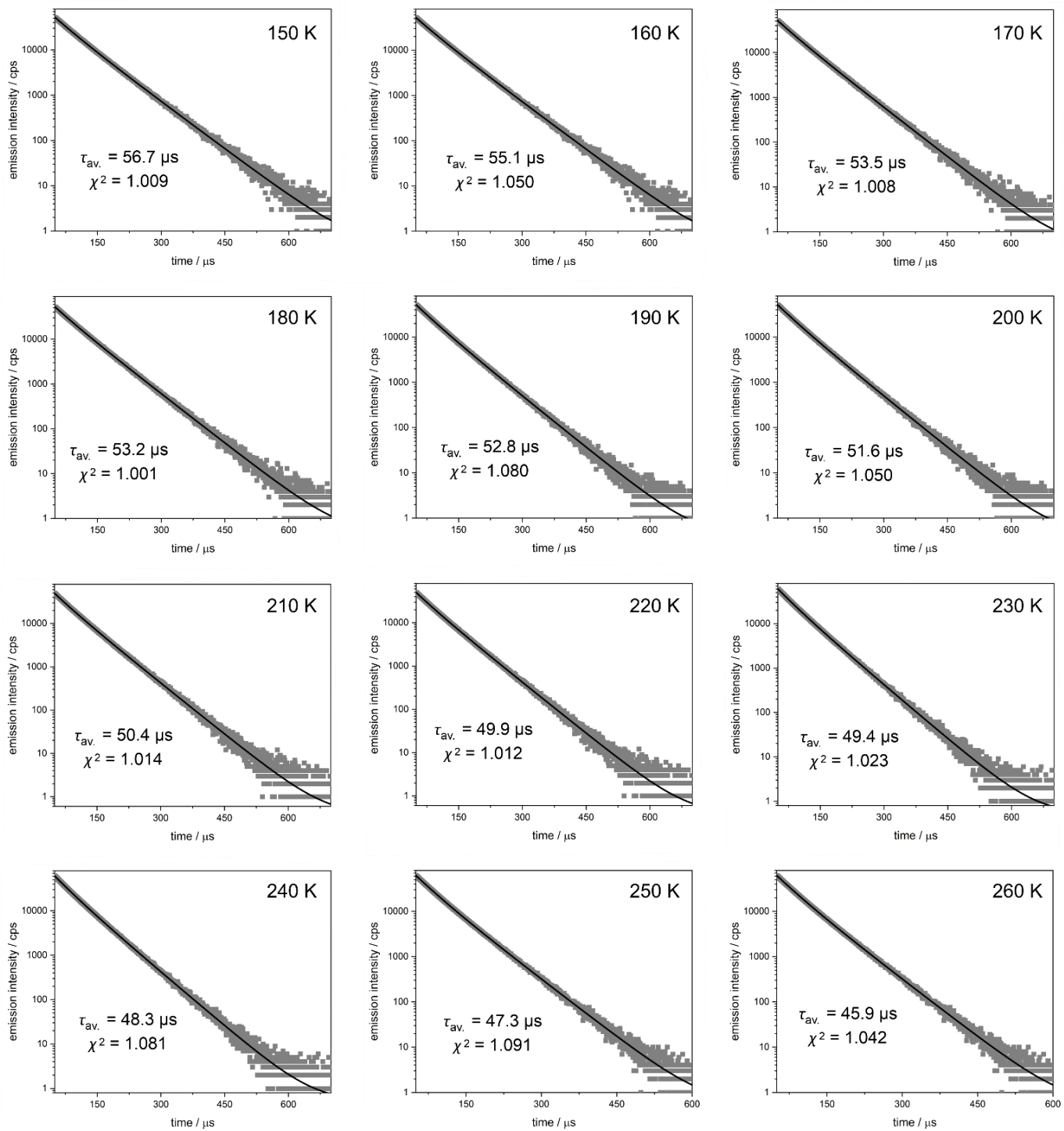


**Fig. S68** (part 2 of 3) Temperature-variable emission decay profiles for **Re<sub>2</sub>-bpen** under  $\lambda_{exc} = 430$  nm and  $\lambda_{em} = 616$  nm, collected for the indicated temperatures from the 30–330 K range (in this part, the region of 150–260 K is shown). The double exponential fitting was applied for each temperature; the related best-fit curve is illustrated by a solid line. The best-fit parameters are roughly presented on the graphs while the detailed values are gathered in Table S75.

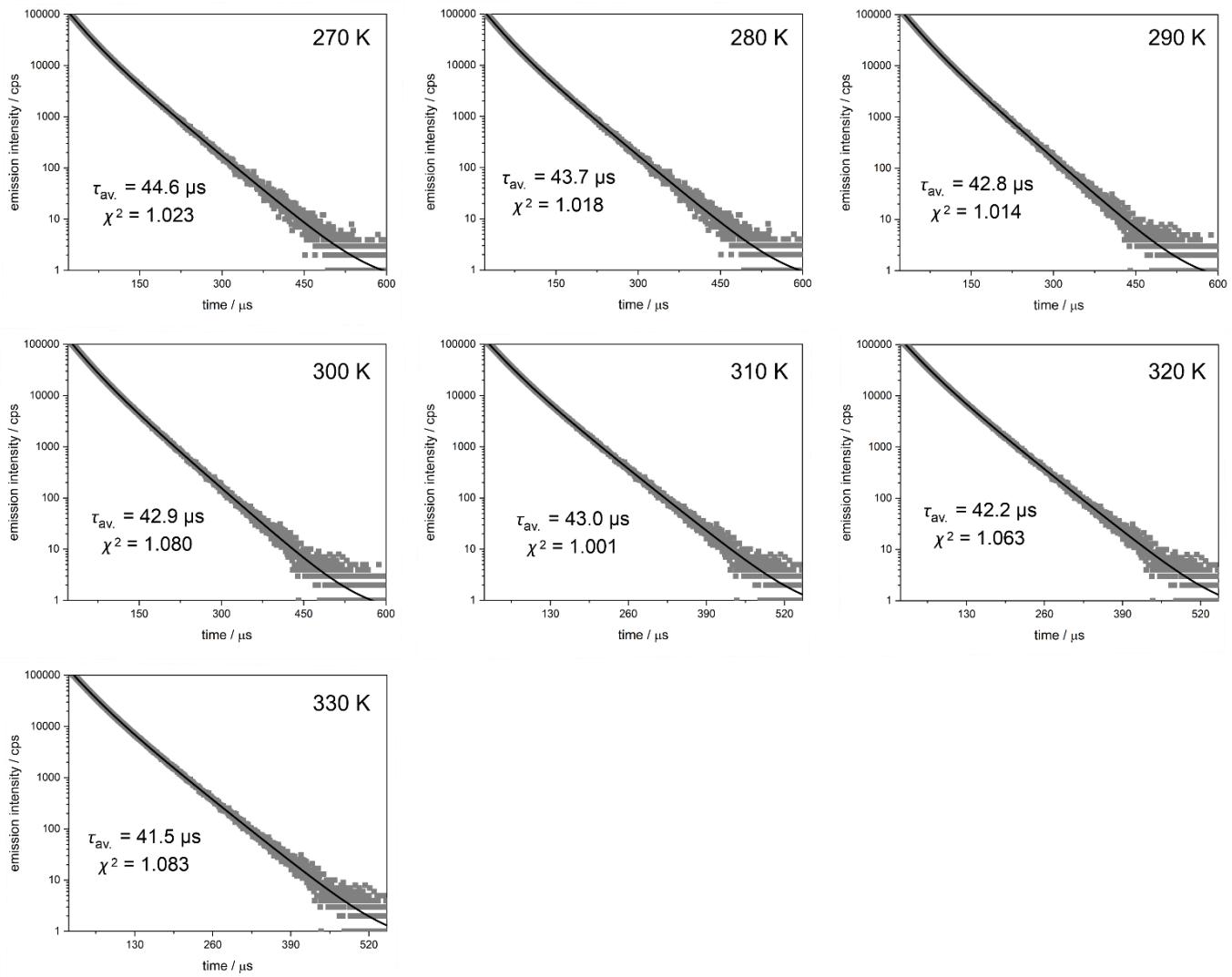


**Fig. S68** (part 3 of 3) Temperature-variable emission decay profiles for **Re<sub>2</sub>-bpen** under  $\lambda_{\text{exc}} = 430 \text{ nm}$  and  $\lambda_{\text{em}} = 616 \text{ nm}$ , collected for the indicated temperatures from the 30–330 K range (in this part, the region of 270–330 K is shown). The double exponential fitting was applied for each temperature; the related best-fit curve is illustrated by a solid line. The best-fit parameters are roughly presented on the graphs while the detailed values are gathered in Table S75.

**Table S75** Best-fit parameters for the emission decay profiles of **Re<sub>2</sub>-bpn** to the double exponential decay function (represented by the  $\tau_1$  and  $\tau_2$  values of emission lifetime components, with the respective contributions given in the brackets next to the lifetime values), and the calculated weighted-average emission lifetime ( $\tau_{\text{av.}}$ ), all presented for the 30–330 K temperature range (see Fig. S68 for the respective emission decay profiles).

parameter	<b>Re<sub>2</sub>-bpn</b>					
	30 K	40 K	50 K	60 K	70 K	80 K
$\tau_1$ (%) / $\mu\text{s}$	74.5 (69.35)	66.6 (51.33)	58.6 (33.31)	54.0 (33.19)	49.4 (33.08)	48.6 (34.88)
$\tau_2$ (%) / $\mu\text{s}$	126.2 (30.65)	108.5 (48.67)	90.9 (66.69)	86.7 (66.81)	82.5 (66.92)	80.1 (65.12)
$\tau_{\text{av.}}$ / $\mu\text{s}$	90.4	87.0	80.1	75.9	71.6	69.1
$\chi^2$	1.084	1.063	1.096	1.005	1.080	1.051
	90 K	100 K	110 K	120 K	130 K	140 K
$\tau_1$ (%) / $\mu\text{s}$	47.9 (36.67)	45.6 (32.64)	43.4 (28.61)	41.5 (26.05)	39.7 (23.48)	38.3 (23.13)
$\tau_2$ (%) / $\mu\text{s}$	77.7 (63.33)	74.3 (67.36)	70.9 (71.39)	68.6 (73.95)	66.4 (76.52)	64.5 (76.87)
$\tau_{\text{av.}}$ / $\mu\text{s}$	66.8	64.9	63.0	61.6	60.1	58.4
$\chi^2$	1.078	1.067	1.016	1.005	1.010	1.021
	150 K	160 K	170 K	180 K	190 K	200 K
$\tau_1$ (%) / $\mu\text{s}$	37.0 (22.79)	35.5 (22.63)	33.9 (22.47)	34.4 (21.94)	34.9 (21.42)	33.2 (21.20)
$\tau_2$ (%) / $\mu\text{s}$	62.6 (77.21)	60.9 (77.37)	59.2 (77.53)	58.5 (78.06)	57.7 (78.58)	56.5 (78.80)
$\tau_{\text{av.}}$ / $\mu\text{s}$	56.7	55.1	53.5	53.2	52.8	51.6
$\chi^2$	1.009	1.050	1.008	1.001	1.080	1.050
	210 K	220 K	230 K	240 K	250 K	260 K
$\tau_1$ (%) / $\mu\text{s}$	31.5 (20.97)	31.8 (20.57)	32.0 (20.17)	31.4 (20.07)	30.8 (19.96)	28.5 (19.74)
$\tau_2$ (%) / $\mu\text{s}$	55.4 (79.03)	54.6 (79.43)	53.8 (79.83)	52.6 (79.93)	51.4 (80.04)	50.2 (80.26)
$\tau_{\text{av.}}$ / $\mu\text{s}$	50.4	49.9	49.4	48.3	47.3	45.9
$\chi^2$	1.014	1.012	1.023	1.081	1.091	1.042
	270 K	280 K	290 K	300 K	310 K	320 K
$\tau_1$ (%) / $\mu\text{s}$	26.3 (19.52)	26.2 (19.47)	26.1 (19.42)	26.3 (18.97)	26.4 (18.52)	25.7 (18.17)
$\tau_2$ (%) / $\mu\text{s}$	49.0 (80.48)	47.9 (80.53)	46.8 (80.58)	46.8 (81.03)	46.7 (81.48)	45.9 (81.83)
$\tau_{\text{av.}}$ / $\mu\text{s}$	44.6	43.7	42.8	42.9	43.0	42.2
$\chi^2$	1.023	1.018	1.014	10.080	1.001	1.063
	330 K	–	–	–	–	–
$\tau_1$ (%) / $\mu\text{s}$	25.1 (17.81)	–	–	–	–	–
$\tau_2$ (%) / $\mu\text{s}$	45.1 (82.19)	–	–	–	–	–
$\tau_{\text{av.}}$ / $\mu\text{s}$	41.5	–	–	–	–	–
$\chi^2$	1.083	–	–	–	–	–

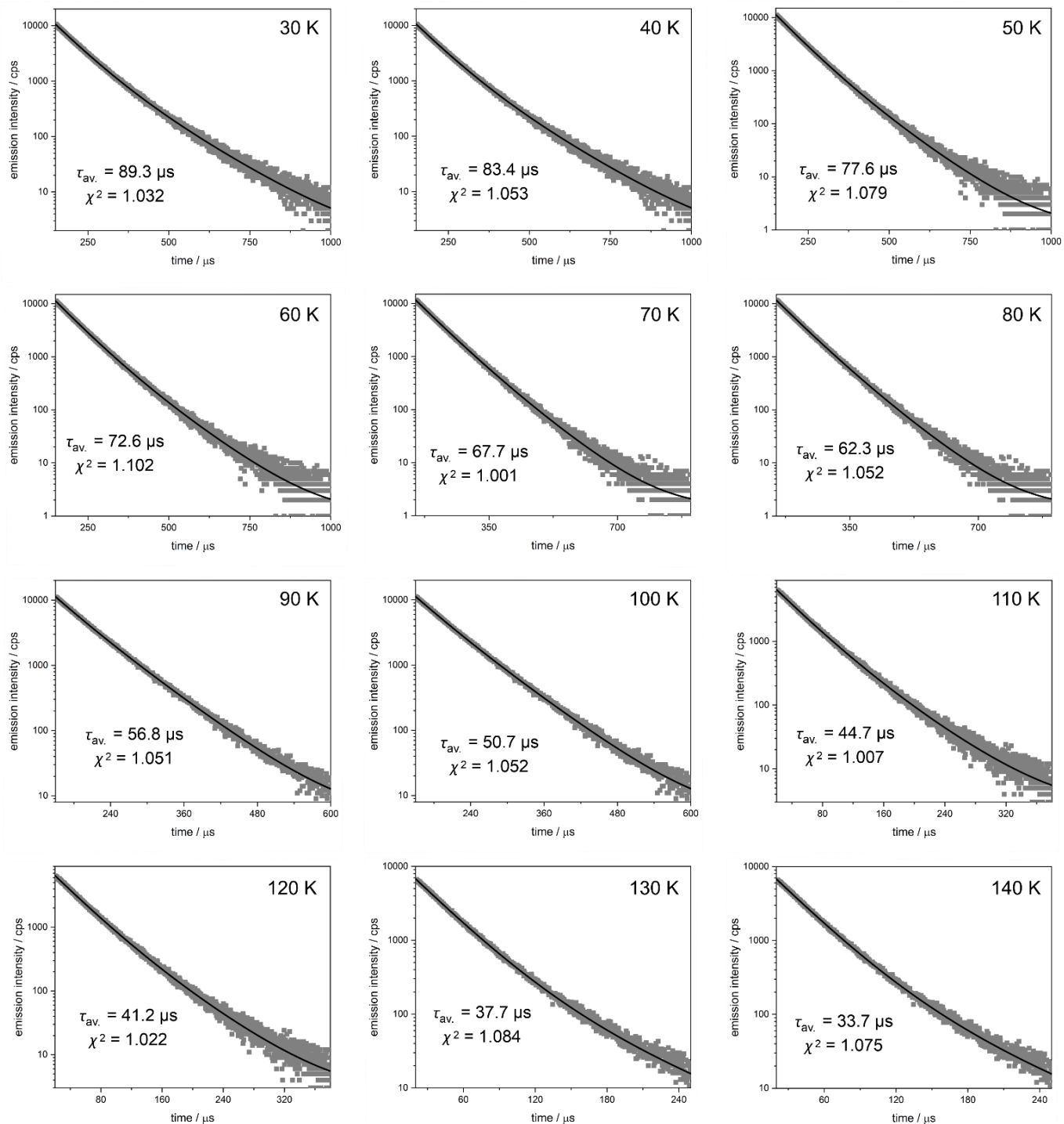


**Fig. S69 (part 1 of 3)** Temperature-variable emission decay profiles for **Re<sub>2</sub>-bpb** under  $\lambda_{exc} = 430$  nm and  $\lambda_{em} = 602$  nm, collected for the indicated temperatures from the 30–330 K range (in this part, the region of 30–140 K is shown). The double exponential fitting was applied for each temperature; the related best-fit curve is illustrated by a solid line). The best-fit parameters are roughly presented on the graphs while the detailed values are gathered in Table S76.

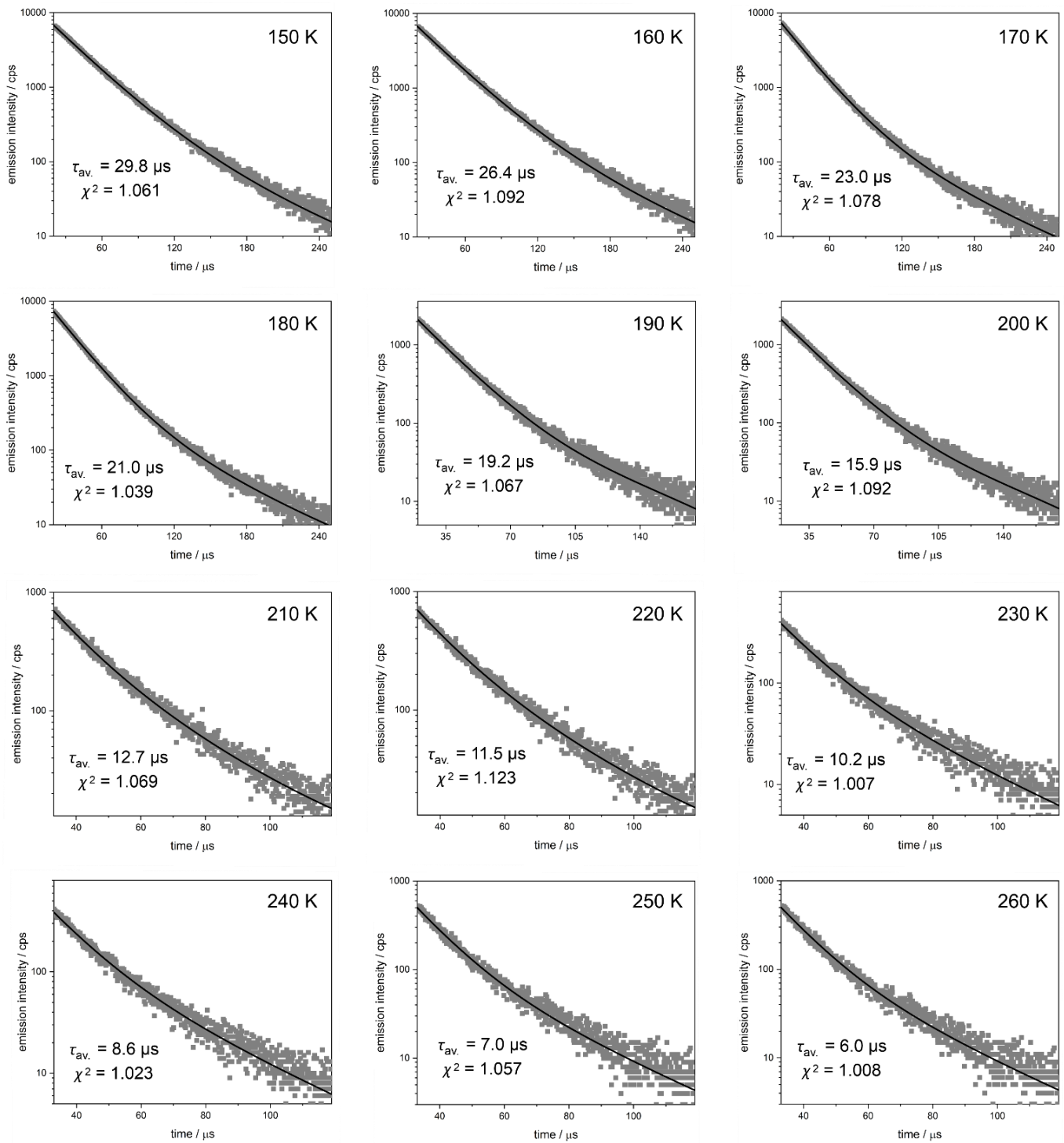


**Fig. S69 (part 2 of 3)** Temperature-variable emission decay profiles for **Re<sub>2</sub>-bpb** under  $\lambda_{\text{exc}} = 430 \text{ nm}$  and  $\lambda_{\text{em}} = 602 \text{ nm}$ , collected for the indicated temperatures from the 30–330 K range (in this part, the region of 150–260 K is shown). The double exponential fitting was applied for each temperature; the related best-fit curve is illustrated by a solid line). The best-fit parameters are roughly presented on the graphs while the detailed values are gathered in Table S76.

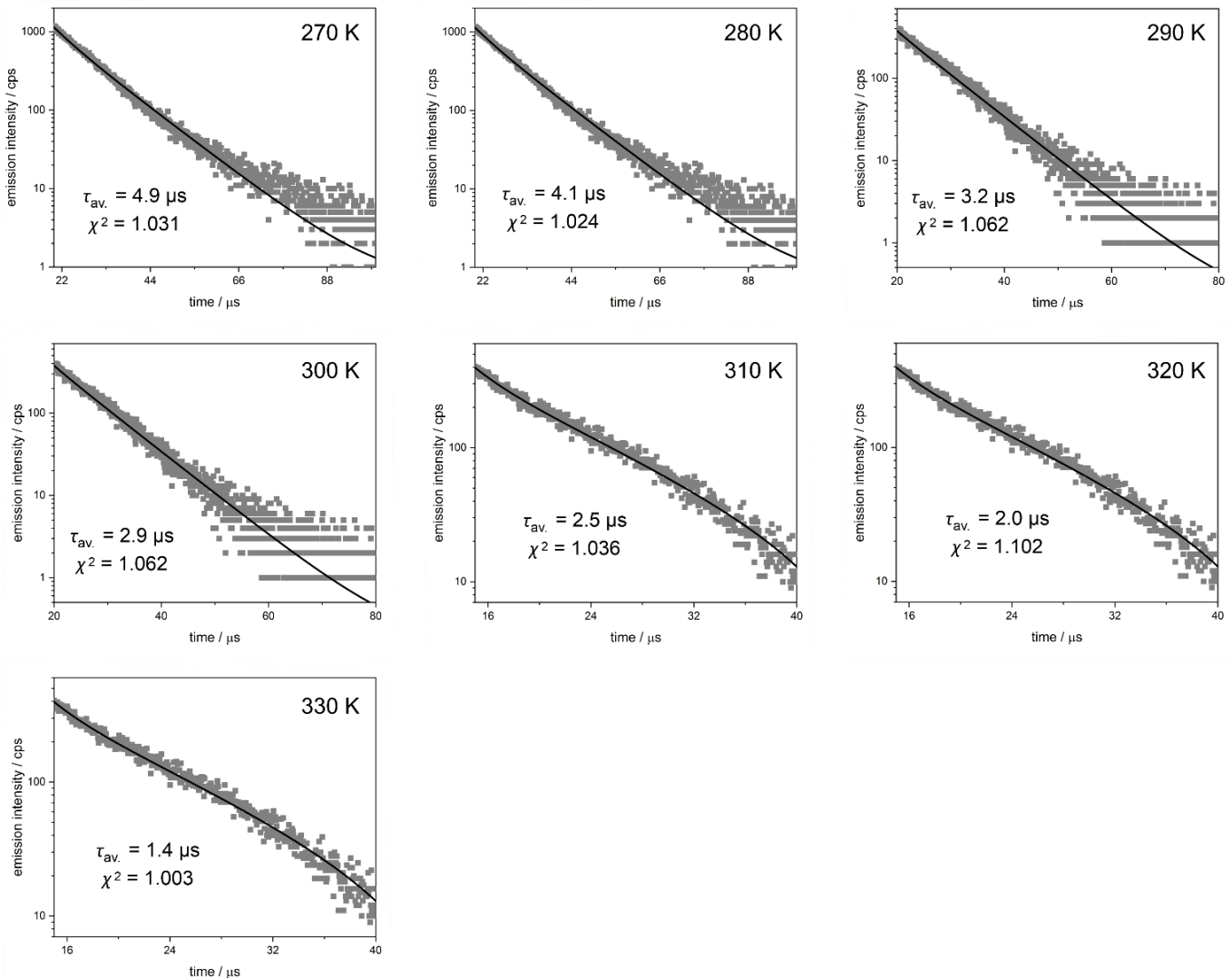


**Fig. S69** (part 3 of 3) Temperature-variable emission decay profiles for **Re<sub>2</sub>-bpb** under  $\lambda_{exc} = 430$  nm and  $\lambda_{em} = 602$  nm, collected for the indicated temperatures from the 30–330 K range (in this part, the region of 270–330 K is shown). The double exponential fitting was applied for each temperature; the related best-fit curve is illustrated by a solid line). The best-fit parameters are roughly presented on the graphs while the detailed values are gathered in Table S76.

**Table S76** Best-fit parameters for the emission decay profiles of **Re<sub>2</sub>-bpb** to the double exponential decay function (represented by the  $\tau_1$  and  $\tau_2$  values of emission lifetime components, with the respective contributions given in the brackets next to the lifetime values), and the calculated weighted-average emission lifetime ( $\tau_{\text{av.}}$ ), all presented for the 30–330 K temperature range (see Fig. S69 for the respective emission decay profiles).

parameter	<b>Re<sub>2</sub>-bpb</b>					
	30 K	40 K	50 K	60 K	70 K	80 K
$\tau_1$ (%) / $\mu\text{s}$	69.9 (68.08)	67.2 (68.80)	64.5 (69.51)	61.6 (69.93)	58.7 (70.36)	53.7 (70.94)
$\tau_2$ (%) / $\mu\text{s}$	130.7 (31.92)	119.1 (31.20)	107.4 (30.49)	98.3 (30.07)	89.2 (29.64)	83.3 (29.06)
$\tau_{\text{av.}}$ / $\mu\text{s}$	89.3	83.4	77.6	72.6	67.7	62.3
$\chi^2$	1.032	1.053	1.079	1.102	1.001	1.052
	90 K	100 K	110 K	120 K	130 K	140 K
$\tau_1$ (%) / $\mu\text{s}$	48.7 (71.52)	44.3 (73.57)	39.9 (75.62)	36.9 (76.89)	33.8 (78.16)	30.3 (79.31)
$\tau_2$ (%) / $\mu\text{s}$	77.4 (28.48)	68.5 (26.43)	59.6 (24.38)	55.6 (23.11)	51.6 (21.84)	46.9 (20.69)
$\tau_{\text{av.}}$ / $\mu\text{s}$	56.8	50.7	44.7	41.2	37.7	33.7
$\chi^2$	1.051	1.052	1.007	1.022	1.084	1.075
	150 K	160 K	170 K	180 K	190 K	200 K
$\tau_1$ (%) / $\mu\text{s}$	26.7 (80.45)	23.8 (82.69)	20.8 (84.93)	19.4 (86.63)	17.9 (88.34)	14.8 (89.22)
$\tau_2$ (%) / $\mu\text{s}$	42.3 (19.55)	38.7 (17.31)	35.2 (15.07)	31.8 (13.37)	28.5 (11.66)	25.7 (10.78)
$\tau_{\text{av.}}$ / $\mu\text{s}$	29.8	26.4	23.0	21.0	19.2	15.9
$\chi^2$	1.061	1.092	1.078	1.039	1.067	1.092
	210 K	220 K	230 K	240 K	250 K	260 K
$\tau_1$ (%) / $\mu\text{s}$	11.6 (90.10)	10.5 (90.73)	9.5 (91.36)	8.0 (91.92)	6.5 (92.47)	5.4 (92.68)
$\tau_2$ (%) / $\mu\text{s}$	23.0 (9.90)	20.9 (9.27)	18.8 (8.64)	16.2 (8.08)	13.7 (7.53)	12.4 (7.32)
$\tau_{\text{av.}}$ / $\mu\text{s}$	12.7	11.5	10.2	8.6	7.0	6.0
$\chi^2$	1.069	1.123	1.007	1.023	1.057	1.008
	270 K	280 K	290 K	300 K	310 K	320 K
$\tau_1$ (%) / $\mu\text{s}$	4.4 (92.9)	3.6 (93.02)	2.8 (93.14)	2.6 (93.38)	2.3 (93.63)	1.8 (93.88)
$\tau_2$ (%) / $\mu\text{s}$	11.1 (7.1)	9.8 (6.98)	8.5 (6.86)	7.3 (6.62)	6.2 (6.37)	4.9 (6.12)
$\tau_{\text{av.}}$ / $\mu\text{s}$	4.9	4.1	3.2	2.9	2.5	2.0
$\chi^2$	1.031	1.024	1.062	1.022	1.036	1.102
	330 K	–	–	–	–	–
$\tau_1$ (%) / $\mu\text{s}$	1.3 (94.13)	–	–	–	–	–
$\tau_2$ (%) / $\mu\text{s}$	3.63 (5.87)	–	–	–	–	–
$\tau_{\text{av.}}$ / $\mu\text{s}$	1.4	–	–	–	–	–
$\chi^2$	1.003	–	–	–	–	–

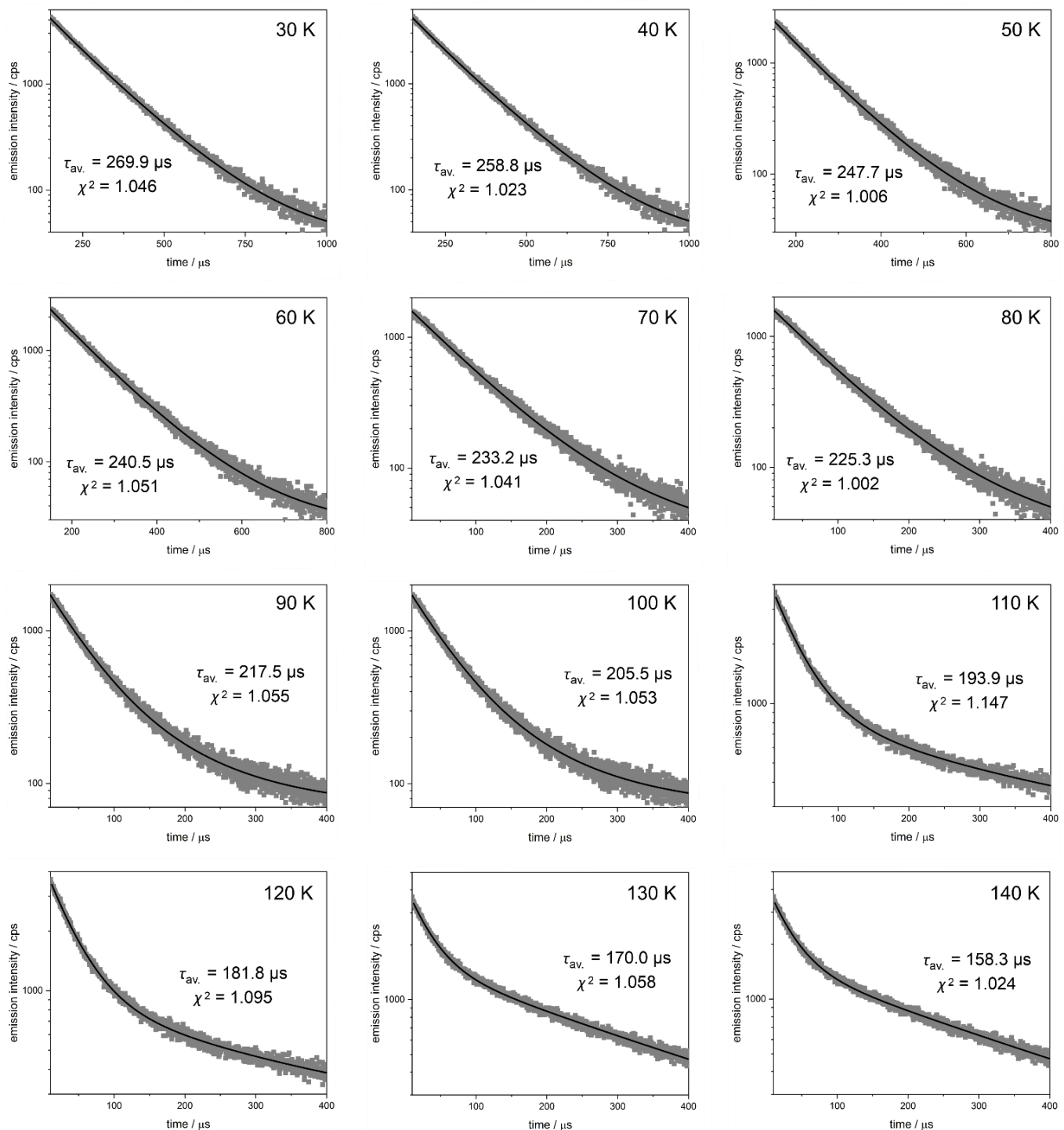


**Fig. S70** (part 1 of 3) Temperature-variable emission decay profiles for **Re<sub>2</sub>-bpbb** under  $\lambda_{\text{exc}} = 430 \text{ nm}$  and  $\lambda_{\text{em}} = 554 \text{ nm}$ , collected for the indicated temperatures from the 30–330 K range (in this part, the region of 30–140 K is shown). The double exponential fitting was applied for each temperature; the related best-fit curve is illustrated by a solid line). The best-fit parameters are roughly presented on the graphs while the detailed values are gathered in Table S77.

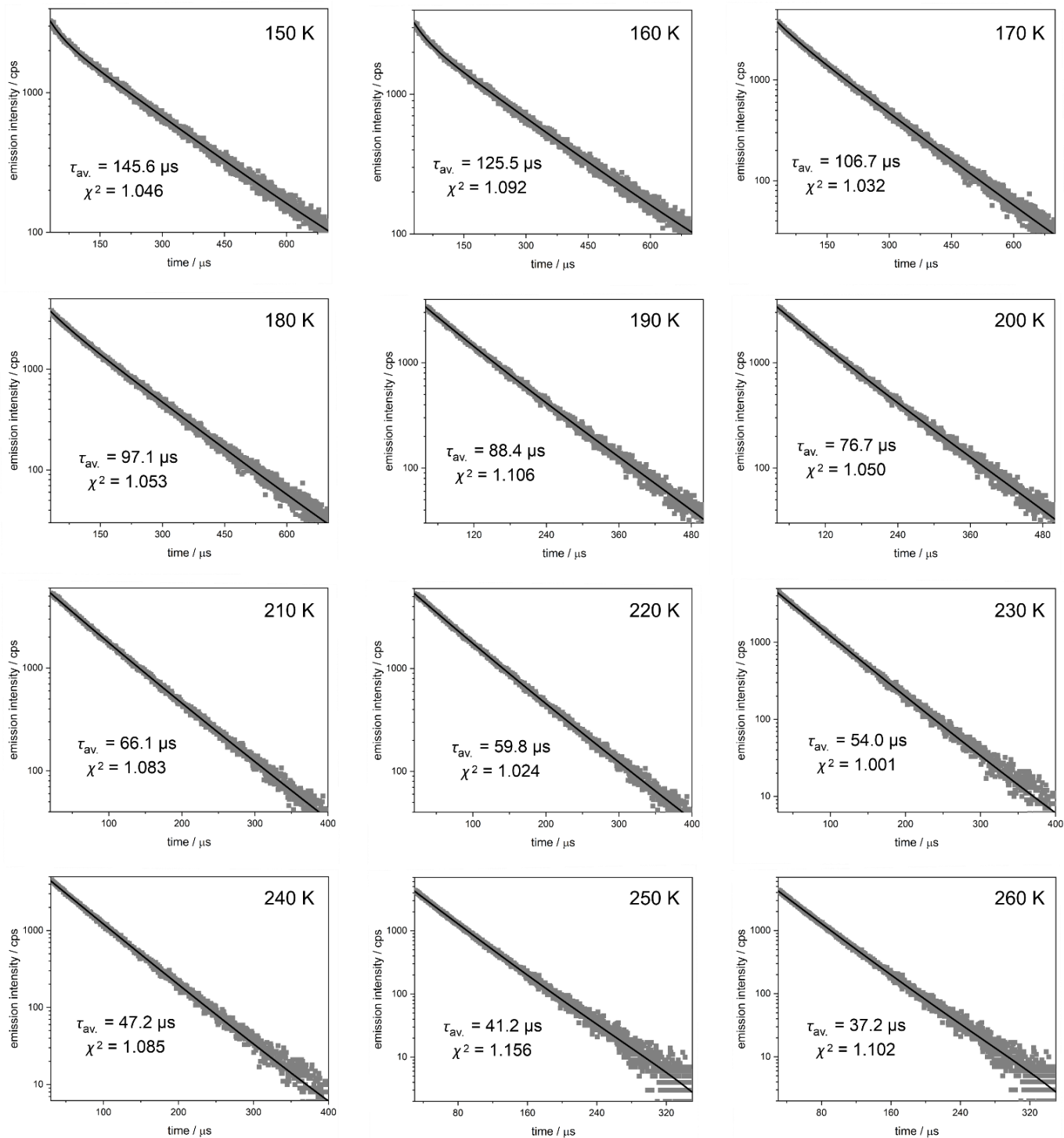


**Fig. S70** (part 2 of 3) Temperature-variable emission decay profiles for **Re<sub>2</sub>-bpbp** under  $\lambda_{exc} = 430$  nm and  $\lambda_{em} = 554$  nm, collected for the indicated temperatures from the 30–330 K range (in this part, the region of 150–260 K is shown). The double exponential fitting was applied for each temperature; the related best-fit curve is illustrated by a solid line). The best-fit parameters are roughly presented on the graphs while the detailed values are gathered in Table S77.

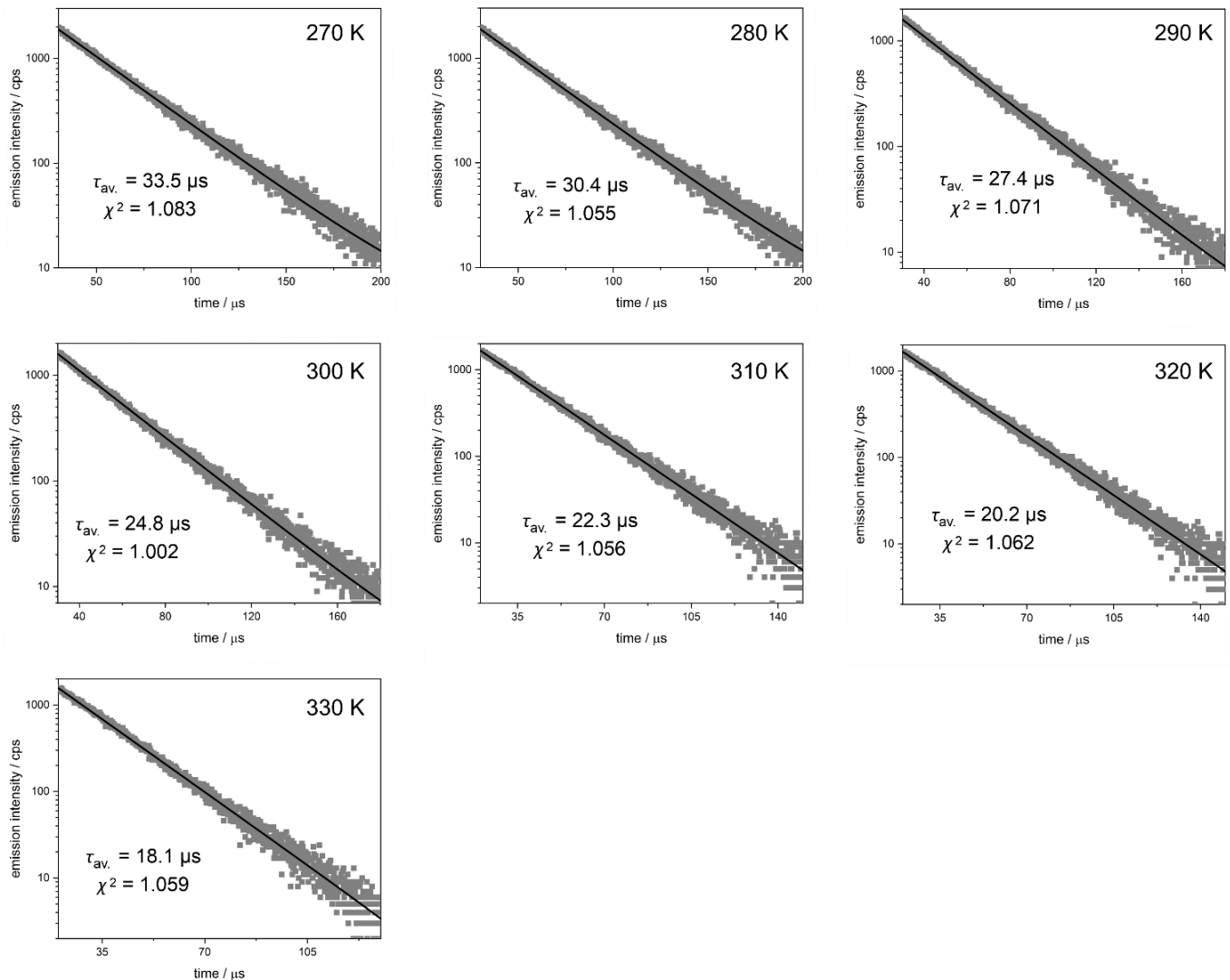


**Fig. S70** (part 3 of 3) Temperature-variable emission decay profiles for **Re<sub>2</sub>-bpbbp** under  $\lambda_{\text{exc}} = 430$  nm and  $\lambda_{\text{em}} = 554$  nm, collected for the indicated temperatures from the 30–330 K range (in this part, the region of 270–330 K is shown). The double exponential fitting was applied for each temperature; the related best-fit curve is illustrated by a solid line). The best-fit parameters are roughly presented on the graphs while the detailed values are gathered in Table S77.

**Table S77** Best-fit parameters for the emission decay profiles of **Re<sub>2</sub>-bpbp** to the double exponential decay function (represented by the  $\tau_1$  and  $\tau_2$  values of emission lifetime components, with the respective contributions given in the brackets next to the lifetime values), and the calculated weighted-average emission lifetime ( $\tau_{\text{av.}}$ ), all presented for the 30–330 K temperature range (see Fig. S70 for the respective emission decay profiles).

parameter	<b>Re<sub>2</sub>-bpbp</b>					
	30 K	40 K	50 K	60 K	70 K	80 K
$\tau_1$ (%) / $\mu\text{s}$	103.5 (26.17)	101.2 (29.68)	98.9 (33.19)	95.0 (34.64)	91.2 (36.09)	90.6 (37.55)
$\tau_2$ (%) / $\mu\text{s}$	328.9 (73.83)	325.3 (70.32)	321.7 (66.81)	317.6 (65.36)	313.4 (63.91)	306.3 (62.45)
$\tau_{\text{av.}}$ / $\mu\text{s}$	269.9	258.8	247.7	240.5	233.2	225.3
$\chi^2$	1.046	1.023	1.006	1.051	1.041	1.002
	90 K	100 K	110 K	120 K	130 K	140 K
$\tau_1$ (%) / $\mu\text{s}$	89.9 (39.01)	87.3 (40.80)	84.6 (42.6)	80.5 (44.49)	76.3 (46.38)	73.8 (44.39)
$\tau_2$ (%) / $\mu\text{s}$	299.1 (60.99)	287.1 (59.20)	275.0 (57.4)	263.0 (55.51)	251.0 (53.62)	225.7 (55.61)
$\tau_{\text{av.}}$ / $\mu\text{s}$	217.5	205.5	193.9	181.8	170.0	158.3
$\chi^2$	1.055	1.053	1.147	1.095	1.058	1.024
	150 K	160 K	170 K	180 K	190 K	200 K
$\tau_1$ (%) / $\mu\text{s}$	71.3 (42.39)	69.9 (44.66)	68.6 (46.93)	66.8 (51.18)	65.1 (55.42)	61.5 (59.60)
$\tau_2$ (%) / $\mu\text{s}$	200.3 (57.61)	170.4 (55.34)	140.4 (53.07)	128.9 (48.82)	117.4 (44.58)	99.1 (40.4)
$\tau_{\text{av.}}$ / $\mu\text{s}$	145.6	125.5	106.7	97.1	88.4	76.7
$\chi^2$	1.046	1.092	1.032	1.053	1.106	1.050
	210 K	220 K	230 K	240 K	250 K	260 K
$\tau_1$ (%) / $\mu\text{s}$	57.8 (63.78)	54.4 (68.70)	51.0 (73.61)	46.0 (83.90)	41.0 (94.18)	37.2 (100)
$\tau_2$ (%) / $\mu\text{s}$	80.9 (36.22)	71.6 (31.30)	62.3 (26.39)	53.5 (16.10)	44.8 (5.82)	–
$\tau_{\text{av.}}$ / $\mu\text{s}$	66.1	59.8	54.0	47.2	41.2	37.2
$\chi^2$	1.083	1.024	1.001	1.085	1.156	1.102
	270 K	280 K	290 K	300 K	310 K	320 K
$\tau_1$ (%) / $\mu\text{s}$	33.5 (100)	30.4 (100)	27.4 (100)	24.8 (100)	22.3 (100)	20.2 (100)
$\tau_2$ (%) / $\mu\text{s}$	–	–	–	–	–	–
$\tau_{\text{av.}}$ / $\mu\text{s}$	33.5	30.4	27.4	24.8	22.3	20.2
$\chi^2$	1.083	1.055	1.071	1.002	1.056	1.062
	330 K	–	–	–	–	–
$\tau_1$ (%) / $\mu\text{s}$	18.1 (100)	–	–	–	–	–
$\tau_2$ (%) / $\mu\text{s}$	–	–	–	–	–	–
$\tau_{\text{av.}}$ / $\mu\text{s}$	18.1	–	–	–	–	–
$\chi^2$	1.059	–	–	–	–	–

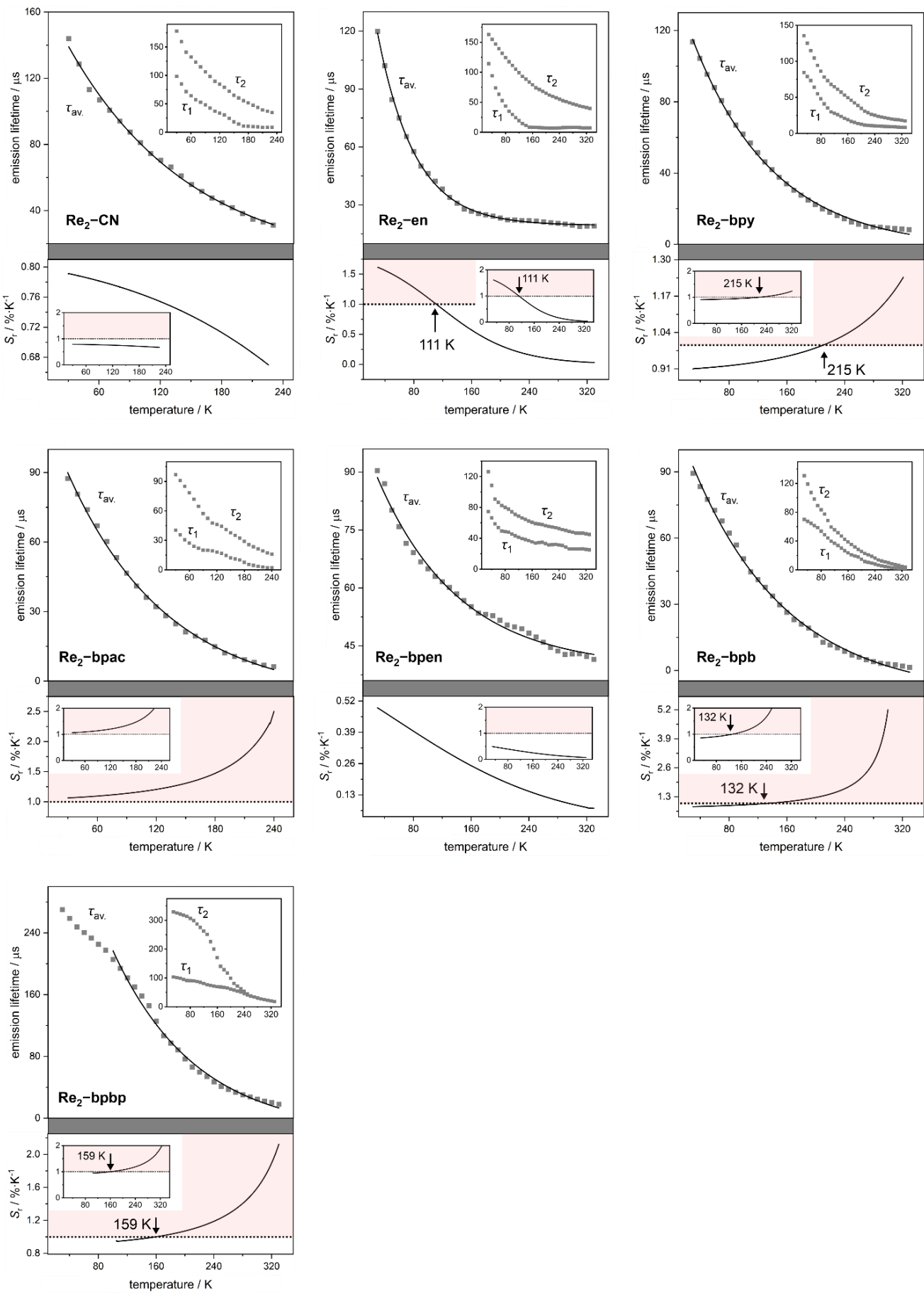


**Fig. S71** Temperature dependencies of emission lifetimes ( $\tau_1$  and  $\tau_2$ ; obtained from fitting to the double exponential decay functions; the insets) and the calculated weighted-average emission lifetime ( $\tau_{\text{av.}}$ ; main graphs) for **Re<sub>2</sub>-CN**, **Re<sub>2</sub>-en**, **Re<sub>2</sub>-bpy**, **Re<sub>2</sub>-bpac**, **Re<sub>2</sub>-bpen**, **Re<sub>2</sub>-bpb**, and **Re<sub>2</sub>-bpbp** (Fig. S64–S70, Tables S71–S77), with the best-fit curves (solid lines) obtained using the exponential fitting, shown together with the relative thermal sensitivity ( $S_T$ ) curves (under the corresponding fits). The resulting best-fit parameters are collected in Table S78.

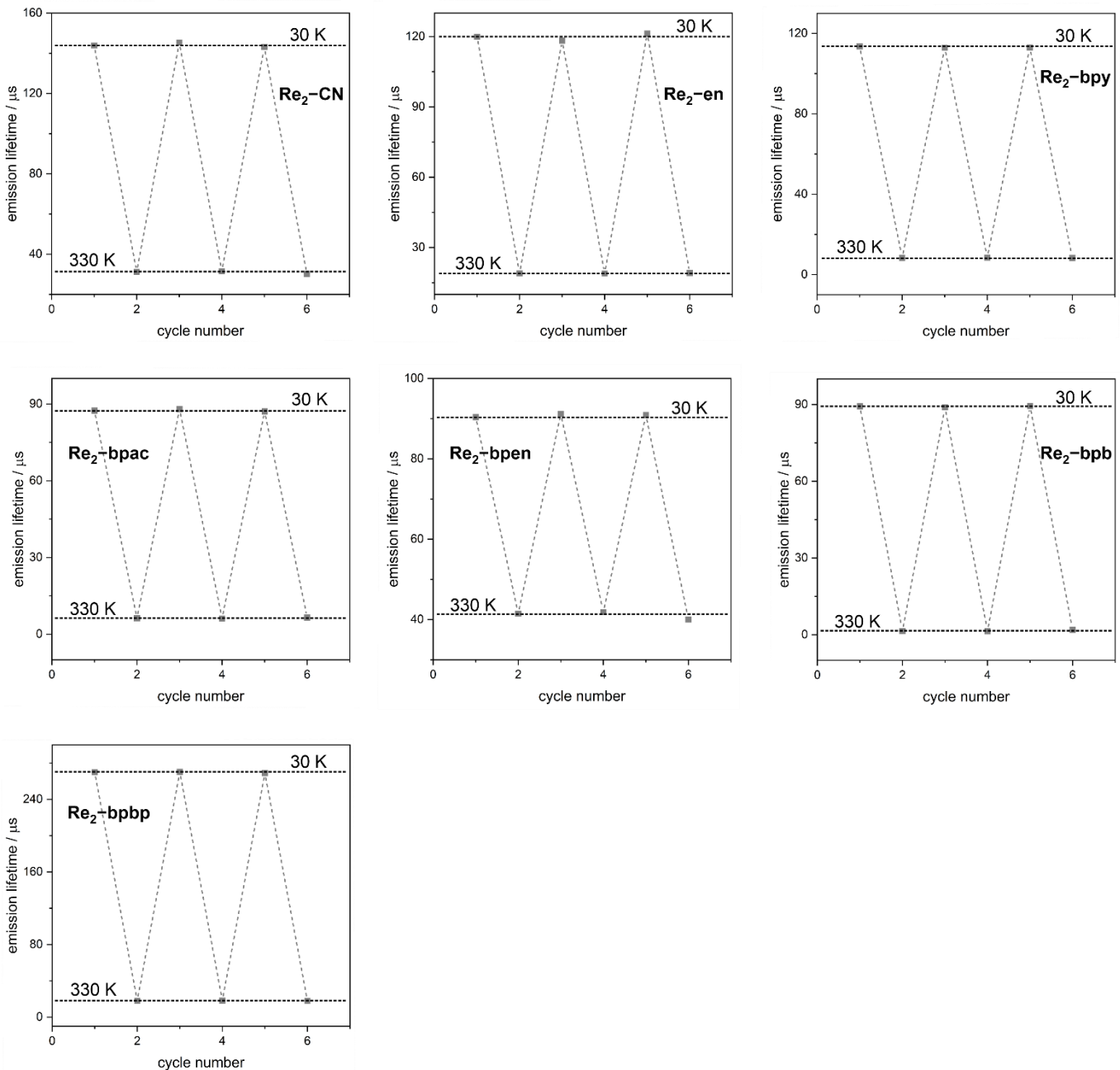


**Fig. S72** Thermal repeatability curves of the application of a weighted-average emission lifetime ( $\tau_{av.}$ ) as a thermometric parameter, presented for six consecutive measurements for **Re<sub>2</sub>-CN**, **Re<sub>2</sub>-en**, **Re<sub>2</sub>-bpy**, **Re<sub>2</sub>-bpac**, **Re<sub>2</sub>-bpen**, **Re<sub>2</sub>-bpb**, and **Re<sub>2</sub>-bpbp** (see Fig. S72 for comparison). Please note **Re<sub>2</sub>-bppe** does not appear here and other Fig./tables related to the optical thermometry based on emission lifetimes as its values of emission lifetimes were too short to be reliably followed experimentally and thus used for optical thermometry.

**Table S78** Best-fit parameters for the exponential fitting of the temperature dependencies of the weighted-average emission lifetime ( $\tau_{\text{av.}}$ ) for **Re<sub>2</sub>-CN**, **Re<sub>2</sub>-en**, **Re<sub>2</sub>-bpy**, **Re<sub>2</sub>-bpac**, **Re<sub>2</sub>-bpee**, **Re<sub>2</sub>-bpb**, and **Re<sub>2</sub>-bpbp**, investigated within the indicated temperature ranges (see Fig. S71 for the visualization of the related best-fit curves and experimental data).

Material	Temp. range / K	Equation: $\tau_{\text{av.}} = A + B \cdot \exp(C \cdot T)$			$\chi^2 / \%$	$S_r^{\max} / \% \cdot K^{-1}$	$T$ for $S_r^{\max} / K$
		A / $\mu s$	B / $\mu s$	C / $K^{-1}$			
<b>Re<sub>2</sub>-CN</b>	30–230	6.2(0.86)	170.2(2.71)	-0.008(0.0006)	99.8	0.79	30
<b>Re<sub>2</sub>-en</b>	30–330	19.3(0.26)	177.7(2.11)	-0.019(0.0003)	99.9	1.61	30
<b>Re<sub>2</sub>-bpy</b>	30–330	-2.4(0.95)	153.6(1.20)	-0.009(0.0002)	99.9	1.24	330
<b>Re<sub>2</sub>-bpac</b>	300–240	-7.4(1.21)	130.8(1.29)	-0.010(0.0004)	99.8	2.50	240
<b>Re<sub>2</sub>-bpee</b>	30–330	39.3(0.98)	64.3(1.22)	-0.009(0.0005)	99.3	0.49	30
<b>Re<sub>2</sub>-bpb</b>	30–330	-11.3(1.49)	130.5(1.31)	-0.008(0.0003)	99.7	5.20	300
<b>Re<sub>2</sub>-bpbp</b>	100–330	-19.1(7.910)	559.9(27.76)	-0.009(0.0007)	99.4	2.12	330

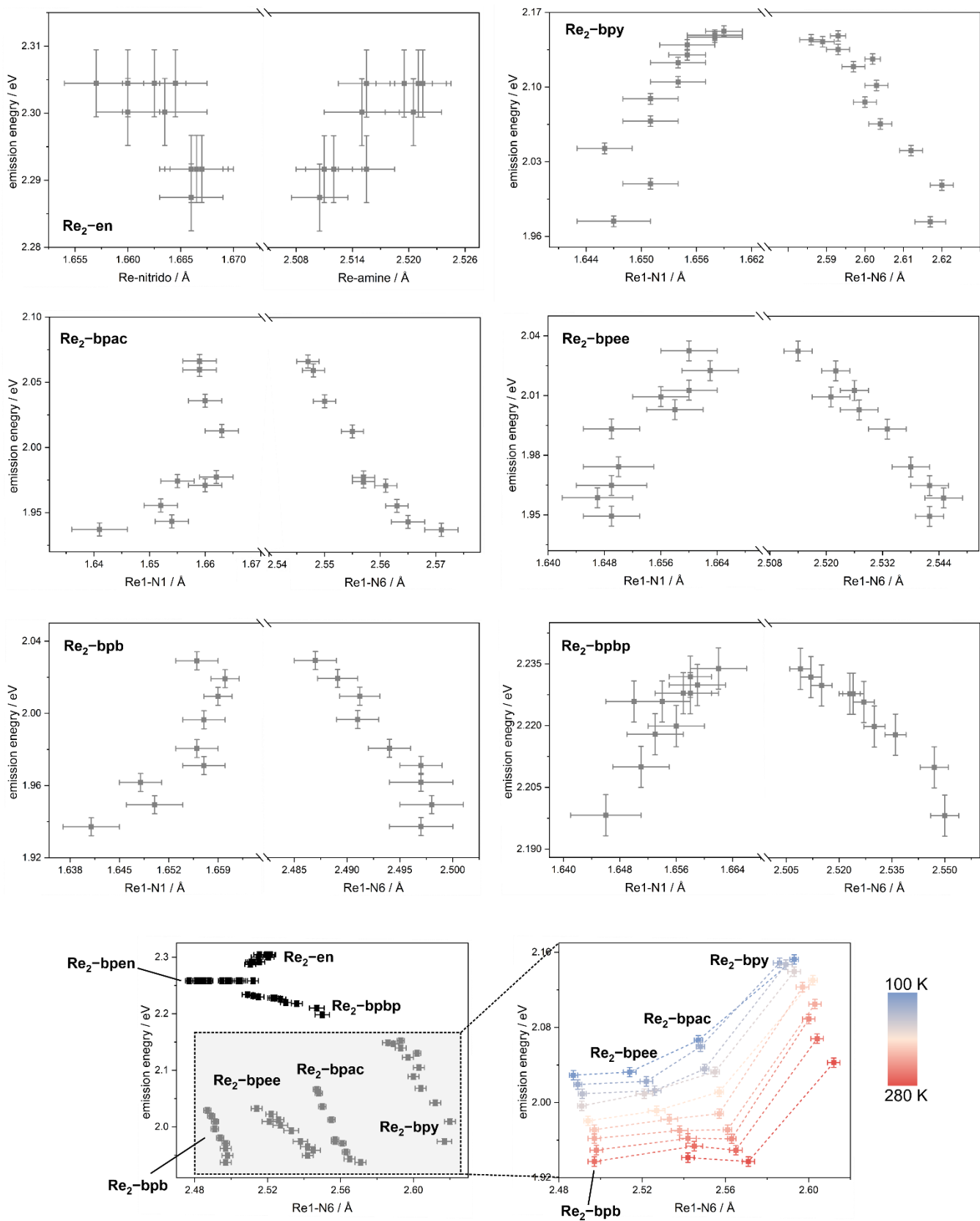


**Fig. S73** The detailed insight into the dependence of emission maximum energy on the Re1-N1 and Re1-N6 bond distances under variable temperature from the 100–280 K range in the whole series of reported materials, i.e., Re<sub>2</sub>-en, Re<sub>2</sub>-bpy, Re<sub>2</sub>-bpac, Re<sub>2</sub>-bpee, Re<sub>2</sub>-bpen, Re<sub>2</sub>-bpb, and Re<sub>2</sub>-bpbp. The bottom part of the figure includes the comparison between the materials while above the separate graphs for each compound are presented.

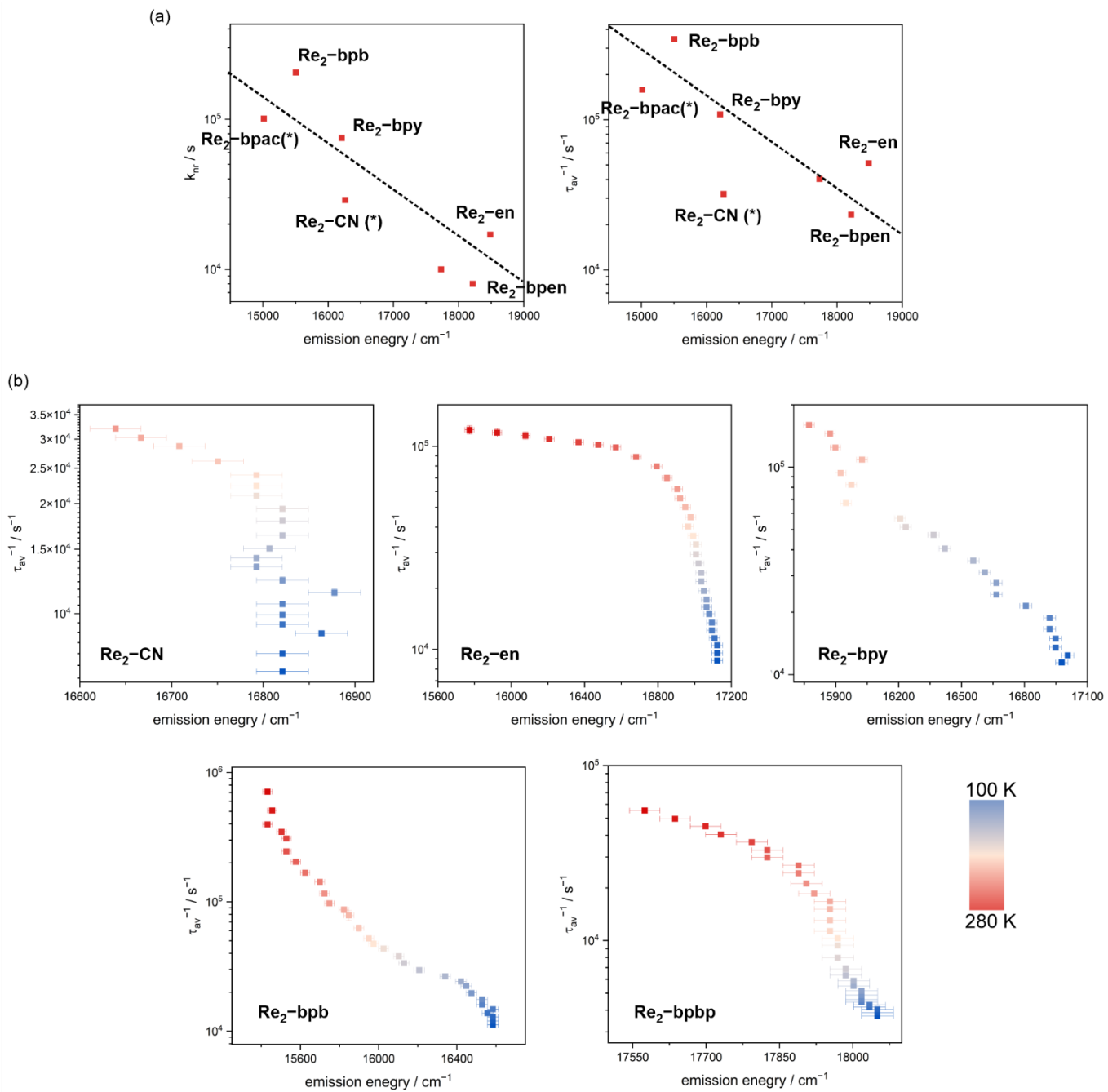


**Fig. S74** The correlation of non-radiative decay rate constant and luminescence lifetime with the emission energies at room temperature within selected materials in the  $\text{Re}_2\text{-L}$  series (a), and the correlation between T-dependent lifetimes and emission energies for  $\text{Re}_2\text{-CN}$ ,  $\text{Re}_2\text{-en}$ ,  $\text{Re}_2\text{-bpy}$ ,  $\text{Re}_2\text{-bpb}$ , and  $\text{Re}_2\text{-bpdp}$ .

## References to the Supporting Information

- S1 – M. Seike, K. Nagata, H. Ikeda, A. Ito, E. Sakuda, N. Kitamura, A. Shinohara and T. Yoshimura, Synthesis and Photoluminescence of Tetracyanidonitridorhenium(V) Complexes with Five-Membered *N*-Heteroaromatic Ligands and Photoluminescence-Intensity Change, *ACS Omega*, 2019, **4**, 21251–21259.
- S2 – L.-J. Luo, Q.-Q. Su, S.-C. Cheng, J. Xiang, W.-L. Man, W.-M. Shu, M.-H. Zeng, S.-M. Yiu, C.-C. Ko and T.-C. Lau, Tunable Luminescent Properties of Tricyanoosmium Nitrido Complexes Bearing a Chelating O<sup>N</sup> Ligand, *Inorg. Chem.*, 2020, **59**, 4406–4413.
- S3 – M. Llunell, D. Casanova, J. Cirera, J. Bofill, P. Alemany, S. Alvarez, M. Pinsky and D. Avnir, Program for the Stereochemical Analysis of Molecular Fragments by Means of Continuous Shape Measures and Associated Tools, SHAPE v. 2.1.; University of Barcelona: Barcelona, Spain, 2013.
- S4 – D. Casanova, J. Cirera, M. Llunell, P. Alemany, D. Avnir and S. Alvarez, Minimal Distortion Pathways in Polyhedral Rearrangements, *J. Am. Chem. Soc.*, 2004, **126**, 1755–1763.
- S5 – H. Ikeda, A. Ito, E. Sakuda, N. Kitamura, T. Takayama, T. Sekine, A. Shinohara and T. Yoshimura, Excited-State Characteristics of Tetracyanidonitridorhenium(V) and -technetium(V) Complexes with N-Heteroaromatic Ligands, *Inorg. Chem.*, 2013, **52**, 6319–6327.
- S6 – M. Liberka, M. Zychowicz, J. Hooper, K. Nakabayashi, S. Ohkoshi and S. Chorazy, Synchronous Switching of Dielectric Constant and Photoluminescence in Cyanidonitridorhenate-Based Crystals, *Angew. Chem. Int. Ed.*, 2023, **62**, e202308284.
- S7 – M. J. Frisch, G. W. Trucks, H. B. Schlegel, G. E. Scuseria, M. A. Robb, J. R. Cheeseman, G. Scalmani, V. Barone, G. A. Petersson, H. Nakatsuji, X. Li, M. Caricato, A. V. Marenich, J. Bloino, B. G. Janesko, R. Gomperts, B. Mennucci, H. P. Hratchian, J. V. Ortiz, A. F. Izmaylov, J. L. Sonnenberg, D. Williams-Young, F. Ding, F. Lipparini, F. Egidi, J. Goings, B. Peng, A. Petrone, T. Henderson, D. Ranasinghe, V. G. Zakrzewski, J. Gao, N. Rega, G. Zheng, W. Liang, M. Hada, J. M. Ehara, K. Toyota, R. Fukuda, J. Hasegawa, M. Ishida, T. Nakajima, Y. Hondo, O. Kitao, H. Nakai, T. Vreven, K. Throssell, J. A. Montgomery, J. E. Peralta, F. Ogliaro, M. J. Bearpark, J. J. Heyd, E. N. Brothers, K. N. Kudin, V. N. Staroverov, T. A. Kobayashi, R. Keith, J. Normand, K. Raghavachari, A. P. Rendell, J. C. Burant, S. S. Iyengar, J. Tomasi, M. Cossi, J. M. Millam, M. Klene, C. Adamo, R. Cammi, J. W. Ochterski, R. L. Martin, K. Morokuma, O. Farkas, J. B. Foresman and D. J. Fox, Gaussian 16, Revision C.01, Gaussian, Inc.: Wallingford CT, United States, 2016.
- S8 – C. Adamo and V. Barone, Toward reliable density functional methods without adjustable parameters: The PBE0 model, *J. Chem. Phys.*, 1999, **110**, 6158–6170.
- S9 – F. Weigend and R. Ahlrichs, Balanced basis sets of split valence, triple zeta valence and quadruple zeta valence quality for H to Rn: Design and assessment of accuracy, *Phys. Chem. Chem. Phys.*, 2005, **7**, 3297–3305.
- S10 – J. Tomasi, B. Mennucci and R. Cammi, Quantum Mechanical Continuum Solvation Models, *Chem. Rev.*, 2005, **105**, 2999–3093.
- S11 – S. Grimme, S. Ehrlich and L. Goerigk, Effect of the damping function in dispersion corrected density functional theory, *J. Comp. Chem.*, 2011, **32**, 1456–1465.
- S12 – M. E. Casida, C. Jamorski, K. C. Casida and D. R. Salahub, Molecular excitation energies to high-lying bound states from time-dependent density-functional response theory: Characterization and correction of the time-dependent local density approximation ionization threshold, *J. Chem. Phys.*, 1998, **108**, 4439–4449.
- S13 – F. Neese, F. Wennmohs, U. Becker and C. Ripplinger, The ORCA quantum chemistry program package, *J. Chem. Phys.*, 2020, **152**, 224108.
- S14 – A. D. Becke, Density-functional exchange-energy approximation with correct asymptotic behavior, *Phys. Rev. A*, 1988, **38**, 3098–3100.
- S15 – C. Lee, W. Yang and R. G. Parr, Development of the Colle-Salvetti correlation-energy formula into a functional of the electron density, *Phys. Rev. B*, 1988, **37**, 785–789.

- S16 – B. De Souza, G. Farias, F. Neese and R. Izsak, Predicting Phosphorescence Rates of Light Organic Molecules Using Time-Dependent Density Functional Theory and the Path Integral Approach to Dynamics, *J. Chem. Theory Comput.*, 2019, **15**, 1896–1904.
- S17 – C. Latouche, D. Skouteris, F. Palazzetti and V. Barone, TD-DFT Benchmark on Inorganic Pt(II) and Ir(III) Complexes, *J. Chem. Theory Comput.*, 2015, **11**, 3281–3289.
- S18 – E. Caldeweyher, S. Ehlert, A. Hansen, H. Neugebauer, S. Spicher, C. Bannwarth and S. A. Grimme, A generally applicable atomic-charge dependent London dispersion correction, *J. Chem. Phys.*, 2019, **150**, 154122.
- S19 – R. Cammi, B. Mennucci and J. Tomasi, Fast Evaluation of Geometries and Properties of Excited Molecules in Solution: A Tamm-Dancoff Model with Application to 4-Dimethylaminobenzonitrile, *J. Phys. Chem. A*, 2000, **104**, 5631–5637.
- S20 – E. Van Lenthe, E. J. Baerends and J. G. Snijders, Relativistic regular two-component Hamiltonians, *J. Chem. Phys.*, 1993, **99**, 4597–4610.
- S21 – C. Van Wüllen, Molecular density functional calculations in the regular relativistic approximation: Method, application to coinage metal diatomics, hydrides, fluorides and chlorides, and comparison with first-order relativistic calculations, *J. Chem. Phys.*, 1998, **109**, 392–399.
- S22 – D. A. Pantazis, X.-Y. Chen, C. R. Landis and F. Neese, All-Electron Scalar Relativistic Basis Sets for Third-Row Transition Metal Atoms, *J. Chem. Theory Comput.*, 2008, **4**, 908–919.
- S23 – M. Bühl, C. Reimann, D. A. Pantazis, T. Bredow and F. Neese, Geometries of Third-Row Transition-Metal Complexes from Density-Functional Theory, *J. Chem. Theory Comput.*, 2008, **4**, 1449–1459.
- S24 – F. Neese, F. Wnnmohs, A. Hansen and U. Becker, Efficient, approximate and parallel Hartree-Fock and hybrid DFT calculations. A ‘chain-of-spheres’ algorithm for the Hartree-Fock exchange, *Chem. Phys.*, 2009, **356**, 98–109.
- S25 – R. Izsák and F. Neese, An overlap fitted chain of spheres exchange method, *J. Chem. Phys.*, 2011, **135**, 144105.
- S26 – F. Neese, Efficient and accurate approximations to the molecular spin-orbit coupling operator and their use in molecular g-tensor calculations, *J. Chem. Phys.*, 2005, **122**, 034107.
- S27 – G. Kresse and J. Furthmüller, Efficiency of ab-initio total energy calculations for metals and semiconductors using a plane-wave basis set, *Comput. Mater. Sci.*, 1996, **6**, 15–50.
- S28 – J. P. Perdew, K. Burke and M. Ernzerhof, Generalized Gradient Approximation Made Simple, *Phys. Rev. Lett.*, 1996, **77**, 3865.
- S29 – A. V. Kruckau, O. A. Vydrov, A. F. Izmaylov and G. E. Scuseria, Influence of the exchange screening parameter on the performance of screened hybrid functionals, *J. Chem. Phys.*, 2006, **125**, 224106.
- S30 – P. E. Blöchl, Projector augmented-wave method, *Phys. Rev. B*, 1994, **50**, 17953–17979.
- S31 – K. Momma and F. Izumi, VESTA 3 for three-dimensional visualization of crystal, volumetric and morphology data, *J. Appl. Crystallogr.*, 2011, **44**, 1272–1276.
- S32 – A. Ćirić and M. D. Dramićanin, LumTHools - Software for fitting the temperature dependence of luminescence emission intensity, lifetime, bandshift, and bandwidth and luminescence thermometry and review of the theoretical models, *J. Lumin.*, 2022, **252**, 119413.